

TECHNICAL REPORT 0-6905-R1A

TxDOT PROJECT NUMBER 0-6905

## **Initial Investigation of Performance of Skewed Reinforcing in Inverted-T Bridge Caps**

Satya Sapath Roy  
Jamshaid Sawab  
Tianmin Zhou  
Y. L. Mo  
Thomas T. C. Hsu

January 2019; Published May 2021

1. Report No. FHWA/TX-21/0-6905-R1A	2. Government Accession No.	3. Recipient's Catalog No.	
4. Title and Subtitle Initial Investigation of Performance of Skewed Reinforcing in Inverted-T Bridge Caps		5. Report Date January 2019; Published May 2021	
		6. Performing Organization Code	
7. Author(s) Satya Sapath Roy, Jamshaid Sawab, Tianmin Zhou, Y. L. Mo, and Thomas T. C. Hsu		8. Performing Organization Report No. 0-6905-R1A	
9. Performing Organization Name and Address University of Houston 4800 Calhoun Road Houston, TX 77204-4003		10. Work Unit No. (TR AIS)	
		11. Contract or Grant No. 0-6905	
12. Sponsoring Agency Name and Address Texas Department of Transportation Research and Technology Implementation Office P. O. Box 5080 Austin, Texas 78763-5080		13. Type of Report and Period Covered Technical Report January 2016–January 2019	
		14. Sponsoring Agency Code	
15. Supplementary Notes Project performed in cooperation with the Texas Department of Transportation and the Federal Highway Administration.			
16. Abstract Many reinforced concrete inverted-T bridge caps (ITBCs) are skew when two roads are not aligned perpendicularly and exceed the angle of 45 degrees based on the construction requirements. The Texas ITBCs are designed using the traditional empirical procedures outlined in the TxDOT Bridge Design Manual (TxDOT BDM) LRFD that conform to the AASHTO (American Association of State Highway and Transportation Officials) LRFD (2014) Bridge Design Specifications. There are no precise calculation methods or guidelines given in the AASHTO LRFD (2014) or TxDOT BDM-LRFD (2015) to design skew ITBCs. However, any kind of improper detailing can cause poor placement of concrete and cracks within the concrete structure which would reduce the load-carrying capacity and increase future maintenance costs. Faster and easier construction can be obtained if the skew transverse reinforcing is utilized and it can provide an alternative approach which will significantly reduce the design complexities and construction period. Accordingly, there is a concern about whether using skewed transverse reinforcement will provide reasonable structural behavior for the skew ITBCs regarding the overall cracking occurrence and structural performance. Therefore, TxDOT research project 0-6905 investigated the structural performance of the skew ITBCs with skew transverse reinforcement and compared it to the performance of the ITBCs with traditional transverse reinforcement considering various variables. The research team investigated the structural behavior and failure modes of the ITBCs utilizing skew transverse reinforcement, emphasizing these aspects: (1) skew angle, (2) detailing of transverse reinforcement, and (3) amount of transverse reinforcement. Based on these three variables, 13 skew ITBC specimens were fabricated: seven in Phase 1 of the test plan and six in Phase 2. Where M is the minimum transverse reinforcements specified in AASHTO, Phase 1 test specimens contain 2M of transverse reinforcement whereas Phase 2 specimens contain M amount. Then the test results were calibrated with 3D FE simulation. A parametric analysis was also performed to understand the overall structural behavior of skew reinforcement in inverted-T bridge bent caps. The test and FE simulation results generated these primary observations: (1) the skew transverse reinforcement arrangement does not weaken the bridge cap's capacity; (2) fewer cracks are observed and the observed maximum crack width is smaller in ITBCs with skewed reinforcing; (3) construction complexities can be significantly reduced and a faster and easier construction process can be achieved when skewed reinforcing is used. Therefore, skew transverse reinforcing could be a better alternative to the traditional one.			
17. Key Words ITBC, inverted-T bridge cap, reinforcement design		18. Distribution Statement No restrictions. This document is available to the public through the National Technical Information Service, Springfield, Virginia 22161; www.ntis.gov.	
19. Security Classif. (of this report) Unclassified	20. Security Classif. (of this page) Unclassified	21. No. of Pages TBD	22. Price

**TxDOT Project 0-6905**

**Initial Investigation of Performance of Skewed  
Reinforcing in Inverted-T Bridge Caps**

**Satya Sapath Roy, Jamshaid Sawab, Tianmin Zhou, Y.L. Mo and Thomas T.C. Hsu**  
**Department of Civil and Environmental Engineering**  
**University of Houston**

**Research Report 0-6905-R1A**

## **DISCLAIMERS**

**Author's Disclaimer:** The contents of this report reflect the views of the authors, who are responsible for the facts and the accuracy of the data presented herein. The contents do not necessarily reflect the official view or policies of the Federal Highway Administration or the Texas Department of Transportation (TxDOT). This report does not constitute a standard, specification, or regulation.

**Patent Disclaimer:** There was no invention or discovery conceived or first actually reduced to practice in the course of or under this contract, including any art, method, process, machine manufacture, design or composition of matter, or any new useful improvement thereof, or any variety of plant, which is or may be patentable under the patent laws of the United States of America or any foreign country.

**Research Supervisor: Y.L Mo**

**Professional Engineer License State and Number: Texas No. 110677 P. E.**

## **ACKNOWLEDGMENTS**

The authors would like to express their gratitude to the Texas Department of Transportation (TxDOT) for their financial support and collaborative efforts for this project. This research is supported by TxDOT for Grant 0-6905. The authors would like to specifically thank the contributions of the project supervisory committee which consists of: Chris Glancy, RTI (Research and Technology Implementation Office); Michael Carlson, HOU; Bobby Bari, HOU; Walter "Ray" Fisher, DAL; Courtney Holle, BRG; Aaron Garza, BRG; Hector Garcia, DOT and Andrew Smyth, DOT. Finally, the authors appreciate the rest of the support staff at the Thomas T.C. Hsu Structural Lab at UH (University of Houston) and the many other researchers who helped with instrumentation, testing, and analysis of results.

## ABSTRACT

For the past several decades, the reinforced concrete inverted-T bridge caps (ITBCs) have been widely used in most of the bridges in Texas and the United States as they are aesthetically pleasing and offer a practical means to increase vertical clearance. Many of the ITBCs are skew when two roads are not aligned perpendicularly and exceed the angle of 45 degrees based on the construction requirements. Most of these ITBCs in Texas are designed using the traditional empirical procedures outlined in the TxDOT Bridge Design Manual (TxDOT BDM) LRFD that conform to the AASHTO (American Association of State Highway and Transportation Officials) LRFD (2014) Bridge Design Specifications. There are no precise calculation methods or guidelines given in the AASHTO LRFD (2014) or TxDOT BDM-LRFD (2015) to design skew ITBCs. For a skew ITBC, the TxDOT Manual states only that hanger and ledge reinforcement should be placed perpendicular to the centerline of the skew bent. The detailing of the skew ends of the bent should be done with a section of skewed stirrups and ledge reinforcements. Typically, the transition of straight bars to the skew bars is carried out over column support where the transverse reinforcement spacing is less critical. The designer of ITBC flares the bars out to match the skew angle while trying to maintain a minimum and maximum spacing based on the outcome of the design calculations. Such detailing of transverse reinforcements creates unequal spacing in both sides of the web producing congestion of reinforcements in one side.

The traditional method of flaring the transverse reinforcement out in skew ITBCs brings in significant complexity in design and during the construction process. In addition, the detailing of the transverse reinforcement has a profound influence on the overall shear capacity of the bent cap as well as the performance of the support ledge. Therefore, any kind of improper detailing can cause poor placement of concrete and cracks within the concrete structure which would reduce the load-carrying capacity and increase future maintenance costs. Faster and easier construction can be obtained if the skew transverse reinforcing is utilized and it can provide an alternative approach which will significantly reduce the design complexities and construction period. Accordingly, there is a concern about whether using skewed transverse reinforcement will provide reasonable structural behavior for the skew ITBCs regarding the overall cracking occurrence and structural performance.

Therefore, under the TxDOT research project 0-6905 (*Performance of Skewed Reinforcing in Inverted-T Bridge Caps*), the structural performance of the skew ITBCs with skew transverse reinforcement is investigated and compared to the performance of the ITBCs with traditional transverse reinforcement considering various variables. The objective of this project was to investigate the structural behavior and failure modes of the ITBCs utilizing skew transverse reinforcement, emphasizing the following aspects: (1) skew angle, (2) detailing of transverse reinforcement, and (3) amount of transverse reinforcement. Based on the above mentioned three variables, 13 skew ITBC specimens were fabricated to be tested in the UH Thomas T.C. Hsu Structural Lab. Out of 13

specimens, seven ITBC specimens belong to Phase 1 of the test plan. In Phase 2 of the test plan, six more specimens were tested. Phase 1 test specimens contain an amount of  $2M$  of transverse reinforcement whereas Phase 2 specimens have an  $M$  amount of transverse reinforcement, where  $M$  is the minimum transverse reinforcements specified in AASHTO. Then the test results are calibrated with 3D FE simulation. A parametric analysis is also performed in order to understand the overall structural behavior of skew reinforcement in inverted-T bridge bent caps taking into account unexplored parameters in the test matrix. From the test and FE simulation results of the ITBC specimens, the primary observations made are as follows: (1) the skew transverse reinforcement arrangement does not weaken the bridge cap's capacity; (2) number of cracks observed are fewer and the observed maximum crack width is smaller in the case of the ITBC with skewed reinforcing; (3) construction complexities can be significantly reduced and a faster and easier construction process can be achieved when skewed reinforcing is used. Therefore, skew transverse reinforcing could be a better alternative to the traditional one.

# TABLE OF CONTENTS

<b>CHAPTER 1: INTRODUCTION</b> .....	<b>1</b>
1.1 PROJECT OVERVIEW .....	1
1.2 PROJECT OBJECTIVES .....	2
1.3 PROJECT SIGNIFICANCE.....	3
1.4 ORGANIZATION .....	3
<b>CHAPTER 2: BACKGROUND OF INVERTED-T BRIDGE CAPS</b> .....	<b>5</b>
2.1 OVERVIEW .....	5
2.2 RECAP OF INVERTED-T BENT CAPS .....	5
2.3 COMPONENTS AND LOAD TRANSFER MECHANISM.....	7
2.4 FAILURE MODES IN INVERTED-T BENT CAP .....	9
2.4.1 Flexure Failure Mode.....	10
2.4.2 Shear Failure Mode.....	10
2.4.3 Torsional Failure.....	11
2.4.4 Failure of Hanger Stirrups .....	11
2.4.5 Ledge Failure due to Punching Shear .....	12
2.4.6 Failure due to Shear Friction.....	12
2.5 DESIGN PROVISIONS FOR ITBC .....	13
2.5.1 Flexure Capacity .....	13
2.5.2 Shear Capacity .....	14
2.5.3 Hanger Capacity of the Transverse Reinforcement .....	15
2.5.4 Torsional Capacity of the Section.....	16
2.5.5 Punching Shear Capacity of the Ledge.....	16
2.5.6 Shear Friction Capacity of the Ledge .....	18
2.5.7 Bearing Capacity of the Ledge .....	19
2.5.8 Diagonal Cracking Between Ledge and Web (Zu et al., 2003) .....	20
2.6 CONCLUSION.....	21
<b>CHAPTER 3: EXPERIMENTAL PROGRAM</b> .....	<b>22</b>
3.1 OVERVIEW .....	22
3.2 TESTING PROGRAM.....	22
3.2.1 Skew Angle.....	22
3.2.2 Detailing of Transverse Reinforcement .....	22

3.2.3	Amount of Transverse Reinforcement.....	22
3.3	DESIGN OF ITBC SPECIMENS.....	23
3.3.1	Phase 1 Specimens.....	25
3.3.2	Phase 2 Specimens.....	29
3.4	FABRICATION OF THE INVERTED-T TEST SPECIMENS .....	32
3.4.1	Steel Reinforcement Properties.....	32
3.4.2	Concrete Mix Design Properties.....	32
3.4.3	Construction of the Test Specimen.....	34
3.5	TEST SETUP.....	39
3.6	INSTRUMENTATIONS .....	46
3.6.1	Load – Displacement Measurement.....	46
3.6.2	Strain Measurement .....	47
3.6.3	Crack Measurement .....	52
3.7	LOADING PROTOCOL .....	52
3.8	SUMMARY.....	53
	<b>CHAPTER 4: EXPERIMENTAL RESULTS .....</b>	<b>54</b>
4.1	OVERVIEW .....	54
4.2	MATERIAL PROPERTIES .....	54
4.2.1	Steel Reinforcement Properties.....	54
4.2.2	Concrete Properties.....	54
4.3	PRIMARY EXPERIMENTAL RESULTS .....	55
4.4	TEST RESULTS.....	58
4.4.1	Phase 1 Specimens.....	58
4.4.2	Phase 2 Specimens.....	84
4.5	DISCUSSIONS OF THE TEST RESULTS.....	101
4.5.1	Comparison of Primary Test Results .....	101
4.5.2	Strength Data Evaluation .....	104
4.5.3	Serviceability Data Evaluation .....	107
4.5.4	Failure Modes of ITBC Specimens.....	123
4.6	CONCLUSIONS.....	126
	<b>CHAPTER 5: FINITE ELEMENT (FE) ANALYSIS .....</b>	<b>128</b>
5.1	OVERVIEW .....	128

5.2	FINITE ELEMENT ANALYSIS OF TEST SPECIMENS.....	128
5.2.1	Finite Element Modeling .....	128
5.2.2	Material Models .....	129
5.2.3	Finite Element Simulated Results.....	137
5.3	PARAMETRIC STUDY .....	139
5.3.1	Comparison of Deformations for Various Skew Angles .....	140
5.3.2	Comparison of Displacements at Service Load .....	140
5.3.3	Stresses in Transverse Rebars at Service Load.....	143
5.3.4	Stresses in Transverse Rebars at Yielding .....	146
5.3.5	Effect of Loading Pad's Location on Transverse Rebars .....	150
5.3.6	Effect of End Face Rebars .....	154
5.3.7	Comparison of Principal Tensile Strain (Cracking Zone) .....	157
5.4	CONCLUSIONS.....	159
	<b>CHAPTER 6: DESIGN RECOMMENDATIONS.....</b>	<b>160</b>
6.1	OVERVIEW .....	160
6.2	GENERAL DESIGN RECOMMENDATIONS.....	160
6.3	PROPOSED CHANGES TO TXDOT PRACTICE.....	163
6.3.1	Current TxDOT Practice.....	163
6.3.2	Proposed Change .....	163
6.4	DESIGN EXAMPLES.....	163
6.4.1	Defining the Bent Cap .....	163
6.4.2	Illustrative Example .....	163
6.5	3D FEA RESULTS OF THE FULL SCALE BENT CAP .....	167
6.6	CONCLUSIONS.....	172
	<b>CHAPTER 7: SUMMARY AND CONCLUSIONS.....</b>	<b>173</b>
7.1	SUMMARY OF THE RESEARCH WORK.....	173
7.2	CONCLUSIONS.....	173
	<b>APPENDIX 1: STRAIN GAUGE LOCATIONS OF TEST SPECIMENS.....</b>	<b>178</b>
	<b>APPENDIX 2 : STRAIN IN THE REBARS OF TEST SPECIMENS .....</b>	<b>191</b>
	<b>APPENDIX 3: ILLUSTRATIVE DESIGN EXAMPLE .....</b>	<b>208</b>

## LIST OF FIGURES

Figure 2.1. Components of a Highway Bridge .....	6
Figure 2.2. Difference between Rectangular and Inverted-T Bent Cap .....	6
Figure 2.3. Components of Inverted-T Bent Cap .....	7
Figure 2.4. Non-Skew and Skew ITBC .....	8
Figure 2.5. Deformations Pattern of Skewed ITBCs .....	9
Figure 2.6. Flexural Failure Modes in Inverted-T Bent Caps.....	10
Figure 2.7. Shear Failure Mode in Inverted-T Bent Cap .....	11
Figure 2.8. Torsional Failure Mode in Inverted-T Bent Cap.....	11
Figure 2.9. Failure of Hanger Stirrups in Inverted-T Bent Cap.....	12
Figure 2.10. Failure due to Punching Shear in Ledge of ITBC .....	12
Figure 2.11. Failure due to Shear Friction in Inverted-T Bent Cap.....	13
Figure 2.12. Shear Friction Consideration:.....	16
Figure 2.13. Shear Friction for Ledge (AASHTO LRFD, 2014).....	18
Figure 2.14. Bearing Consideration: .....	19
Figure 2.15. Crack at West End Face of Southwest Inverted-T Bent.....	20
Figure 3.1. Main Components of Inverted-T Bridge Cap.....	25
Figure 3.2. Reinforcing details of Phase 1 ITBCs: .....	28
Figure 3.3. Reinforcing Details of Phase 2 ITBCs: .....	31
Figure 3.4. Partial Reinforcing Details of Phase 1 Specimens: .....	35
Figure 3.5. Partial Reinforcing Details of Phase 2 Specimens: .....	36
Figure 3.6. Fabrication of Specimens: .....	38
Figure 3.7. Schematic View of the Test Setup for ITBC Specimens .....	40
Figure 3.8. Support Conditions for the Test .....	41
Figure 3.9. Elevation view of the loading frame A and B with dimension details.....	42
Figure 3.10. Elevation view of the loading frame C with dimension details.....	43
Figure 3.11. Primary components of test frame during fabrication stage:.....	44
Figure 3.12. Test Setup of ITBC Specimen in UH Laboratory .....	45
Figure 3.13. Instrumentation:.....	47
Figure 3.14. Strain Gauge Installation: .....	49
Figure 3.15. Typical Strain Gauges Arrangement and Location .....	51

Figure 3.16. Crack Width Measurement.....	52
Figure 4.1. ITBC Showing the Shear Spans .....	56
Figure 4.2. Force-displacement Curve of Specimen ITBC-0-T-2M: .....	59
Figure 4.3. Cracking of Specimen ITBC-0-T-2M: .....	60
Figure 4.4. Strain Behavior of Specimen ITBC-0-T-2M Rebars : .....	61
Figure 4.5. Force-displacement Curve of ITBC-30-T-2M: .....	63
Figure 4.6. Force-displacement Curve of ITBC-30-S-2M: .....	64
Figure 4.7. Cracking of Specimen ITBC-30-T-2M: .....	65
Figure 4.8. Cracking of Specimen ITBC-30-S-2M: .....	66
Figure 4.9. Strain Behavior of Specimen ITBC-30-T-2M Rebars: .....	67
Figure 4.10. Strain Behavior of Specimen ITBC-30-S-2M Rebars:.....	68
Figure 4.11. Force-displacement Curve of ITBC-45-T-2M: .....	70
Figure 4.12. Force-displacement Curve of ITBC-45-S-2M : .....	71
Figure 4.13. Cracking of Specimen ITBC-45-T-2M: .....	73
Figure 4.14. Cracking of Specimen ITBC-45-S-2M: .....	74
Figure 4.15. Strain Behavior of Specimen ITBC-45-T-2M Rebars: .....	75
Figure 4.16. Strain Behavior of Specimen ITBC-45-S-2M Rebars :.....	77
Figure 4.17. Force-displacement Curve of ITBC-60-T-2M: .....	79
Figure 4.18. Force-displacement Curve of ITBC-60-S-2M: .....	80
Figure 4.19. Cracking of Specimen ITBC-60-T-2M: .....	81
Figure 4.20. Cracking of Specimen ITBC-60-S-2M: .....	82
Figure 4.21. Strain Behavior of Specimen ITBC-60-T-2M Rebar: .....	83
Figure 4.22. Strain Behavior of Specimen ITBC-60-S-2M Rebars:.....	84
Figure 4.23. Force-displacement curve of ITBC-30-T-M: .....	86
Figure 4.24. Force-displacement curve of ITBC-30-S-M: .....	87
Figure 4.25. Cracking of Specimen ITBC-30-T-M: .....	88
Figure 4.26. Cracking of Specimen ITBC-30-S-M: .....	89
Figure 4.27. Force-displacement curve of ITBC-45-T-M: .....	91
Figure 4.28. Force-displacement curve of ITBC-45-S-M : .....	92
Figure 4.29. Cracking of Specimen ITBC-45-T-M: .....	93
Figure 4.30. Cracking of Specimen ITBC-45-S-M: .....	95

Figure 4.31. Force-displacement curve of ITBC-60-T-M: .....	97
Figure 4.32. Force-displacement curve of ITBC-60-S-M: .....	97
Figure 4.33. Cracking of Specimen ITBC-60-T-M: .....	99
Figure 4.34. Cracking of Specimen ITBC-60-S-M: .....	100
Figure 4.35. Force-displacement Curve:.....	102
Figure 4.36. Normalized Force-displacement Curve of Test Specimens .....	106
Figure 4.37. Cracking Pattern at Failure Stage for Specimen ITBC-0-T-2M .....	110
Figure 4.38. Cracking Pattern at Failure Stage for Specimen ITBC-30-T-2M .....	111
Figure 4.39. Cracking Pattern at Failure Stage for Specimen ITBC-30-S-2M.....	112
Figure 4.40. Cracking Pattern at Failure Stage for Specimen ITBC-45-T-2M .....	113
Figure 4.41. Cracking Pattern at Failure Stage for Specimen ITBC-45-S-2M.....	114
Figure 4.42. Cracking Pattern at Failure Stage for Specimen ITBC-60-T-2M .....	115
Figure 4.43. Cracking Pattern at Failure Stage for Specimen ITBC-60-S-2M.....	116
Figure 4.44. Cracking Pattern at Failure Stage for Specimen ITBC-30-T-M .....	117
Figure 4.45. Cracking Pattern at Failure Stage for Specimen ITBC-30-S-M.....	118
Figure 4.46. Cracking Pattern at Failure Stage for Specimen ITBC-45-T-M .....	119
Figure 4.47. Cracking Pattern at Failure Stage for Specimen ITBC-45-S-M.....	120
Figure 4.48. Cracking Pattern at Failure Stage for Specimen ITBC-60-T-M .....	121
Figure 4.49. Cracking Pattern at Failure Stage for Specimen ITBC-60-S-M.....	122
Figure 4.50. Punching Shear Failure of Ledges in ITBC-60-T-2M .....	124
Figure 4.51. Plan View of Partial Reinforcement Arrangement for ITBC-60-T-2M.....	124
Figure 4.52. Punching Shear Failure of Ledges in ITBC-60-S-2M.....	125
Figure 4.53. Torsional cracking profile at peak load : .....	126
Figure 4.54. Torsional cracking profile at peak load: .....	126
Figure 5.1. 3D FE Model of ITBC-0-T-2M.....	128
Figure 5.2. 3D Finite Element Mesh of ITBC in ABAQUS:.....	129
Figure 5.3. Plan View of Partial Reinforcing in ABAQUS .....	133
Figure 5.4. Stress-Strain Curves of Concrete in Tension and Compression.....	134
Figure 5.5. Stress-Strain Curve of Mild Steel.....	134
Figure 5.6. Comparison of Force – Displacement Curves.....	139
Figure 5.7. Deformations of skew ITBCs for Various Skew Angles .....	140

Figure 5.8. Displacement at Service Load for Various Skew Angle .....	143
Figure 5.9. Transverse Rebar Stresses at Service Load for Various Skew Angle .....	145
Figure 5.10. Stresses in Hanger Rebars at Yielding: .....	149
Figure 5.11. Different Configurations of Loading Pads .....	151
Figure 5.12. Stresses in Transverse Rebars for Various C .....	153
Figure 5.13. End Face Details.....	154
Figure 5.14. Stresses in Transverse Rebars for Various Skew Angles .....	156
Figure 5.15. Comparison of Principal Tensile Strain at Service Load .....	159
Figure 6.1. Typical Stirrup Details ~ Plan View .....	162
Figure 6.2. Typical Bent Cap Cross Section.....	164
Figure 6.3. Typical Bent Cap Cross Section at End Face .....	165
Figure 6.4. Partial Elevation View Over a Column .....	166
Figure 6.5 Partial Plan view Reinforcement Detailing (Shows S, M & N Bars).....	166
Figure 6.6. 3D Finite Element Model of the Designed Bent Cap with Skew Angle $43^{\circ}$ .....	168
Figure 6.7. Partial 3D Finite Element Mesh of the Designed Bent Cap.....	169
Figure 6.8. Tensile stress Contour at Service Load (With End Face Rebars) .....	170
Figure 6.9. Tensile stress Contour at Service Load (Without End Face Rebars) .....	171

## LIST OF TABLES

Table 3.1. Test Matrix of ITBC Specimens .....	23
Table 3.2. ITBC Rebar Details .....	32
Table 3.3. Typical PCC Mixture Design for Test Specimens.....	33
Table 3.4. Typical SCC Mixture Design for Test Specimens.....	34
Table 4.1. Yield Strength of Steel Rebars.....	54
Table 4.2. Mean Compressive Strength of ITBC Specimens .....	55
Table 4.3. Summary of Test Results .....	57
Table 4.4. Summary of Primary Test Results of 30 <sup>0</sup> Skew ITBCs.....	103
Table 4.5. Summary of Primary Test Results of 45 <sup>0</sup> Skew ITBCs.....	103
Table 4.6. Summary of Primary Test Results of 60 <sup>0</sup> Skew ITBCs.....	104
Table 4.7. Observation of Diagonal Cracks at the End Face of ITBCs .....	108
Table 4.8. Summary of Number of Flexural Shear Cracks Count.....	109
Table 5.1. Material Parameters for the Concrete Damaged Plasticity Model .....	136

# **CHAPTER 1: INTRODUCTION**

## **1.1 PROJECT OVERVIEW**

Inverted-T bridge caps (ITBC) are used extensively in Texas and throughout the rest of the United States because they are aesthetically pleasing and offer a practical means to increase the vertical clearance of bridges. Many of these inverted-T bridge structures are skew, some in excess of 45 degrees, based on the angle of the bridges crossing roadways, waterways, or railways. Most of these ITBC in Texas are designed using the traditional empirical procedures outlined in the TxDOT (Texas Department of Transportation) Bridge Design Manual-LRFD that conforms to the AASHTO (American Association of Highway and Transportation Officials) LRFD (2014) Bridge Design Specifications. There are no precise calculation methods or guidelines given in the AASHTO LRFD or TxDOT Bridge Design Manual-LRFD to design skew ITBC. The TxDOT Bridge Design Manual states only that hanger and ledge reinforcement should be placed perpendicular to the centerline of the skew bent. The detailing of the skew ends of the bent should be done with a section of skew stirrups and ledge reinforcements. Typically, the transition of straight bars to the skew bars is carried out over a column support where the transverse reinforcement spacing is less critical. The designer of ITBC flares the bars out to match the skew angle while trying to maintain a minimum and maximum spacing based on the outcome of the design calculations.

Such detailing of transverse reinforcement in skew ITBC brings complexity into the design and construction process. This transverse reinforcement has a profound influence on the overall shear capacity of the bent cap as well as the performance of the support ledge. Therefore, any kind of improper detailing can cause poor placement of concrete and cracks within the concrete structure which would reduce the load carrying capacity and increase future maintenance costs. Faster and easier construction can be obtained if the skew transverse reinforcing steel is utilized and it can provide an alternative approach which will significantly reduce the design complexities and construction period. Accordingly, there is a concern about whether using skew transverse reinforcement will provide reasonable structural behavior for the skew ITBC regarding the overall cracking occurrence and structural performance. Therefore, it is necessary to analyze the structural performance of the skew ITBC with skew transverse reinforcement and compare the performance to the traditional ITBC.

The ACI (American Concrete Institute) 318-14 states that nominal torsional moment strength increases if the area enclosed by the centerline of the outermost closed transverse torsional reinforcement is increased. By providing skew transverse reinforcement in skew ITBC as a replacement for traditional reinforcement, the area enclosed by the centerline of the outermost closed loop reinforcement is increased. Thus, skew transverse reinforcement has the potential to decrease the effects of torsion coming onto the skew ITBC. But there has not been adequate research to back this theory. A lack

of experimental research has thwarted this approach so far. So far, no significant research has been undertaken to study the performance of skew transverse reinforcement in ITBC. A thorough experimental and analytical research is carried out through this project to verify the potential beneficial effects of using skew reinforcement instead of traditional reinforcement.

The research program has been divided into two phases which consist of a total of 13 ITBC test specimens. The test matrix with different test parameters for the inverted-T bridge cap specimens is presented in Table 3.1. In the first phase, seven inverted-T bent cap specimens are considered. There are three critical parameters considered in the test matrix. They include the skew angle, the detailing of transverse reinforcement, and the amount of transverse reinforcements. Four values of the skew angles considered in this study are 0, 30, 45, and 60 degrees. Two types of the transverse reinforcement detailing are considered, including traditional reinforcing (presently used by TxDOT) and skewed reinforcing (proposed). The amount of transverse reinforcement considered is twice the minimum transverse reinforcement (2M) and the minimum transverse reinforcements (M) specified by AASHTO LRFD (2014). The inverted-T bridge cap specimens with the 2M and M amount of transverse reinforcements are fabricated in Phase 1 and Phase 2 of the test plan, respectively. Moreover, in the Phase 2 specimens, end face reinforcements (U1 and U2 bars) and the G bars are provided in both ends of the inverted-T bridge cap to investigate the propagation of diagonal cracks at the re-entrant corner between the ledge and the web at the end faces of the exterior portions of the ITBCs. The structural performance of the inverted-T bent caps with traditional transverse reinforcement is compared with the performance of the bent caps designed with proposed transverse reinforcement detailing. The strength and serviceability are two main aspects that are taken into consideration to evaluate the performance of the inverted-T bent caps. Moreover, the simulation of test members is performed in order to understand the overall structural behavior of skewed reinforcement in inverted-T bridge caps. Later, the developed numerical models are calibrated against the test results for the further numerical simulation, taking into account unexplored parameters in the test matrix.

## **1.2 PROJECT OBJECTIVES**

The objectives of this project are summarized as follows:

1. To investigate the effect of skewed transverse reinforcement with skew angle,  $0^{\circ}$ ,  $30^{\circ}$ ,  $45^{\circ}$ , and  $60^{\circ}$  in inverted-T bent caps.
2. To compare and evaluate the structural performance of skewed transverse reinforcement with traditional transverse reinforcement in ITBCs in regards to strength criteria with a focus on shear capacity and torsional effects.
3. To compare and evaluate the structural performance of skewed transverse reinforcement with traditional transverse reinforcement in ITBCs in terms of

serviceability criteria considering the number of cracks, cracking widths and failure mode.

4. The ITBC test specimens will be modeled in 3D Finite Element software ABAQUS and all the test results will be calibrated. Additional parameters that were not considered in the proposed test matrix will be investigated in detail to establish enough databases.
5. The general design recommendations and changes to the TxDOT practice to design skewed reinforcements in ITBCs will be proposed.

### **1.3 PROJECT SIGNIFICANCE**

This project will provide the following benefits to the TxDOT and other stakeholders:

1. By replacing a traditional transverse reinforcement with a skewed one, proper placement of concrete and less complex fabrication of reinforcement could be ensured. As a result, the construction costs involved would be reduced.
2. Skewed reinforcement would reduce the congestion in the skew region of the bent cap. As a result, proper placement of concrete could be achieved. It would reduce the complexity in detailing the skew region of the bent cap by providing uniform spacing and same size reinforcing bars. Therefore, lesser working hours and laborers would be required for the fabrication/construction of the ITBC with skewed reinforcement.
3. So far, no significant research has been undertaken to study the performance of skewed transverse reinforcement in ITBC. A lack of experimental research has thwarted the use of skewed reinforcing. Therefore, there are no specific design guidelines for the design of skewed reinforcements in inverted-T bent caps, which makes the design unreliable with increased risks of failure. By providing proper design guidelines for different skew angles, high levels of lifetime uncertainties and risks of failure could be prevented. The skew reinforcement approach could reduce the replacement cost and increase the reliability thereby benefiting the TxDOT and other stakeholders financially.

### **1.4 ORGANIZATION**

This report is divided into seven chapters. Chapter 1 introduces an overview and the objectives of the research in addition to an outline of this report. Chapter 2 presents a background and literature review of the past relevant work along with failure modes in inverted-T bent cap research. A general background of the design provisions and behavior of inverted-T bent caps is also presented. The experimental program and testing process considered under the scope of the project is described in detail in Chapter 3. An overview of the test specimens and the fabrication of the specimens are presented. The test setup and instrumentation are described and the overall test procedure is outlined. Chapter 4

demonstrates the results obtained after testing inverted-T bent cap specimens under static compression loading. Criteria for strength and serviceability evaluation are detailed. Comparisons of strength, diagonal cracking load, and the crack width progression are presented for the experimental variables covered in this project. 3D Finite Element Analysis (FEA) of all the test specimens is presented in Chapter 5 along with parametric studies considering more variables. An overview of the design recommendations is presented in Chapter 6. All the findings and conclusions of the research program are summarized in Chapter 7.

## **CHAPTER 2: BACKGROUND OF INVERTED-T BRIDGE CAPS**

### **2.1 OVERVIEW**

In this chapter is an overview of the theoretical background of inverted-T bent cap including design and behavior. The AASHTO LRFD Bridge Design Specifications and TxDOT Bridge Design Manual are discussed. Local and global failure modes are briefly described. The difference between skew and non-skew bent cap is outlined. The effect of torsion on the skewed bent cap has been discussed.

### **2.2 RECAP OF INVERTED-T BENT CAPS**

The fundamental components of a highway bridge can be categorized into three parts including superstructure (deck slab, girder), substructure (pier, abutment, cap, bearing), and foundation (pile, well foundation) as shown in Figure 2.1. A bent is another terminology in regard to substructure which can be described as an assembly of columns and a bent cap beam which serves as intermediate support between bridge spans that resist and transfer vertical loads and lateral loads (seismic and wind) from the superstructure to the foundation. The bent cap beam is provided to carry longitudinal girders and to transfer the loads to the bent columns. The concrete bent caps are typically classified as Drop bent cap, Integral bent cap and Inverted-T bent cap which may be cast-in-place or precast and may be either conventionally reinforced or prestressed.

The inverted-T bent cap can be described as a bent cap constructed in the form of an inverted-T with a provision on the ledge on each side of the web for supporting the girders to achieve economic and speedy bridge construction schemes. Such bent caps are significantly adopted in bridge construction to reduce the elevation of bridges and to improve available clearance beneath the girders (Gomez, 2012). Inverted-T beams can be simply supported, cantilevered over simple supports, or constructed monolithically with columns or piers. The main difference between inverted-T bent caps and rectangular bent caps can be seen in Figure 2.2.

- ❖ In the case of the inverted-T bent cap, the provided ledge system reduces the overall depth by avoiding deep cross members as compared to typical rectangular bent caps resulting in lower abutments and shorter approaches for the bridge. Also, this structural system is aesthetically pleasing and offers a practical means for increasing the vertical clearance.
- ❖ The bridge girders are supported on ledges near the bottom of the beam, effectively loading the cap along its tension cord. This arrangement generates a tension field in the web at the loading points as forces are “hung” from the tension chord to the top of the beam. In contrast, compression-chord loaded beams are not subjected to such concentrated tension fields in the web as the load is applied to the upper part of the beam (Fernandez, 2012).

- ❖ The forces are applied to ledges at a considerably larger distance away from the centerline of the web which set up greater twisting forces on the web. With the traffic approaching the bent cap, girder reactions on one of the ledges instigate twisting towards the approaching load. After the passage of traffic, the twisting is promoted in the opposite direction.

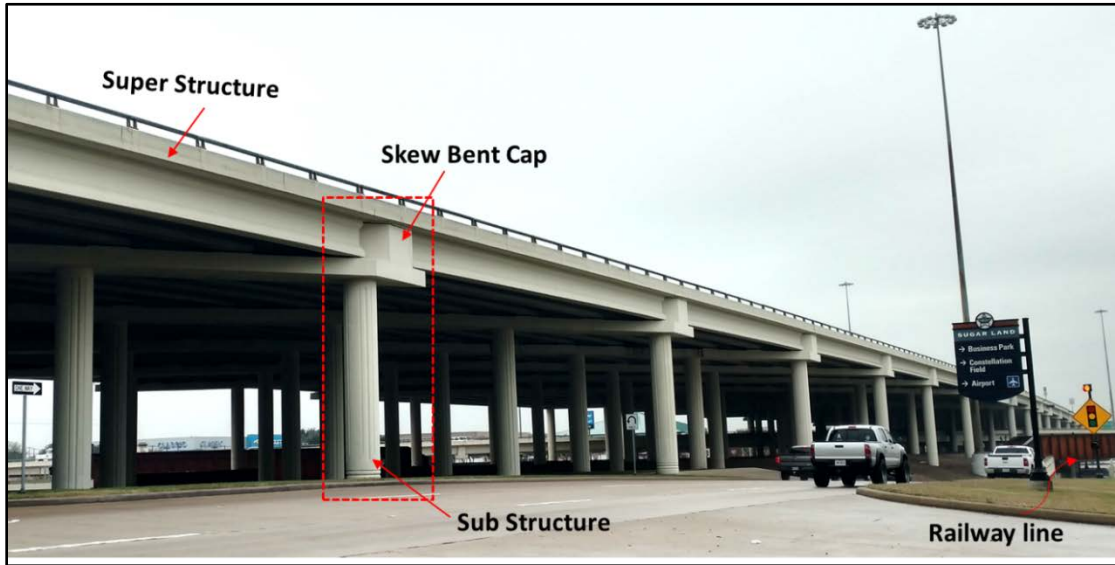


**Figure 2.1. Components of a Highway Bridge**

In keeping with the above advantages, inverted-T beams are extensively used in Texas as bridge bent caps. When the roadways, waterways, or railways are not perpendicular to the bridge at intersections, skew bridges are provided to safely carry traffic. Use of these skew “Inverted-T bent cap” bridge structures is common throughout Texas. The skew angle of many of these bridge structures is more than 45 degrees.

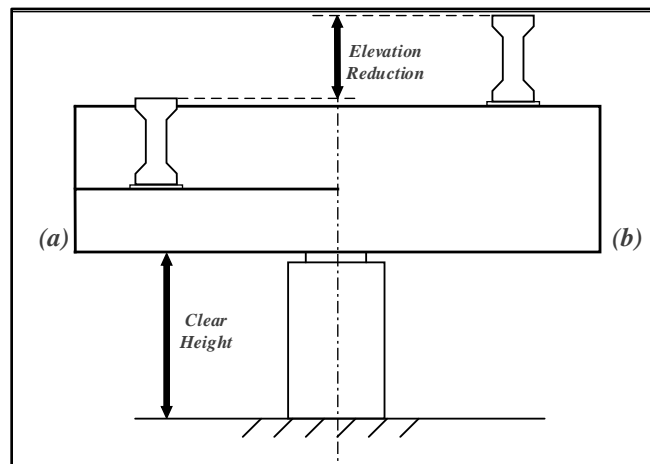


**Figure 2.2. Difference between Rectangular and Invreted-T Bent Cap  
(a) rectangular bent cap and (b) inverted-T bent cap**

### 2.3 COMPONENTS AND LOAD TRANSFER MECHANISM

As shown in Figure 2.3, the inverted-T bent cap is comprised of two main parts which include web and ledges. Load from the girders on the top face of the ledge of an inverted-T beam imposes vertical tensile forces (hanger tension) near the bottom of the web. The stem or web is designed with hanger reinforcement which plays an important role in transferring the concentrated loads applied at bearing pads to the stem and also sustains the shear forces generated in the inverted-T beam.

The ledges are provided at the bottom of the cap such that the loads are applied through them to the beam and the ledge reinforcement is provided to resist flexure, shear friction, and axial tension forces in the cantilevered ledge. Furthermore, the longitudinal and lateral bending of the ledge of an inverted-T bent cap produce a very complex stress distribution in the flange. The state of combined stress in an inverted-T beam cannot be obtained by simple stress cases. Hence, the design of reinforcement for the web and for the ledge of an inverted-T section imposes special problems (Mirza et.al 1985).

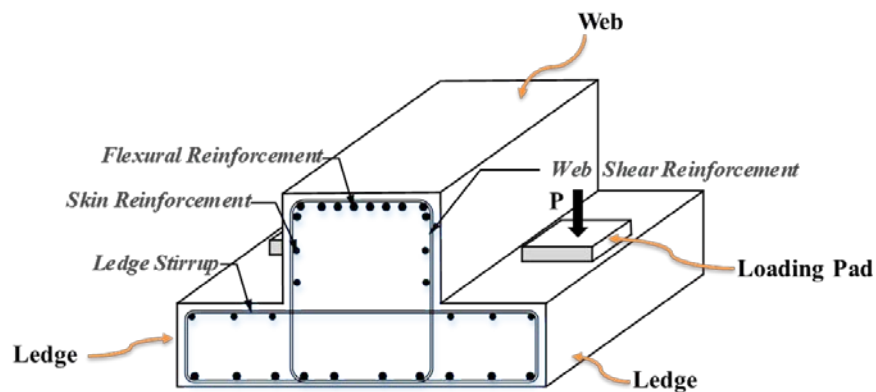
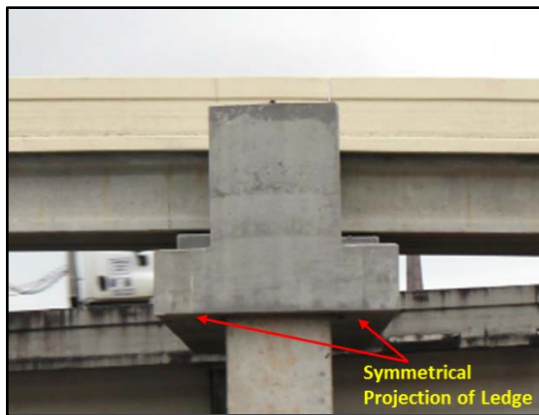


**Figure 2.3. Components of Inverted-T Bent Cap**

The inverted-T bent cap is encountered by torsion with every passage of live load across the bent cap. As the live load approaches the bent cap, girder reactions cause torsion of the bent cap towards the approaching load. The direction of twist reverses after the passage of live loads on girders that react on the opposite ledge overhang of the inverted-T beam. Hence, the passage of traffic tends to make the twist a reversing phenomenon. Moreover, in the case of the skewed inverted-T bent cap the effect of torsion is even very high due to unsymmetrical projection of the ledges and unsymmetrical locations of bearing pads on both sides of the web as shown in the Figure 2.4. This torsional effect increases with the increase in the skew angle.



(a) Skew angle 0 deg



(b) Skew angle ~ 45 deg

**Figure 2.4. Non-Skew and Skew ITBC**

For example, Figure 2.5 shows the deformation patterns at the end of the bridge cap at the service load, corresponding to two different values of the skew angle 0 degree and 45 degree. As can be seen from the figure, there are unsymmetrical deformations in both the ledges in case of 45-degree skew bent cap whereas the deformations are symmetric and equal for the case of zero-degree skew bent cap. Even though the same amount of load is applied to each of the loading pads, the unsymmetrical deformations in skew cases are caused by torsional moments generated by the unsymmetrical locations of bearing pads on the ledges of the bridge cap and because of the effect of torsional moment, the shear is additive in one leg and subtractive in other leg of the stirrups.

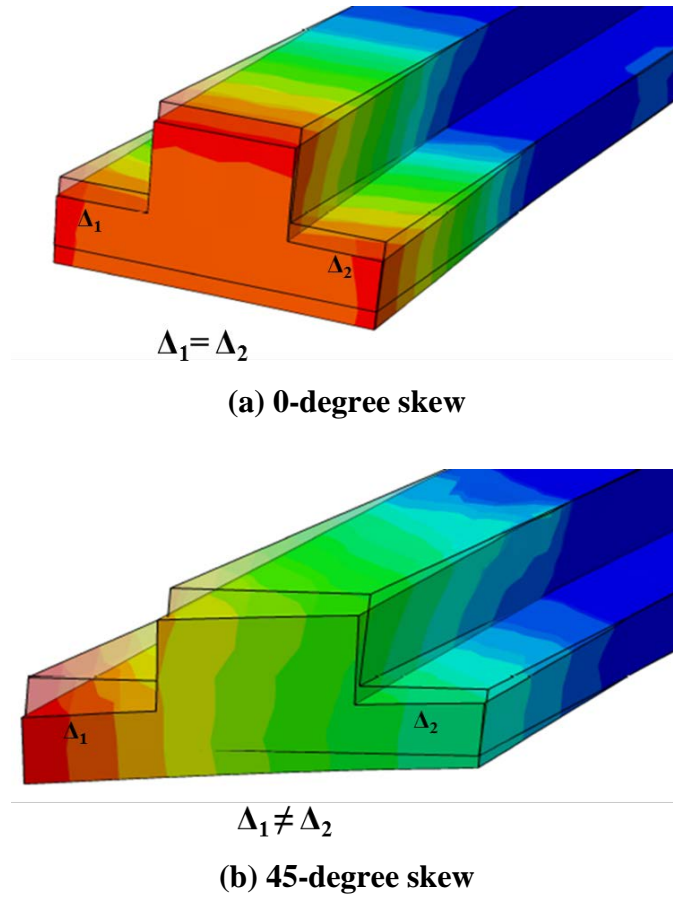


**Figure 2.5. Deformations Pattern of Skewed ITBCs**

#### **2.4 FAILURE MODES IN INVERTED-T BENT CAP**

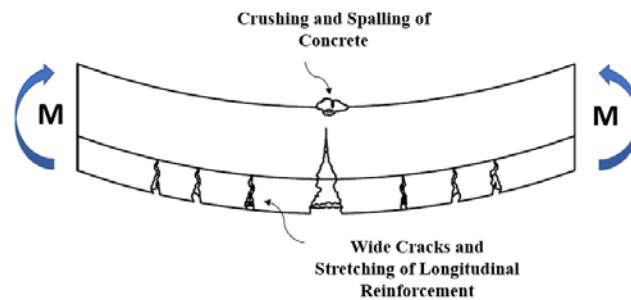
The strength of a reinforced concrete inverted-T bent cap is limited to the strength of the weakest components that participate in holding the applied loads. Mirza et al. (1983) defined six failure modes of the inverted-T bent cap based on their physical tests. The six modes of failure include flexure failure, shear failure, torsion failure, punching shear failure, shear friction failure, and hanger failure depending on the design parameters and loading conditions. The failure of hanger stirrups, the ledge failure due to punching shear and the failure due to loss of shear friction are considered as local failure modes of the inverted-T bridge cap, which are non-ductile in nature. The inverted-T bent cap can undergo failure in flexure, shear, torsion mode or any combination of the three failure modes only if the bent cap satisfies the local strength requirement for each of the hanger action of web stirrups, ledge punching shear and ledge shear friction. The similar failure modes are expected in the case of skew inverted-T bent caps. A brief description of each failure mode proposed by Mirza and Furlong (1983) are explained in the following section.

### 2.4.1 Flexure Failure Mode

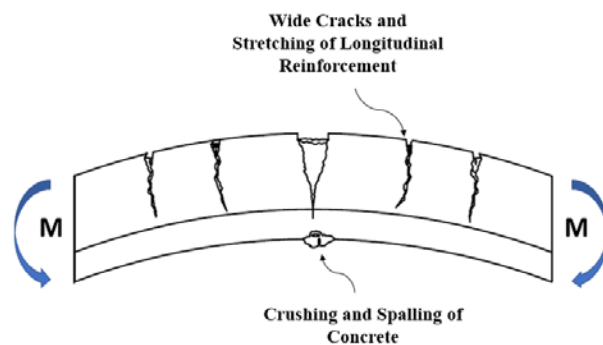
An inverted-T bent cap can be said to undergo the flexural failure when the resistance of the bent cap to flexural deformation starts to decrease. The flexure failure of the bent cap is characterized by the yielding and subsequent failing of longitudinal rebars at higher deformations. This is accompanied by cracking, crushing, and spalling of concrete at the surface of maximum compressive strain as shown in Figure 2.6. The specimen is said to be subjected to failure after the compressive resistance is exhausted with the spalling or flaking of concrete at the compression zone.

### 2.4.2 Shear Failure Mode

Inverted-T bent caps subjected to loading under an effective shear span-to-depth ratio ( $a/d$ ) will fail in shear when the stirrups at the critical region between the support and point of application of the load yield. Furthermore, the yielding of the stirrups occurs across a large crack which extends diagonally along the side faces of the web until the shear strength or compressive strength of uncracked concrete is exhausted as shown in Figure 2.7. This failure mode is considered to be under shear.



(a) Flexural Failure -Positive Moment



(b) Flexural Failure -Negative Moment

**Figure 2.6. Flexural Failure Modes in Inverted-T Bent Caps**

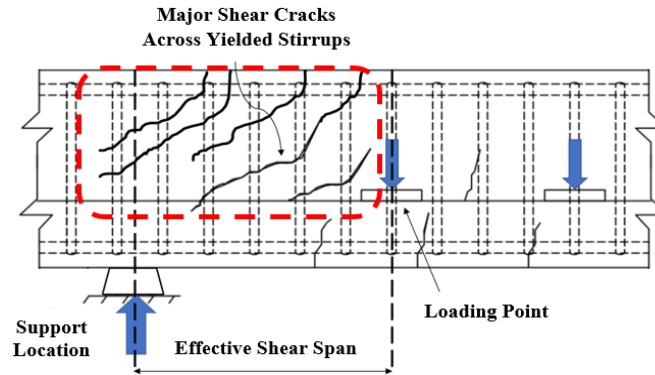


**Figure 2.7. Shear Failure Mode in Inverted-T Bent Cap**

### 2.4.3 Torsional Failure

Torsional distress in inverted-T bent caps appears in the form of diagonal tension cracks that extend in a spiral pattern from one face of the member to the adjacent face as shown in Figure 2.8. The diagonal cracks keep extending in length and in width with respect to the increase in the torsional forces until reinforcement across the crack yields. The member is considered to fail in torsion when the longitudinal and transverse reinforcements crossing the diagonal cracks yield.

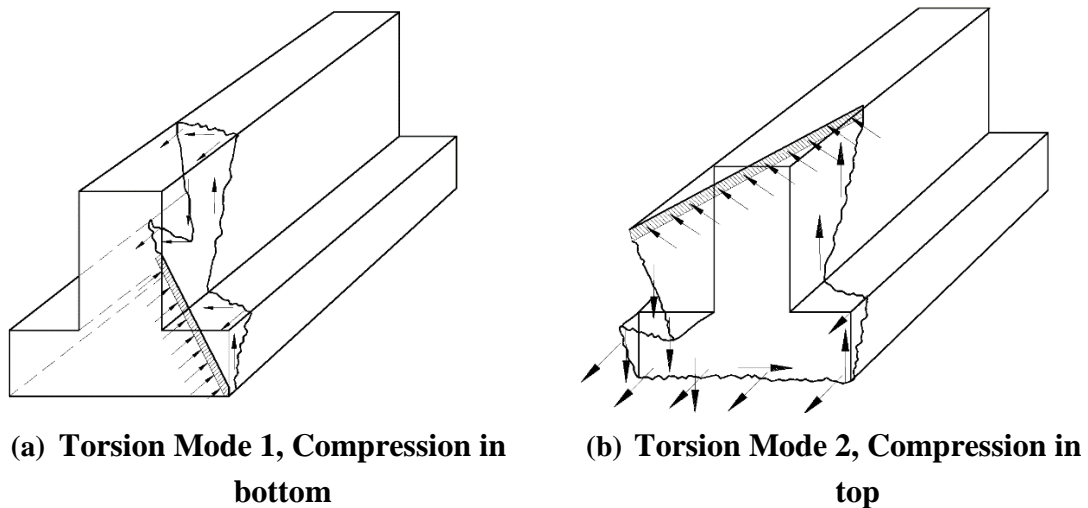


**Figure 2.8. Torsional Failure Mode in Inverted-T Bent Cap**

### 2.4.4 Failure of Hanger Stirrups

Failure of hanger stirrups initiates with the occurrence of vertical separation between the flange and the web at the top portion of the flange as shown in Figure 2.9. The separation arises as a local phenomenon near the location of girder's bearing plate, however, as the stirrups provided around bearing plate yield, the flange gradually deflects and causes more hangers to share the applied concentrated girder load. The failure happens

after all stirrups in the form of hangers undergo yielding. Thus, it is required to design the ledge adequately strong to distribute the girder loads longitudinally.

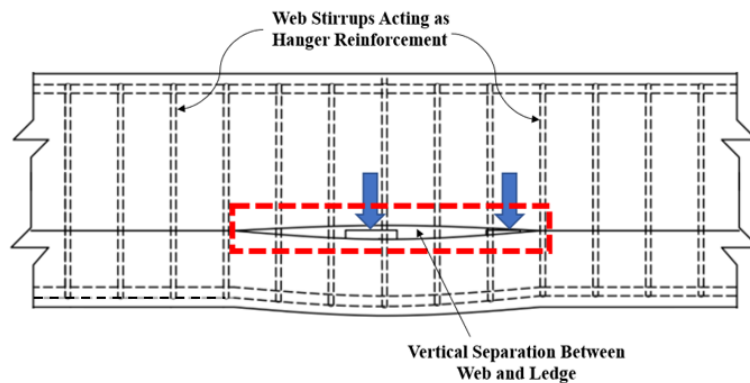


**Figure 2.9. Failure of Hanger Stirrups in Inverted-T Bent Cap**

#### 2.4.5 Ledge Failure due to Punching Shear

The failure of the ledge due to punching shear occurs when the forces resulting from the bridge girders that are very large in magnitude punch out the portion beneath a bearing pad in the form of a truncated pyramid of concrete. The failure is detected by the appearance of diagonal tension cracks ascending from the edge of the bearing plate. The explosive nature of punching shear failure is characterized by wide cracks followed by crushing and spalling of concrete since the ledge is subjected to failure due to downward movements as shown in Figure 2.10.

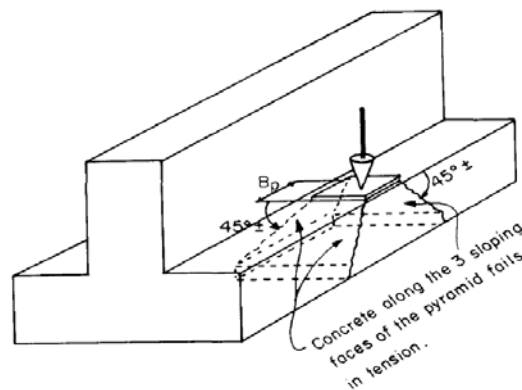


**Figure 2.10. Failure due to Punching Shear in Ledge of ITBC**

#### 2.4.6 Failure due to Shear Friction

The shear friction failure encountered at the interface of the web and ledge along the length of the web can be attributed to the local loss of resistance to the load because the ledge supporting girders tend to deform away from the web, and at the same time it has a

propensity to deflect downward due to the loss of shear strength along the face of the web. While the transverse bars acting in flexure placed at the top of the ledge experience yielding, the ledge resistance in shear friction along the face of the web turns out to be incapable of retaining the girder forces and may allow deformation of the ledge downward along the face of the web. Figure 2.11 shows the shear friction failure mode.

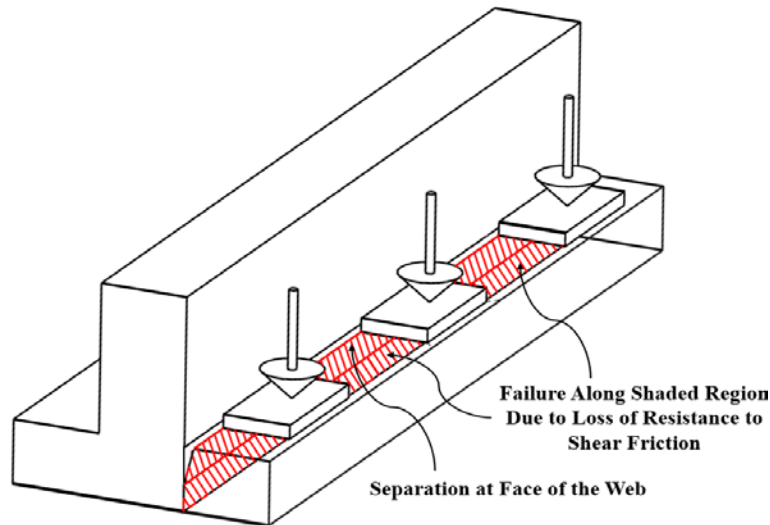


**Figure 2.11. Failure due to Shear Friction in Inverted-T Bent Cap**

## **2.5 DESIGN PROVISIONS FOR ITBC**

Inverted-T bent caps in the state of Texas are designed utilizing the conventional empirical procedures defined in the TxDOT Bridge Design Manual (TxDOT, 2015) which conform to the requirements in the AASHTO LRFD Bridge Design Specifications (AASHTO, 2014). According to the TxDOT Bridge Design Manual, the placement of hanger and ledge reinforcement should be perpendicular to the centerline of the skew bent. In addition, the detailing of the skew ends of the bent should be done with a section of skew stirrups and ledge reinforcement. It is also recommended that the distance from the exterior bearing pad to the end of the inverted-T bent cap should be at least 24 inches to prevent excessive hanger and ledge reinforcement provision and to satisfy the adequate punching shear capacity requirement. Further, it is suggested that extra vertical reinforcement be provided across the end surfaces of the ledge to resist cracking. In this section, the design provisions for various components of inverted-T bridge caps are summarized as per the AASHTO LRFD Bridge Design Specifications (2014) and TxDOT Bridge Design Manual–LRFD (2015):

### **2.5.1 Flexure Capacity**

The flexure theory for beam members has been widely accepted for many years, and it has only minor variations among the available design codes or guidelines. In this

section, the nominal flexural strength according to AASHTO LRFD (2014) can be calculated as follows.

$$M_n = A_s f_y \left( d - \frac{a}{2} \right) \quad (2.1)$$

$$a = c \beta_1 \quad (2.2)$$

$$c = \frac{A_s f_y}{0.85 f'_c \beta_1 b} \quad (2.3)$$

where

$M_n$  = nominal flexural resistance (kips.in.);  $A_s$  = area of longitudinal reinforcements (in<sup>2</sup>);  $f_y$  = yield strength of longitudinal reinforcements (ksi);  $d$  = effective depth of the inverted-T bent cap (in.);  $a$  = depth of equivalent stress block (in.);  $c$  = depth of cross section under compression under ultimate load (in.);  $f'_c$  = specified strength of concrete at 28 days in psi; and  $b$  = effective web/ledge width (in.)

## 2.5.2 Shear Capacity

The shear capacity can be calculated using the guidelines provided in the AASHTO LRFD (2014). The detailed equations for the calculation of shear capacity are presented below.

The nominal shear strength  $V_n$  of a concrete member described by AASHTO LRFD (2014) Eq. 5.8.3.3-1 can be evaluated using Eq. (2.4) as follows:

$V_n$  is lesser of:

$$(V_c + V_s + V_p) \text{ and } 0.25 f'_c b_v d_v + V_p \quad (2.4)$$

$$V_c = 0.0316 \beta \sqrt{f'_c} \text{ (ksi) } b_v d_v \quad (2.5)$$

$$V_s = \frac{A_v f_y d_v \cot \theta}{s} \quad (2.6)$$

The shear resistance of a concrete member in Eq. (2.4) is separated into the components,  $V_c$ , which relies on tensile and shear stresses in the concrete and component  $V_s$ , which relies on tensile stresses in the transverse reinforcement. The expression for  $V_c$  and  $V_s$  applies to both pre-stressed and non-pre-stressed sections.

### 2.5.2.1 Minimum Transverse Reinforcement

The minimum transverse reinforcement as per AASHTO LRFD 5.8.2.5-1 is given by:

$$A_{v\_min} = 0.0316 \sqrt{f'_c} \frac{S_{bar_s} b_v}{f_y} \quad (2.7)$$

where

$V_n$  = nominal shear strength;  $V_c$  = contribution of shear strength of concrete;  $V_s$  = contribution of shear strength of shear reinforcements;  $f'_c$  = specified strength of concrete at 28 days in psi;  $b_v$  = effective web width (in.);  $d_v$  = effective shear depth (in.);  $\hat{a}$  = factor indicating ability of diagonally cracked concrete to transmit tension and shear;  $A_v$  = area of shear reinforcement within a distance  $S$  (in.<sup>2</sup>);  $f_y$  = yield strength of shear reinforcements;  $\theta$  = angle of inclination of diagonal compressive stresses (degrees); and  $S$  = spacing of transverse reinforcement (in.)

### 2.5.3 Hanger Capacity of the Transverse Reinforcement

Generally, the design strength of transverse reinforcements in the inverted-T bent cap is controlled by its hanger capacity. Hanger capacity should be large enough to transfer the ultimate load from the ledge into the web to prevent the local failure. As per the AASHTO LRFD 5.13.2.5.5 guidelines, the hanger capacity of the transverse reinforcements will be calculated using the equations as follows:

#### Interior Girder

$V_n$  is a minimum of :

$$\left\{ \frac{A_{hr}f_y}{S_{bar_s}} (S) \right. \quad (2.8)$$

$$0.063\sqrt{f'_c}b_f d_f + \frac{A_{hr}f_y}{S_{bar_s}} (W + 2d_f) \quad (2.9)$$

#### Exterior Girder

$V_n$  is a minimum of :

$$V_n \text{ for the interior girder} \quad (2.10)$$

$$\frac{A_{hr}f_y}{s_{bars}} \left( \frac{S}{2} + c \right) \quad (2.11)$$

$$0.063\sqrt{f'_c}b_f d_f + \frac{A_{hr}f_y}{S_{bars}} \left( \frac{W+2d_f}{2} + c \right) \quad (2.12)$$

where

$V_n$  = nominal hanger capacity;  $A_{hr}$  = area of one leg of hanger reinforcement as illustrated in Figure 2.12 (a) (in.<sup>2</sup>);  $S$  = spacing of bearing places (in.);  $S_{bars}$  = spacing of hanger bars (in.);  $d_f$  = distance from the top of ledge to compression reinforcement as illustrated in Figure 2.12 (b) (in.); and  $b_f$  = full width of the flange as shown in Figure 2.12(b) (in.)

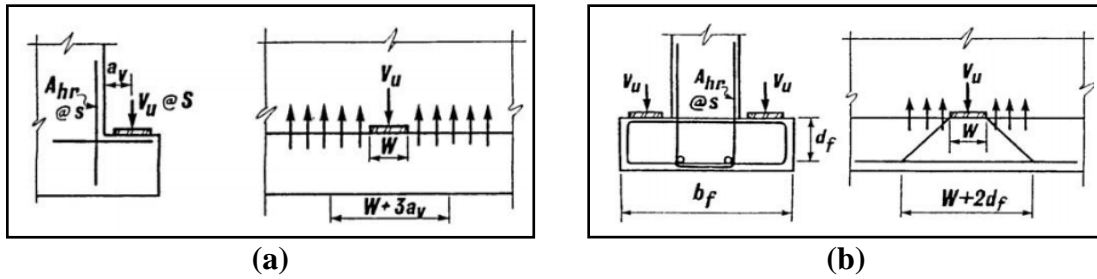


**Figure 2.12. Shear Friction Consideration:**  
**(a) Single-Ledge Hanger Reinforcement and (b) Inverted T-Beam Hanger Reinforcement (AASHTO LRFD, 2014)**

### 2.5.4 Torsional Capacity of the Section

According to the ACI 318-11 Section 11.5.3.6, which conforms to the AASHTO LRFD (2014) Section 5.8.3.6.2-1, the nominal torsional moment strength in terms of stirrup yield strength is:

$$T_n = \frac{2A_o A_t f_{yt}}{s} \cot \theta \quad (2.13)$$

where

$A_o = 0.85A_{oh}$ ;  $\theta$  shall not be taken smaller than 30 degrees nor larger than 60 degrees;  $A_{oh}$  = the area enclosed by the centerline of the outermost closed transverse torsional reinforcement having a yield strength of  $f_{yt}$ ; and  $A_t$  = the amount of transverse reinforcement. It is evident from Eq. (2.13) that nominal torsional moment strength increases if the area enclosed by the centerline of the outermost closed transverse torsional reinforcement is increased.

By providing skew transverse reinforcement in skew inverted-T bridge caps as a replacement for normal reinforcement, the area enclosed by the centerline of the outermost closed hoop torsional reinforcement is increased. Thus, skew transverse reinforcing has the potential to reduce the effects of torsion coming onto the skew inverted-T bridge caps. However, there has not been adequate research to back this theory. Thorough experimental and analytical research is needed to verify the possible effects of using skew reinforcement over normal reinforcement.

### 2.5.5 Punching Shear Capacity of the Ledge

Punching shear is a two-way action that usually is very brittle, sudden, and it occurs locally. Thus, punching shear always plays a very significant role while designing the inverted-T bent cap. The mechanism for punching shear failure in the ledge can form when girder reactions exceed the tensile strength of concrete along the surface of the truncated pyramid. The ledge should be deep enough to prevent punching shear failure. The stirrups that intersect the face of the truncated pyramid can help support the concentrated load if

anchorage of the stirrups can be developed above and below the face of the truncated pyramid. However, no such help from the stirrups is included in the punching shear equation because this would require cumbersome checks on the design and detailing of the stirrups.

In this section, the punching shear strength shall be evaluated using the equations given in AASHTO LRFD (2014) and TxDOT BDM-LRFD (2015).

#### 2.5.5.1 AASHTO LRFD, 2014

The following equations give the punching shear capacity of the inverted-T beam ledge according to AASHTO LRFD 5.13.2.5.4 (Eq. (2.14) through Eq. (2.16)).

For all interior pads, or exterior pads where the end distance  $C$  is greater than  $S/2$ , the nominal punching shear capacity is given by:

$$V_n = 0.125 \sqrt{f'_c} (W + 2L + 2 d_e) d_e \quad (2.14)$$

For all exterior pads where the end distance  $C$  is less than  $S/2$  and  $C-0.5W$  is less than  $d_e$ , the punching shear capacity is calculated as:

$$V_n = 0.125 \sqrt{f'_c} (W + L + d_e) d_e \quad (2.15)$$

For all exterior pads where the end distance  $C$  is less than  $S/2$  and  $C - 0.5W$  is greater than  $d_e$ , the punching shear capacity is calculated as:

$$V_n = 0.125 \sqrt{f'_c} (0.5W + L + d_e + c) d_e \quad (2.16)$$

where

$V_n$  = nominal punching shear strength;  $f'_c$  = specified strength of concrete at 28 days in ksi;  $W$  = width of bearing pad (in.);  $L$  = length of bearing pad (in.);  $d_e$  = effective depth from extreme compression fiber to the centroid of the tensile force (in.); and  $c$  is the distance from the ledge end to the center of the exterior load (in.). These equations require that the truncated pyramids of adjacent loads do not overlap. In cases where overlapping occurs the AASHTO Code requires an investigation of the combined surface areas to be conducted.

#### 2.5.5.2 TxDOT Bridge Design Manual – LRFD, 2015

The TxDOT Bridge Design Manual, 2015 recommends  $d_e$  be replaced by  $d_f$  in all the equations suggested by AASHTO LRFD, where  $d_f$  = the effective distance between the positive bending reinforcements to the top of the ledge. As per the TxDOT Bridge Design Manual, for all interior girders, the nominal punching shear capacity is given as follows [Eq. (2.17) through Eq. (2.19)]:

$$V_n = 0.125 \sqrt{f'_c} (W + 2L + 2 d_f) d_f \quad (2.17)$$

For all exterior girders, the punching shear capacity is calculated as the minimum of:

$$V_n = 0.125 \sqrt{f'_c} (W + L + 2 d_f) d_f \quad , \text{ and (2.18)}$$

$$V_n = 0.125 \sqrt{f'_c} (0.5W + L + d_f + c) d_f \quad (2.19)$$

### 2.5.6 Shear Friction Capacity of the Ledge

The ledge of an inverted-T bent cap acts as a cantilever beam, continuous longitudinally along the web. The web provides the support for the ledge as a fixed edge. Shear friction failure may occur due to slippage or shearing off the ledge along the face of the web as a result of shear friction loss. The flexural steel normal to the shearing face must be adequate in order to develop a normal force large enough to maintain the frictional shear. As per AASHTO LRFD 5.13.2.5.2, the effective ledge length resisting shear friction shall not exceed  $S$ ,  $W + 4a_v$  or  $2c$ . Where  $S$  is the spacing of girders (in.),  $W$  is the width of the bearing pad (in.),  $a_v$  is the distance from the face of the web to load (in.), and  $c$  is the distance from the ledge end to the center of the exterior load (in.) as shown in Figure 2.13.

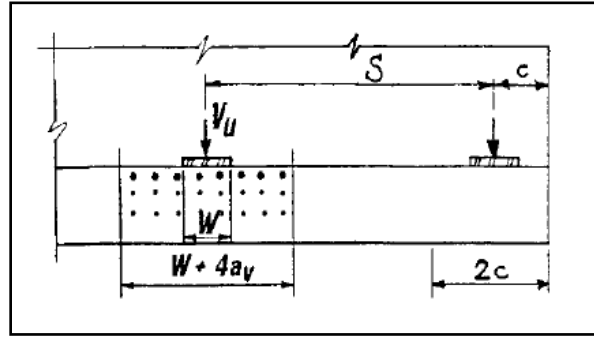


Figure 2.13. Shear Friction for Ledge (AASHTO LRFD, 2014)

The shear friction capacity of the ledge where the shear-friction reinforcement is perpendicular to the shear plane is given by the equation specified in ACI 318-14 Code Section 11.6.4, which conforms to the AASHTO LRFD (2014) as follows:

$$V_n = C_1 A_{cv} + \mu (A_{vf} f_y + P_c) \quad (2.20)$$

The minimum shear friction reinforcement as per AASHTO LRFD 5.8.4.4-1 is given by:

$$A_{vf\_min} = \frac{(0.05 \text{ ksi}) \cdot A_{cv}}{f_y} \quad (2.21)$$

$$A_{cv} = d_e \cdot b_s \quad (2.22)$$

where

$V_n$  = nominal shear resistance of the interface plane (kips);  $c_1$  = cohesion factor ( $c_1 = 0$  for corbel and ledges);  $A_{cv}$  = area of concrete considered to be engaged in interface shear transfer ( $\text{in.}^2$ ), interior beams: minimum of  $(W + 4a_v, S)$  times  $d_e$ , exterior beams: minimum of  $(W + 4a_v, S, 2c)$  times  $d_e$ ;  $d_e$  = depth of ledge from bottom surface to center of gravity of top tension steel (in.);  $\mu$  = the appropriate value of the coefficient of friction as given in

ACI Code Section 11.6.4.3 = 1.4 for normal weight concrete placed monolithically;  $A_{vf}$  = Area of shear friction steel (in.<sup>2</sup>); and  $P_c$  = permanent net compressive force normal to the shear plane (kips).

The provisions neglect any cohesion in the concrete area and consider only the friction shear strength provided by the prestressed and mild reinforcement at the ledge web interface. The width of the interface area is considered equal to the width of the loading plate plus four times the distance from the face of the web to the center of the load ( $a_v$ ).

### 2.5.7 Bearing Capacity of the Ledge

The load on the bearing pad propagates along a truncated pyramid whose top has the area  $A_1$  and whose base has the area  $A_2$  as shown in Figure 2.14.  $A_1$  is the loaded area (the bearing pad area:  $L \times W$ ).  $A_2$  is the area of the lowest rectangle contained wholly within the support (the inverted-T bridge cap).  $A_2$  must not overlap the truncated pyramid of another load in either direction, nor can it extend beyond the edges of the cap in any direction. Bearing resistance of the ledges based on AASHTO LRFD Eq. 5.7.5-2 shall be taken as:

$$V_n = 0.85 \times f'_c \times A_1 \times m \quad (2.23)$$

where

$V_n$  = nominal bearing resistance (kip);  $A_1$  = area under bearing device (in.<sup>2</sup>);  $A_2$  = a notational area defined as shown in Figure 2.14, (in.<sup>2</sup>)

$$m = \text{modification factor} = \sqrt{\frac{A_2}{A_1}} \leq 2.0 \quad (2.24)$$

$$A_1 = W \times L \quad (2.25)$$

$$A_2 = W_2 \times L_2 \quad (2.26)$$

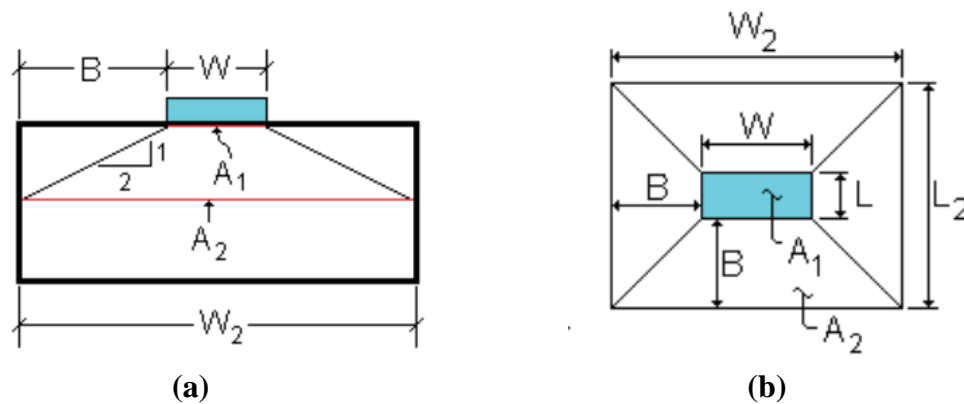


**Figure 2.14. Bearing Consideration:**  
**(a) Elevation view of bearing area and (b) Plan view of bearing area**

### 2.5.8 Diagonal Cracking Between Ledge and Web (Zu et al., 2003)

Inverted-T bent caps used across the state of Texas add to pleasant aesthetics and increase the vertical clearance but are susceptible to diagonal cracking which frequently occurs between the cantilever ledge and the web at the service load condition as shown in Figure 2.15. Such cracks impart the appearance of structural distress, and further expansion of crack width can lead to the corrosion of reinforcement and the shortening of the service life of bridges. To address these concerns, TxDOT funded research project 0-1854 under the title of “Crack control for ledges in inverted-T bent caps,” Report No. 0-1854-5 (Zhu et al. 2003), with the objective of obtaining a better understanding of the crack control criteria for ledges in inverted-T bent caps.

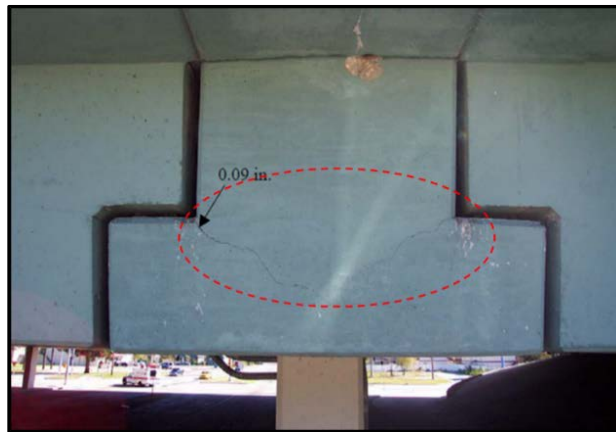


**Figure 2.15. Crack at West End Face of Southwest Inverted-T Bent**

From the experimental work performed by the research team, following observations were made:

1. The hanger spacing had no apparent influence on the distribution of hanger bar strains along the span and consequently, no effect was observed on the effective distribution width of hanger bars.
2. At the interior spans of the inverted-T bent cap, the provision of diagonal bars proved to be an effective way to control the crack width.
3. An addition of diagonal bars at the end faces of cantilever spans was not as helpful as in the interior spans. The most effectual variable discovered to control the crack width was the distance from the end face to the most exterior load.
4. It was observed that limiting the service load to a “critical load” where crack widths begin to widen rapidly, can contribute to controlling the diagonal crack width at the end faces.

Thus, based on the research work, it was concluded that the most reliable and effective means of minimizing the diagonal crack width at the end faces is to increase the

distance from the end face to the most exterior load. An addition of diagonal bars will not be an appropriate alternative to control the crack width.

## **2.6 CONCLUSION**

The AASHTO LRFD Bridge Design Specifications and TxDOT Bridge Design Manual are discussed. Local and global failure modes are briefly described. The inverted-T specimens are designed with the formula described in this section keeping an view in the yielding of transverse stirrups. The specimens are designed in a such a way that the shear stirrups should yield bfore it should fail in other failure modes.

## **CHAPTER 3: EXPERIMENTAL PROGRAM**

### **3.1 OVERVIEW**

This chapter provides an insight into the design, fabrication, and construction of inverted-T bridge caps as well as the structural testing procedure adopted for test specimens under the research work. The material properties such as the compressive strength of concrete and yield strength of steel rebars are also presented in this chapter. Based on the scope of the research, 13 specimens of the inverted-T bent cap are designed and fabricated taking into consideration the predetermined test variables which include skew angle, the detailing of transverse reinforcement, and the amount of transverse reinforcements. The experimental program was designed to evaluate the effect of the test variables on the performance of skew transverse reinforcement in the inverted-T bent caps. This chapter explains the test set-up and instrumentation installed for the half-scaled specimens and loading protocol followed for testing specimens.

### **3.2 TESTING PROGRAM**

An extensive testing program is proposed to achieve the objectives of the research project. The experimental program is comprised of 13 ITBC test specimens designed by considering the following test variables to investigate their effect on the structural performance of inverted-T bridge caps.

#### **3.2.1 Skew Angle**

Inverted-T bent caps with skew angles of 0, 30, 45 and 60 degrees are considered under the scope of the work.

#### **3.2.2 Detailing of Transverse Reinforcement**

Two types of transverse reinforcement detailing are taken into consideration which include traditional reinforcement as used by TxDOT and skewed reinforcement as proposed under the research scope. In case of specimens designed in accordance with TxDOT provisions, the spacing between transverse reinforcement is not uniform whereas for skew reinforcement, the spacing is constant throughout the length of the specimen.

#### **3.2.3 Amount of Transverse Reinforcement**

The amount of transverse reinforcement considered is equivalent to twice the minimum reinforcement (2M) and the minimum transverse reinforcement (M) as specified in the AASHTO LRFD (2014). The entire test plan has been divided into two phases based on the amount of reinforcement in which the inverted-T bent cap specimens in the “Phase-1” are provided with the 2M amount of transverse reinforcement, and “Phase-2” specimens are provided with the M amount of transverse reinforcement.

Table 3.1 demonstrates the test matrix which includes nomenclature for test specimens and variables considered in the experimental program.

### 3.3 DESIGN OF ITBC SPECIMENS

From the point of view of design and analysis, an inverted-T bridge cap essentially behaves like an inverted-T beam. The capacity of a reinforced concrete inverted-T beam is limited to the strength of the weakest components that participate in transferring the applied loads. The various components of the inverted-T bridge cap with the most typical design terminology are shown in Figure 3.1.

The present study primarily focuses on the shear and torsion behavior of normal and skew transverse reinforcing in inverted-T bridge caps for four different skew angles ( $0^{\circ}$ ,  $30^{\circ}$ ,  $45^{\circ}$ , and  $60^{\circ}$ ). Accordingly, during the design stage of the test specimens, it is ensured that the flexure and all other local failure modes must be prevented before the yielding capacity of the transverse stirrups is reached. In other words, the flexure capacity, hanger capacity of transverse stirrups, punching shear capacity, and shear friction capacity of the ledge should be large enough, so that the shear and torsional capacities of the transverse stirrups can be achieved in the test. This is necessary in order to capture, evaluate and compare the performance of normal and skew reinforcing in skew inverted-T bridge caps.

The flexure capacity, shear capacity, hanger capacity, punching shear capacity, and shear friction capacity of zero-degree skew inverted-T bridge caps, which is defined as the control specimen in this research, are calculated based on various code provisions described in the earlier chapter. The smallest strength obtained from these calculations was considered as the governing failure mode.

**Table 3.1. Test Matrix of ITBC Specimens**

No.	Specimen I.D.	Skew Angle				Detailing of Transverse Steel		Amount of Transverse Steel	
		$0^{\circ}$	$30^{\circ}$	$45^{\circ}$	$60^{\circ}$	Traditional (T)	Skew (S)	2M	M
1	ITBC-0-T-2M	X				X		X	
2	ITBC-30-T-2M		X			X		X	
3	ITBC-30-T-M		X			X			X
4	ITBC-30-S-2M		X				X	X	
5	ITBC-30-S-M		X				X		X
6	ITBC-45-T-2M			X		X		X	

No.	Specimen I.D.	Skew Angle				Detailing of Transverse Steel		Amount of Transverse Steel	
		0°	30°	45°	60°	Traditional (T)	Skew (S)	2M	M
7	ITBC-45-T-M			X		X			X
8	ITBC-45-S-2M			X			X	X	
9	ITBC-45-S-M			X			X		X
10	ITBC-60-T-2M				X	X		X	
11	ITBC-60-T-M				X	X			X
12	ITBC-60-S-2M				X		X	X	
13	ITBC-60-S-M				X		X		X

**Nomenclature:**

ITBC: Inverted-T Bridge Cap

Skew Angle: 0°/30°/45°/60°

Detailing of Transverse Reinforcement: Traditional (T) and Skew (S)

Amount of Transverse Reinforcement: 2\* Minimum AASHTO (2M) and Minimum AASHTO (M)

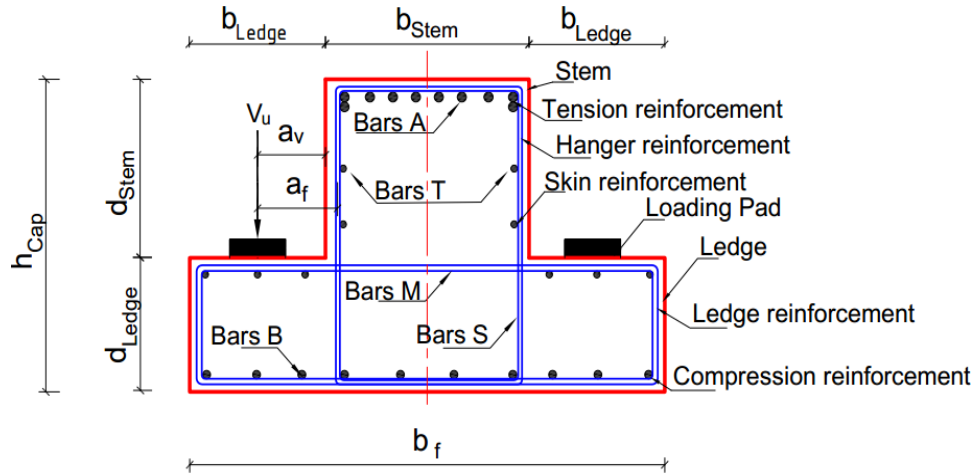


**Figure 3.1. Main Components of Inverted-T Bridge Cap**

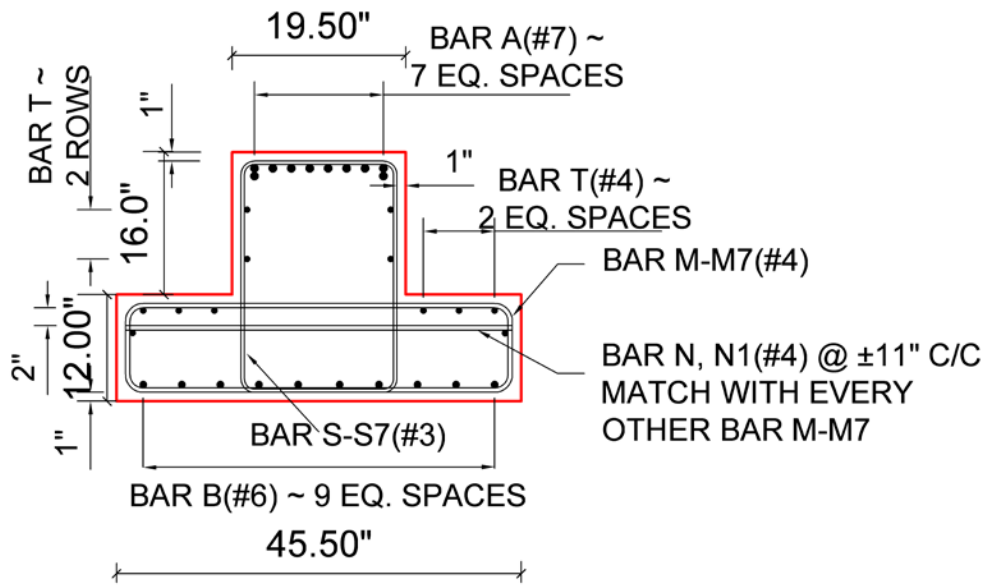
**Terminology:**

**$b_{Ledge}$  = Width of the ledge,  $b_{Stem}$  = Width of the stem,  $d_{Ledge}$  = Depth of the ledge,  $d_{Stem}$  = Depth of the stem,  $h_{cap}$  = Total height of the cap,  $b_f$  = Total width of the flange,  $a_v$  = The distance from the face of the stem to the center of the loading pad and  $a_f$  = The distance from the central line of hanger reinforcement to the center of the loading pad**

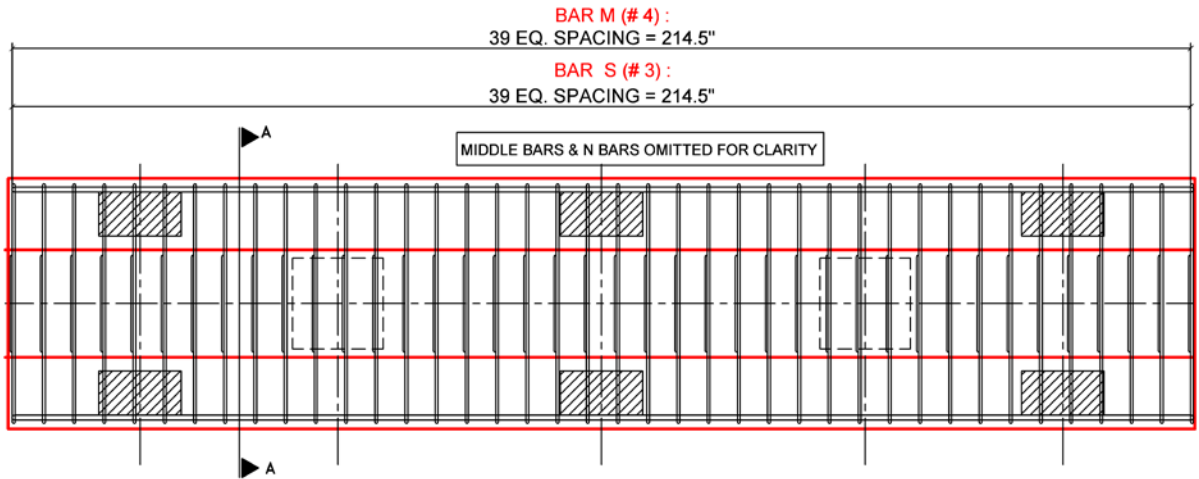
The total length of the inverted-T bridge cap specimen considered for this study is 18 feet. The height of each of both the ledge and stem is 12 inches and 16 inches, respectively, whereas the width of each of both the ledge and stem is 45.5 inches and 19.5 inches, respectively.

**3.3.1 Phase 1 Specimens**

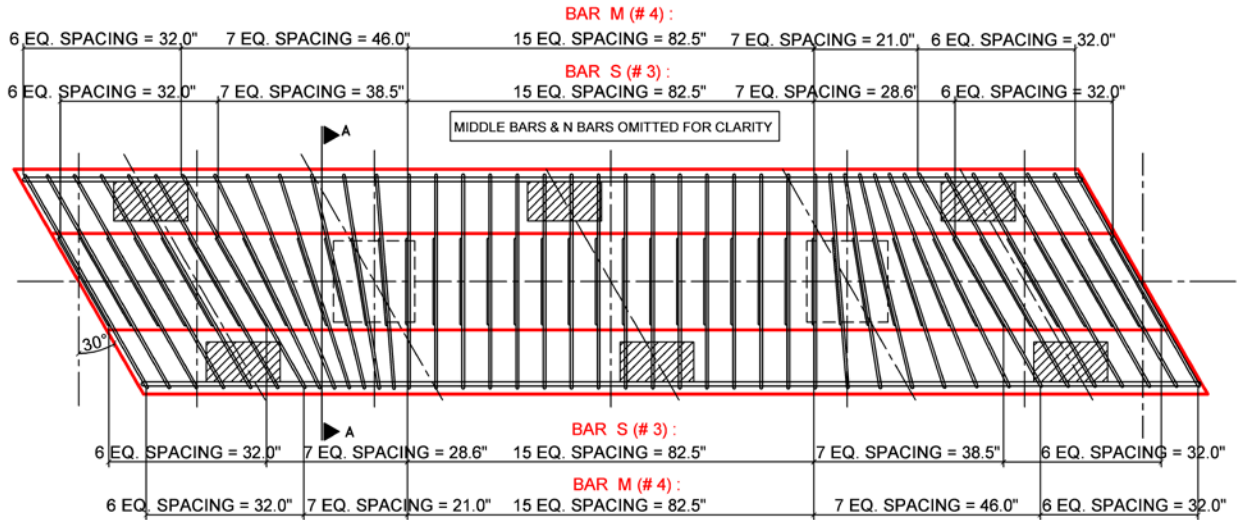
Phase 1 specimens, which include ITBC-0-T-2M, ITBC-30-T-2M, ITBC-30-S-2M, ITBC-45-T-2M, ITBC-45-S-2M, ITBC-60-T-2M, and ITBC-60-S-2M, have a 2M amount of transverse reinforcement in all the specimens. These specimens do not have the vertical reinforcements at the end faces. Figures 3.2(a)–3.2(h) show the cross-sectional view of reinforcement details and the plan view of the reinforcement details of all the inverted-T bridge cap specimens for Phase 1 of the test plan.



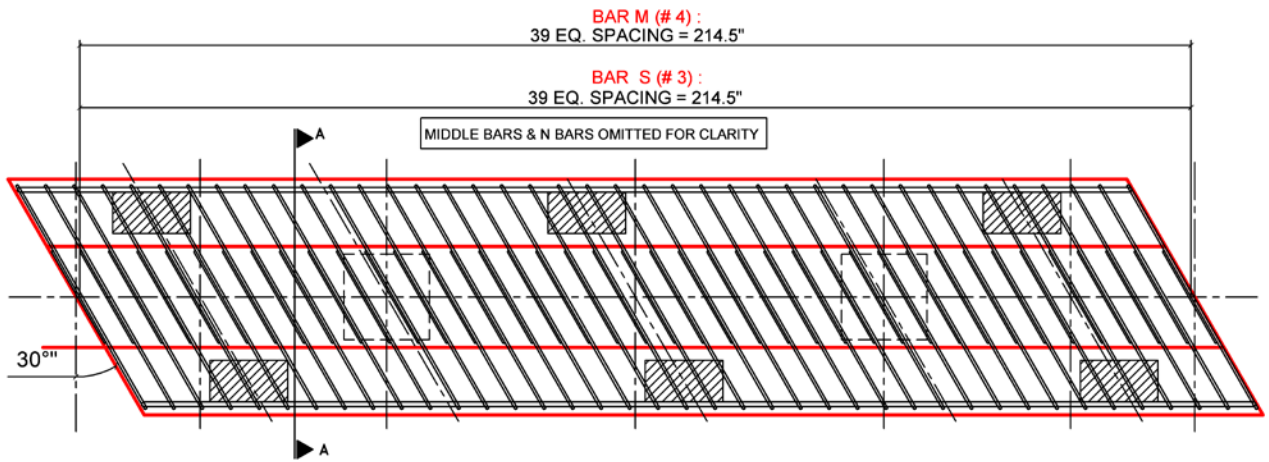
(a)



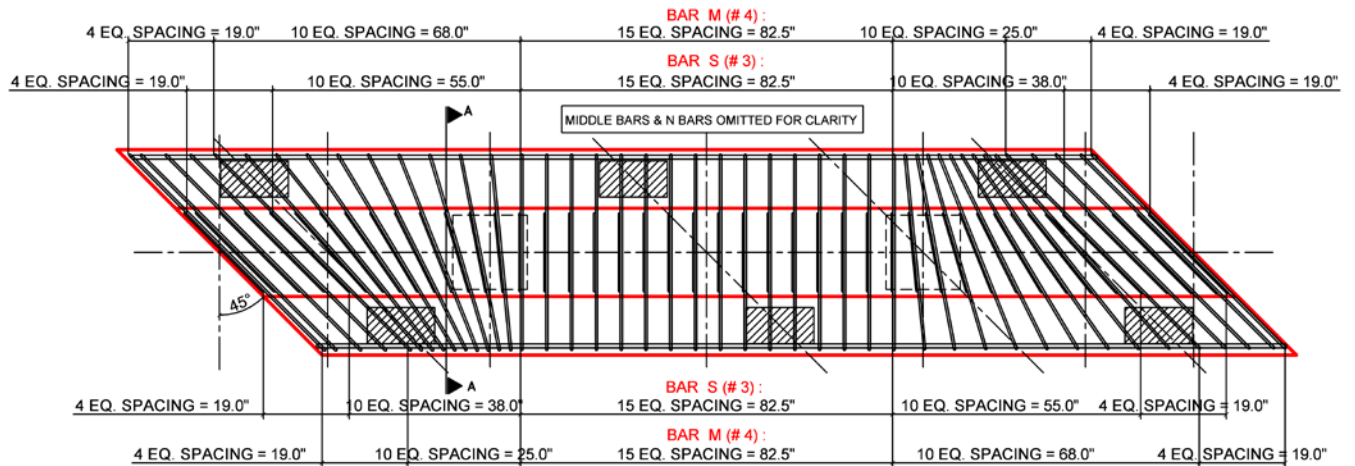
(b)



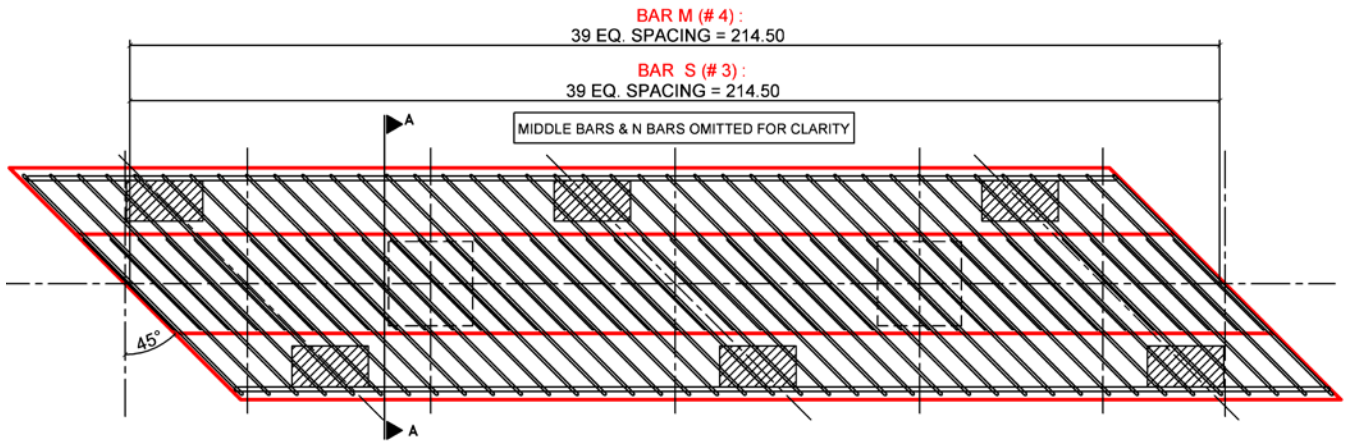
(c)



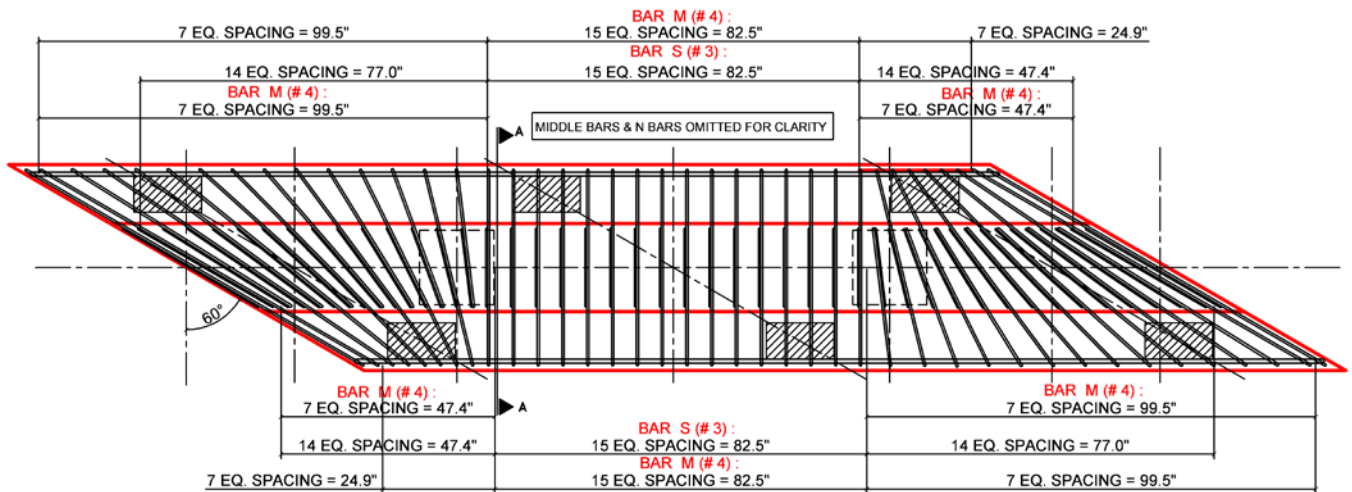
(d)



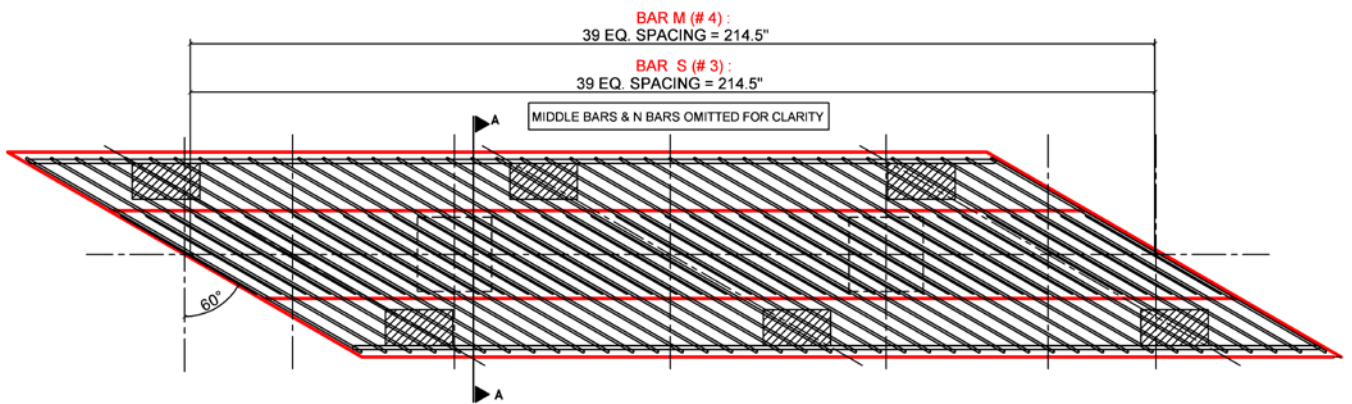
(e)



(f)



(g)



(h)

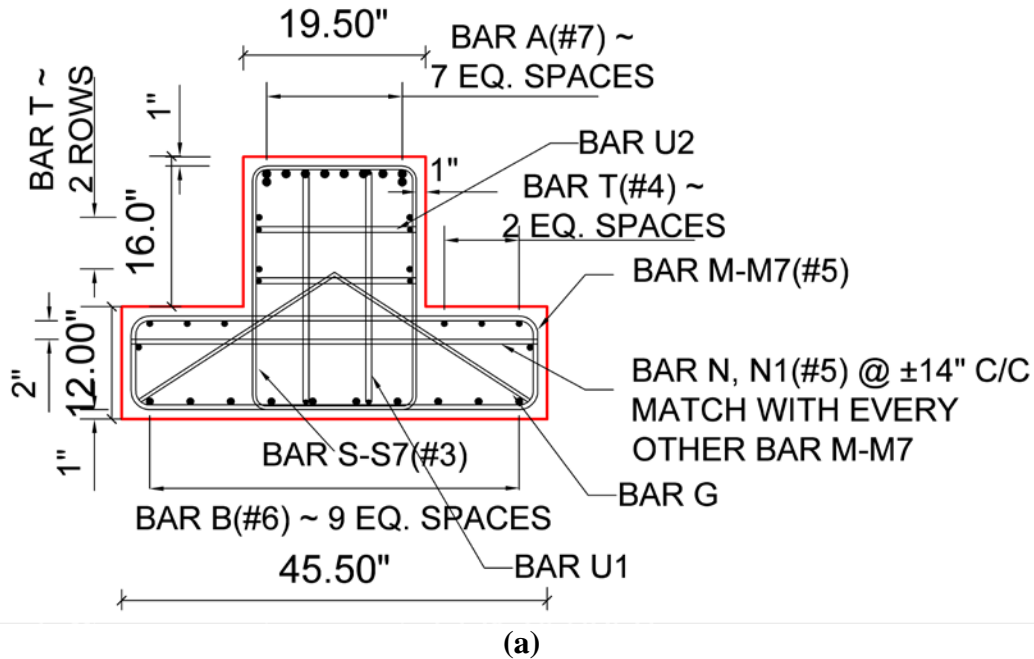
Figure 3.2. Reinforcing details of Phase 1 ITBCs:

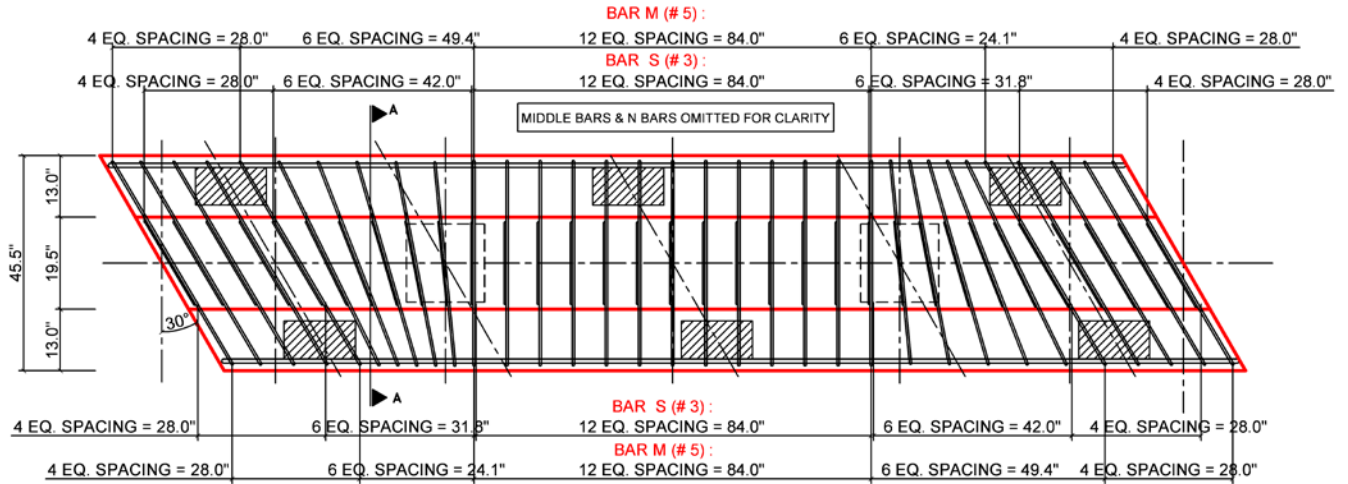
- (a) Typical reinforcing details at Section AA and (b) Plan view reinforcing details (c) Plan view reinforcing details of ITBC-30-T-2M, (d) Plan view reinforcing details of ITBC-30-S-2M, (e) Plan view reinforcing details of ITBC-45-T-2M, (f) Plan view

**reinforcing details of ITBC-45-S-2M, (g) Plan view reinforcing details of ITBC-60-T-2M and (g) Plan view reinforcing details of ITBC-60-S-2M**

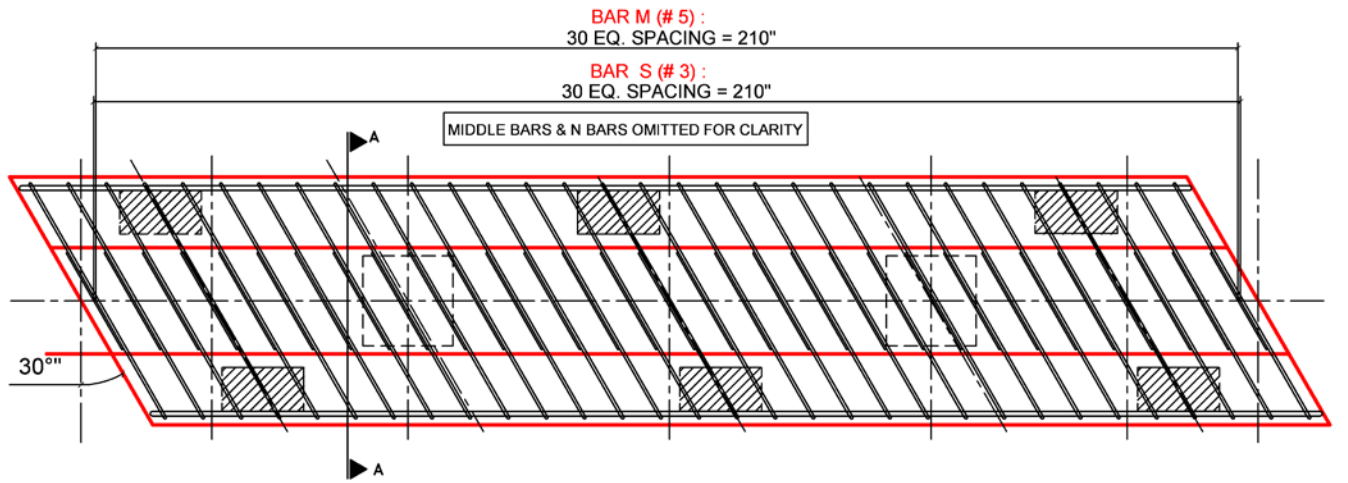
**3.3.2 Phase 2 Specimens**

Phase 2 specimens, which include ITBC-30-T-M, ITBC-30-S-M, ITBC-45-T-M, ITBC-45-S-M, ITBC-60-T-M, and ITBC-60-S-M, have M amount of transverse reinforcement in all the specimens. In addition, in all the Phase 2 specimens, end face reinforcements (U1 and U2 bars) and the G bars are provided in both ends of the inverted-T bridge cap to control the formation of cracks. Figures 3.3(a)–3.3(g) show the plan view of the reinforcement details of all the inverted-T bridge cap specimens for Phase 2 of the test plan.

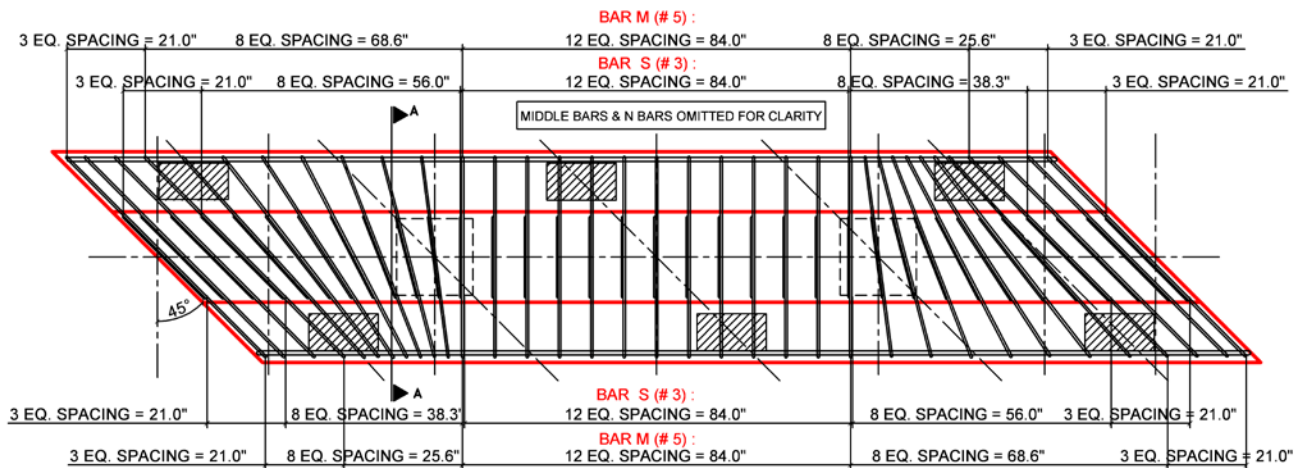




(b)



(c)



(d)

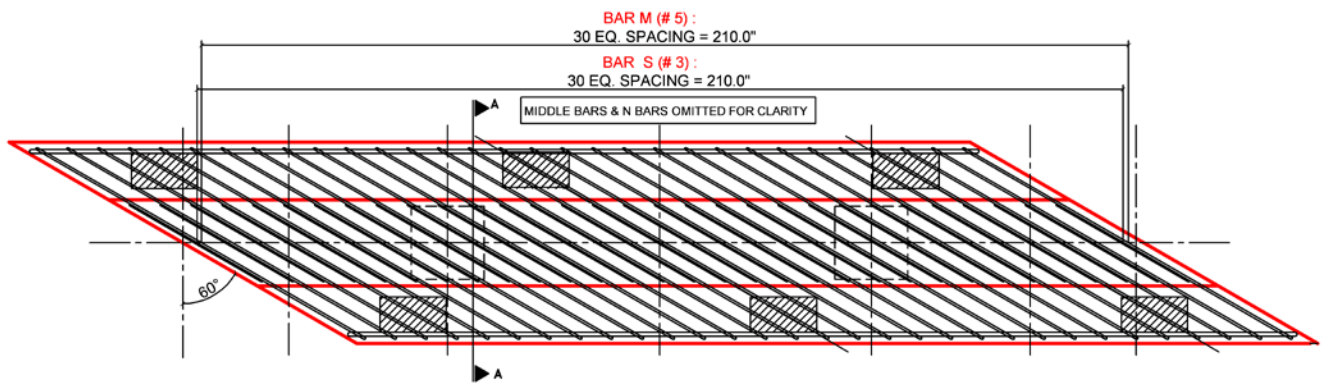
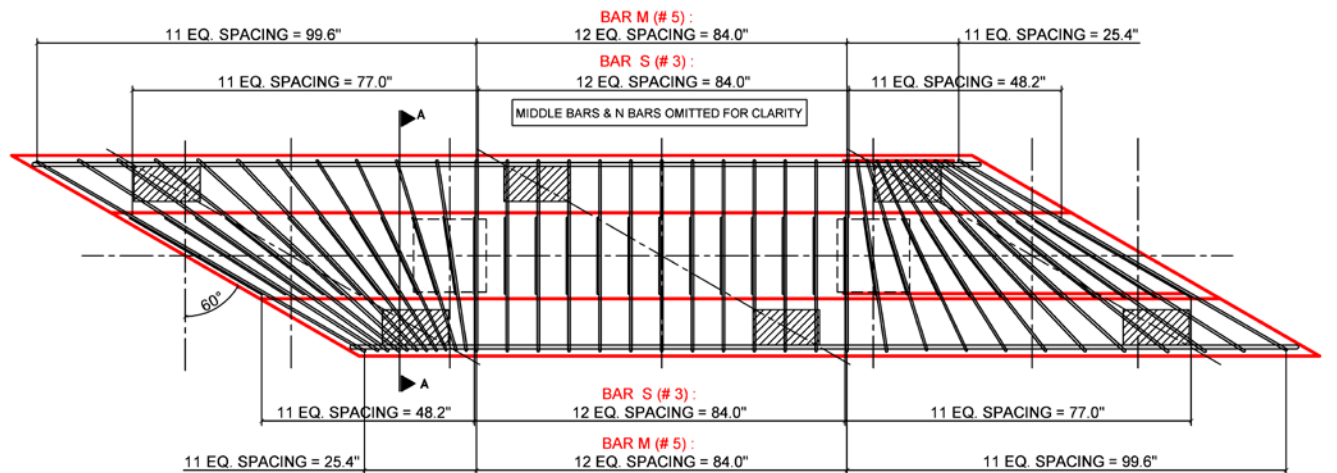
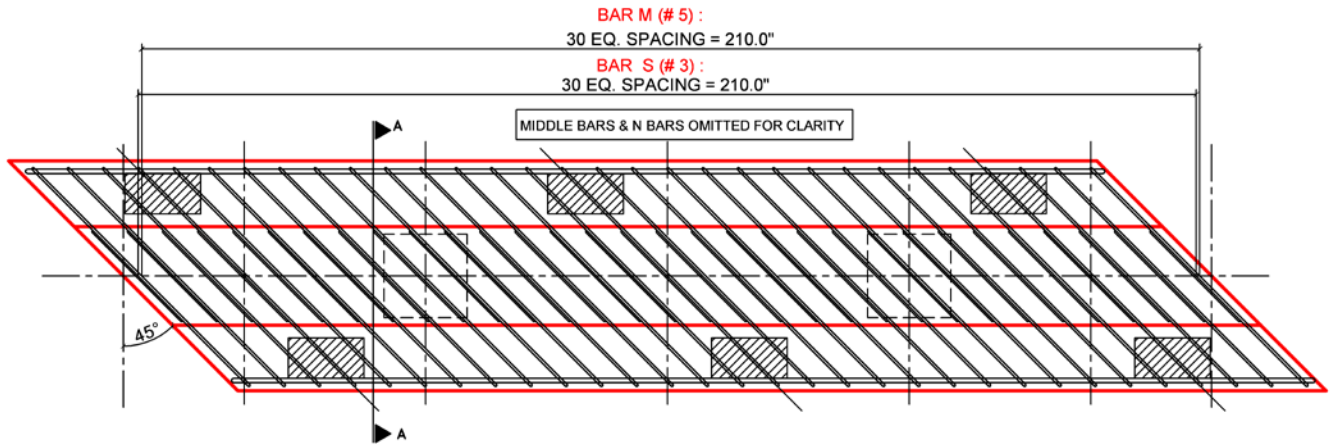


**Figure 3.3. Reinforcing Details of Phase 2 ITBCs:**  
**(a) Typical end face reinforcing details, (b) Plan view reinforcing details of SITBC-30-T-M, (c) Plan view reinforcing details of SITBC-30-S-M, (d) Plan view reinforcing details of SITBC-45-T-M, (e) Plan view reinforcing details of SITBC-45-**

**S-M, (f) Plan view reinforcing details of SITBC-60-T-M and (g) Plan view reinforcing details of SITBC-60-S-M**

**3.4 FABRICATION OF THE INVERTED-T TEST SPECIMENS**

The inverted-T bent cap specimens were constructed utilizing the steel and wood formworks to facilitate the fabrication process and ensure the dimensional accuracy. Specimens were subjected to curing of 28 days before testing process. The following section depicts the properties of the materials and fabrication process practiced during the construction of test specimens.

**3.4.1 Steel Reinforcement Properties**

Grade 60 deformed bars satisfying the requirements of ASTM A615 were used for all steel reinforcement. Each bar size was tested to determine actual yield strength in accordance with ASTM A370 testing procedures. Deformed mild steel #3 reinforcing bars were used as transverse reinforcement (S Bars), which act as hanger and shear reinforcements. The yield strength of #3 rebars ( $f_{yt}$ ) is 66.0 ksi. The various size of rebars used in the construction of ITBC specimens are summarized in Table 3.2.

**Table 3.2. ITBC Rebar Details**

Rebar Name	Rebar Size
Bar A	#7
Bar B	#6
Bar S	#3
Bar M	#4, #5
Bar N	#4, #5
Bar U1	#3
Bar U2	#3
Bar G	#5

**3.4.2 Concrete Mix Design Properties**

As per TxDOT specifications, typically the concrete strengths for the construction of inverted-T bridge caps should be around 3600 psi. Specimens 1, 2, 4, 6 and 8 (in Table 3.1) were cast in August of 2016. These specimens were cast with a cement/cementitious ratio of 0.6 which is generally the same as the mix design “wanted by TxDOT.” The ready-mix concrete had a mixture proportion by weight per  $yd^3$  as shown in Table 3.3.

**Table 3.3. Typical PCC Mixture Design for Test Specimens**

<b>Material Specifications</b>	<b>Quantity per yd<sup>3</sup></b>
Type 3 Portland cement (ALAMO III)	310 lb
Water	27.36 gallons
Water /Cement ratio	0.44
Class F Fly ash	207 lb
CA: Pioneer Hanson Arena 1” limestone aggregate	1673 lb
FA: Pioneer Hanson Arena natural sand	1540 lb
Admixture: Sika Visco-crete 2110	21 oz
Sika Plastiment	6 oz
Ambient temperature	82 -93 °F
Entrapped air	2%
Slump	6   2 inches

During the casting of the first five specimens, areas of congested reinforcement were encountered, and it was difficult to vibrate those areas for the purpose of concrete compaction. The next batch of casting, which was done in August of 2017 onwards, included specimens 3, 5, 7, 9, 10, 11, 12 and 13 as mentioned in Table 3.1. These specimens had areas of even more congestion of reinforcement due to higher skew angles. Therefore, based on a suggestion from the construction company, SCC (Self Compacting Concrete) with the same compressive strength was used to solve the above-mentioned difficulty. SCC utilizes high doses of High Range Water Reducer (HRWR, AKA Superplasticizer), Viscosity Modifying Agent (VMA), and Air Entraining Agent to increase the rheology and workability of the concrete. In SCC, the concrete flows under its own weight and consolidates without the need for much external vibration. SCC is used where there is a congestion of reinforcement or difficulty in performing the necessary external vibration. SCC was especially needed for the 60° specimens as there was heavy congestion of reinforcement in the fanning out zone, and it continued to be used for the remaining specimens to maintain consistency. The SCC mix design is supposed to have some differences as compared to conventional concrete as it includes a higher dose of HRWR, VMA, and Air Entraining Agent. However, the SCC mix design proportion used for the remaining specimens is expected to yield the same compressive strength as that of the conventional concrete which was used for the first batch of specimens (1, 2, 4, 6, and 8). The ready-mix self-compacting concrete had a mixture proportion by weight per yd<sup>3</sup> as shown in Table 3.4.

**Table 3.4. Typical SCC Mixture Design for Test Specimens**

<b>Material Specifications</b>	<b>Quantity per yd<sup>3</sup></b>
Type 3 Portland cement (ALAMO III)	474 lb
Water	30.12 gallons
Water /Cement ratio	0.35
Class F Fly ash	255 lb
CA: Pioneer Hanson Arena 1” limestone aggregate	1507 lb
FA: Pioneer Hanson Arena natural sand	1441.2 lb
Admixture: Sika Viscocrete 2110	37.2 oz
Sika Plastiment	4 oz
High Range Water-Reducing Admixture: Sika R-4	4 oz
Air	2.5 oz
Ambient temperature	60-70 °F
Entrapped air	4.8%
Spread value	21-23”

Mean Concrete Compressive strength was measured by six 4-inch X 8-inch cylinders for each specimen cast (following ASTM C31 procedures) and tested in accordance with ASTM C39 simultaneously with each specimen on the same day of testing.

### 3.4.3 Construction of the Test Specimen

The test specimens were constructed using materials and methods typically used in TxDOT practice. Out of a total of 13 ITBC specimens mentioned in the test matrix, five specimens were constructed in the month of August 2016, which include five Phase 1 specimens (ITBC-0-T-2M, ITBC-30-T-2M, ITBC-30-S-2M, ITBC-45-T-2M and ITBC-45-S-2M,). In the month of August, 2017, six more specimens were constructed including two Phase 1 specimens (ITBC-60-T-2M and ITBC-60-S-2M) and four Phase 2 specimens (ITBC-45-T-M, ITBC-45-S-M, ITBC-60-T-M, and ITBC-60-S-M). Two more Phase 2 specimens (ITBC-30-T-M and ITBC-30-S-M) were fabricated in the month of January, 2018. Figures 3.4(a)–3.4(g) and Figures 3.5(a)–3.5(f) present the photographs of a partial reinforcement arrangement during construction of Phase 1 and Phase 2 test specimens, respectively.



(a)



(b)



(c)



(d)



(e)



(f)



(g)

**Figure 3.4. Partial Reinforcing Details of Phase 1 Specimens:**

(a) Specimen ITBC-0-T-2M, (b) Specimen ITBC-30-T-2M, (c) Specimen ITBC-30-S-2M, (d) Specimen ITBC-45-T-2M, (e) Specimen ITBC-45-S-2M, (f) Specimen ITBC-60-T-2M and (g) Specimen ITBC-60-S-2M



(a)



(b)



(c)



(d)



(e)



(f)

**Figure 3.5. Partial Reinforcing Details of Phase 2 Specimens:**  
(a) Specimen ITBC-30-T-M, (b) Specimen ITBC-30-S-M, (c) Specimen ITBC-45-T-M, (d) Specimen ITBC-45-S-M, (e) Specimen ITBC-60-T-M and (f) Specimen ITBC-60-S-M

All the specimens were constructed at the precast concrete company, Flexicore of Texas, under stringent quality control supervision. Cage assembly, strain gauge

instrumentation, and casting took approximately one week per ITBC specimen. Specimens were cured for at least 28 days before testing. Reinforcing steel was ordered from another company, NUCOR, and rebars were cut and bent before being shipped to the Flexicore company. Upon assembling of the steel cages [Figure 3.6(a)], strain gauges were pasted to the steel reinforcement as described in Section 3.6. The specimens were then moved to the casting area [Figure 3.6 (b)] and placed into the steel and wood forms [Figure 3.6 (c)]. For each specimen, a slump test was conducted according to ASTM C143. Water was added to each mix to adjust the slump to the target value of  $6 \pm 2$  inches. Concrete was placed using a one-cubic yard bucket lifted by an overhead crane as shown in Figure 3.6 (d). Internal vibrators were used to ensure proper consolidation of concrete [Figure 3.6 (e)]. After the initial setting, the top surface was finished [Figure 3.6 (f)] and covered with a plastic sheet to limit water evaporation from the specimen. For each specimen, six numbers of standard 4" x 8" test cylinders were cast following ASTM C31 procedures [Figure 3.6 (g)], and the mean compressive strength was tested in accordance with ASTM C39 on the same day of testing for each specimen. When the desired strength of the specimens was achieved, forms were removed and specimens were uncovered and stored in the store yard of the Flexicore company [Figure 3.6 (h)].



(a)



(b)



(c)



(d)



(e)



(f)



(g)



(h)

**Figure 3.6. Fabrication of Specimens:**

**(a) Cage assembly and instrumentation, (b) Cage being moved to casting area, (c) Re-bar cage in the steel and wood formwork, (d) Placing of concrete (e) Internal**

**vibrators, (f) Top surface finishing, (g) Casting of 4" x 8" cylinders and (h)  
Specimen after removing the form work**

### **3.5 TEST SETUP**

The testing frame was designed similar to the frame used in TxDOT Project 0-1854 (Crack Control for Ledges in Inverted 'T' Bent Caps) performed at the University of Houston. The schematic view of the loading frame setup and the support arrangement is shown in Figure 3.7 and Figure 3.8, respectively.

The loading frame has been specially designed to have a working capacity much greater than the capacity of the test specimens. There is a total of three vertical loading frames. The loading frames are connected to the two longitudinal wide flange beams, which are anchored to the strong floor. Each vertical steel frame is equipped with a corresponding hydraulic actuator. Three hydraulic actuators, two with a capacity of 600 kips each and one with a capacity of 330 kips, are used to apply the loads to the skew bridge bent cap specimens. The detailed elevation view of the three loading frames is shown in Figures 3.9 and 3.10.

The actuators are controlled by a versatile FlexTest GT system that allows both the load control and the displacement control procedures. The load is applied by the displacement control loading protocol, ensuring the same amount of load in each of the six pedestals during the tests. In the displacement control mode, all three actuators are controlled manually. Each of the outputs (loads) from the two end actuators is read, and the same load is input to the middle actuator so that the same loading in each of the six loading pads can be maintained. The spreader beam attached to the actuators transfers the load from the actuators to the ledge of the inverted-T test specimen through the loading pads as shown in Figure 3.7. The loading pads are placed on the lead sheet to distribute the load uniformly and to eliminate the stress concentration under the loading pads. Each test is estimated to last 4 to 5 hours.

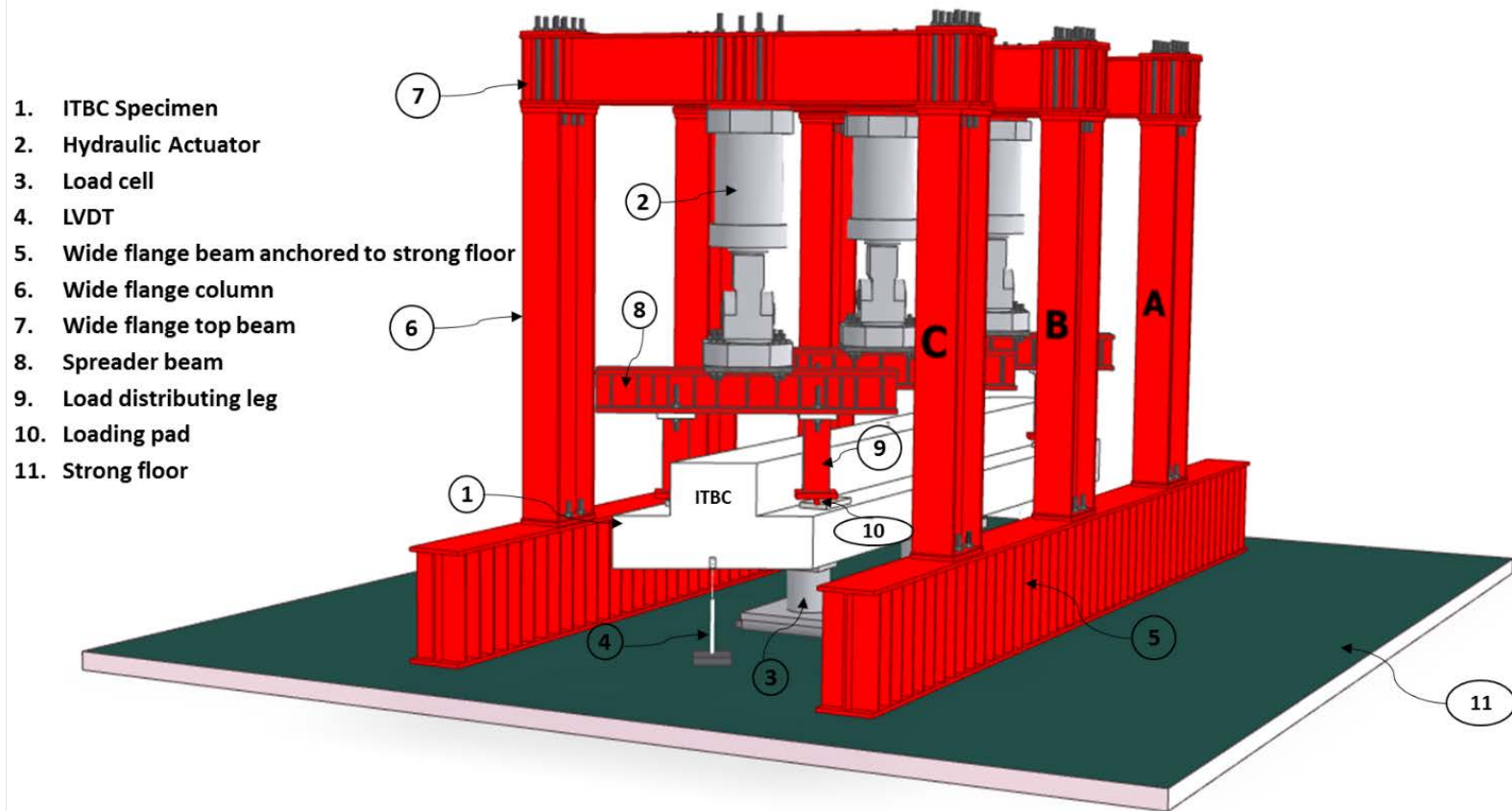
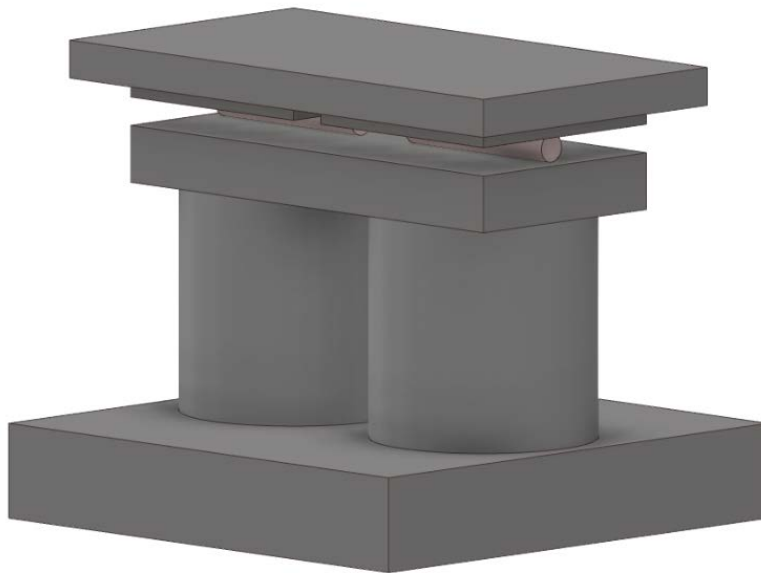


Figure 3.7. Schematic View of the Test Setup for ITBC Specimens



**(a) Roller Support (1000 kip Load Cell)**



**(b) Hinge Support (500 kip Load Cell)**

**Figure 3.8. Support Conditions for the Test**

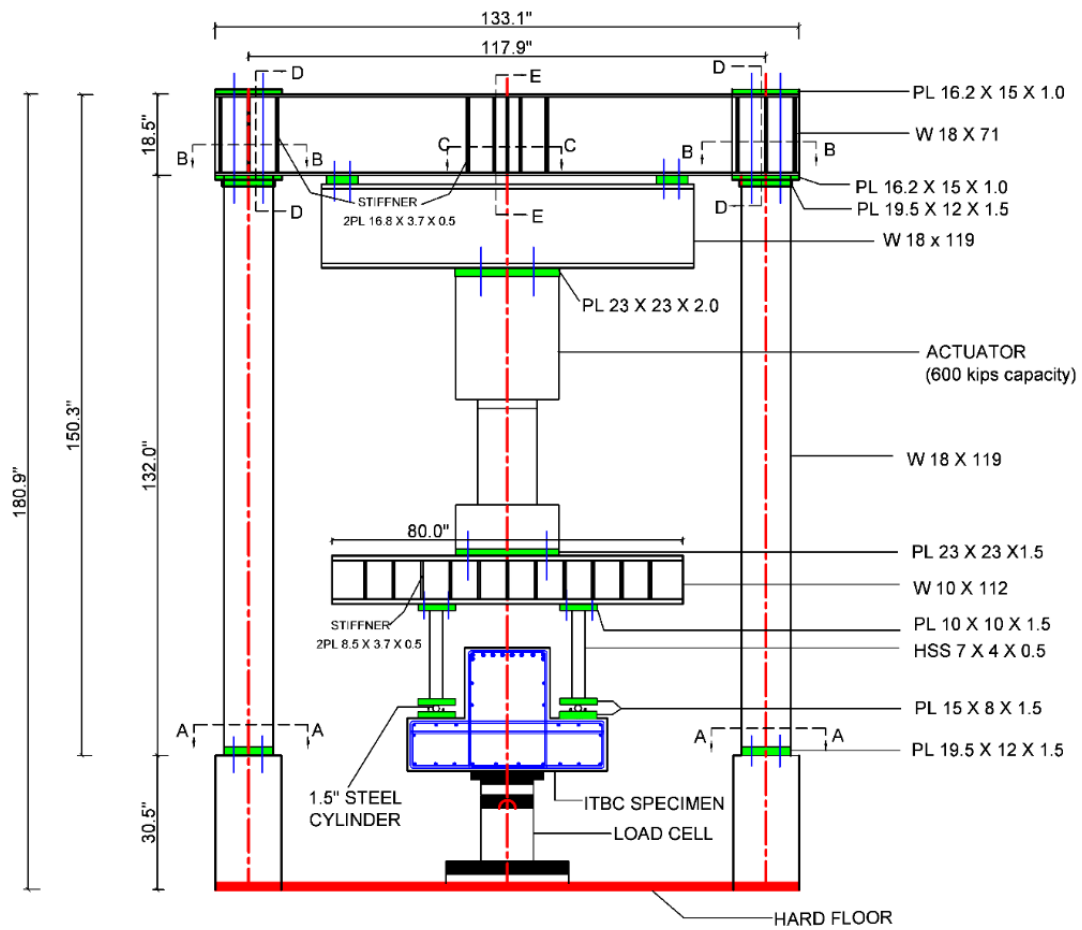


**Figure 3.9. Elevation view of the loading frame A and B with dimension details**

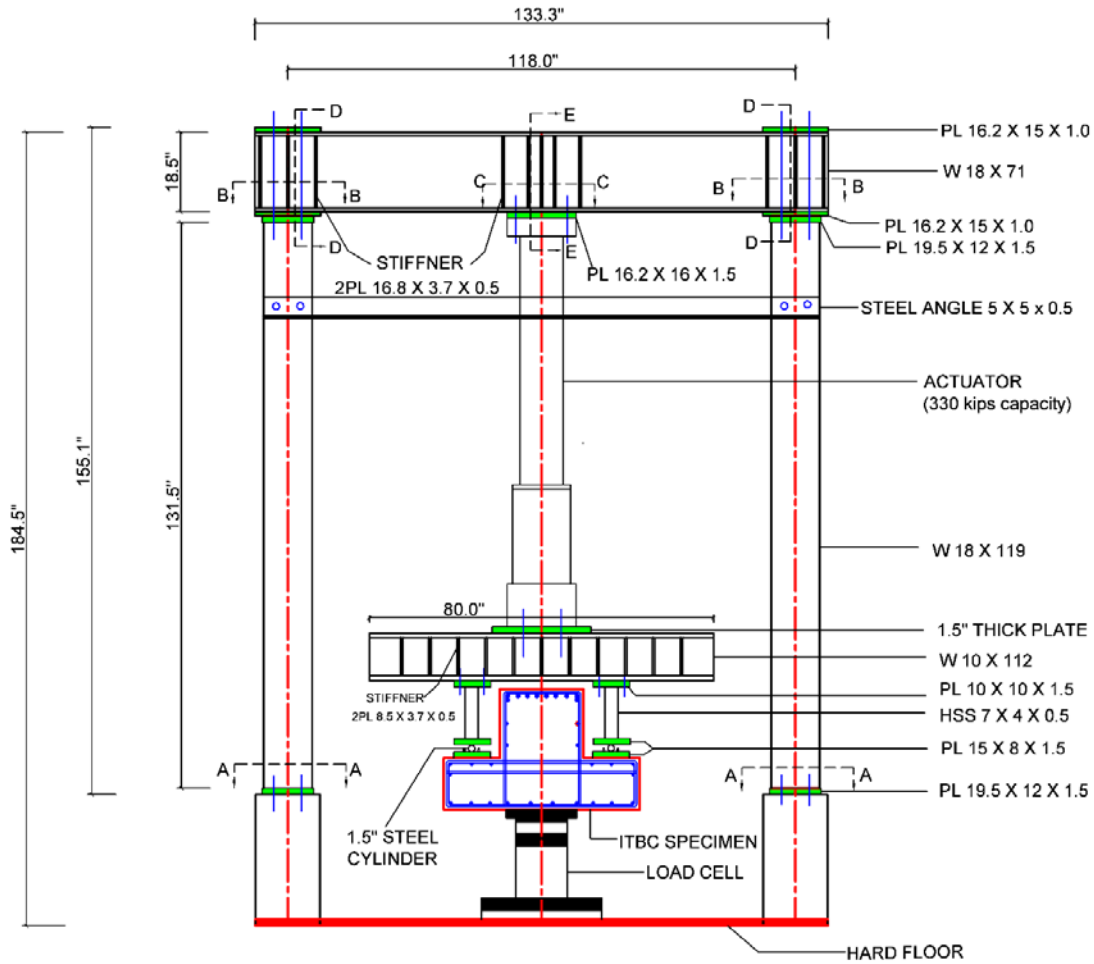


**Figure 3.10. Elevation view of the loading frame C with dimension details**

The primary components of the loading frames setup at the fabrication stage, such as the top beams, vertical wide flange columns, spreader beam, and load distributing legs, are shown in Figure 3.11. The complete test setup of the loading frame with the inverted-T bridge cap test specimen at the UH lab is depicted in Figure 3.12.



(a)



(b)



(c)



(d)

**Figure 3.11. Primary components of test frame during fabrication stage:**  
**(a) Top beams of the test frame, marked as [7] in Figure 3.7, (b) Columns of the test frame, marked as [6] in Figure 3.7, (c) Spreader beams, marked as [5] in Figure 3.7 and (d) Load distributing legs, marked as [9] in Figure 3.7**

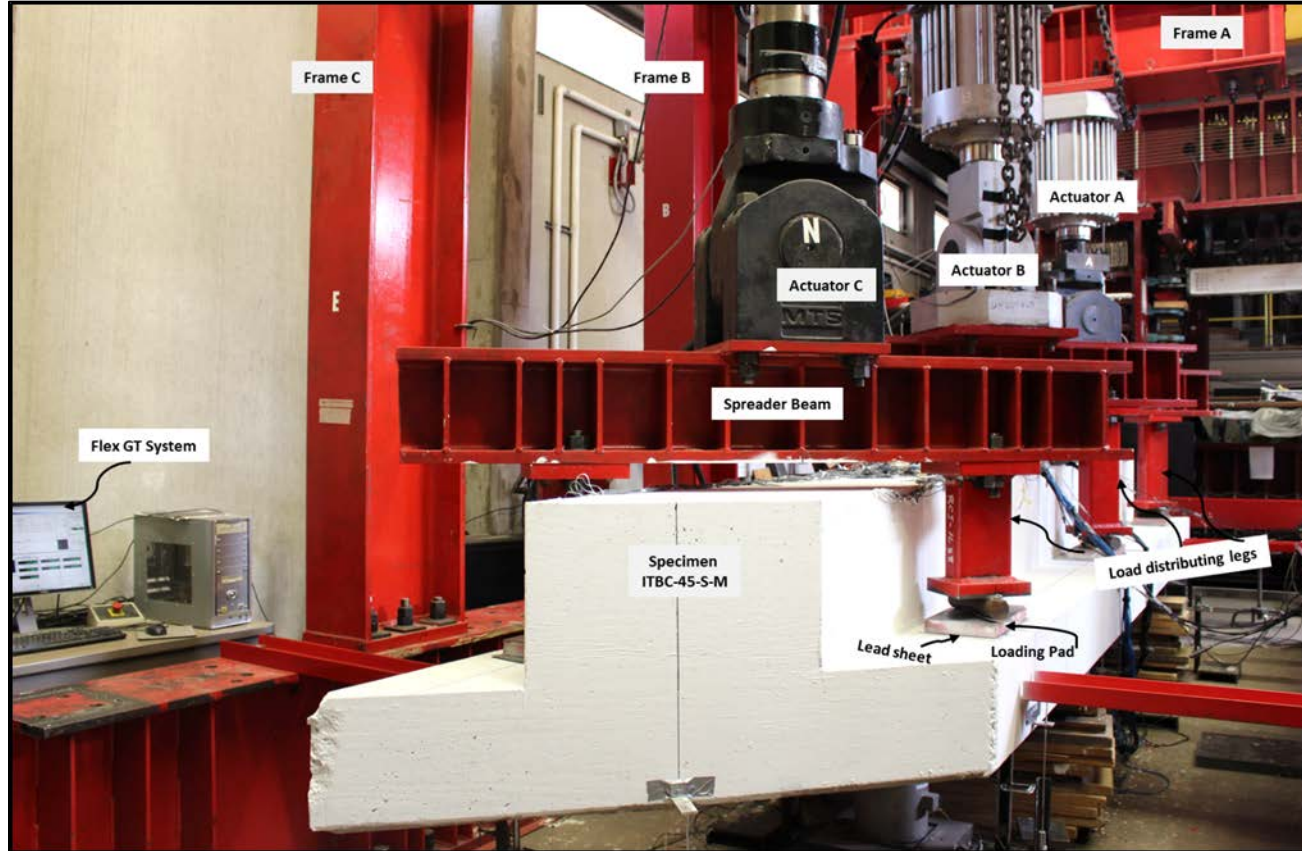


**Figure 3.12. Test Setup of ITBC Specimen in UH Laboratory**

### **3.6 INSTRUMENTATIONS**

The structural testing performed on each of the inverted-T bridge cap specimens comprised of a data set received from different instruments installed to obtain observations and readings in terms of strain, loads, displacements and crack widths. The instruments mounted during all tests include strain gages (strain measurement), load cells (applied load/reaction measurement), linear potentiometers and LVDTs (displacement measurement) whereas crack widths were noted using a crack comparator.

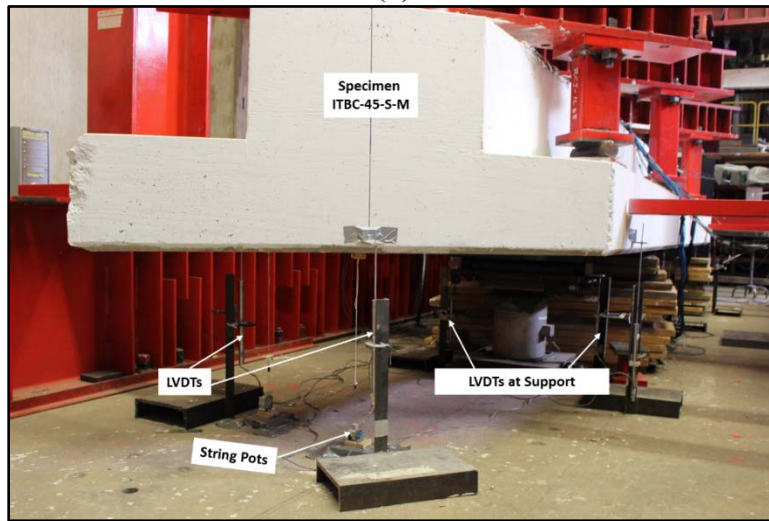
#### **3.6.1 Load – Displacement Measurement**

Each inverted-T bridge cap specimen is supported at the bottom by three reaction load cells, two with a capacity of 500 kips each and one with a capacity of 1000 kips, which is used to check the force equilibrium of the structural system during the tests. The roller support has a load cell with a capacity of 1000 kips, and the hinge support has two load cells with a capacity of 500 kips each, as shown in Figure 3.8.

The linear variable differential transformer (LVDT) and string potentiometers were attached to the specimen to monitor and record the displacement of the test specimen during the test. The arrangement for this is shown in Figure 3.13(a) and Figure 3.13(b). LVDTs were placed vertically at two support locations and at both ends of the specimen to measure the settlement of the supports and the total deflection of each specimen, respectively. The net deflection of the specimens was calculated by subtracting the support settlement from the total deflection. In addition to LVDTs, the string potentiometers were placed under each loading point of the specimen to monitor the deflection during the test. The reaction force obtained from the load cell was plotted against the net displacement obtained from the LVDT to establish the desired load-deflection curve of each specimen.



(a)



(b)

**Figure 3.13. Instrumentation:**

**(a) Load cell arrangement at the support locations, (b) LVDT and String Potentiometer for deflection measurements**

### 3.6.2 Strain Measurement

Strain gauges model FLA-5-11-5LT manufactured by Tokyo Sokki Kenkyujo Co., Ltd. were affixed to the longitudinal, transverse (hanger) and ledge reinforcement at the locations of maximum expected strain to monitor and record the tensile strain in the test specimens. The installation procedure of the strain gauges is depicted in Figure 3.13. First, the bar deformations were removed using a grinder, without significantly reducing the cross section of the bar [Figure 3.14 (a)]. The cleared surface was polished with sand paper to provide a smooth planar surface that was then cleaned using conditioner (which is acidic in nature) [Figure 3.14 (b)] followed by a neutralizer (which is alkaline in nature) [Figure

3.14 (c)] with the help of cotton balls. Then the catalyst was applied on the back of each strain gauge [Figure 3.14 (d)] followed by applying the M-bond adhesive [Figure 3.14 (e)]. Strain gauges were glued to the cleaned surface with the help of butter paper [Figure 3.14 (f)] and covered with polyurethane coating [Figure 3.14 (h)], followed by nitrile rubber coating [Figure 3.14 (i)] to waterproof them. Finally, the strain gauges were wrapped in butyl rubber tape [Figure 3.14 (j)], followed by aluminum foil tape [Figure 3.14(k)] to further isolate them and the ends were perfectly sealed [Figure 3.14 (l)].



**Figure 3.14. Strain Gauge Installation:**

**(a) Grinding off bar deformations, (b) Cleaning of grinded surface using acidic conditioner, (c) Cleaning of grinded surface using alkaline neutralizer, (d) Applying catalyst to the back of strain gauge, (e) Applying the adhesive, (f) Pasting strain gauges to steel bar with butter paper, (g) Glued strain gauge allowed to dry, (h) Applying polyurethane coating, (i) Applying nitrile rubber coating, (j) Isolating with butyl rubber tape, (k) Covering with aluminum foil and (l) Installation ends with perfectly sealing**

The yield stress of transverse stirrups (#3) is found to be 66.00. Therefore, the rebars are considered as yielded when the tensile strain in the hanger stirrups (#3 rebars) becomes 0.0023. Figure 3.15 shows the typical arrangement and locations of strain gauges in the primary reinforcements in test specimen ITBC-0-T-2M. The strain gauges are marked by a certain notation for better understanding. The strain gauge notation NES1-NES20, SES1-SES20, NWS1-NWS20, SWS1-SWS20, NEU1- NWU1, SEU1- SWU1, NEG1- NWG1, SEG1- SWG1 are represented as follows:

- N/S: North/South side of the test specimen.
- E/W: East/West leg of transverse stirrups (S Bars), U Bars, and G Bars.
- S/M/L/U/G: S Bars/M Bars/Longitudinal Bars/U Bars/G Bars.
- 1,2,3,4-20: the S and M rebar's number.

The strain gauge locations for all other test specimens are shown in Appendix 1. Explanations for of the strain gauge locations at each type of rebars are described below:

- NES1 shows the strain value of the east leg of the first (#1) S bar on the North side of the test specimen.
- NWS1 shows the strain value of the west leg of the first (#1) S bar on the North side of the test specimen.
- NM5 shows the strain value of the fifth (#5) M bar on the North side of the test specimen. NL shows the strain value of the longitudinal rebar on North side of the test specimen.
- SL shows the strain value of the longitudinal rebar on the South side of the test specimen. NEU1 shows the strain value of the east leg of the first (#1) U bar on the North side of the test specimen.
- NWU1 shows the strain value of the west leg of the first (#1) U bar on the North side of the test specimen.
- NEG1 shows the strain value of the east leg of the first (#1) G bar on the North side of the test specimen.
- NWG1 shows the strain value of the west leg of the first (#1) G bar on the North side of the test specimen.

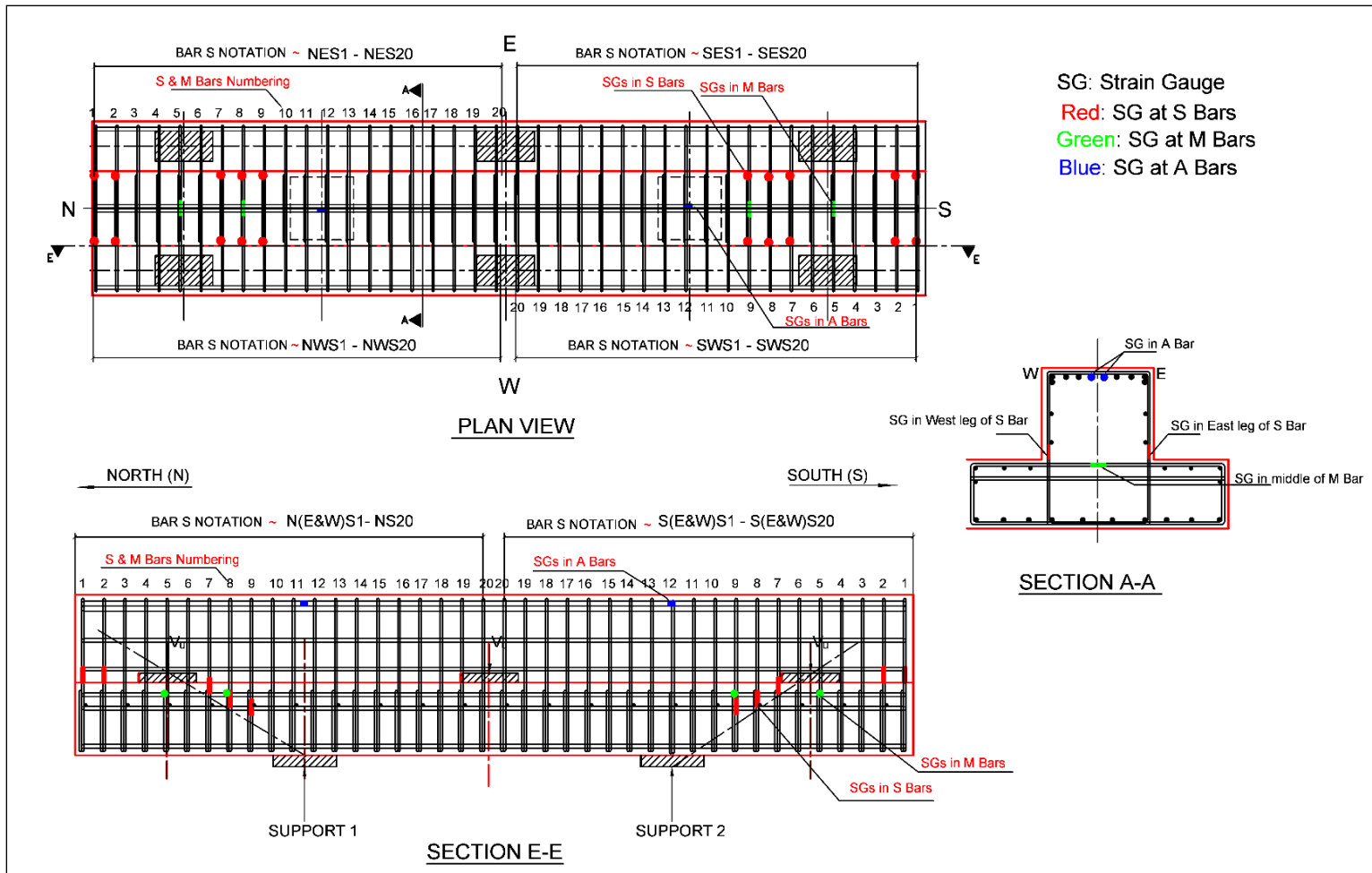
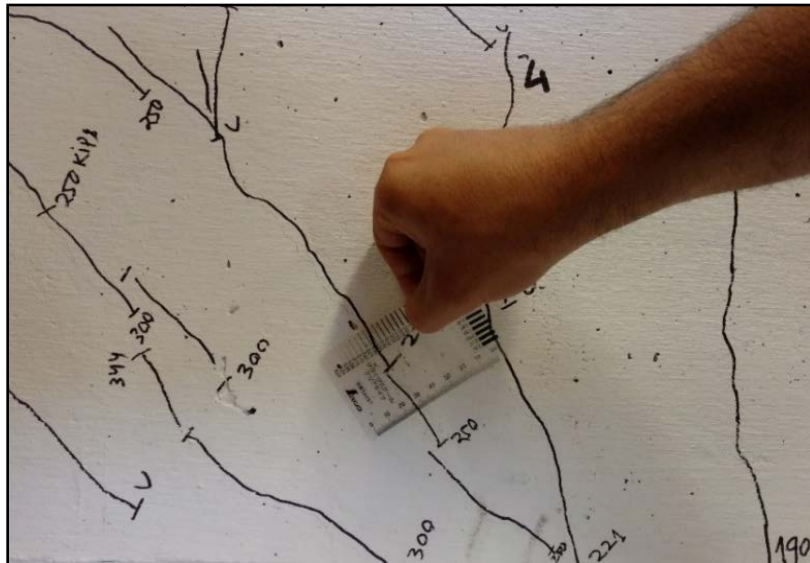


Figure 3.15. Typical Strain Gauges Arrangement and Location

### 3.6.3 Crack Measurement

Flexure and diagonal shear crack widths were measured on each side of the specimens between each load increment using crack comparators as shown in Figure 3.16. Independent measurements were taken by two students and then averaged to get the accurate crack width. Several cracks were selected arbitrarily to be monitored at the same location throughout the entire test. The maximum diagonal crack width on each face was recorded between each load increment and at the end of each test. In addition, a total number of cracks that developed in the web and the ledge of the specimen were measured for comparison after completion of each test.



**Figure 3.16. Crack Width Measurement**

### 3.7 LOADING PROTOCOL

The specimens were loaded in an orientation as shown in Figure 3.12. The load was applied directly to the ledges of the specimens using hydraulic actuators, two with a capacity of 600 kips each and one with a capacity of 330 kips. The reactions were measured through the load cells beneath the ITBC specimen. The actuators are controlled by a versatile FlexTest GT system that allows both the load control as well as displacement control procedures. The load is applied by the displacement control loading protocol, ensuring the same amount of load in each of the six pedestals throughout the tests. In the displacement control mode, all three actuators are controlled manually.

Load was applied monotonically to the specimens in 25-kip increments prior to cracking and 50-kip increments after the appearance of the first flexural shear crack. After each load increment, cracks were marked and measured, and photographs were taken. When the applied load approached an estimated capacity, the loading process was continued until reaching the failure mode.

### **3.8 SUMMARY**

Details of the design, fabrication and experimental program are provided in this report. Experimental variables studied in this project are skew angle, orientation of transverse reinforcements and amount of transverse reinforcements. Thirteen skew inverted-T bridge cap specimens with the variables mentioned above were fabricated and tested with a constant shear span to a depth ratio of 1.4. The design procedure used for obtaining test specimen details is also outlined. In addition, fabrication of specimens, material properties, and construction details are provided in this report. Steel rebar strains, applied loads, reaction forces, and ITBC deflections were monitored throughout the entire tests. Crack width measurements were taken between each load increment.

## CHAPTER 4: EXPERIMENTAL RESULTS

### 4.1 OVERVIEW

A total of 13 inverted-T bent cap specimens are tested in Phase 1 and Phase 2 of the test plan under static compression loading to evaluate and compare the performance of skewed transverse reinforcement with respect to traditional transverse reinforcement. As discussed earlier, the primary variables taken into consideration for the research work include skew angle of bent cap, detailing of transverse reinforcement, and amount of transverse reinforcement. The specimens have been designed in a manner to achieve the yielding of shear reinforcements and avoid any other type of local failure mode such as punching shear failure, hanger stirrup failure, or failure due to shear friction before the yielding of transverse stirrups. The following sections present the test results for each of the 13 specimens in terms of load-displacement characteristics, load-strain behavior, crack patterns observed at peak loads, and corresponding failure modes.

### 4.2 MATERIAL PROPERTIES

#### 4.2.1 Steel Reinforcement Properties

Grade 60 deformed bars satisfying the requirements of ASTM A615 are used for all steel reinforcement. Each bar size was tested to determine actual yield strength in accordance with ASTM A370 testing procedures. Deformed mild steel #3 reinforcing bars were used as transverse reinforcement (S Bars), which act as hanger and shear reinforcements. The yield strength of #3 rebars ( $f_{yt}$ ) is 66.0 ksi. The measured material properties of the reinforcements for each of the rebars provided in the test specimen are summarized in Table 4.1.

**Table 4.1. Yield Strength of Steel Rebars**

Rebar size	#7 Bars	#6 Bars	#5 Bars	#4 Bars	#3 Bars
Yield strength (ksi) ( $f_{yt}$ )	73.30	69.57	68.65	67.54	66.00

#### 4.2.2 Concrete Properties

The details of the concrete mix design proportion are reported in the previous chapter. Mean Concrete Compressive strength was measured by six 4 inch x 8 inch cylinders for each specimen cast (following ASTM C31 procedures) and tested (in accordance with ASTM C39) simultaneously with each specimen on the same day of testing. Actual strengths varied from 7300 to 8900 psi. A summary of the concrete compressive strength of all specimens is presented in Table 4.2.

**Table 4.2. Mean Compressive Strength of ITBC Specimens**

<b>Sr.No</b>	<b>Specimen</b>	<b>Compressive Strength <math>f'_c</math> (ksi)</b>
1	ITBC-0-T-2M	7.3
2	ITBC-30-T-2M	7.5
3	ITBC-30-S-2M	7.3
4	ITBC-45-T-2M	7.6
5	ITBC-45-S-2M	7.8
6	ITBC-60-T-2M	8.7
7	ITBC-60-S-2M	8.9
7	ITBC-30-T-M	7.9
9	ITBC-30-S-M	7.2
10	ITBC-45-T-M	8.3
11	ITBC-45-S-M	8.2
12	ITBC-60-T-M	6.8
13	ITBC-60-S-M	8.1

Even though the compressive strength of the concrete turned out to be higher than the target strength of 3.6 ksi, the compressive strength of concrete is not a critical parameter for this research. The effect of the compressive strength can be normalized by dividing the shear force by  $(\sqrt{f'_c} * b_w * d)$ , where  $f'_c$  is the compressive strength of concrete on the day of testing,  $b_w$  is the width of the web of the bent cap and  $d$  is the effective depth of the bent cap. Moreover, the difference of  $f'_c$  between the traditional ITBC and the corresponding skew ITBC specimen is not significant. This method of investigation has also been implemented by many researchers such as UT Austin for TxDOT Research Project 0-6416, Report No. FHWA/TX-13/0-6416-1, where the compressive strength of concrete was not a critical parameter.

### **4.3 PRIMARY EXPERIMENTAL RESULTS**

Primary experimental results of strength and serviceability of the tests conducted on each of the seven ITBC specimens are discussed in the following sections. Figure 4.1 illustrates the shear spans. Table 4.3 represents the summary of all the test results. The variables used in Table 4.3 are defined as follows:

$f'_c$  = compressive strength of concrete at the time of testing measured, psi.

$b_w$  = width of the web, in.

$d$  = distance from extreme compression fiber to centroid of tensile reinforcement of the web, in.

$f_{y\_A}$  = yield strength of the top longitudinal reinforcement (Bar A), ksi.

$f_{y\_B}$  = yield strength of the bottom longitudinal reinforcement (Bar B), ksi.

$f_{y\_S}$  = yield strength of the transverse reinforcement (Bar S), ksi.

$f_{y\_M}$  = yield strength of the ledge reinforcement (Bar M), ksi.

$f_{y\_T}$  = yield strength of the skin reinforcement (Bar T), ksi.

$a$  = shear span measured from the center of the reaction plate to the central line of the external loading pads as shown in **Note 1**, in.

$a_1, a_2$  = distance measured from the center of the reaction plate to the center of the external farthest and closest loading pads respectively, as shown in **Note 1**, in.

$a/d$  = shear span to depth ratio

$V_{Crack}$  = reaction force when the first flexural crack formed, kips.

$V_{Peak}$  = maximum reaction force carried in the critical section of the test specimen, kips.

**Note 1:** a typical plan view of skew ITBC showing the notations of  $a$ ,  $a_1$ , and  $a_2$

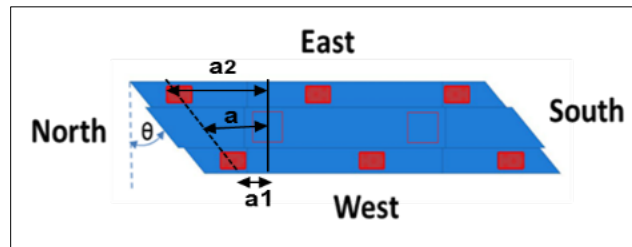


**Figure 4.1. ITBC Showing the Shear Spans**

**Table 4.3. Summary of Test Results**

Specimen ID	f <sub>c</sub> (ksi)	b <sub>w</sub> (in)	d (in)	f <sub>y_A</sub> (ksi)	f <sub>y_B</sub> (ksi)	f <sub>y_S</sub> (ksi)	f <sub>y_M</sub> (ksi)	F <sub>y_T</sub> (ksi)	a (in)	a1 (in)	a2 (in)	a/d (ratio)	a1/d (ratio)	a2/d (ratio)	V <sub>Crack</sub> (kips)	V <sub>Peak</sub> (kips)	$\frac{V_{Peak}}{\sqrt{f_c} b_w d}$
ITBC-0-T-2M	7.3	19.5	24.5	73.3	69.57	66	67.54	67.54	36	36.0	36	1.5	1.5	1.5	115	338	9.13
ITBC-30-T-2M	7.5	19.5	24.5	73.3	69.57	66	67.54	67.54	36	26.6	45.4	1.5	1.1	1.9	128	384	9.28
ITBC-30-S-2M	7.3	19.5	24.5	73.3	69.57	66	67.54	67.54	36	26.6	45.4	1.5	1.1	1.9	127	381	9.33
ITBC-45-T-2M	7.6	19.5	24.5	73.3	69.57	66	67.54	67.54	36	19.8	52.2	1.5	0.8	2.1	115	369	8.86
ITBC-45-S-2M	7.8	19.5	24.5	73.3	69.57	66	67.54	67.54	36	19.8	52.2	1.5	0.8	2.1	132	361	8.56
ITBC-60-T-2M	8.7	19.5	24.5	73.3	69.57	66	67.54	67.54	36	8.0	64	1.5	0.3	2.6	105	321	7.20
ITBC-60-S-2M	8.9	19.5	24.5	73.3	69.57	66	67.54	67.54	36	8.0	64	1.5	0.3	2.6	113	317	7.03
ITBC-30-T-M	7.9	19.5	24.5	73.3	69.57	66	67.54	67.54	36	26.6	45.4	1.5	1.1	1.9	109	376	8.85
ITBC-30-S-M	7.2	19.5	24.5	73.3	69.57	66	67.54	67.54	36	26.6	45.4	1.5	1.1	1.9	98	371	9.15
ITBC-45-T-M	8.3	19.5	24.5	73.3	69.57	66	67.54	67.54	36	19.8	52.2	1.5	0.8	2.1	116	302	6.94
ITBC-45-S-M	8.2	19.5	24.5	73.3	69.57	66	67.54	67.54	36	19.8	52.2	1.5	0.8	2.1	105	347	8.02
ITBC-60-T-M	6.8	19.5	24.5	73.3	69.57	66	67.54	67.54	36	8.0	64	1.5	0.3	2.6	82	300	7.61
ITBC-60-S-M	8.1	19.5	24.5	73.3	69.57	66	67.54	67.54	36	8.0	64	1.5	0.3	2.6	108	312	7.26

## 4.4 TEST RESULTS

A total of 13 inverted-T bent cap specimens were tested under static compression loading to evaluate and compare the performance of skewed transverse reinforcement with respect to traditional transverse reinforcement in the test specimens. The following sections present the comprehensive test results for each of the 13 specimens in terms of load-displacement characteristics, load-strain behavior, crack patterns observed at peak loads, and corresponding failure modes. The given specimen was arranged to test under static compression loading in an experimental set-up of three testing frames as described in Chapter 3. The orientation of the specimens during all tests was kept constant, and the stability of the specimens was checked before starting the loading process. The load was applied using a displacement control approach with a 25-kip load increment before cracking and a 50-kip load increment after the appearance of the first flexural crack. The load-displacement curve is marked with different stages (denoted by numbers in red color) observed during the test from the initial loading up to the failure stage of the specimen. All the stages represented in the curves are briefly justified below the figure number. The X-axis of the force-displacement curve represents the displacement recorded by LVDTs in inches whereas the Y-axis represents a support reaction obtained from the load cell in kips. The rebar numbering and locations of strain gauges for all the ITBC specimens are described in Appendix 1. The reaction force, strain values at first yielding, and peak at yielding of critical rebars for all the specimens are shown in Appendix 2.

### 4.4.1 Phase 1 Specimens

Phase 1 specimens, which include ITBC-0-T-2M, ITBC-30-T-2M, ITBC-30-S-2M, ITBC-45-T-2M, ITBC-45-S-2M, ITBC-60-T-2M and ITBC-60-S-2M, have 2M amount of transverse reinforcement but do not have the vertical reinforcements at the end faces.

#### 4.4.1.1 Specimen ITBC-0-T-2M

The load-displacement curve for specimen ITBC-0-T-2M is demonstrated in Figure 4.2. During the testing process, the first flexural crack (Crack 1) was encountered at a load of 109 kips as shown in Figure 4.3(a). In addition, with a gradual increment in the applied load, several other flexural and shear cracks were observed, as depicted in Figure 4.3(b) to Figure 4.3(d).

The strain gauges attached to the longitudinal bars (A bars), ledge stirrups (M bars), and hanger stirrups (S bars) provided the measurements of tensile strain produced in the respective rebars. With the increasing load, the strains produced in the bars were monitored to note the yielding of rebars. The yielding of rebars is considered to have occurred when the strain reached the value of 0.0023. At a support reaction of 238 kips, the first yielding of the transverse stirrup (NWS1) located at the northwest end face region of the specimen is observed. The flexural shear crack width recorded at the first yielding stage is 0.012 in

Figure 4.3(d). After the first yielding of rebar at 238 kips, the other transverse stirrups located at the south and north end region including SES1, NWS2, NES1 and NES2 immediately underwent yielding at 240 kips, 244 kips, 245 kips, and 248 kips, respectively. Following this, the bars between the support and exterior loading pads, NES8, SWS9, SES7, and NWS7 yielded at a reaction force of 320 kips, 320 kips, 324 kips, and 326 kips, respectively. The strain gauges which did not reach the strain value of 0.0023 within the peak support reaction were considered to be not yielded.

After subsequent application of load, at a support reaction of 336 kips, Crack 3 was developed between the ledge and web at the end faces of the specimen, i.e. north and south end face. Further, the crack width drastically increased at a peak support reaction of 338 kips and at the same time the load carrying capacity started to drop. This peak support reaction corresponds to the shear load of 226 kips. A considerable number of shear cracks with evident crack width were observed at the north as well as at the south end of the specimen. For this specimen, two types of failure modes were observed at the peak stage. Initially, the shear failure was observed due to yielding of shear reinforcements further followed by the separation of the ledge from the web at both of the end face overhang parts as a result of failure of the transverse rebars at the end. Figure 4.3(e) and Figure 4.3(f) show the north and south end of the specimen at failure stage, respectively.

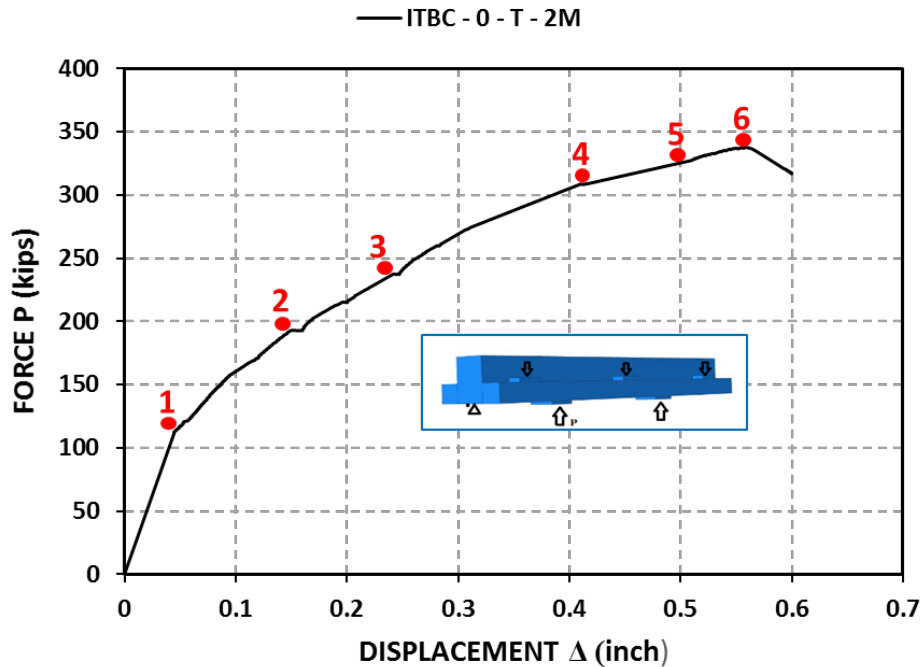


**Figure 4.2. Force-displacement Curve of Specimen ITBC-0-T-2M:**

- 1: First flexure crack at 109 kips, 2: First flexural shear crack at 190 kips, 3: Yielding of transverse rebars at the end face (beyond the shear span) at 238 kips, 4: Diagonal crack appears in the ledge at the end face at 309 kips, 5: Yielding of transverse rebars at shear span region at 320 kips, 6: Peak load at 338 kips**

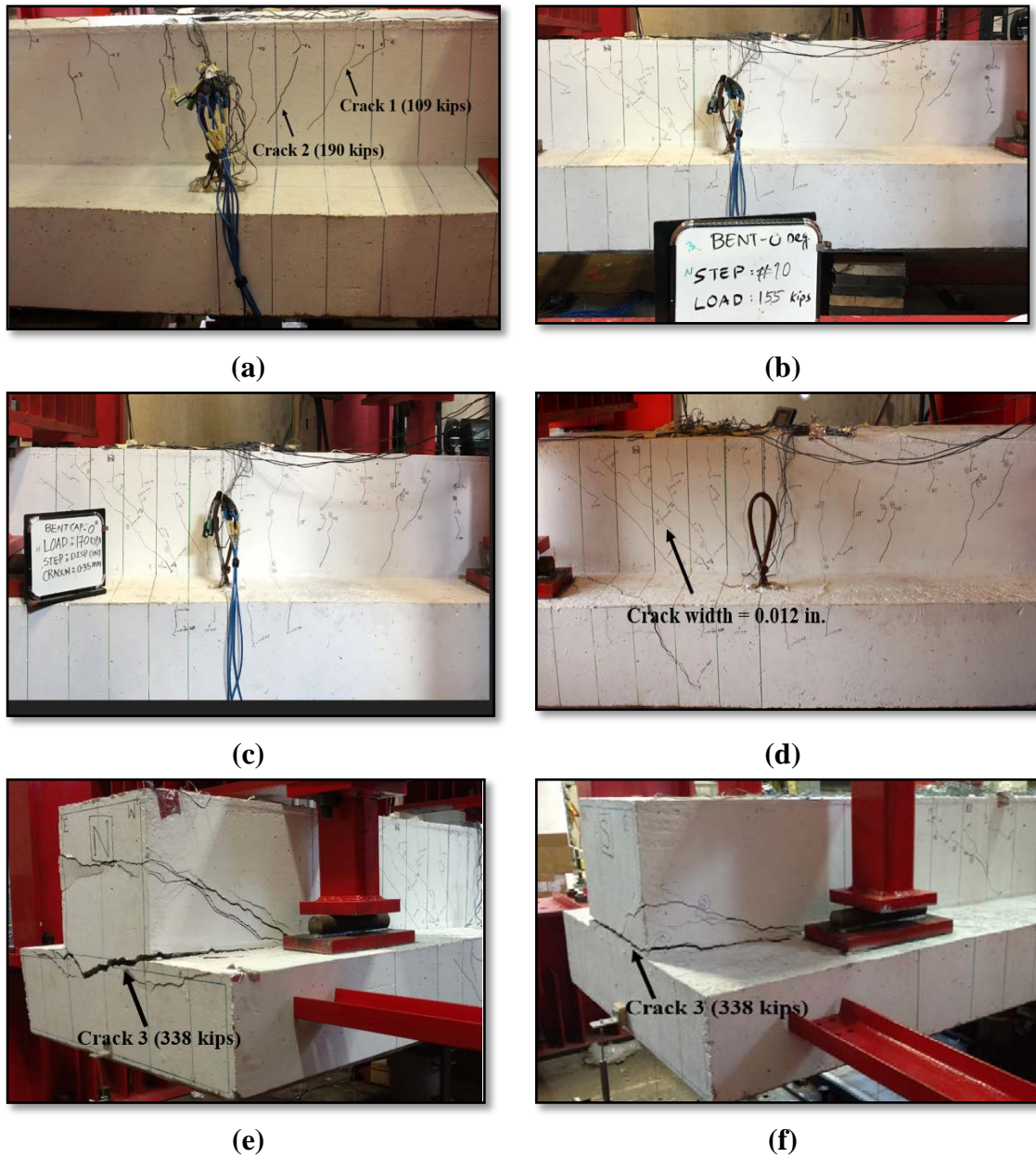


**Figure 4.3. Cracking of Specimen ITBC-0-T-2M:**

- (a) Flexure and flexural shear cracks, (b) Flexural shear cracks at 155 kips, (c) Flexural shear cracks at 170 kips, (d) Crack width measured at first yielding, (e) North end of specimen at failure, (f) South end of specimen at failure**

Figures 4.4(a)-4.4(f) represent the tensile strain trend of selective rebars with respect to the support reaction including hanger stirrups (NES1, NES2, SES1, SES2, and SWS2) and the ledge bar (NM5). The strain gauges which attained the strain value of 0.0023 are considered to be yielded at the corresponding load. Figure 4.4(a)-(e) indicate the yielding point for each of the strain gauges which show that the rebars including NES1,

NES2, SES1, SES2, and SWS2 reached the yielding state whereas the north ledge bar remained un-yielded [Figure 4.4 (f)].

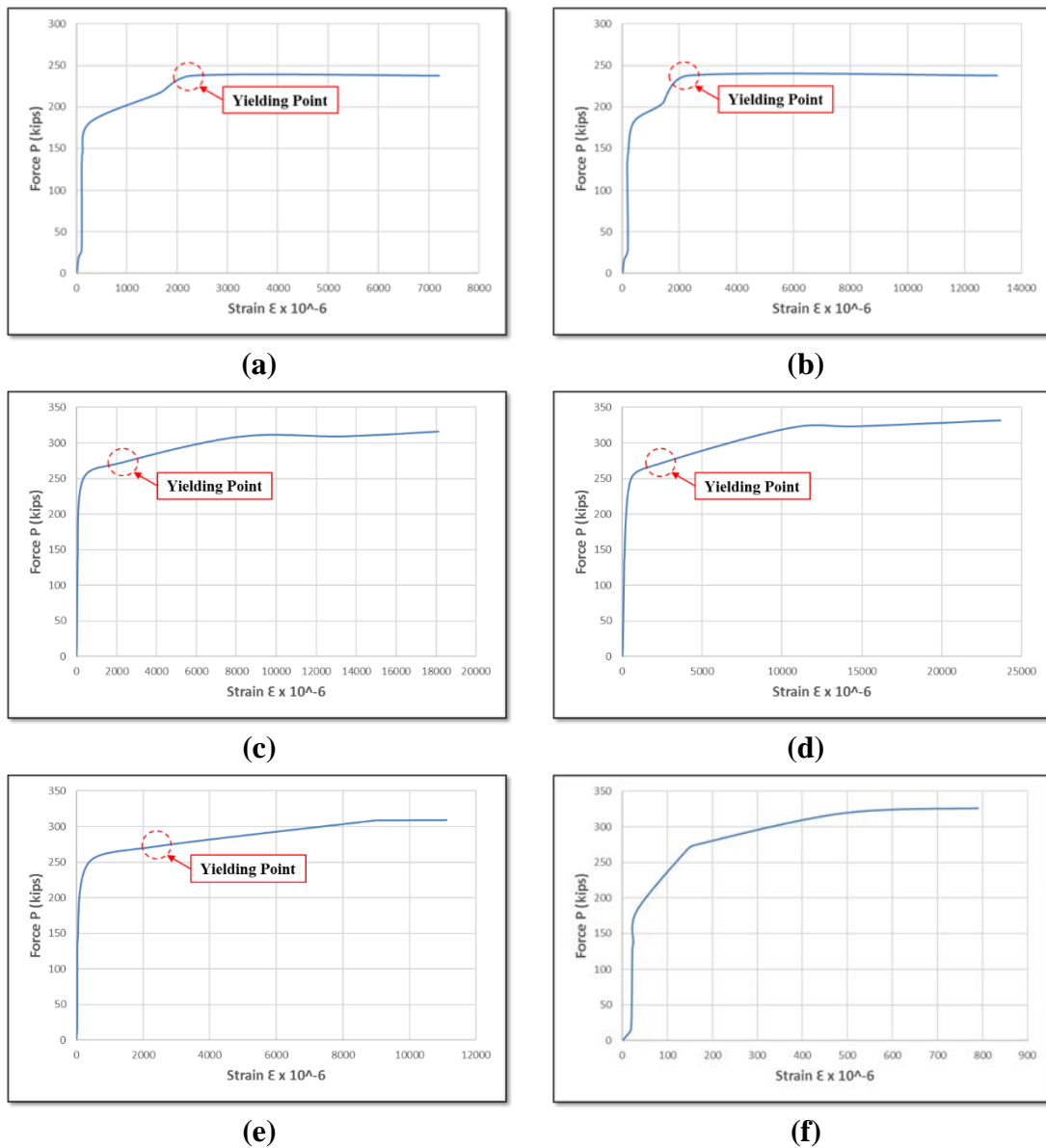


**Figure 4.4. Strain Behavior of Specimen ITBC-0-T-2M Rebars :**

**(a) Force-strain trend for rebar NES1, (b) Force-strain trend for rebar NES2, (c) Force-strain trend for rebar SES1, (d) Force-strain trend for rebar SES2, (e) Force-strain trend for rebar SWS2, (f) Force-strain trend for rebar NM5**

#### 4.4.1.2 Specimen ITBC-30-T-2M

The reaction force-displacement curve for Specimen ITBC-30-T-2M is shown in Figure 4.5. As shown in Figure 4.7(a), flexural crack Crack1 was first observed at a load of 128 kips. Subsequently, flexural shear cracks (Cracks 2 to 4) were observed at a load

from 187 kips to 230 kips. The first yielding of transverse stirrups occurred in the northeast end overhang part of the specimen at a support reaction of 321 kips. Subsequently, the rebars located between the support and exterior loading pads, NES9 and SES8, yielded at a support reaction force of 346 kips and 351 kips, respectively. The strain profile of these stirrups is shown in Figures 4.9(d) and 4.9(e), respectively. The flexural shear crack pattern observed at yielding of the transverse stirrups at the north and south ends are shown in Figure 4.7 (b) and Figure 4.7 (c), respectively. The maximum flexural shear crack width at yielding was measured as 0.013 in.

As shown in Figure 4.7(d), diagonal cracks Crack5 and Crack6 were observed on the end face of the ledge at a support reaction of 346 kips and 358 kips, respectively. Furthermore, crack Crack7 occurred between the ledge and the web on the end face of the specimen at a support reaction of 381 kips, as shown in Figure 4.7(e). The width of crack Crack7 increased significantly at a peak support reaction of 384 kips and the load carrying capacity of the specimen started to drop. The peak support reaction of 384 kips corresponds to an individual actuator load (shear load) of 256 kips. The failure mode of the specimen was primarily attributed to the shear failure caused by the yielding of the shear reinforcements, followed by the formation of wide cracks between the ledge and the web at both the end face overhang parts of the ITBC specimen due to the failure of the transverse rebars at the end. The north and south ends of the test specimen at failure are shown in Figure 4.7(f) and Figure 4.7(g), respectively. The maximum flexural shear crack width at peak was measured as 0.021in [Figure 4.7(h)]. The strain profiles of longitudinal rebars, ledge stirrups and hanger stirrups are shown in Figure 4.9.

#### **4.4.1.3 Specimen ITBC-30-S-2M**

As shown in Figure 4.6, the reaction force obtained from the load cell was plotted against the displacement obtained from the LVDT to get the complete load-displacement curve for Specimen ITBC-30-S-2M. As shown in Figure 4.8(a), flexural crack Crack1 was first observed at a load of 127 kips. Subsequently, flexural shear cracks (Cracks 2 to 5) were observed at a load of 190 kips. The first yielding of transverse stirrups occurred in the north-east end overhang part (NES1) of the specimen at a support reaction of 332 kips. Subsequently, the rebars located between the support and exterior loading pads, NWS8 and SES8, yielded at a support reaction force of 347 kips and 354 kips, respectively. The strain profile of these stirrups is shown in Figures 4.10(c) and 4.10(d), respectively.

The flexural shear crack pattern observed at yielding of the transverse stirrups at the north and south ends are shown in Figure 4.8(b) and 4.8(c), respectively. The maximum flexural shear crack width at yielding was measured as 0.01 in. As shown in Figure 4.8(d), diagonal cracks Crack6 and Crack7 were observed on the end face of the ledge at a support reaction of 344 kips and 356 kips, respectively. Most of the shear reinforcements in the over hang portion were yielded at a support reaction of 350 kips to 379 kips. Furthermore, crack Crack8 occurred between the ledge and the web on the end face of the specimen at a

support reaction of 379 kips, as shown in Figure 4.8(e). The width of crack Crack8 increased significantly at a peak support reaction of 381 kips and the load carrying capacity of the specimen started to drop. The peak support reaction of 381 kips corresponds to an individual actuator load (shear load) of 254 kips. The failure mode of the specimen was primarily attributed to the shear failure caused by the yielding of the shear reinforcements, followed by the separation of the ledge from the web at both end face overhang parts of the ITBC specimen due to the failure of the transverse rebars at the end. The test specimens at failure are shown in Figure 4.8(f) and Figure 4.8(g), respectively. The maximum flexural shear crack width at peak was measured as 0.016 in [Figure 4.8(h)]. The strain profiles of longitudinal rebars, ledge stirrups and hanger stirrups are shown in Figure 4.11.

From the strain values of both the 30° skewed specimens it can be inferred that the strain of longitudinal rebars and ledge stirrups at peak load are less than the yielding strain, 0.0023. Therefore, the specimen was safe in flexure and also in other local modes. Only yielding happens in the hanger stirrups during the test.

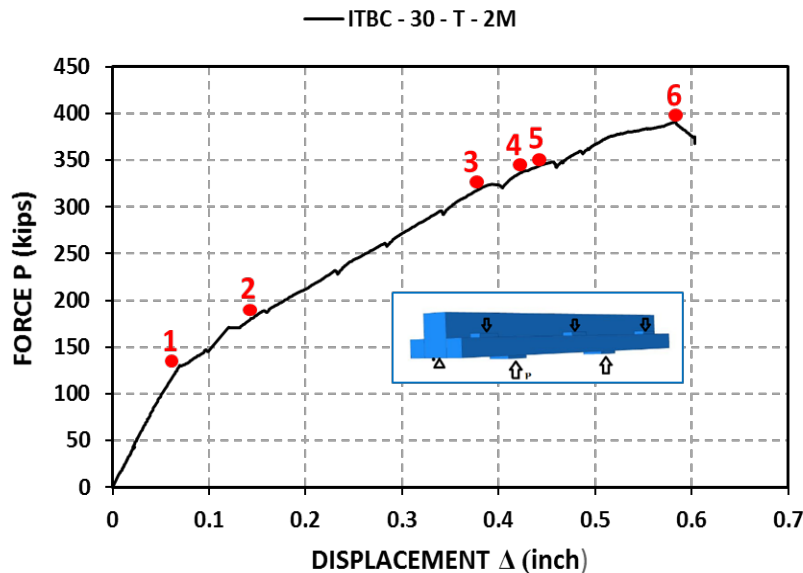


**Figure 4.5. Force-displacement Curve of ITBC-30-T-2M:**

- 1: First flexure crack at 128 kips, 2: First flexural shear crack at 187 kips, 3: Yielding of transverse rebars at the end face (beyond the shear span) at 321 kips, 4: Yielding of transverse rebars at shear span region at 346 kips, 5: Diagonal crack appears in the ledge at the end face at 346 kips, 6: Peak load at 384 kips**

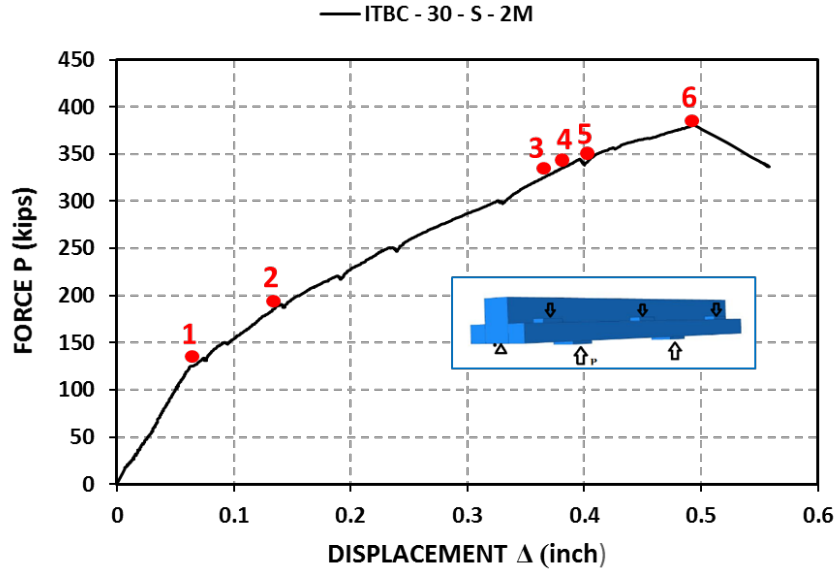
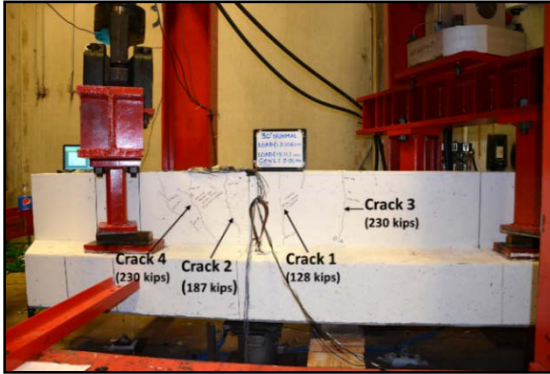


Figure 4.6. Force-displacement Curve of ITBC-30-S-2M:

- 1: First flexure crack at 127 kips, 2: First flexural shear crack at 190 kips, 3: Yielding of transverse rebars at the end face (beyond the shear span) at 332 kips, 4: Diagonal crack appears in the ledge at the end face at 344 kips, 5: Yielding of transverse rebars at shear span region at 347 kips, 6: Peak load at 381 kips



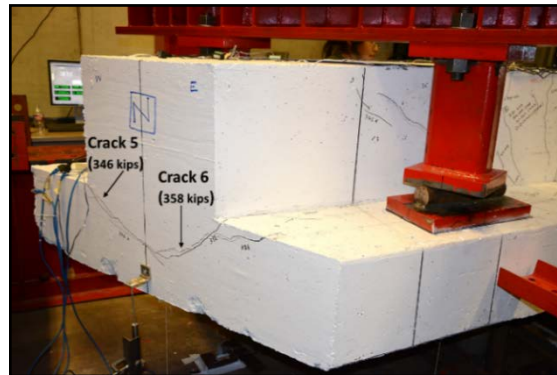
(a)



(b)



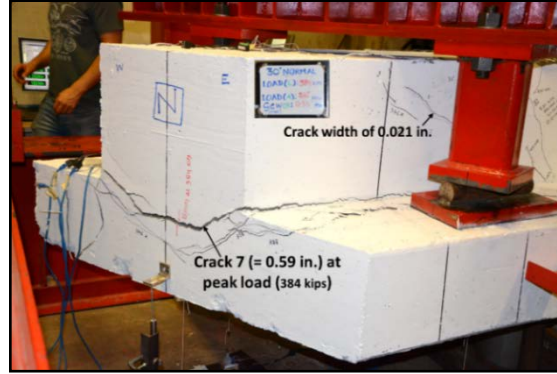
(c)



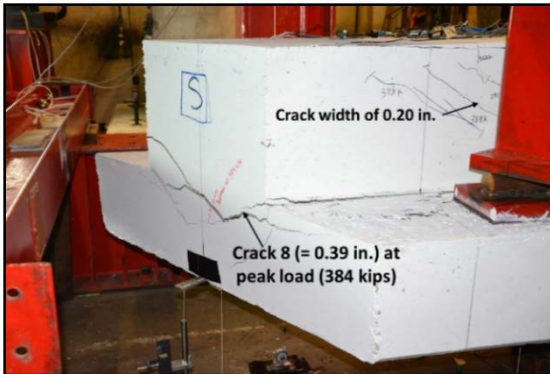
(d)



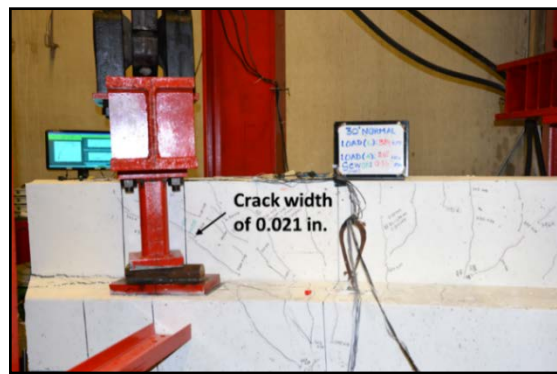
(e)



(f)



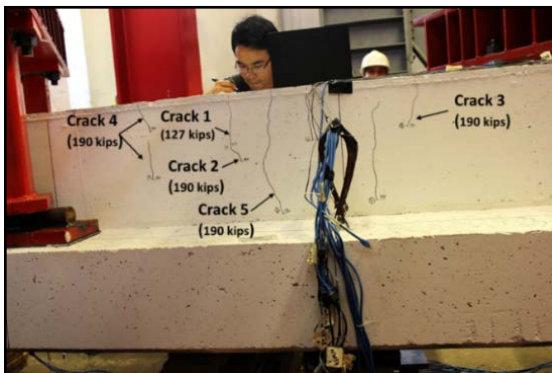
(g)



(h)

**Figure 4.7. Cracking of Specimen ITBC-30-T-2M:**

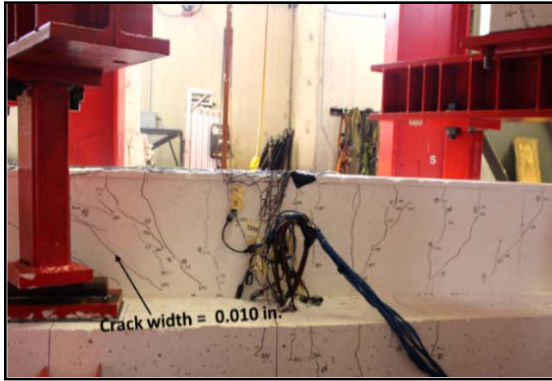
(a) Flexure and flexure shear cracks, (b) Flexural shear crack at yielding on north face, (c) Flexural shear crack at yielding on south face, (d) Diagonal crack at the end face of the ledge, (e) Cracks between the ledge and the web in the end face of the specimen, (f) North face of the specimen at failure, (g) South face of the specimen at failure and (h) Maximum shear crack width at peak



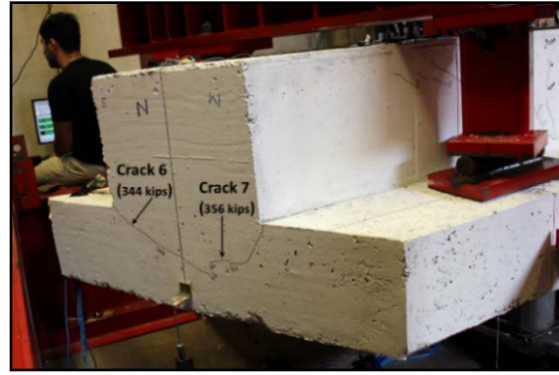
(a)



(b)



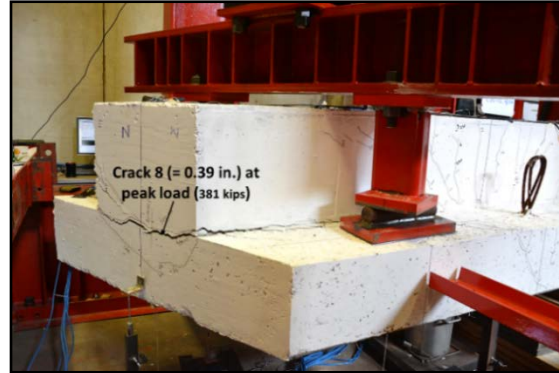
(c)



(d)



(e)



(f)



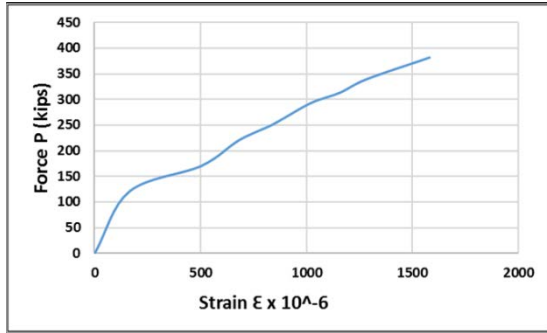
(g)



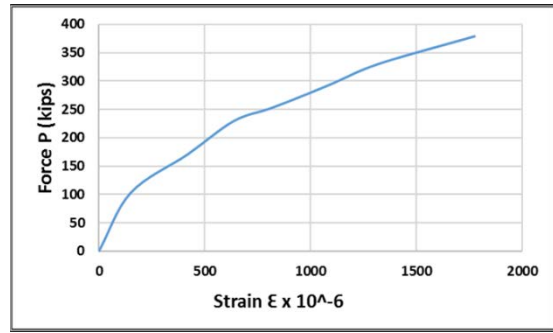
(h)

**Figure 4.8. Cracking of Specimen ITBC-30-S-2M:**

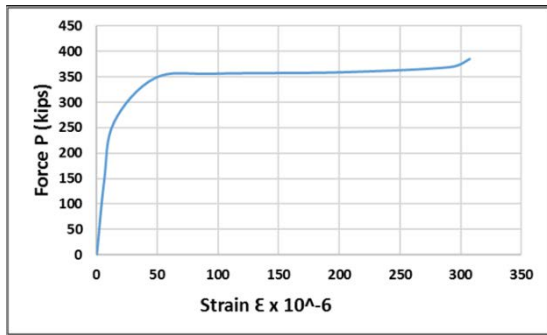
(a) Flexure and flexure shear cracks, (b) Flexural shear crack at yielding on north face, (c) Flexural shear crack at yielding on south face, (d) Diagonal crack at the end face of the ledge, (e) Cracks between the ledge and the web in the end face of the specimen, (f) North face of the specimen at failure, (g) South face of the specimen at failure and (h) Maximum shear crack width at peak



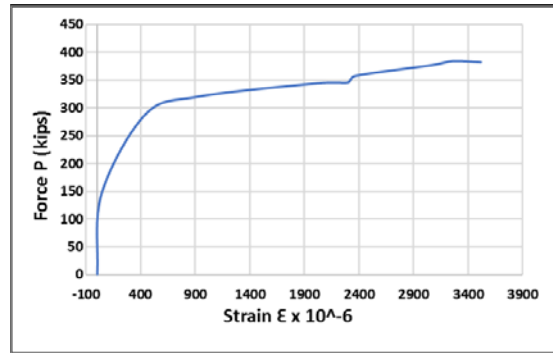
(a)



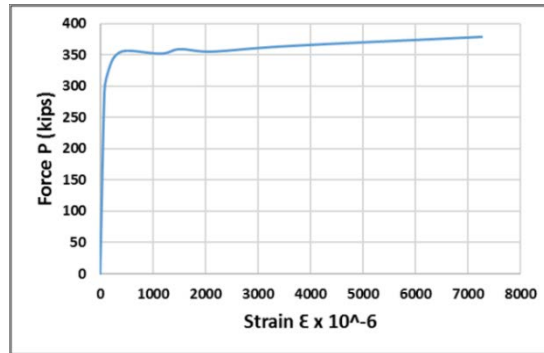
(b)



(c)



(d)



(e)

**Figure 4.9. Strain Behavior of Specimen ITBC-30-T-2M Rebars:**

- (a) Strain profile of a longitudinal bar NL, (b) Strain profile of a longitudinal bar SL, (c) Strain profile of a ledge rebar SM5 at loading point, (d) Strain profile of NES9, (e) Strain profile of SES8**

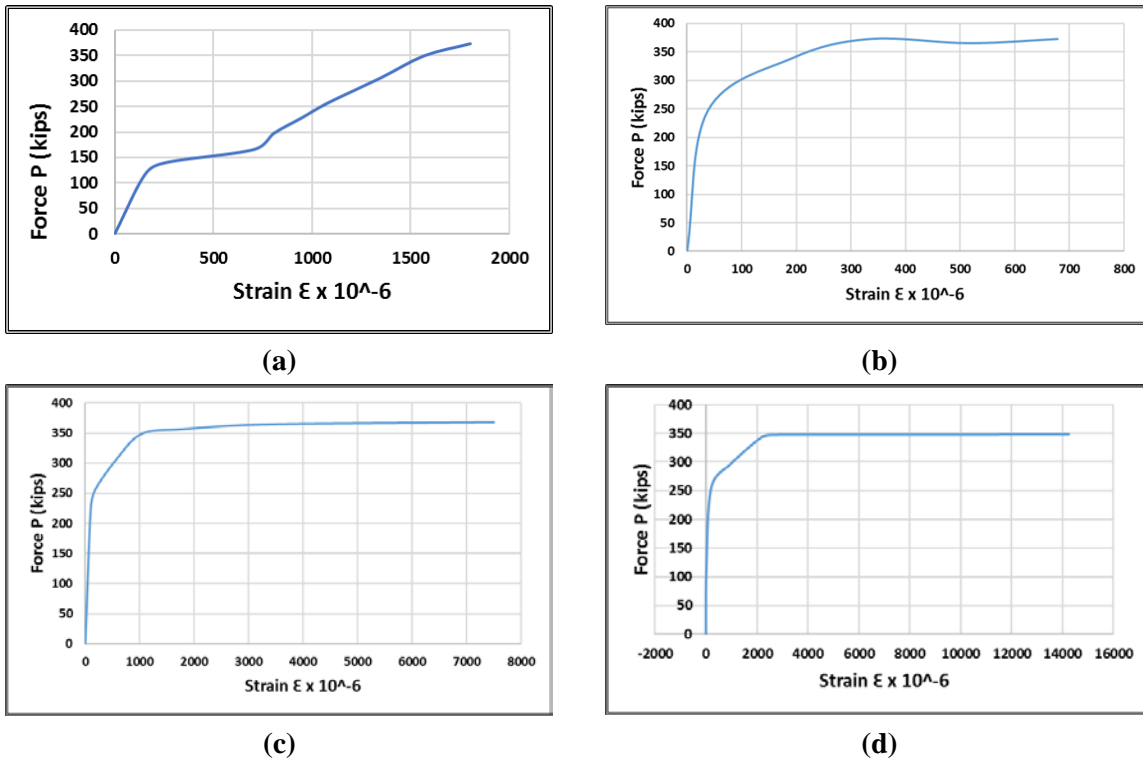


**Figure 4.10. Strain Behavior of Specimen ITBC-30-S-2M Rebars:**  
**(a) Strain profile of a longitudinal bar at north side, (b) Strain profile of a ledge rebar at north side at loading point, (c) Strain profile of SES8, (d) Strain profile of NES1**

#### 4.4.1.4 Specimen ITBC-45-T-2M

Figure 4.11 shows the reaction force-displacement curve for Specimen ITBC-45-T-2M. As shown in Figure 4.13(a), the first flexural crack Crack1 was first observed at a load of 115 kips. Subsequently, flexural shear cracks (Cracks 2 to 5) were observed at a load from 165 kips to 200 kips as shown in Figure 4.13(b). The loads applied by the actuators were progressively increased and the strains in the longitudinal reinforcements (A bars), ledge stirrups (M bars) and hanger stirrups (S bars) were monitored. The transverse stirrups in the north end overhang part of the specimen started yielding at a support reaction of 271 kips. At this loading stage, the strains in the shear stirrups (NES1) reached a value greater than 0.0023, which is the yielding strain of the rebars. Subsequently, the rebars located between the support and exterior loading pads, NES7 and NWS8, yielded at a support reaction force of 324 kips and 336 kips, respectively.

As shown in Figure 4.13(c), diagonal crack Crack 6 was observed on the long end face of the ledge at a support reaction of 255 kips. Furthermore, crack Crack7 occurred on the end face of the specimen at a support reaction of 300 kips, as shown in Figure 4.13(d). Crack Crack8 occurred on the short end face of the ledge at a support reaction of 358 kips as shown in Figure 4.13(e). The width of cracks Crack6 and Crack7 increased significantly

at a peak support reaction of 369 kips and the load carrying capacity of the specimen started to drop. The peak support reaction of 369 kips corresponds to shear load of 246 kips. The failure mode of the specimen was primarily attributed to the shear and torsion failure caused by the yielding of the transverse reinforcements. Moreover, a large number of wide cracks were observed at both end faces of the specimen. The north and south ends of the test specimen at failure are shown in Figure 4.13(f) and 4.13(g), respectively. The maximum flexural shear crack width at peak was measured as 0.020 in Figures 4.13(h) and 4.13(i). The strain profiles of longitudinal rebars, ledge stirrups and hanger stirrups are shown in Figure 4.15.

#### **4.4.1.5 Specimen ITBC-45-S-2M**

As shown in Figure 4.12, the reaction force obtained from the load cell was plotted against the net displacement obtained from the LVDT to get the complete load-displacement curve for Specimen ITBC-45-S-2M. As shown in Figure 4.14(a), flexural cracks Crack1 and Crack2 were first observed at a support reaction of 132 kips. Subsequently, a flexural shear crack (Crack3) was observed at a support reaction of 164 kips, as shown in Figure 4.14(b). The loads applied by the actuators were progressively increased and the strains in the longitudinal reinforcements (A bars), ledge stirrups (M bars) and hanger stirrups (S bars) were monitored.

The shear stirrups in the overhang part started yielding at a support reaction of 293 kips. At this loading stage, the strains in the shear stirrups (NES1) reached values greater than 0.0023, which is the yielding strain of the rebar. Subsequently, the rebars located between the support and exterior loading pads, NES8 and NES7, yielded at a support reaction force of 320 kips and 324 kips, respectively. The strain profile of some of these shear stirrups is shown in Figure 4.15.

As shown in Figures 4.14(c) and 4.14(d), diagonal cracks Crack4 and Crack5 were observed on the end face of the ledge at a support reaction of 251 kips and 295 kips, respectively. The transverse reinforcements in the overhang portion (NES8, SWS7, SES8 and SES9) were yielded at a support reaction of 295 kips to 361 kips. Furthermore, crack Crack6 occurred between the ledge and the web on the end face of the specimen at a support reaction of 320 kips, as shown in Figure 4.15(e). The width of crack Crack6 increased significantly at a peak support reaction of 361 kips and the loads on the specimen started to drop. The peak support reaction of 361 kips corresponds to an individual actuator load (shear load) of 241 kips. The failure mode of the specimen was primarily attributed to the shear failure caused by the yielding of the shear reinforcements and with a large number of torsional cracks at both ends of the specimen. The north and south ends of the test specimen at failure are shown in Figures 4.14(f) and 4.14(g), respectively. The maximum flexural shear crack width at peak was measured as 0.018 in. The flexural shear crack pattern at the peak load is shown in Figure 4.14(h). The strain profiles of longitudinal rebars, ledge stirrups and hanger stirrups are shown in Figure 4.16.

From the strain values of both the 45° skewed specimens, it can be inferred that the strain of longitudinal rebars and ledge stirrups at peak load are less than the yielding strain, 0.0023. Therefore, the specimen has enough flexure capacity. Only yielding happens in the hanger stirrups during the test. In addition, in both the 45° ITBC specimens wide shear and torsional cracks are observed due to higher skew angles, whereas Such cracks are not encountered in case of 30° ITBC specimens.

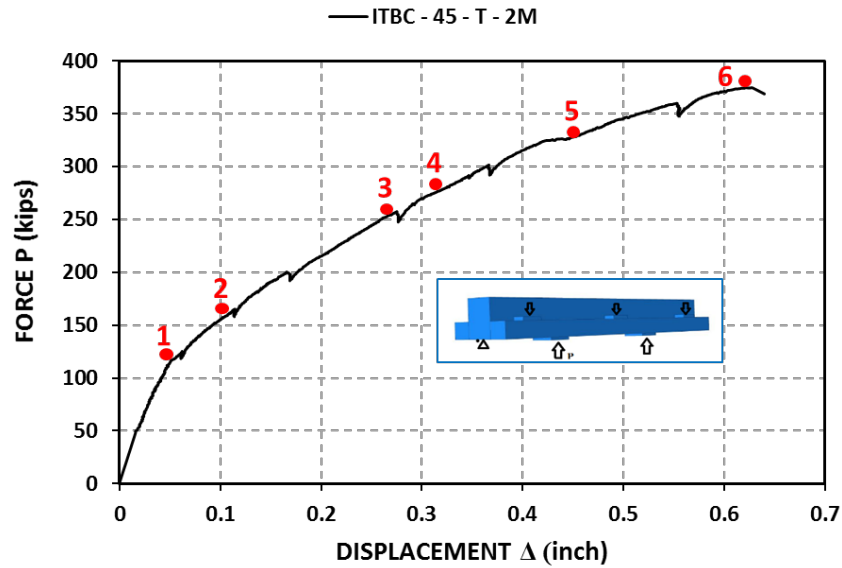


**Figure 4.11. Force-displacement Curve of ITBC-45-T-2M:**  
**1: First flexure crack at 115 kips, 2: First flexural shear crack at 165 kips, 3: Diagonal crack appears in the ledge at the end face at 255 kips, 4: Yielding of transverse rebars at the end face (beyond the shear span) at 271 kips, 5: Yielding of transverse rebars at shear span region at 324 kips, 6: Peak load at 369 kips**

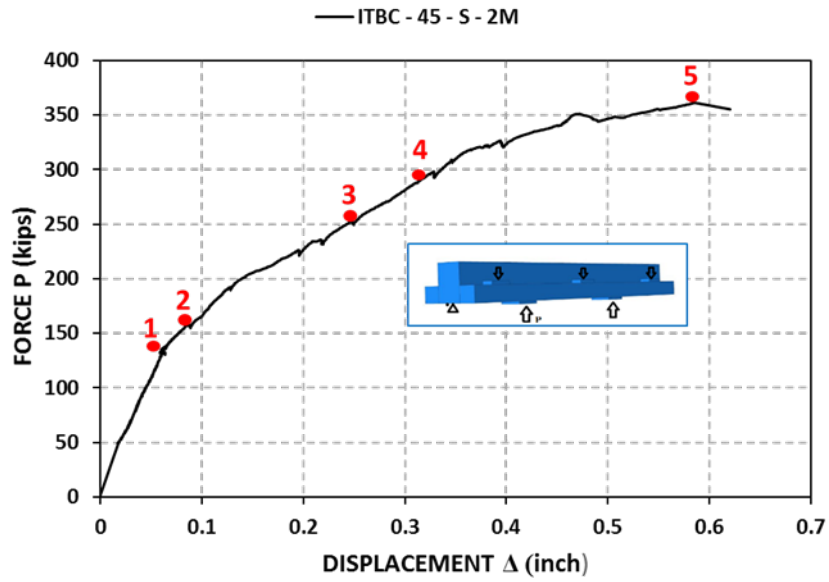
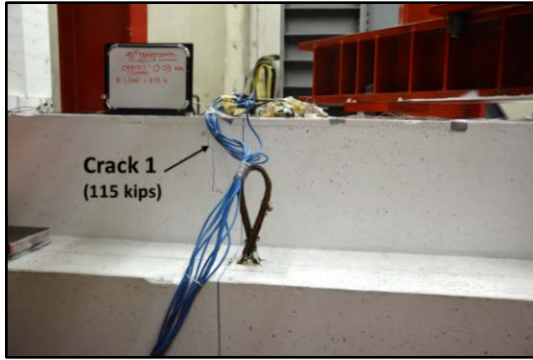
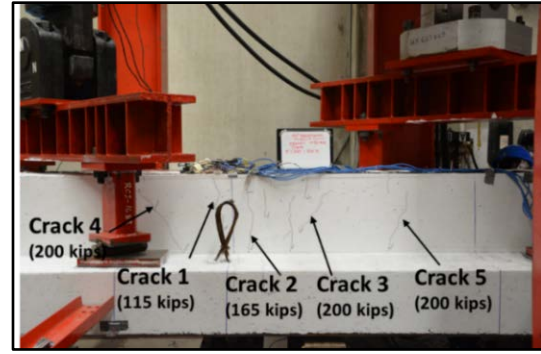


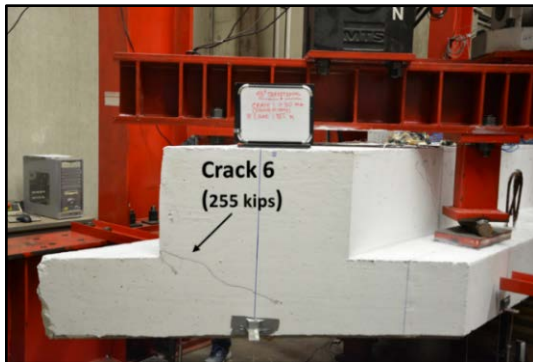
**Figure 4.12. Force-displacement Curve of ITBC-45-S-2M :**  
**1: First flexure crack at 132 kips, 2: First flexural shear crack at 164 kips, 3:**  
**Diagonal crack appears in the ledge at the end face at 251 kips, 4: Yielding of**  
**transverse rebars at 293 kips, 5: Peak load at 361 kips**



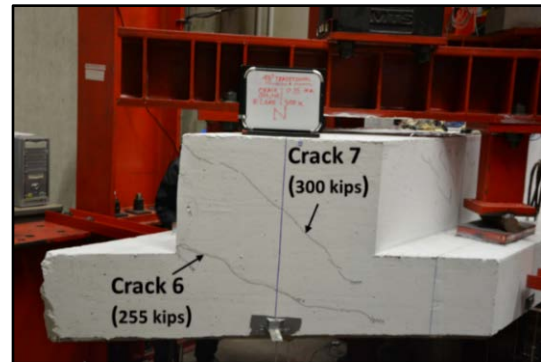
(a)



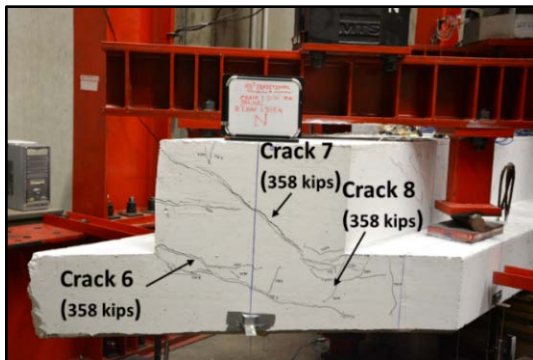
(b)



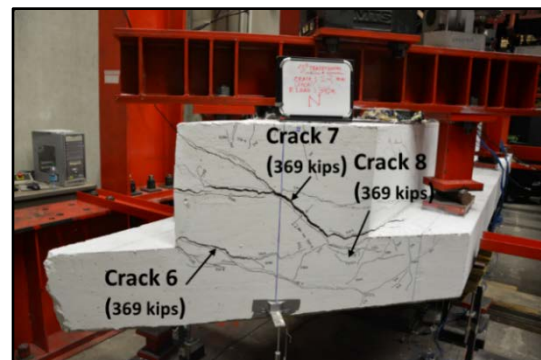
(c)



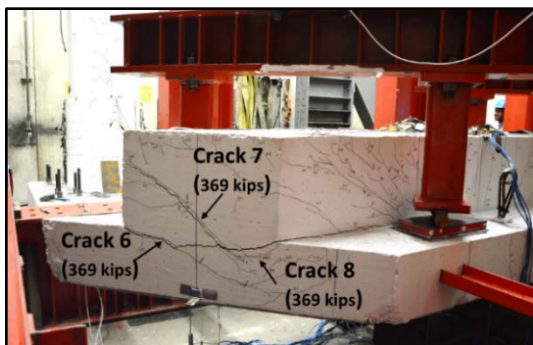
(d)



(e)



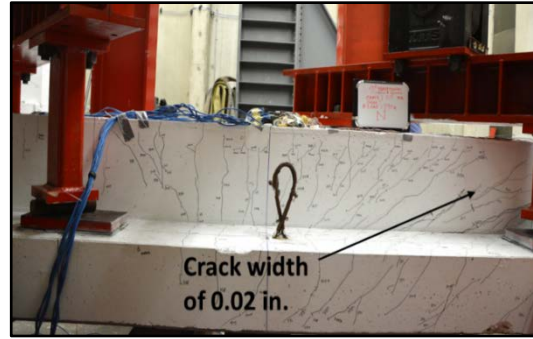
(f)



(g)



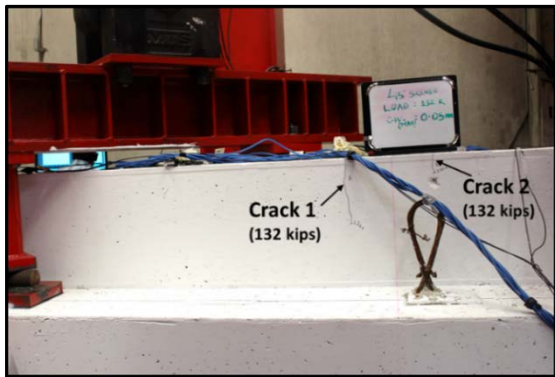
(h)



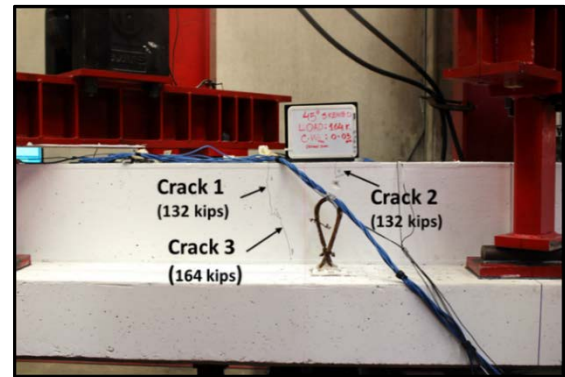
(i)

**Figure 4.13. Cracking of Specimen ITBC-45-T-2M:**

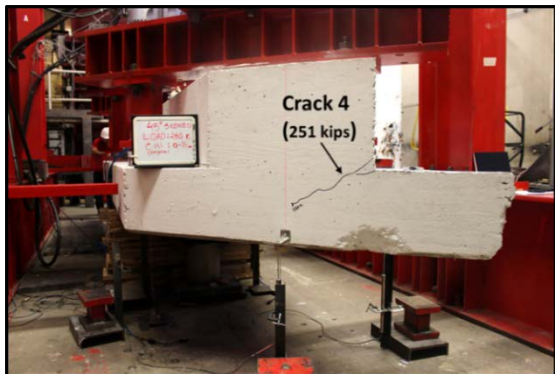
**(a) First flexure crack, (b) Flexure and flexure shear cracks at 200 kips, (c) Diagonal crack at the end face of the ledge at 255 kips, (d) Diagonal crack at the end face of the ledge at 300 kips, (e) Diagonal crack at the end face of the ledge at 358 kips, (f) North face of the specimen at failure, (g) South face of the specimen at failure, (h) Maximum shear crack width at peak at north-east side and (i) Maximum shear crack width at peak at north-west side**



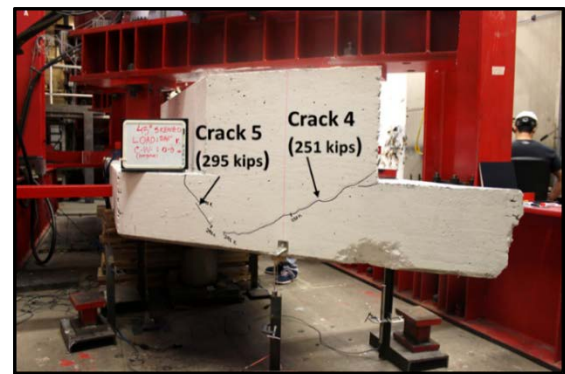
(a)



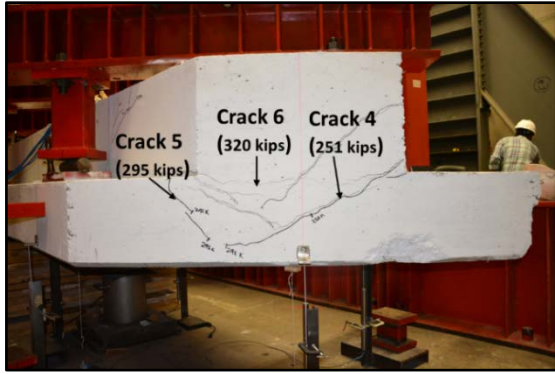
(b)



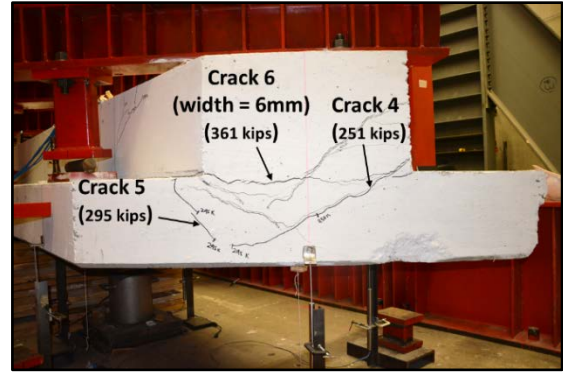
(c)



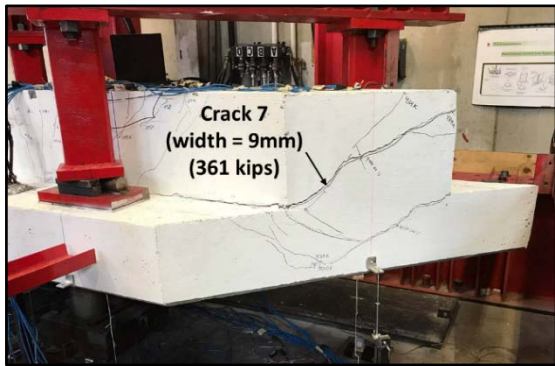
(d)



(e)



(f)



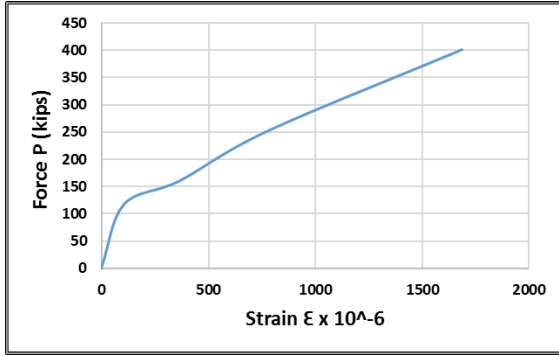
(g)



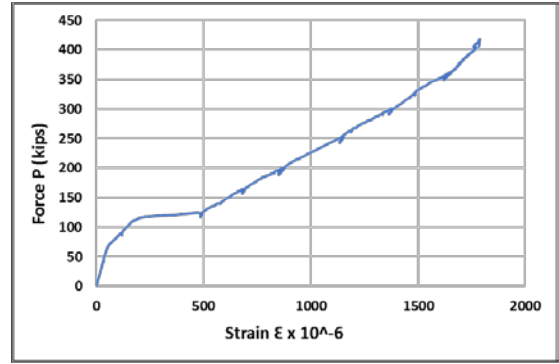
(h)

**Figure 4.14. Cracking of Specimen ITBC-45-S-2M:**

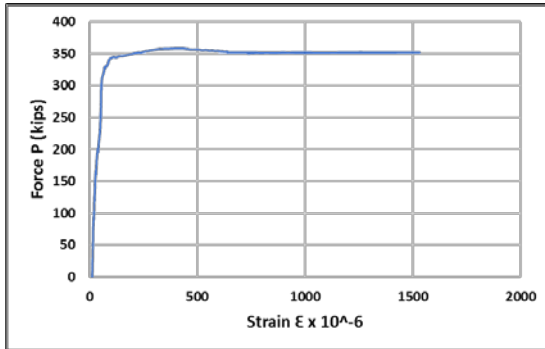
**(a) Flexure crack, (b) Flexure and flexure shear cracks at 164 kips, (c) Diagonal crack at the end face of the ledge at 251 kips, (d) Diagonal crack at the end face of the ledge at 295 kips, (e) Cracks between the ledge and the web in the end face of the specimen, (f) North face of the specimen at failure, (g) South face of the specimen at failure, (h) Maximum shear crack width at peak at north-east side**



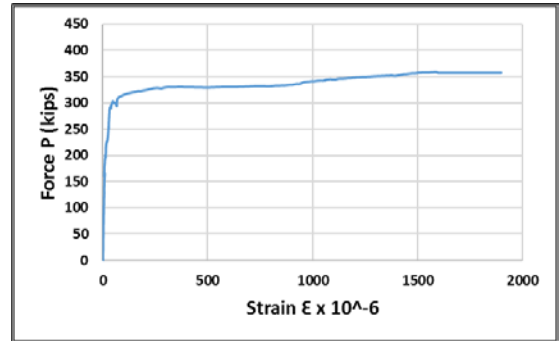
(a)



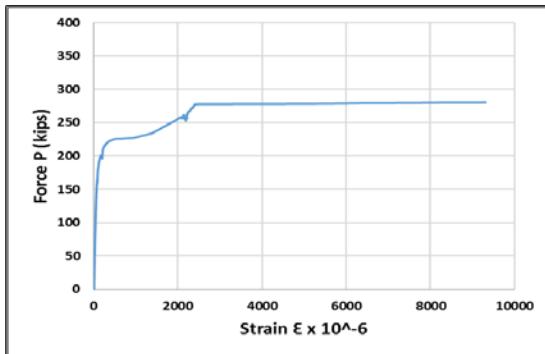
(b)



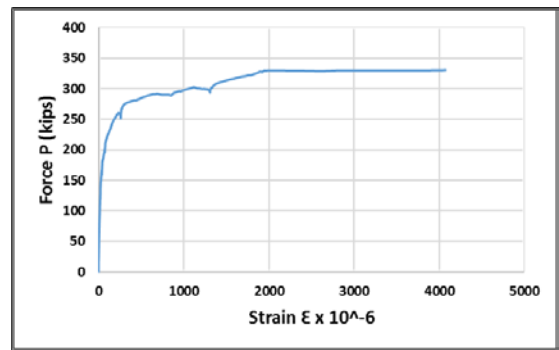
(c)



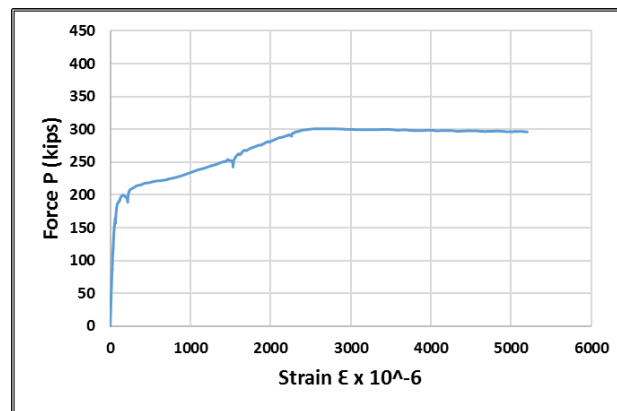
(d)



(e)



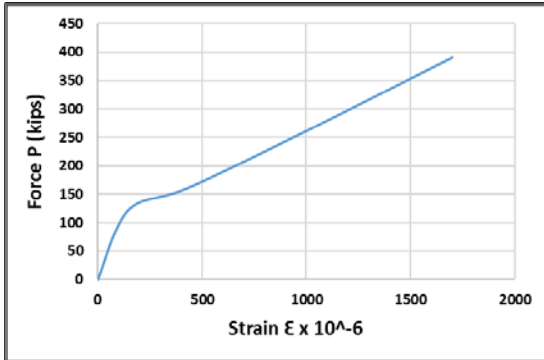
(f)



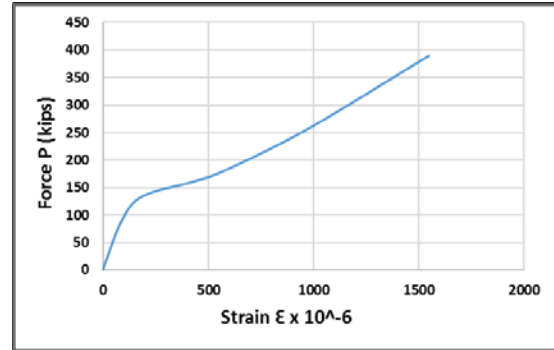
(g)

Figure 4.15. Strain Behavior of Specimen ITBC-45-T-2M Rebars:

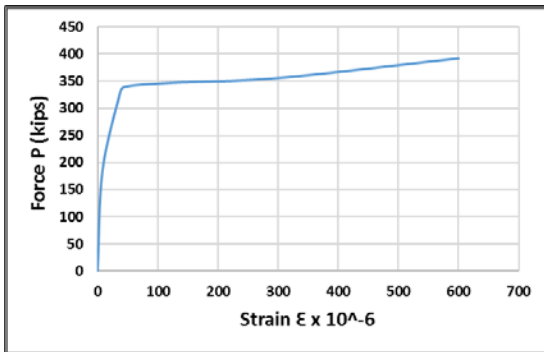
(a) Strain profile of a longitudinal bar NL, (b) Strain profile of a longitudinal bar SL, (c) Strain profile of a ledge rebar NM5, (d) Strain profile of ledge rebar SM5, (e) Strain profile of NES1, (f) Strain profile of NES7 and (g) Strain profile of SWS1



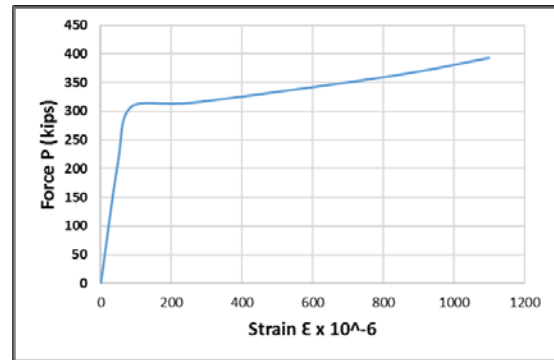
(a)



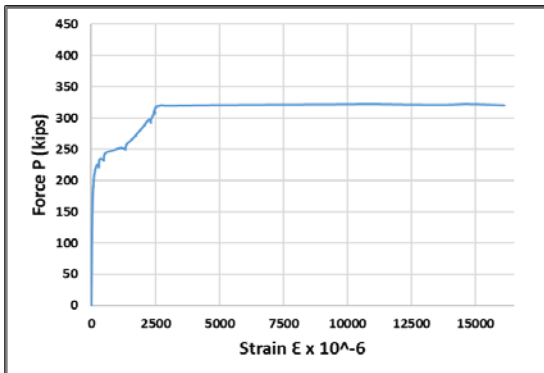
(b)



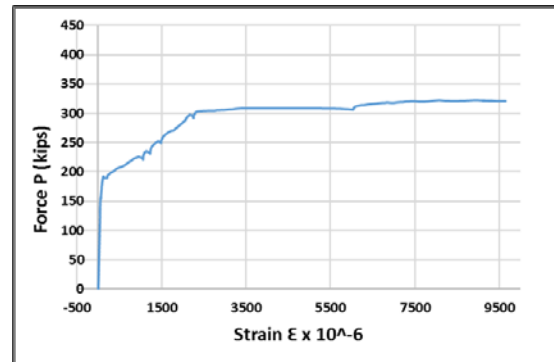
(c)



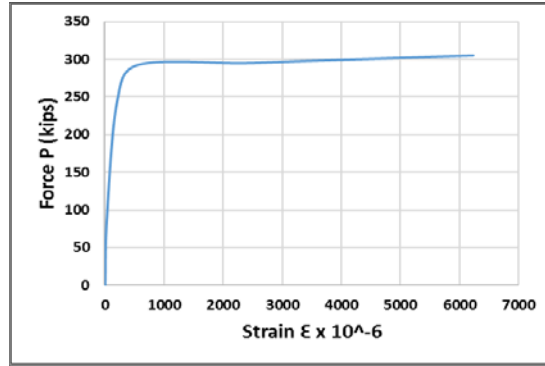
(d)



(e)



(f)



(f)

**Figure 4.16. Strain Behavior of Specimen ITBC-45-S-2M Rebars :**

**(a) Strain profile of a longitudinal bar at north side, (b) Strain profile of a longitudinal bar at South side, (c) Strain profile of a ledge rebar at north side at loading point, (d) Strain profile of ledge rebar at north side at loading point, (e) Strain profile of NES1, (f) Strain profile of NES7 and (g) Strain profile of SWS1**

#### 4.4.1.6 Specimen ITBC-60-T-2M

As shown in Figure 4.17, the reaction force obtained from the load cell was plotted against the net displacement obtained from the LVDTs to get the complete load-displacement curve for Specimen ITBC-60-T-2M. As shown in Figure 4.19(a), flexural cracks C1 and C2 were observed at a support reaction of 105 kips. Subsequently, flexural shear cracks C3 to C12 were observed at a support reaction from 126 kips to 190 kips, as shown in Figure 4.19(b). The loads applied by the actuators were progressively increased and the strains in the longitudinal reinforcements (A bars), ledge stirrups (M bars) and hanger stirrups (S bars) were closely monitored. The first yielding of transverse stirrups occurred in the north end overhang part of the specimen at a support reaction of 171 kips. At this loading stage, the strains in the shear stirrups (NES1), which is located at the north end face, was measured as 0.0023, which was the yielding strain of the S bars. Subsequently, the rebars located between the support and exterior loading pads, NES5 and NES8, yielded at a support reaction force of 234 kips and 294 kips, respectively.

As shown in Figure 4.19(c), diagonal crack C13 was observed on the end face of the ledge (long side) at a support reaction of 150 kips. Furthermore, torsional cracks C14 - C17 occurred on the end face of the test specimen at a support reaction from 157 kips-260 kips, as shown in Figure 4.19(d). Afterward, the width of torsional cracks C13-C17 increased significantly at a peak support reaction of 304 kips and the carrying load of the specimen started to drop. The peak support reaction of 321 kips corresponds to an individual actuator load (shear load) of 202 kips. The failure mode of the specimen was primarily attributed to the torsional failure caused by a large number of torsional cracks and the yielding of the transverse shear reinforcements at both ends of the specimen. Many torsional cracks were observed in both ends of the specimen at failure, which was not

observed in previous tests for smaller skew angle ( $30^{\circ}$  and  $45^{\circ}$ ) inverted-T bent cap specimens. Moreover, the failure of the ledges due to punching shear mechanism was also observed at both ends of the specimen at the peak reaction load. The maximum torsional crack width at the peak was measured as 0.45 inches. The north and south ends of the test specimen at failure are shown in Figure 4.19(e) and 4.19(f), respectively. The maximum flexural shear crack width at peak was measured as 0.020 in. Figure 4.21(a) to Figure 4.21(f) represent the tensile strain trend of selective rebars with respect to the support reaction including hanger stirrups (NES1, NES2 and SWS1), ledge bars (NEM4 and NEM6) and longitudinal bar (NL). The strain gauges which attained the strain value of 0.0023 are considered to be yielded at the corresponding load.

#### **4.4.1.7 Specimen ITBC-60-S-2M**

As shown in Figure 4.18, the reaction force obtained from the load cell was plotted against the net displacement obtained from the LVDTs to get the complete load-displacement curve for Specimen ITBC-60-S-2M. As shown in Figure 4.20(a), flexural crack C1 was observed at a support reaction of 113 kips. Subsequently, flexural shear cracks C2 to C10 were observed at a support reaction from 113 kips to 203 kips, as shown in Figure 4.20(b). The loads applied by the actuators were progressively increased and the strains in the longitudinal reinforcements (A bars), ledge stirrups (M bars) and hanger stirrups (S bars) were monitored. The transverse stirrups (S bars) in the south end overhang part (SWS1) of the specimen started yielding at a support reaction of 210 kips. At this loading stage, the strains in the shear stirrups (SWS1) reached the value greater than 0.0023, which is the yielding strain of the transverse rebars. Subsequently, the rebars located between the support and exterior loading pads (shear span region), SWS5, NES5 and SWS6, yielded at a support reaction force of 245 kips, 262 kips and 267 kips respectively.

As shown in Figure 4.20(c), diagonal crack C11 was observed on the end face of the ledge (long side) at a support reaction of 157 kips. Furthermore, torsional cracks C13 - C16 occurred on the end face of the test specimen at a support reaction from 157 kips to 246 kips, as shown in Figure 4.20(d). Afterward, as the load application is progressively increased, the width of torsional cracks C13-C16 increased significantly up to a peak support reaction of 317 kips and the carrying load of the specimen started to drop. The peak support reaction of 317 kips corresponds to an individual actuator load (shear load) of 212 kips. The failure mode of the specimen was primarily attributed to the torsional failure caused by a large number of torsional cracks and the yielding of the transverse reinforcements at both ends of the specimen. Moreover, the failure of the ledges due to the punching shear mechanism was also observed at both ends of the specimen at the peak reaction load, which was also noticed in the 60-degree skew specimen with traditional reinforcements. The north and south ends of the test specimen at failure are shown in Figures 4.20(e) and 4.20(f), respectively. The punching shear crack profile for the north

and south side ledges are shown in Figures 4.20(g) and 4.20(h), respectively. Such torsional cracks and punching shear mechanism of the ledges were not observed in previous tests for smaller skew angle ( $0^{\circ}$ ,  $30^{\circ}$  and  $45^{\circ}$ ) inverted-T bent cap specimens. The maximum torsional crack width at the peak load was measured as 0.32 inches. The maximum flexural shear crack width at the peak load was measured as 0.020 in.

Figure 4.22(a) to Figure 4.22(f) represent the tensile strain trend of selective rebars with respect to the support reaction including hanger stirrups (NES1, NES2 and SWS1), ledge bars (NEM4 and SWM8) and longitudinal bar (NL). The strain gauges which attained the strain value of 0.0023 are considered to be yielded at the corresponding load. Figure 4.22(a-c) indicate the yielding point for each of the strain gauges which show that the rebars including NES1, NES2, and SWS1 reached the yielding state whereas NEM4, SWM8 and the (north) longitudinal bar remained unyielded [(Figure 4.22(d-f)].

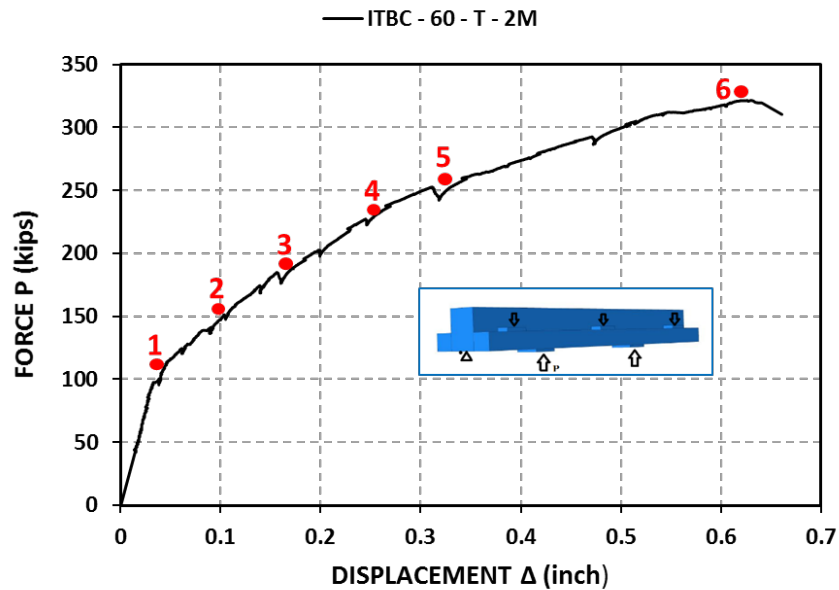


**Figure 4.17. Force-displacement Curve of ITBC-60-T-2M:**

**1: First flexure crack at 105 kips, 2: Diagonal crack appears in the ledge at the end face at 150 kips, 3: Yielding of transverse rebars (S bars) at the end face (outside the shear span) at 171 kips, 4: Yielding of transverse rebars (S bars) at shear span region at 234 kips, 5: Yielding of ledge rebars (M bars) at 254 kips and 6: Peak load at 321 kips**

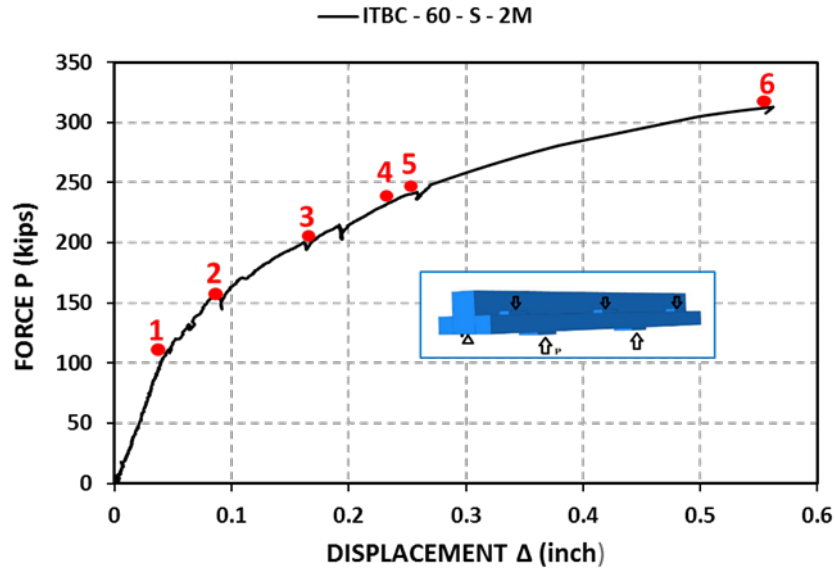
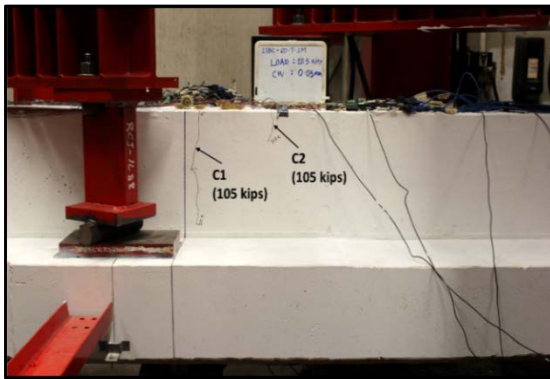
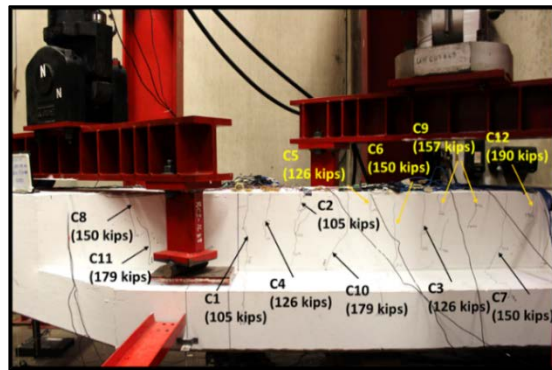


Figure 4.18. Force-displacement Curve of ITBC-60-S-2M:

1: First flexure crack at 113 kips, 2: Diagonal crack appears in the ledge at the end face at 157 kips, 3: Yielding of transverse rebars (S bars) at the end face (outside of the shear span) at 210 kips, 4: Yielding of ledge rebars (M bars) at 238 kips, 5: Yielding of transverse rebars (S bars) at shear span region at 245 kips and 6: Peak load at 317 kips



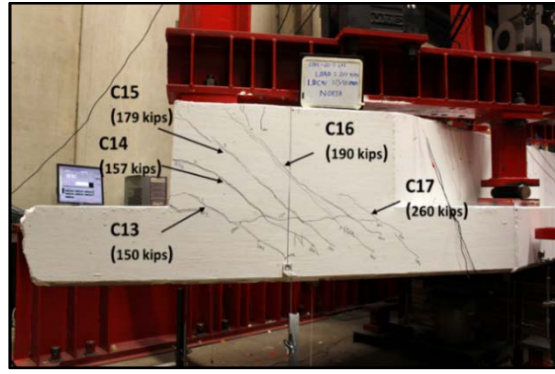
(a)



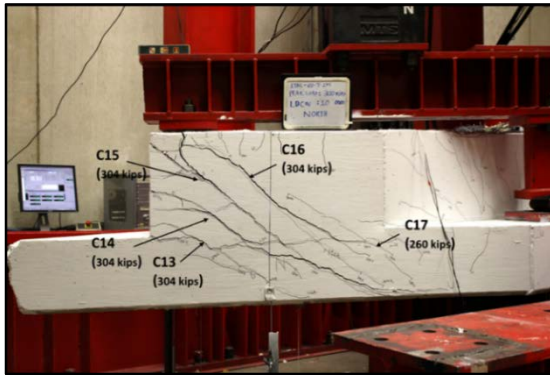
(b)



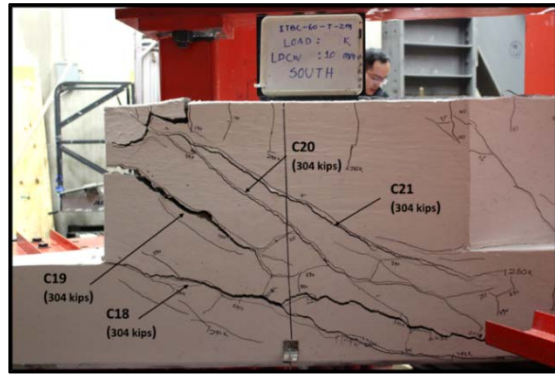
(c)



(d)



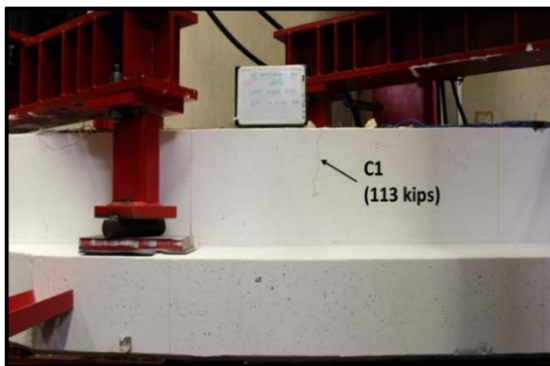
(e)



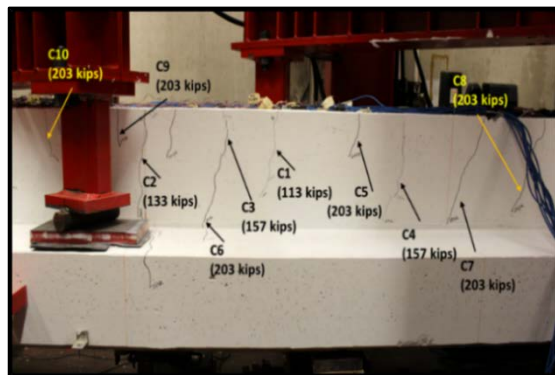
(f)

**Figure 4.19. Cracking of Specimen ITBC-60-T-2M:**

- (a) Flexural cracks at 105 kips (b) Flexural shear cracks at 190 kips (c) Diagonal crack at the end face of the ledge at 150 kips (d) Diagonal cracks at the end face of the ledge at 260 kips (e) North face of the specimen at 304 kips (f) South face of the specimen at 304 kips



(a)



(b)

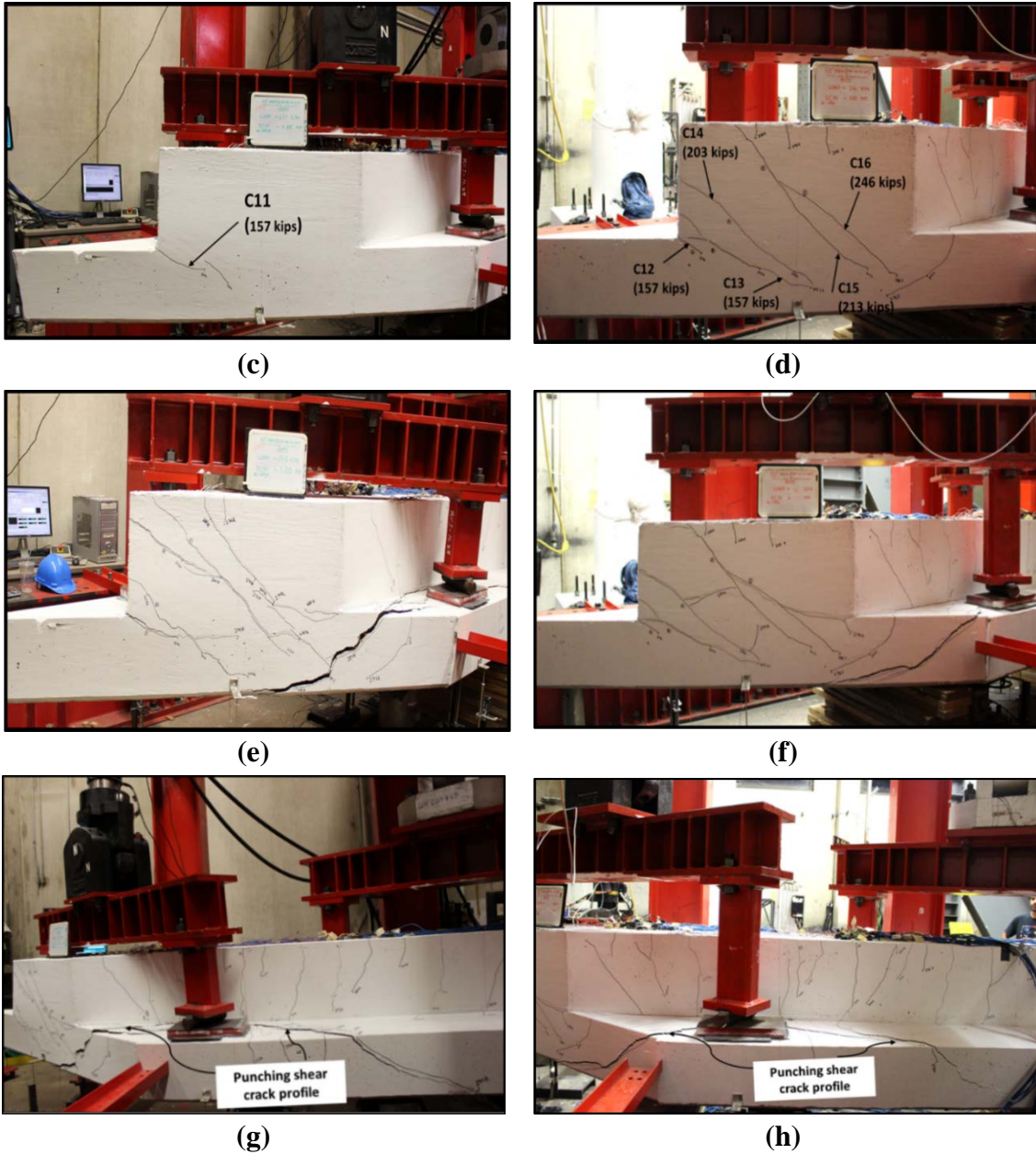
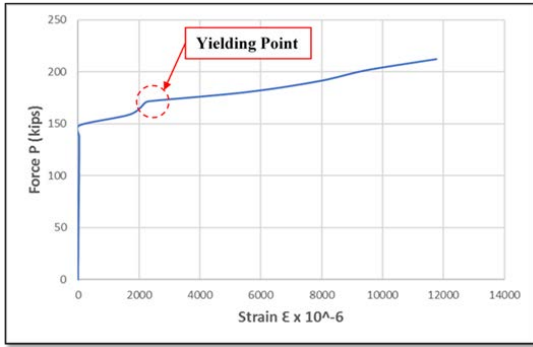
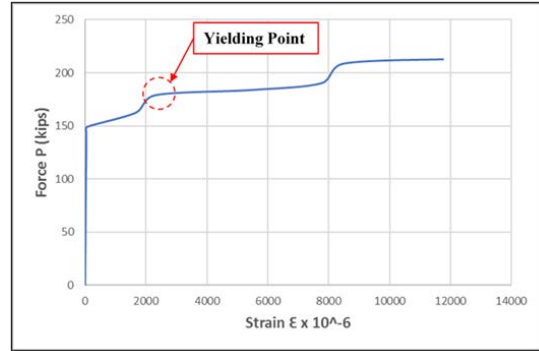


**Figure 4.20. Cracking of Specimen ITBC-60-S-2M:**

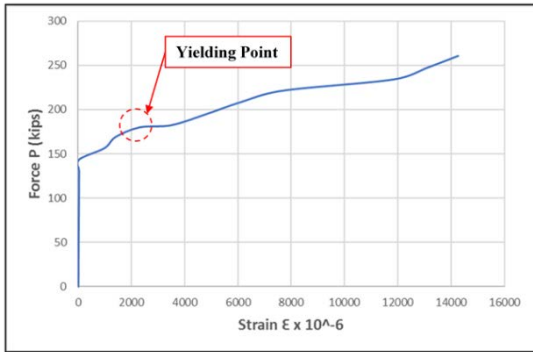
(a) Flexural crack at 113 kips (b) Flexural shear cracks profile at 203 kip (c) Diagonal crack at the end face of the ledge at 157 kips (d) Diagonal cracks at the end face of the ledge at 246 kips (e) North face of the specimen at failure (f) South face of the specimen at failure (g) Punching shear crack profile of the ledge at north side of the specimen (h) Punching shear crack profile of the ledge at south side of the specimen



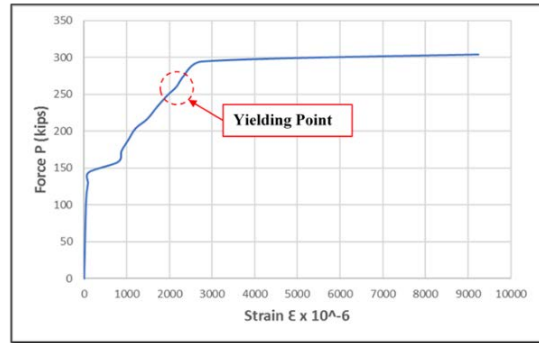
(a)



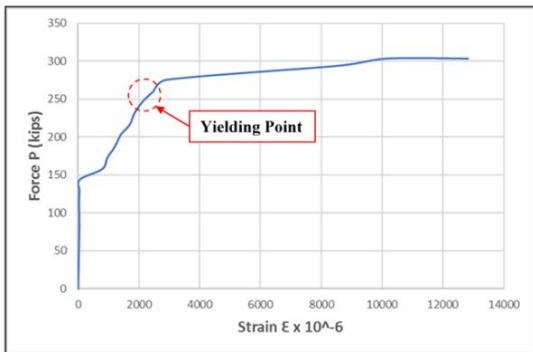
(b)



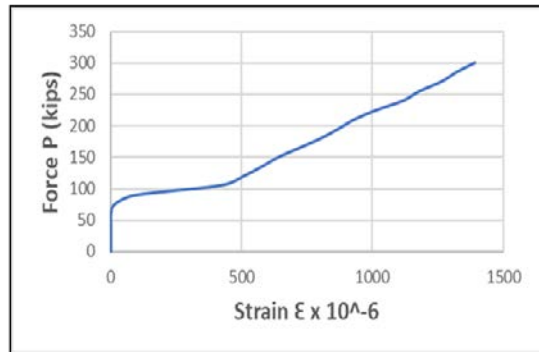
(c)



(d)

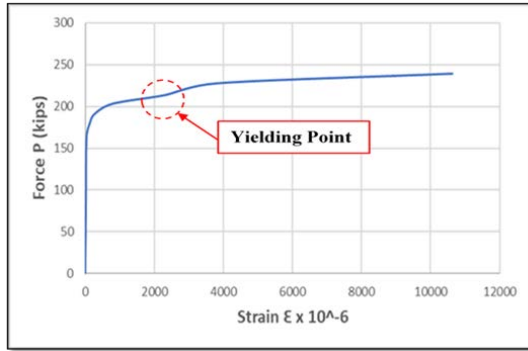


(e)

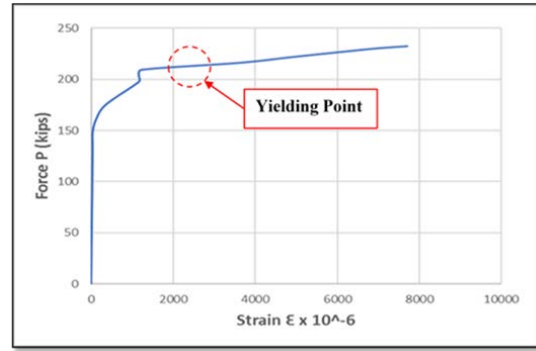


(f)

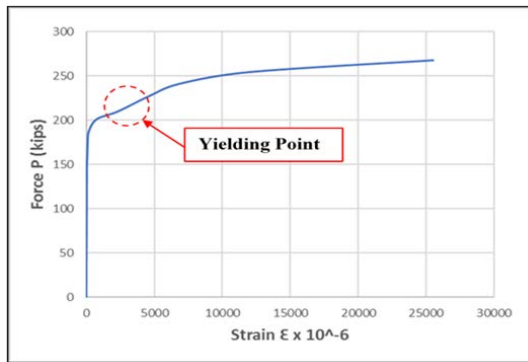
**Figure 4.21. Strain Behavior of Specimen ITBC-60-T-2M Rebar:**  
**(a) Load-strain trend for rebar NES1, (b) Load-strain trend for rebar SWS1, (c) Load-strain trend for rebar NES2, (d) Load-strain trend for rebar NEM4, (e) Load-strain trend for rebar NEM6, (f) Load-strain trend for rebar SL**



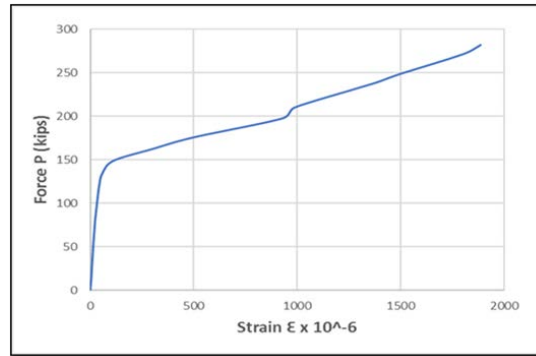
(a)



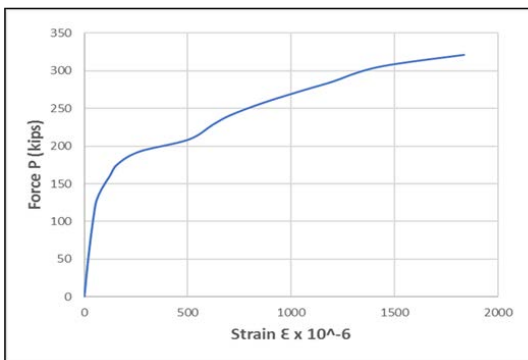
(b)



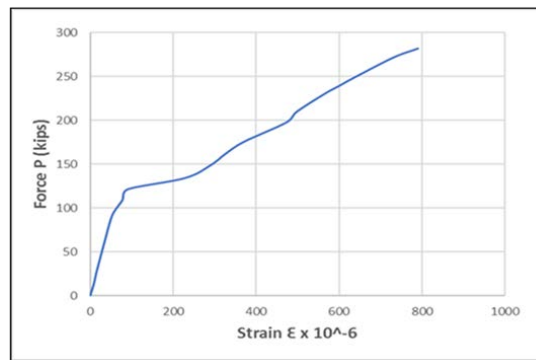
(c)



(d)



(e)



(f)

**Figure 4.22. Strain Behavior of Specimen ITBC-60-S-2M Rebars:**

**(a) Load-strain trend for rebar NES1, (b) Load-strain trend for rebar NES2, (c) Load-strain trend for rebar SWS1, (d) Load-strain trend for rebar NEM4, (e) Load-strain trend for rebar SWM8, (f) Load-strain trend for rebar NL**

#### 4.4.2 Phase 2 Specimens

Phase 2 specimens, which include ITBC-30-T-M, ITBC-30-S-M, ITBC-45-T-M, ITBC-45-S-M, ITBC-60-T-M, and ITBC-60-S-M, have M amount of transverse reinforcement in all the specimens. In addition, in all the Phase 2 specimens, end face reinforcements (U1 and U2 bars) and the G bars are provided in both the ends of inverted-T bridge cap to control the formation of crack. The following sections present the test

results for each of six specimens in terms of load-displacement characteristics, load-strain behavior, crack patterns observed at peak loads and corresponding failure modes.

#### **4.4.2.1 Specimen ITBC-30-T-M**

The reaction force acquired from the load cell was plotted against the net displacement obtained from the LVDTs to obtain the complete load-displacement curve of Specimen ITBC-30-T-M, as shown in Figure 4.23. As shown in Figure 4.25(a), the first flexural crack C1 was observed at a support reaction of 109 kips. Subsequently, with the increase of load, flexural shear cracks C4 to C9 were observed between support reactions of 109 kips and 250 kips, as shown in Figure 4.25(b).

As the loads applied by the actuators were gradually increased, the transverse stirrups (S bars) located in the overhang part started yielding at a support reaction of 292 kips. At this loading stage, the strains in the shear stirrups (NES6) reached a value greater than 0.0023, which is the yielding strain of the transverse rebars. The second set of yielding of transverse stirrups (NES7) occurred at a support reaction of 298 kips.

As shown in Figure 4.25(c), diagonal cracks C10 (on the long side) and C11 (on the short side) were observed on the end face of the ledge at a support reaction of 345 kips and 360 kips, respectively. These cracks were also observed in Specimen ITBC-30-T-2M at a support reaction of 346 kips and 358 kips, respectively, which implies such diagonal cracks on the end face of inverted-T bridge caps do not necessarily depend on the transverse reinforcement ratio.

The width of flexural shear cracks C1–C9 increased significantly as the support reaction reached a peak of 376 kips. The load carrying capacity of the specimen dropped as the peak support reaction was reached. The peak support reaction of 376 kips corresponds to an individual actuator load (shear load) of 251 kips. The failure mode of the specimen was primarily attributed to the shear failure caused by the yielding of shear reinforcements at both ends of the specimen and followed by the initial crushing of the compression strut in the web. The crack pattern of the specimen at peak is shown in Figures 4.25(d)–4.25(e). The maximum flexural shear crack width at the peak load was measured to be 0.15 in.

#### **4.4.2.2 Specimen ITBC-30-S-M**

As shown in Figure 4.24, the reaction force obtained from the load cell was plotted against the net displacement obtained from the LVDTs to obtain the complete load-displacement curve for Specimen ITBC-30-S-M. As indicated in Figure 4.26(a), the first set of flexural cracks C1 and C2 was observed at a support reaction of 98 kips. Subsequently, with the increase of load, flexural shear cracks C2 to C13 were observed between support reactions of 98 kips and 250 kips, as shown in Figure 4.26(b).

With the progressive increase of the actuator load, the transverse stirrups (S bars) located in the overhang part started yielding at a support reaction of 295 kips. At this

loading stage, the strains in the shear stirrups (NES6) reached a value greater than 0.0023, which is the yielding strain of the transverse rebars. The second set of yielding of transverse stirrups (NES7) occurred at a support reaction of 299 kips, followed by SWS7 at 316 kips. As shown in Figure 4.26(c), diagonal crack C14 was observed on the end face of the ledge (long side) at a support reaction of 330 kips, where the diagonal crack C15 was observed (Figure 4.26(d)) at 350 kips. These cracks were also encountered in Specimen ITBC-30-S-2M at a support reaction of 344 kips and 356 kips respectively, which implies that such diagonal cracks on the end face of inverted-T bridge caps do not necessarily depend on its transverse reinforcement ratio.

The width of flexural shear cracks C1–C13 increased significantly as the support reaction attained a peak of 371 kips. The load carrying capacity of the specimen dropped as the peak support reaction was reached. The peak support reaction of 371 kips corresponds to an individual actuator load of 247 kips. The failure mode of the specimen was primarily attributed to the shear failure caused by the yielding of shear reinforcements at both ends of the specimen and followed by the initiation of crushing of compression strut in the web. The crack pattern of the specimen at the peak load is shown in Figures 4.26(e)-4.26(j). The maximum flexural shear crack width at the peak load was measured to be 0.18 in.

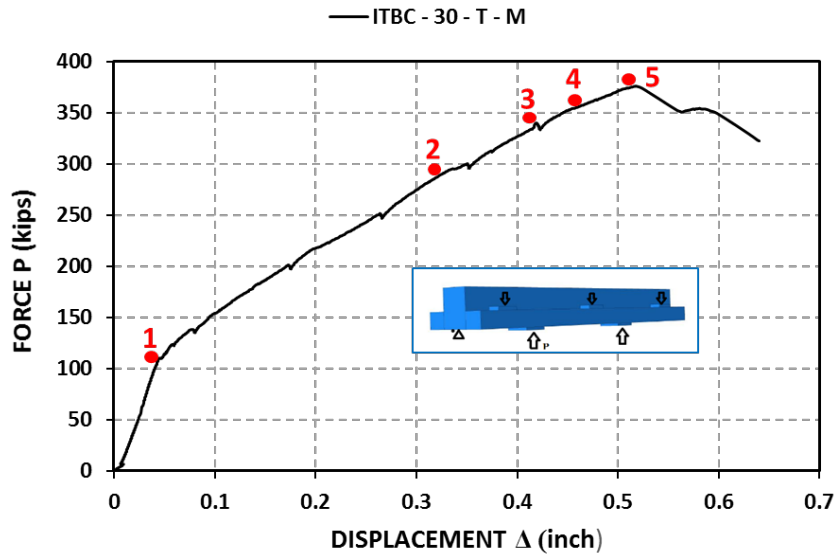


**Figure 4.23. Force-displacement curve of ITBC-30-T-M:**

- 1: First flexure crack at 109 kips, 2: First yielding of transverse rebars (S bars) at 292 kips, 3: Diagonal crack in the ledge at the end face at 345 kips, 4: Diagonal crack in the ledge at the short end face at 360 kips, 5: Peak load at 376 kips**

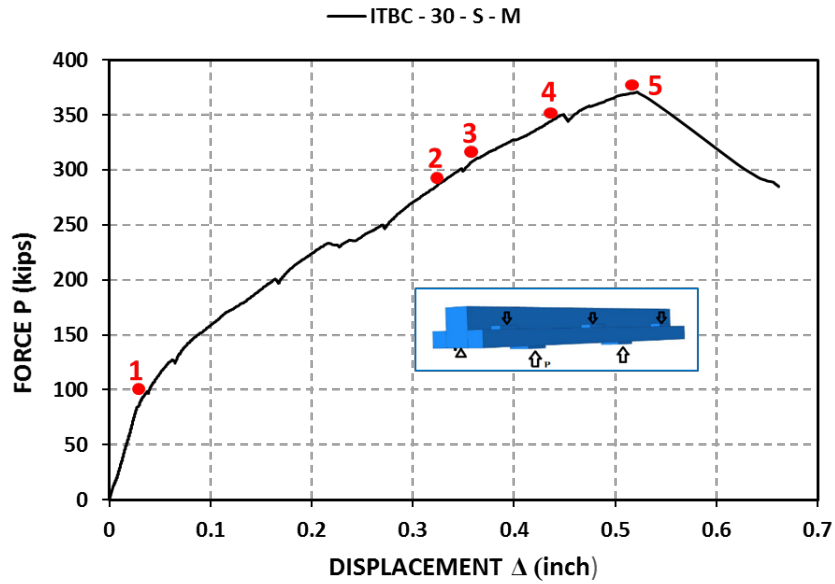
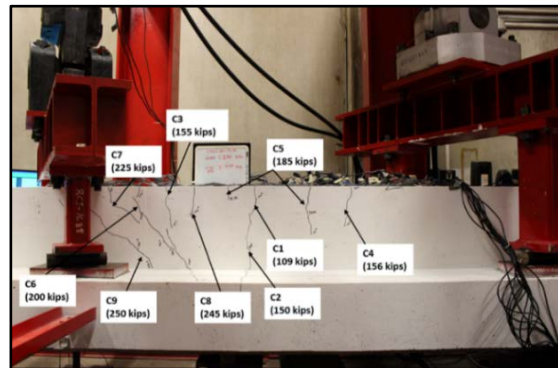


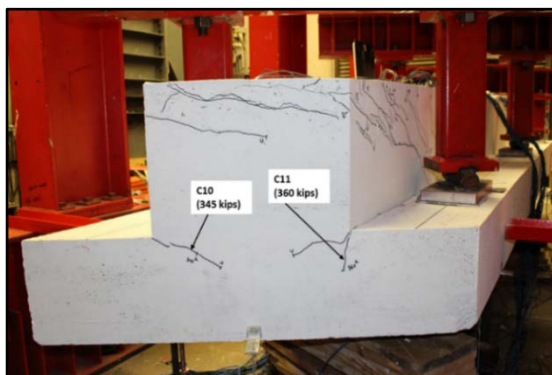
**Figure 4.24. Force-displacement curve of ITBC-30-S-M:**  
**1: First flexure crack at 98 kips, 2: First yielding of transverse rebars (S bars) at 295 kips, 3: Diagonal crack in the ledge at the long end face at 330 kips, 4: Diagonal crack in the ledge at the short end face at 350 kips, 5: Peak load at 371 kips**



(a)



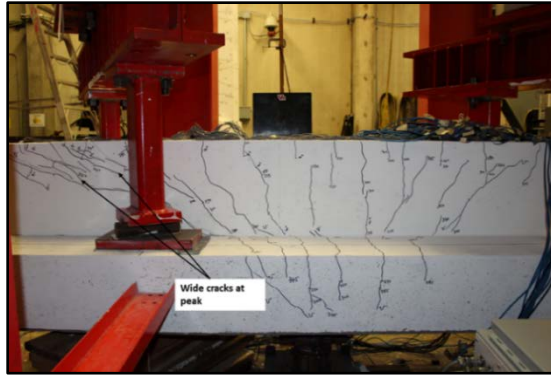
(b)



(c)

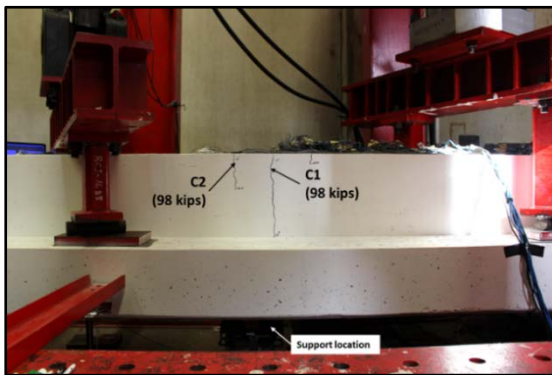


(d)

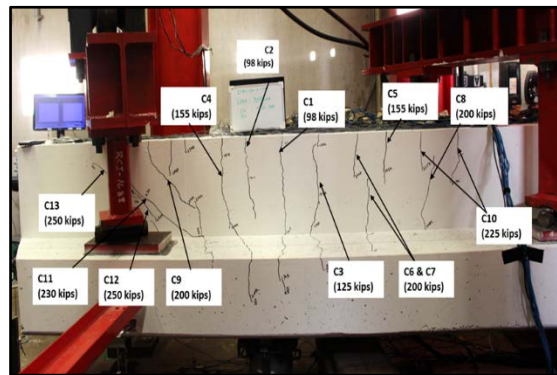


(e)

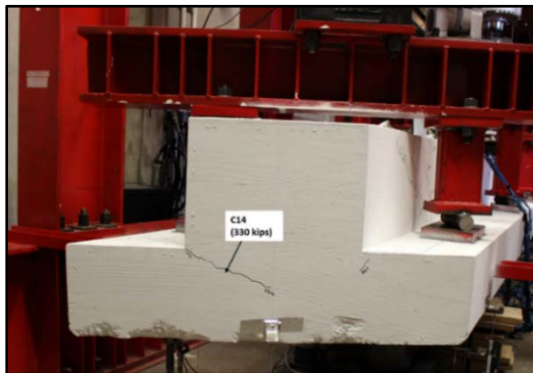
**Figure 4.25. Cracking of Specimen ITBC-30-T-M:**  
**(a) Flexural cracks at 109 kips (b) Flexural shear cracks profile at 250 kips (c) Diagonal crack at the end face of the ledge (d) South-west side of the specimen at peak and (e) South-east side of the specimen at peak**



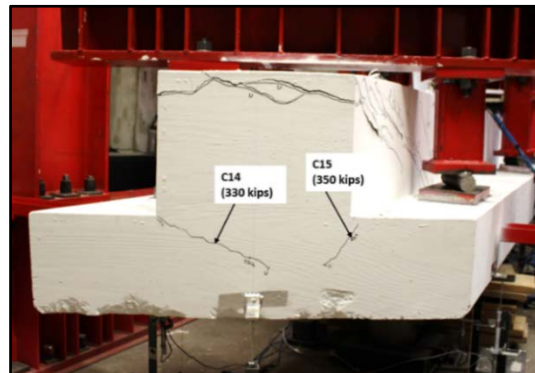
(a)



(b)



(c)



(d)

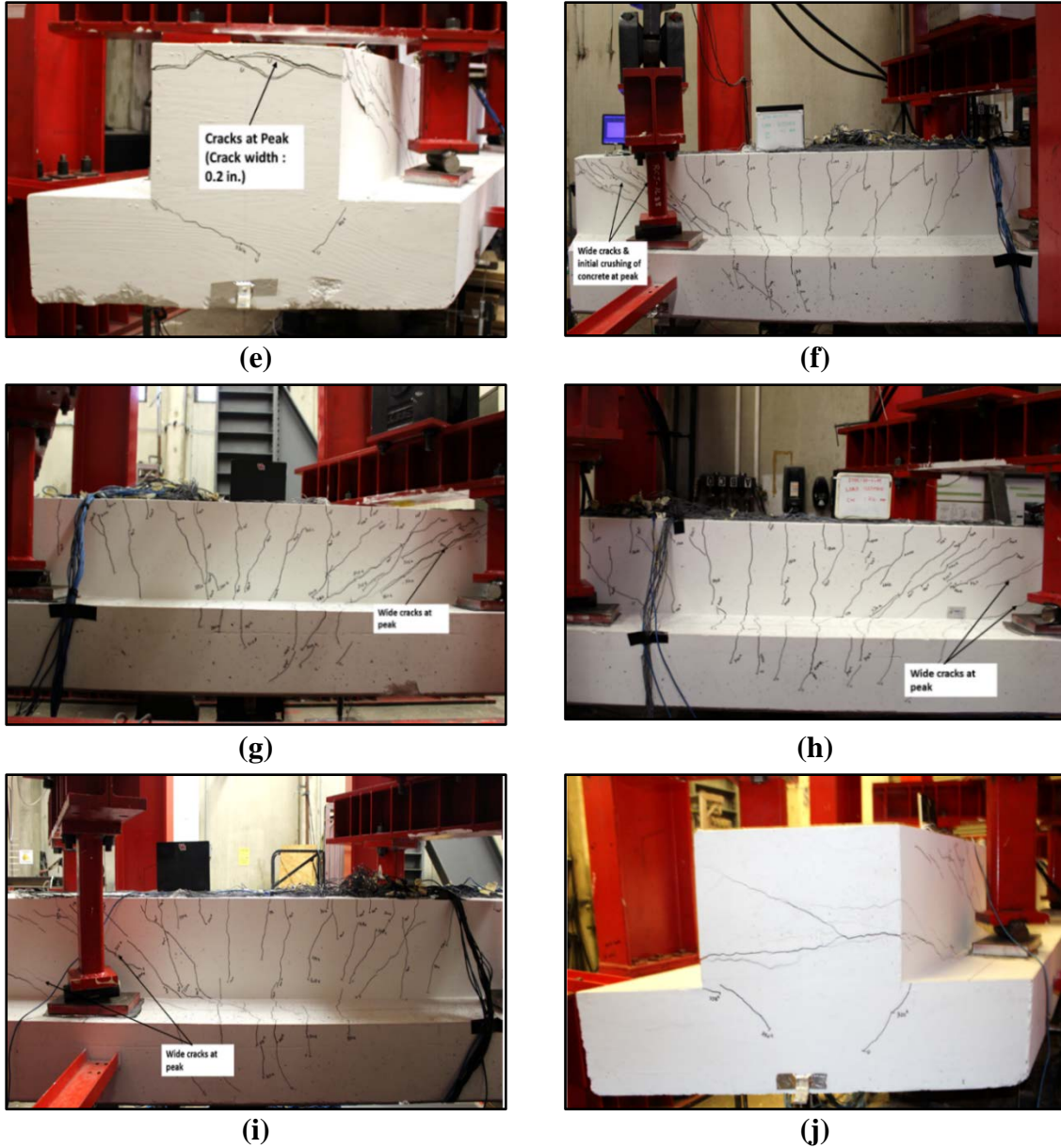


**Figure 4.26. Cracking of Specimen ITBC-30-S-M:**

**(a) Flexural cracks at 98 kips (b) Flexural shear cracks profile at 250 kips (c) Diagonal crack at the end face of the ledge at 330 kips (d) Diagonal crack at the end face of the ledge at 350 kips (e) North end face of the specimen at peak (f) North-east side of the specimen at peak (g) North-east side of the specimen at peak (h) South-east side of the specimen at peak (i) South-East side of the specimen at peak and (j) South end face of the specimen at failure**

#### **4.4.2.3 Specimen ITBC-45-T-M**

The reaction force acquired from the load cell was plotted against the net displacement obtained from the LVDTs to obtain the complete load-displacement curve of

Specimen ITBC-45-T-M, as shown in Figure 4.27. As shown in Figure 4.29(a), the first set of flexural cracks C1, C2 and C3 were observed at a support reaction of 116 kips. Subsequently, with the increase of load, flexural shear cracks C4 to C10 were observed between support reactions of 116 kips and 256 kips, as shown in Figure 4.29(b).

As the loads applied by the actuators were gradually increased, the transverse stirrups (S bars) located in the overhang part started yielding at a support reaction of 252 kips. At this loading stage, the strains in the shear stirrups (NES7) reached a value greater than 0.0023, which is the yielding strain of the transverse rebars. The second set of yielding of transverse stirrups (NWS4) occurred at a support reaction of 269 kips, followed by NWS5 at 276 kips.

As shown in Figure 4.29(c), diagonal crack C11 was observed on the end face of the ledge (long side) at a support reaction of 256 kips. This crack was also observed in Specimen ITBC-45-T-2M at a support reaction of 255 kips, which implies such diagonal cracks on the end face of inverted-T bridge caps do not depend on the transverse reinforcement ratio.

The width of flexural shear cracks C1–C10 increased significantly as the support reaction reached a peak of 302 kips. The load carrying capacity of the specimen dropped as the peak support reaction was reached. The peak support reaction of 302 kips corresponds to an individual actuator load of 201 kips. The failure mode of the specimen was primarily attributed to the shear failure caused by the yielding of shear reinforcements at both ends of the specimen and followed by the crushing of the compression strut in the web. The cracking pattern of the specimen at peak is shown in Figures 4.29(d)-4.29(i). The maximum flexural shear crack width at the peak load was measured as 0.2 in.

#### **4.4.2.4 Specimen ITBC-45-S-M**

As shown in Figure 4.28, the reaction force obtained from the load cell was plotted against the net displacement obtained from the LVDTs to obtain the complete load-displacement curve for Specimen ITBC-45-S-M. As indicated in Figure 4.30(a), the first flexural crack C1 was observed at a support reaction of 105 kips. Subsequently, with the increase of load, flexural shear cracks C2 to C8 were observed between support reactions of 105 kips and 250 kips, as shown in Figure 4.30(b).

With the progressive increase of the actuator load, the transverse stirrups (S bars) located in the overhang part started yielding at a support reaction of 261 kips. At this loading stage, the strains in the shear stirrups (SES5) reached a value greater than 0.0023, which is the yielding strain of the transverse rebars. The second set of yielding of transverse stirrups SWS7 occurred at a support reaction of 274 kips followed by NWS5 at 287 kips. Appendix 1 describes the rebar numbering and locations for all the ITBC specimens.

As shown in Figure 4.30(c), diagonal crack C9 was observed on the end face of the ledge (long side) at a support reaction of 250 kips, whereas the diagonal crack C10 was observed [Figure 4.30(d)] at 300 kips. These cracks were also encountered in Specimen

ITBC-45-S-2M at a support reaction of 251 kips and 295 kips, respectively, which implies that such diagonal cracks on the end face of inverted-T bridge caps do not depend on its transverse reinforcement ratio.

The width of flexural shear cracks C1–C8 increased significantly as the support reaction attained a peak of 347 kips. The load carrying capacity of the specimen dropped as the peak support reaction was reached. The peak support reaction of 347 kips corresponds to an individual actuator load (shear load) of 231 kips. The failure mode of the specimen was primarily attributed to the shear failure caused by the yielding of shear reinforcements at both ends of the specimen and followed by the crushing of the compression strut in the web. The cracking pattern of the specimen at peak is shown in Figures 4.30 (e)–4.30(j). The maximum flexural shear crack width at the peak load was measured as 0.20 in.

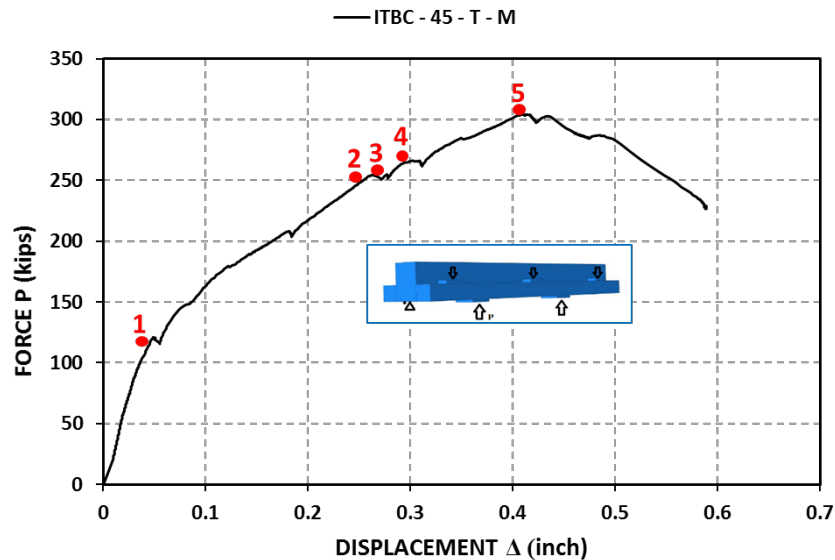


**Figure 4.27. Force-displacement curve of ITBC-45-T-M:**

**1: First flexure crack at 116 kips, 2: Diagonal crack appears in the ledge at the end face at 256 kips, 3: First yielding of transverse rebars (S bars) at 252 kips, 4: Second set yielding of transverse rebars (S bars) at 268 kips and 5: Peak load at 302 kips**

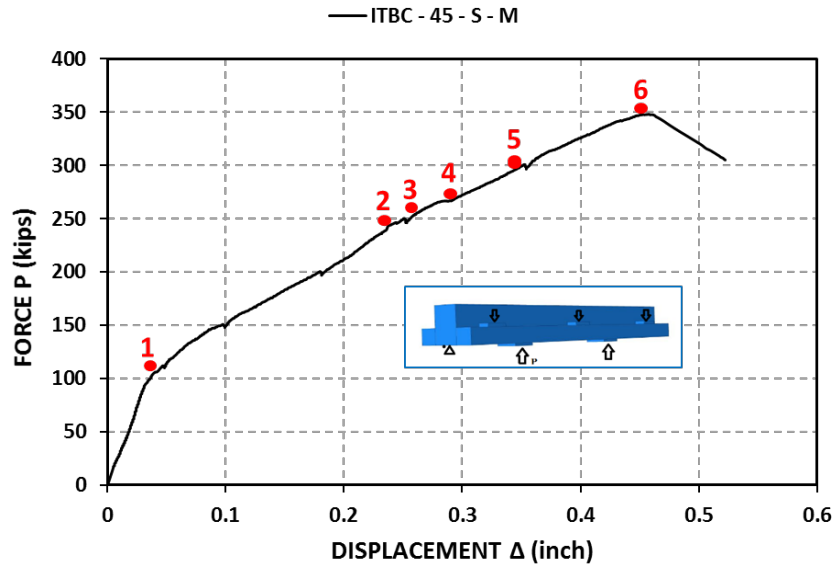
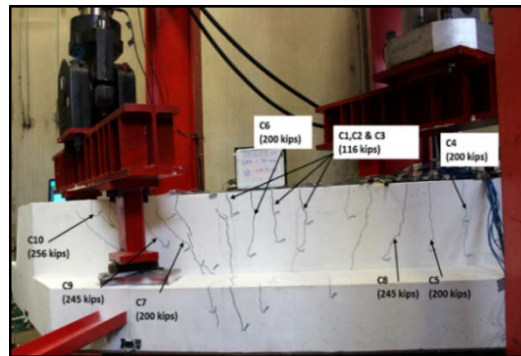


**Figure 4.28. Force-displacement curve of ITBC-45-S-M :**

- 1: First flexure crack at 105 kips, 2: Diagonal crack appears in the ledge at the long end face at 250 kips, 3: First yielding of transverse rebar (S bars) at 261 kips, 4: Second set of yielding of transverse rebar (S bars) at 274 kips, 5: Diagonal crack appears in the ledge at the short end face at 300 kips, 6: Peak load at 347 kips**



**(a)**



**(b)**



**(c)**



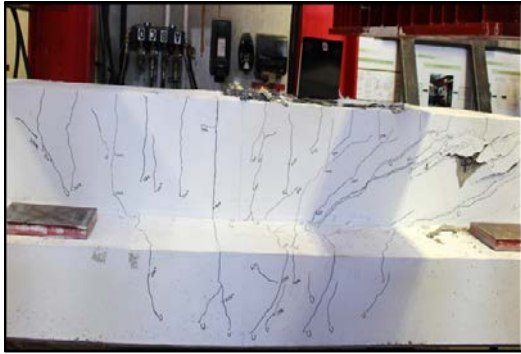
**(d)**



(e)



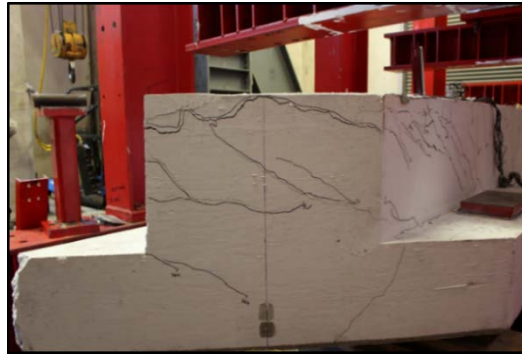
(f)



(g)



(h)



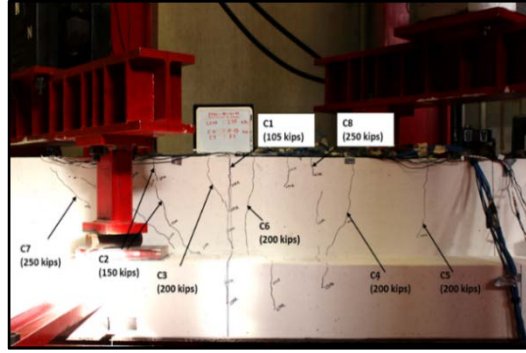
(i)

**Figure 4.29. Cracking of Specimen ITBC-45-T-M:**

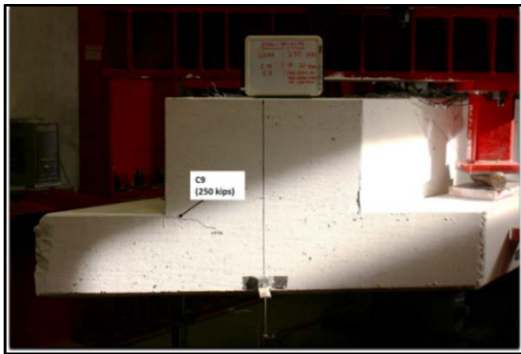
**(a) Flexural cracks at 116 kips (b) Flexural shear cracks profile at 256 kips (c) Diagonal crack at the end face of the ledge at 256 kips (d) North end face of the specimen at peak (e) North-west side of the specimen at peak (f) North-east side of the specimen at peak (g) South-west side of the specimen at peak (h) South-east side of the specimen at peak and (i) South end face of the specimen at failure**



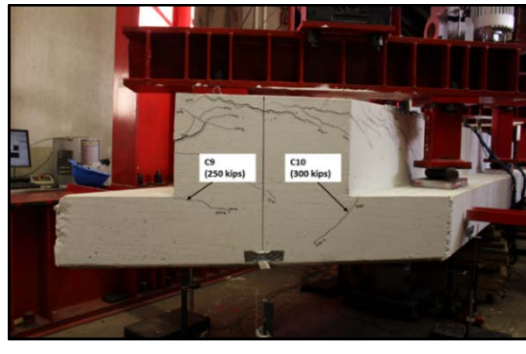
(a)



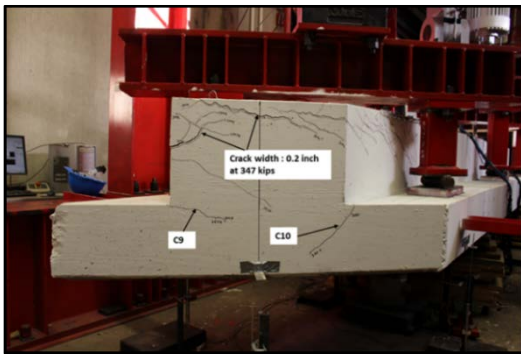
(b)



(c)



(d)



(e)



(f)



(g)



(h)



**Figure 4.30. Cracking of Specimen ITBC-45-S-M:**

**(a) Flexural crack at 105 kips (b) Flexural shear cracks profile at 250 kips (c) Diagonal crack at the end face of the ledge at 250 kips (d) Diagonal crack at the end face of the ledge at 300 kips (e) North end face of the specimen at peak (f) North-west side of the specimen at peak (g) North-east side of the specimen at peak (h) South-west side of the specimen at peak (i) South-east side of the specimen at peak and (j) South end face of the specimen at failure**

#### **4.4.2.5 Specimen ITBC-60-T-M**

As shown in Figure 4.31, the reaction force obtained from the load cell was plotted against the net displacement obtained from the LVDTs to obtain the complete load-displacement curve for Specimen ITBC-60-T-M. As indicated in Figure 4.33(a), the first set of flexural cracks C1, C2 and C3 was observed at a support reaction of 82 kips. Subsequently, with the increase of load, flexural shear cracks C4 to C15 were observed between support reactions of 82 kips and 185 kips, as shown in Figure 4.33(b).

With the progressive increase of the actuator load, the transverse stirrups (S bars) located in the overhang part started yielding at a support reaction of 221 kips. At this loading stage, the strains in the shear stirrups (strain gauge NES2) reached a value greater than 0.0023, which is the yielding strain of the transverse rebars. The second set of yielding of transverse stirrups (strain gauge NES1) occurred at a support reaction of 229 kips.

As shown in Figure 4.33(c), diagonal crack C16 of Specimen TBC-60-T-M was observed on the end face of the ledge (long side) at a support reaction of 160 kips. The crack also occurred in Specimen ITBC-60-T-2M at a support reaction of 150 kips, which implies that such diagonal cracks on the end face of inverted-T bridge caps do not necessarily depend on its transverse reinforcement ratio.

The width of flexural shear cracks C1–C16 increased significantly as the support reaction attained a peak of 300 kips. The load carrying capacity of the specimen dropped as the peak support reaction was reached. The peak support reaction of 300 kips corresponds to an individual actuator load (shear load) of 200 kips. The failure mode of the specimen was primarily attributed to the shear failure caused by the yielding of shear

reinforcements at both overhangs ends of the specimen and followed by the initiation of the crushing of compression strut in the web. The crack pattern of the specimen at the peak load is shown in Figures 4.33(d)- 4.33(i). The maximum flexural shear crack width at the peak load was measured to be 0.196 in.

#### **4.4.2.6 Specimen ITBC-60-S-M**

As shown in Figure 4.32, the reaction force obtained from the load cell was plotted against the net displacement obtained from the LVDTs to obtain the load-displacement curve for Specimen ITBC-60-S-M. Figure 4.34(a) shows the test setup of specimen ITBC-60-S-M during the test. As indicated in Figure 4.34(b), the first flexural crack C1 was observed at a support reaction of 108 kips. Subsequently, with the increase of load, flexural shear cracks C2 to C14 were observed between support reactions of 108 kips and 250 kips, as shown in Figure 4.34(c).

With the gradual increase of the actuator load, the transverse stirrups (S bars) located in the overhang part started yielding at a support reaction of 241 kips. At this loading stage, the strains in the shear stirrups (strain gauge NES2) reached a value greater than 0.0023, which is the yielding strain of the transverse rebars. The second set of yielding of transverse stirrups (strain gauge NES1) occurred at a support reaction of 248 kips. The rebar numbering and locations for all the ITBC specimens are described in Appendix 1. The reaction force at yielding, strain values at first yielding and peak force of critical rebars, where strain gauges are affixed during the fabrication stage, are shown in Appendix 2.

As shown in Figure 3.30(d), diagonal crack C15 of Specimen ITBC-60-S-M was observed on the north end face of the ledge (long side) at a support reaction of 156 kips, where as in the south side such crack, C16 was observed at 160 kips (Figure 4.34(e)). These cracks also occurred in Specimen ITBC-60-S-2M at a support reaction of 157 kips, which implies that such diagonal cracks on the end face of inverted-T bridge caps do not necessarily depend on its transverse reinforcement ratio.

The width of flexural shear cracks C1–C16 increased as the support reaction attained a peak of 312 kips. The load carrying capacity of the specimen dropped as the peak support reaction was reached. The peak support reaction of 312 kips corresponds to an individual actuator load (shear load) of 208 kips. The failure mode of the specimen was primarily attributed to the shear failure caused by the yielding of shear reinforcements at both overhangs ends of the specimen and followed by the initiation of crushing of the compression strut in the web. The crack pattern of the specimen at the peak load is shown in Figures 4.34(f)–4.34(k). The maximum flexural shear crack width at the peak load was measured to be 0.11 in.

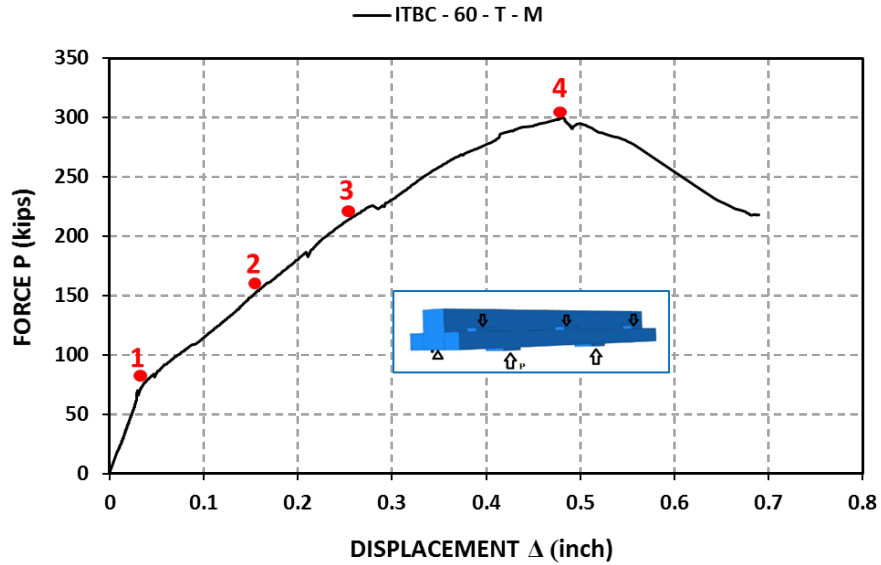


**Figure 4.31. Force-displacement curve of ITBC-60-T-M:**  
**(1: First flexure crack at 82 kips, 2: Diagonal crack in the ledge at the long end face at 160 kips, 3: First yielding of transverse rebar (S bars) at 221 kips, 4: Peak load at 300 kips)**

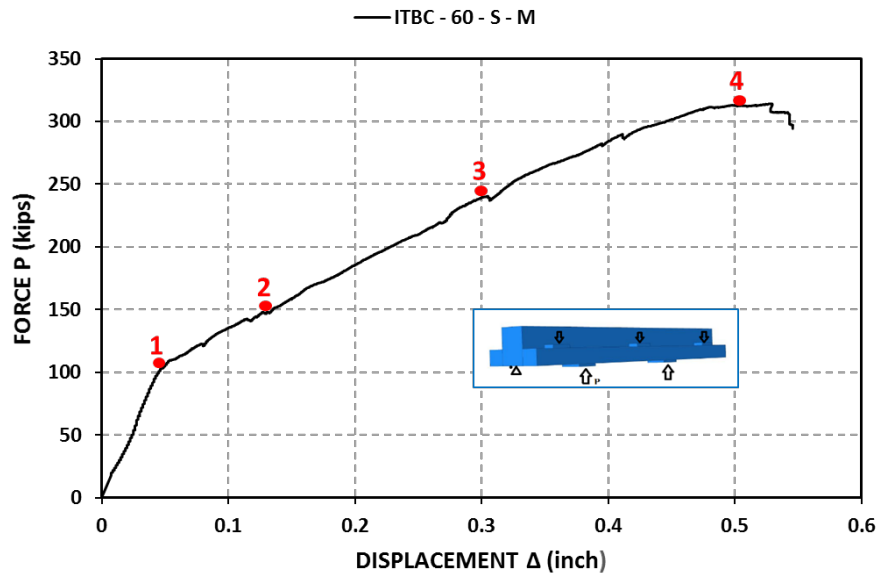
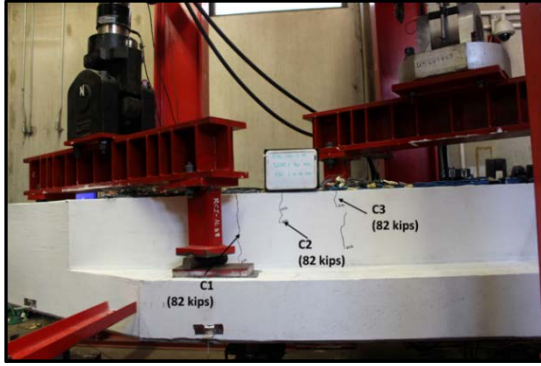
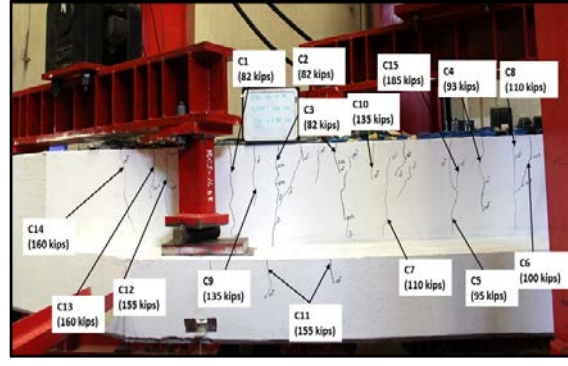


**Figure 4.32. Force-displacement curve of ITBC-60-S-M:**  
**(1: First flexure crack at 108 kips, 2: Diagonal crack in the ledge at the long end face at 156 kips, 3: First yielding of transverse rebar (S bars) at 241 kips, 4: Peak load at 312 kips)**



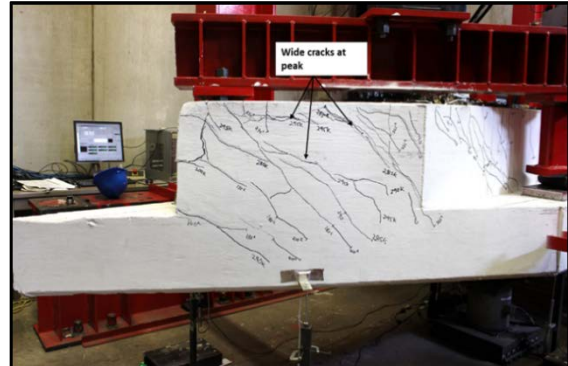
(a)



(b)



(c)



(d)



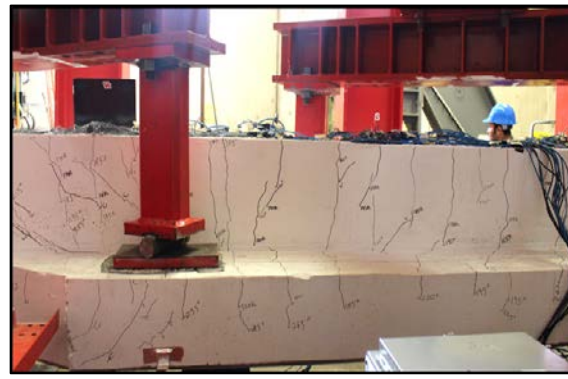
(e)



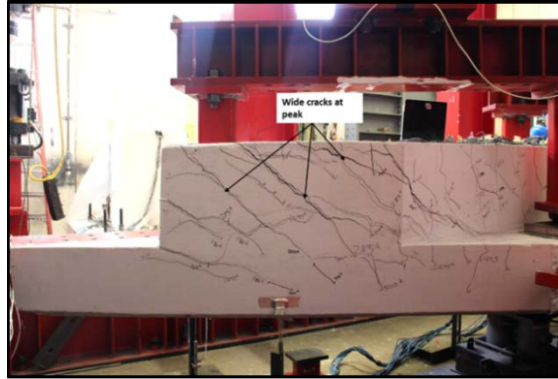
(f)



(g)



(h)



(i)

**Figure 4.33. Cracking of Specimen ITBC-60-T-M:**

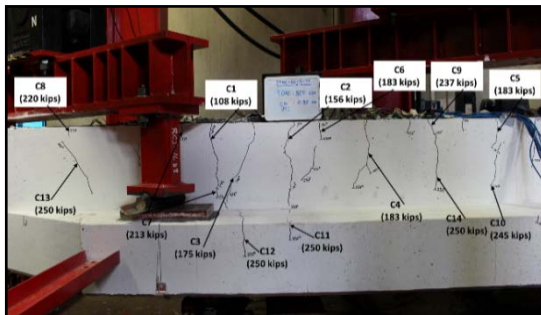
- (a) Flexural cracks at 82 kips (b) Flexural shear cracks profile at 185 kips (c) Diagonal crack at the end face of the ledge at 160 kips (d) North end face of specimen ITBC-60-T-M at peak (e) North-west side of specimen ITBC-60-T-M at peak (f) North-east side of specimen ITBC-60-T-M at peak (g) South-west side of specimen ITBC-60-T-M at peak (h) South-East side of specimen ITBC-60-T-M at peak and (i) South end face of specimen ITBC-60-T-M at failure



(a)



(b)



(c)



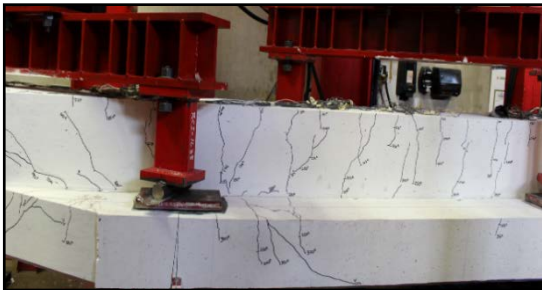
(d)



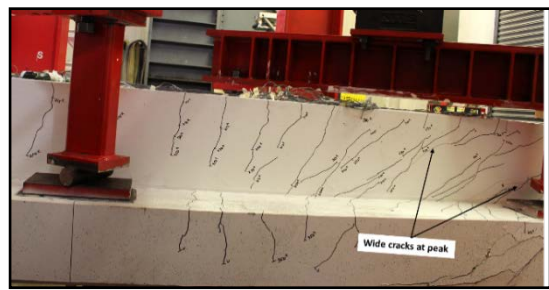
(e)



(f)



(g)



(h)



(i)



(j)



(k)

**Figure 4.34. Cracking of Specimen ITBC-60-S-M:**

(a) Test setup (b) Flexural cracks at 108 kips, (c) Flexural shear cracks profile at 250 kips, (d) Diagonal crack at the north end face at 156 kips, (e) Diagonal crack at the south end face at 160 kips, (f) North end face of specimen ITBC-60-S-M at peak, (g)

**North-west side of specimen ITBC-60-S-M at peak, (H) North-east side of specimen ITBC-60-S-M at peak, (i) South end face of specimen ITBC-60-S-M at peak, (j) South-West side of specimen ITBC-60-S-M at peak and (k) South-east side of specimen ITBC-60-S-M at peak**

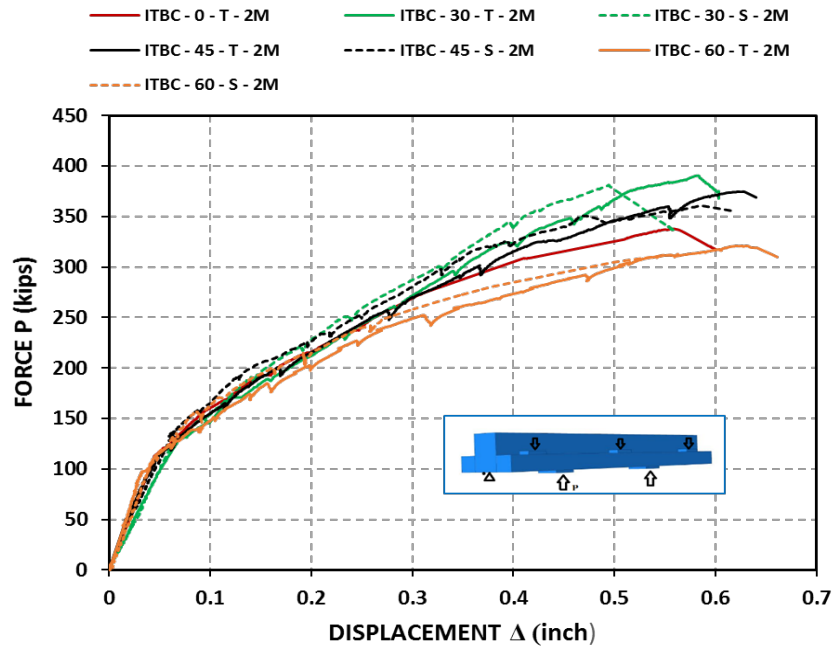
## **4.5 DISCUSSIONS OF THE TEST RESULTS**

This section provides a comparison of inverted-T bent cap specimens from Phase-1 as well as Phase-2 in terms of strength and serviceability criteria when subjected to static compression loading. With respect to the strength criterion, normalized load-displacement curves are compared. In addition, from the serviceability point of view, the following sections compare the occurrence of various types of cracks, and crack patterns at failure mode as well as respective crack width comparison. Also, the section elaborates on the punching shear observed in 60° skewed inverted-T bent cap specimens from Phase 1 and Phase 2 of the experimental program.

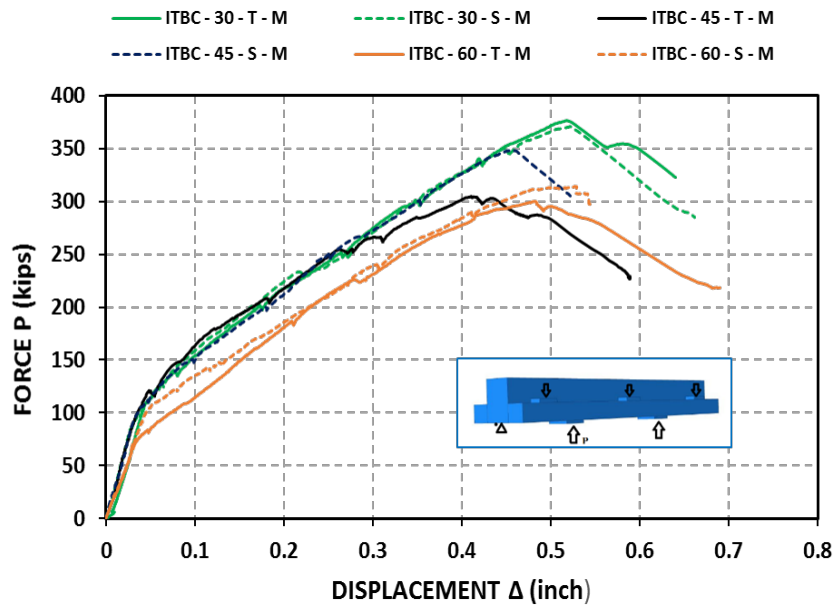
### **4.5.1 Comparison of Primary Test Results**

Figures 4.35(a) and 4.35(b) present the force-displacement curves for all Phase 1 and Phase 2 specimens, respectively. From both the figures it is evident that the behavior of all the force-displacement curves of 30°, 45°, and 60° skew ITBC specimens with traditional and skewed reinforcing is similar. Specimens with a 60° skew angle have a lower capacity of 15-18% than others. This is because the torsional effect is more in the case of higher skew angles, thereby reducing the peak load carrying capacity. Tables 4.4, 4.5 and 4.6 summarize the primary test results of 30°, 45°, and 60°, skew ITBC specimens with traditional and skew reinforcing, respectively. Primary results show that there is no significant difference between the specimens with two types of reinforcing detailing in terms of the capacity because the peak capacity for both types of specimens is very close. Moreover, the first yielding load of transverse stirrups of the specimens with skew reinforcing is higher than that of traditional reinforcing.

From the serviceability point of view (i.e. cracking), inverted-T bridge caps with skew transverse reinforcements has comparatively better performance than that with traditional transverse reinforcements. The diagonal shear crack in the web at peak reaction force for all the specimens with traditional reinforcing is higher than the skewed reinforcing. Such a better performance of skewed reinforcing can be attributed to even distribution (spacing) of hanger and ledge rebars. In the case of traditional reinforcing, the designer of the inverted-T bridge cap flares the bars out to match the skew angle while trying to maintain a minimum and maximum spacing based on the outcome of the design calculations, thereby creating the unequal spacing of transverse reinforcements at both sides of the inverted-T bridge cap. By using skew reinforcing, the unequal spacing of transverse rebars can be avoided and better performance could be achieved by reducing the reinforcement congestion.



(a)



(b)

**Figure 4.35. Force-displacement Curve:**  
**(a) Phase-1 specimens and (b) Phase-2 specimens**

**Table 4.4. Summary of Primary Test Results of 30<sup>0</sup> Skew ITBCs**

Test Result	Specimens			
	Phase 1		Phase 2	
	ITBC-30-T-2M	ITBC-30-S-2M	ITBC-30-T-M	ITBC-30-S-M
First flexural cracking (kips)	128	127	109	98
Yielding of transverse reinforcement (kips)	321	332	292	295
First diagonal crack at the end face (kips)	346	344	345	330
Peak load (kips)	384	381	376	371
Maximum diagonal shear crack width at the peak load (in.)	0.021	0.016	0.18	0.15

**Table 4.5. Summary of Primary Test Results of 45<sup>0</sup> Skew ITBCs**

Test Result	Specimens			
	Phase 1		Phase 2	
	ITBC-45-T-2M	ITBC-45-S-2M	ITBC-45-T-M	ITBC-45-S-M
First flexural cracking (kips)	115	132	116	105
Yielding of transverse reinforcement (kips)	271	293	252	261
First diagonal crack at the end face (kips)	255	251	256	250
Peak load (kips)	369	361	302	347
Maximum diagonal shear crack width at the peak load (in.)	0.020	0.018	0.2	0.2

**Table 4.6. Summary of Primary Test Results of 60° Skew ITBCs**

Test Result	Specimens			
	Phase 1		Phase 2	
	ITBC-60-T-2M	ITBC-60-S-2M	ITBC-60-T-M	ITBC-60-S-M
First flexural cracking (kips)	105	113	82	108
Yielding of transverse reinforcement (kips)	171	210	221	241
First diagonal crack at the end face of the ledge (kips)	150	157	160	156
Peak reaction (kips)	321	317	300	311
Maximum diagonal shear crack width at the peak load (in.)	0.020	0.017	0.19	0.11

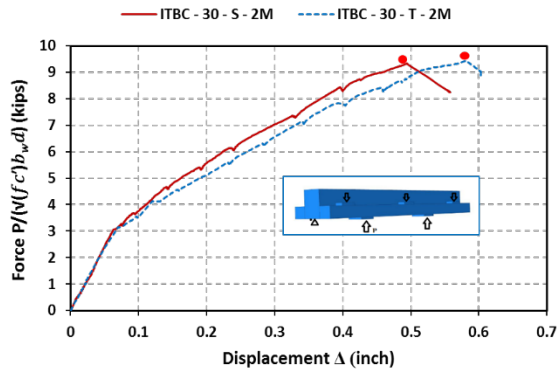
#### 4.5.2 Strength Data Evaluation

As presented in the previous section of experimental results, the force-displacement curves for all ITBC specimens from Phase 1 and Phase 2 were plotted and summarized in terms of first flexural cracking load, diagonal cracking load, yielding of transverse stirrups, and peak load. The peak load ( $V_{Peak}$ ) obtained after performing the test is the maximum shear carried at the critical section.

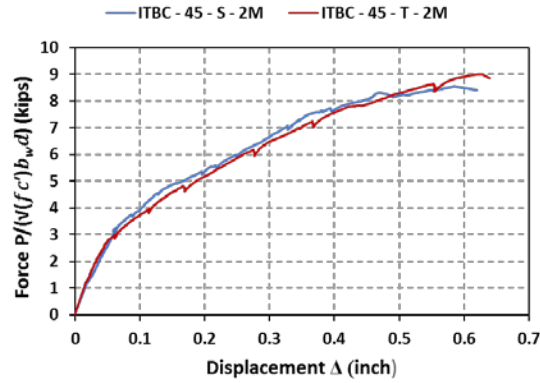
To compare the results of Phase 1 and Phase 2 skew test specimens considered under the experimental program, the normalized load-displacement curves are plotted as shown in Figure 4.36(a)-(f). The reaction force (shear force) obtained from the load cell was normalized by dividing it with  $\sqrt{f'_c} b_w d$  and plotted with the displacement obtained from the LVDT since the shear strength of an inverted-T section is associated with the compressive strength of the concrete. The X-axis represents the displacement (inches) recorded by LVDTs, and the Y-axis represents the normalized shear force obtained by dividing it with  $\sqrt{f'_c} b_w d$  to incorporate the effect of difference in concrete strength.

It can be observed from Figure 4.36 (a)-(f) that the normalized shear capacities of the skew ITBC specimens with traditional transverse reinforcement and skewed transverse reinforcement from Phase 1 and Phase 2 are very close and vary only up to the difference of five percent. However, to some extent the displacement at the peak force for specimens with traditional reinforcement is greater than that of specimens with skew reinforcing. This can be attributed to the fact that the ITBC designed with a traditional reinforcement type has a greater amount of reinforcement and smaller spacing as compared to the skewed reinforcement type. The normalized capacities of all the specimens can be compared with the help of values provided in Table 4.3 as well as from Figure 4.36. It is observed that the normalized shear capacity of all 60° skewed specimens including ITBC-60-T-2M, ITBC-

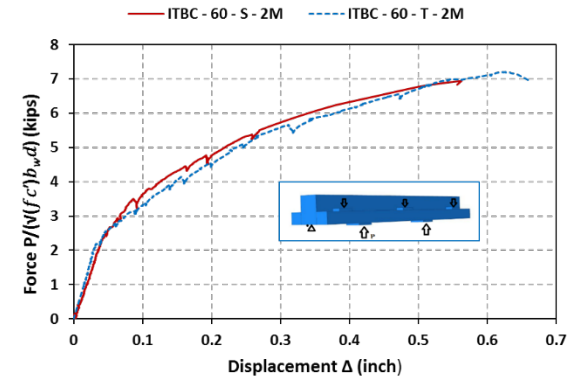
60-S-2M, ITBC-60-T-M, and ITBC-60-S-M is lesser as compared to the shear capacity of the other test specimens. It is found that the normalized shear capacity of 30<sup>0</sup> skewed ITBC specimens in Phase 1 is 6 % and 23% more than the capacity of 45<sup>0</sup> and 60<sup>0</sup> skewed ITBC specimens, respectively. Further, the average capacity of 30<sup>0</sup> skewed ITBC specimens in Phase 2 is 16 % and 18% more than the capacity of 45<sup>0</sup> and 60<sup>0</sup> skewed ITBC specimens, respectively. Thus, it is evident that the shear capacity of the inverted-T bent caps decreases with the increase of the skew angle.



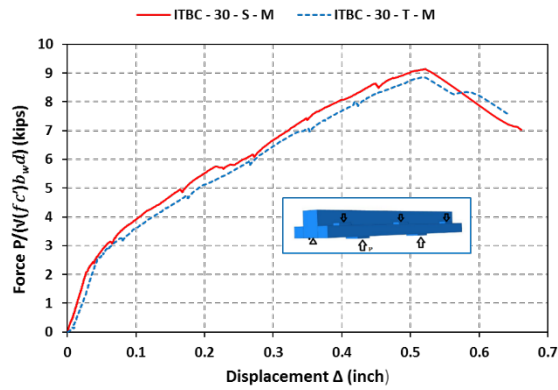
(a) ITBC-30-T-2M and ITBC-30-S-2M



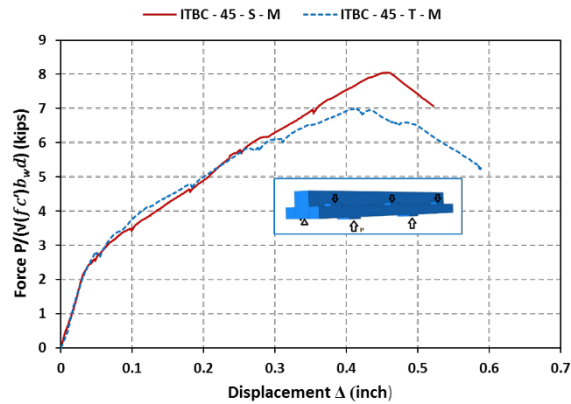
(b) ITBC-45-T-2M and ITBC-45-S-2M



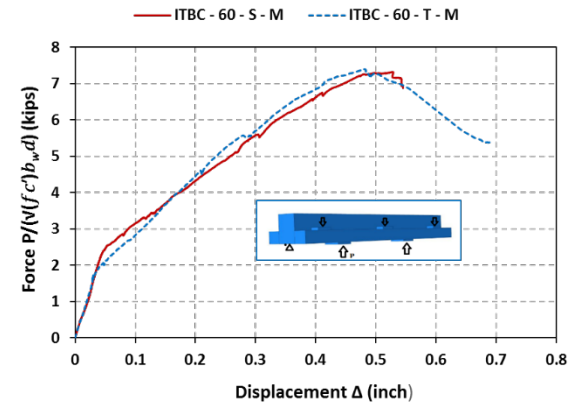
(c) ITBC-60-T-2M and ITBC-60-S-2M



(d) ITBC-30-T-M and ITBC-30-S-M



(e) ITBC-45-T-M and ITBC-45-S-M



(f) ITBC-60-T-M and ITBC-60-S-M

Figure 4.36. Normalized Force-displacement Curve of Test Specimens

### 4.5.3 Serviceability Data Evaluation

The major factors considered under the serviceability performance of the test specimens include comparison of Phase 1 and Phase 2 specimens in terms of cracking pattern, number of cracks observed, and occurrence of diagonal crack as well as respective failure modes. This section also discusses the punching shear failure of ledges observed in 60° skewed ITBC specimens in Phase 1 of the experimental program.

#### 4.5.3.1 Cracking Pattern

Figure 4.37 (a-d) to Figure 4.49 (a-d) represent the cracking pattern obtained for all the test specimens in the experimental program at the failure stage. For all ITBC specimens, the first flexural crack occurred at a close load range between 105 kips to 128 kips except for the specimen ITBC-60-T-M, in which the flexural crack occurred comparatively earlier at 80 kips. The maximum flexural shear crack width noted for Phase 1 specimens was comparatively lower than Phase 2 specimens. In Phase 1 specimens, for ITBC-0-T-2M, the maximum flexural crack width obtained was 0.012 in whereas for ITBC-60-T-2M and ITBC-60-S-2M specimens, the flexural shear crack width was equal to 0.020 in. In case of Phase 2 specimens, the maximum flexural shear crack width reached by ITBC-60-T-M and ITBC-60-S-M was 0.196 inches and 0.11 inches, respectively. As both of the 60° skewed specimens in Phase 1 and Phase 2 were subjected to torsional failure producing a large number of torsional cracks in the end regions of the specimens. Thus, it is seen that for Phase 1 and Phase 2, skewed specimens, the crack widths observed for the specimens with traditional transverse reinforcement were higher than the specimens designed with proposed skewed transverse reinforcement.

#### 4.5.3.2 Diagonal Crack at the Cantilever Ledge and Web

The diagonal crack was observed to be developed in all ITBC test specimens. Table 4.7 shows the reaction force (kips) at which the first diagonal crack appeared at the re-entrant corner between the cantilever ledge and the web at the end faces of the exterior portions of the ITBCs. For the 0° skewed specimen (ITBC-0-T-2M), the diagonal crack appeared at 336 kips on the north and south end faces which was very close to the value of peak load [Figure 4.36 (a-b)]. On the other hand, for all 60° skewed specimens, the diagonal crack appeared at earlier load stage between 150 kips to 160 kips on a longer side at the north as well as the south end faces [Figure 4.41 (a-b)–Figure 4.42 (a-b)]. For 30° and 45° skewed test specimens the diagonal cracks were observed between 250 and 346 kips. The effect of the higher skew angle may have contributed in the early stage development of the diagonal crack in skewed specimens. In the case of ITBC-60-S-M, the diagonal crack was also observed on short sides at the north as well as the south end faces at the loads of 250 kips and 265 kips, respectively. For Phase 2 specimens, the special type of reinforcing bars (G bars: inverted-V shape) were incorporated to prevent the generation of diagonal crack,

however, the specified rebars did not help in preventing the development of diagonal cracks. The diagonal cracks appeared for higher skew angle at a lower load.

**Table 4.7. Observation of Diagonal Cracks at the End Face of ITBCs**

Sr.No	Specimens	Diagonal crack at the re-entrant corner between the cantilever ledge and the web (kips)	Avg. Load (kips)
1	ITBC-30-T-2M	346	341
2	ITBC-30-S-2M	344	
3	ITBC-30-T-M	345	
4	ITBC-30-S-M	330	
5	ITBC-45-T-2M	255	253
6	ITBC-45-S-2M	251	
7	ITBC-45-T-M	256	
8	ITBC-45-S-M	250	
9	ITBC-60-T-2M	150	166
10	ITBC-60-S-2M	157	
11	ITBC-60-T-M	160	
12	ITBC-60-S-M	156	

#### 4.5.3.3 Number of Flexural Shear Cracks

Table 4.8 represents the total number of cracks observed in all ITBC test specimens. In terms of the overall cracking pattern obtained during the loading stage as well as the failure stage, Specimen ITBC-0-T-2M in Phase 1 received a smaller number of flexural, flexural shear, and shear cracks as compared to all other skewed specimens, as seen from Table 4.8. This could be attributed to the considerably higher crack width reached by the failure crack causing the separation of the ledge from the web at both end face overhang parts.

In case of the skewed ITBC specimens in Phase 1, a significantly higher number of cracks were observed in the specimen with traditional reinforcement as compared to the specimen with proposed skewed reinforcement. Especially, the number of shear cracks developed in the end regions at peak load was substantially higher in number, as evident from Figure 4.37 (c-d)–4.42(c-d). Similarly, in Phase 2, the number of cracks observed in the case of the specimen with traditional transverse reinforcement was higher than the

specimen with proposed skewed reinforcement. However, the difference between the number of cracks was not as high as observed for Phase 1. This behavior of the specimens could be attributed to the arrangement of transverse reinforcement in ITBCs designed by a traditional method. In the traditionally designed specimens, the end regions are characterized by the uneven spacing of rebars as a result of induced transition from straight bars to the skew bars. This causes uneven spacing between transverse reinforcing bars at the end regions. On the other hand, the ITBC specimens designed with proposed skewed reinforcement have evenly spaced transverse reinforcement throughout the length of the specimen, thus providing a better performance in terms of cracking.

**Table 4.8. Summary of Number of Flexural Shear Cracks Count**

Specimen ID	Total number of flexural shear cracks observed at peak load				
	Northeast	Southwest	Northwest	Southeast	Total #
ITBC-00-T-2M	16	18	19	21	74
ITBC-30-T-2M	26	25	25	26	102
ITBC-30-S-2M	17	17	17	21	72
ITBC-45-T-2M	31	31	26	35	123
ITBC-45-S-2M	20	15	20	26	81
ITBC-60-T-2M	13	27	31	37	114
ITBC-60-S-2M	12	13	21	22	68
ITBC-30-T-M	14	15	23	26	78
ITBC-30-S-M	13	13	20	24	70
ITBC-45-T-M	14	13	20	28	84
ITBC-45-S-M	19	16	19	26	80
ITBC-60-T-M	26	24	26	27	103
ITBC-60-S-M	24	22	22	23	91

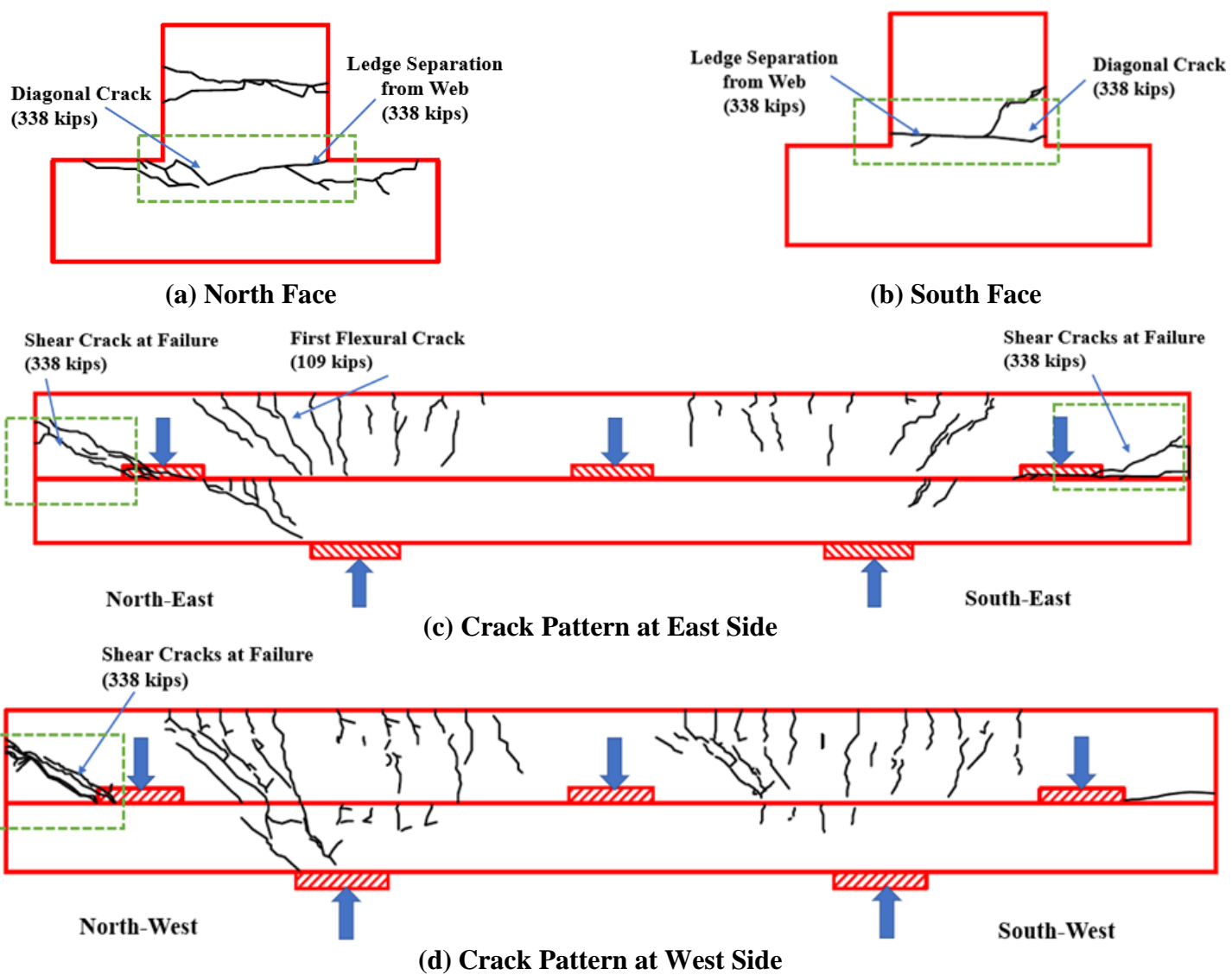
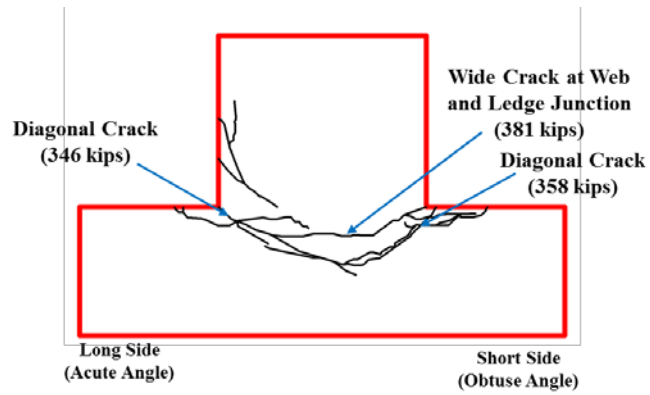
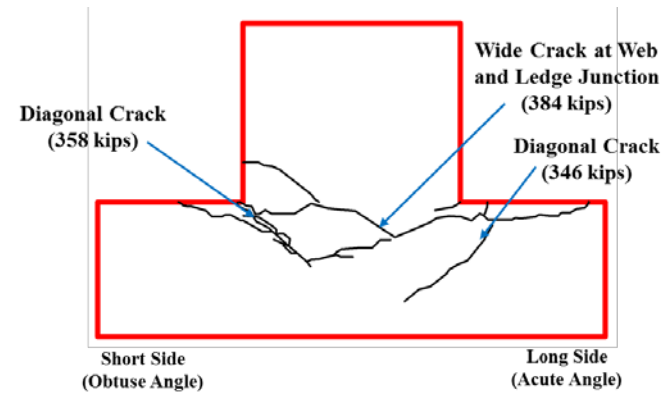


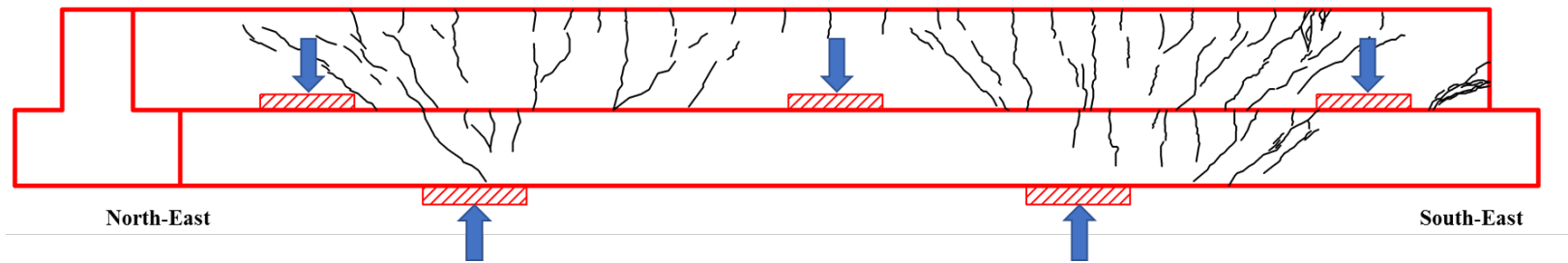
Figure 4.37. Cracking Pattern at Failure Stage for Specimen ITBC-0-T-2M



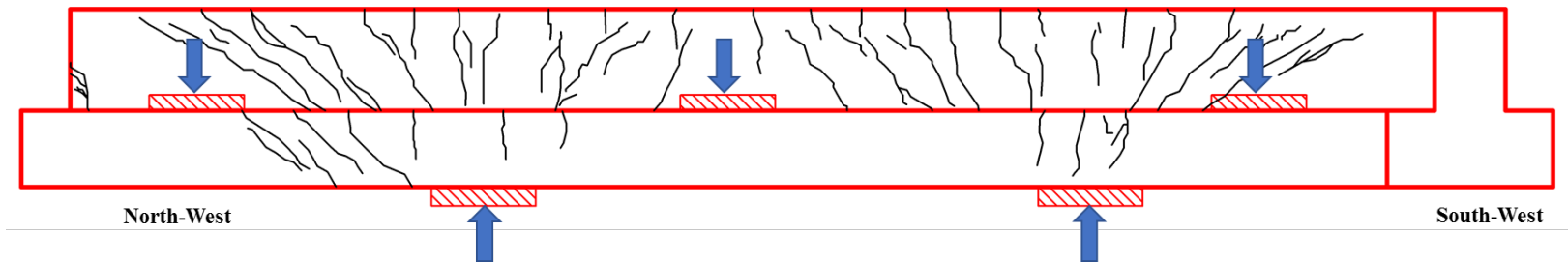
(a) North Face



(b) South Face

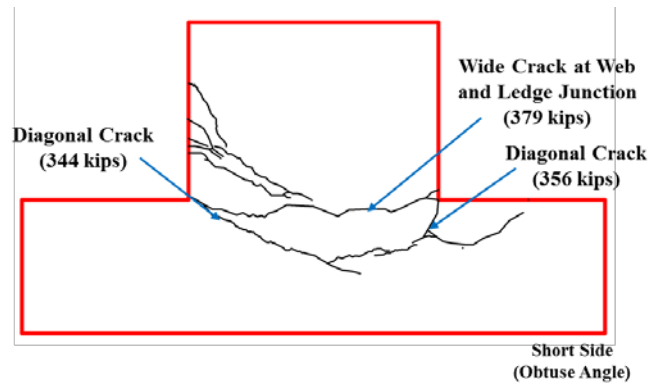


(c) Crack Pattern at East Side

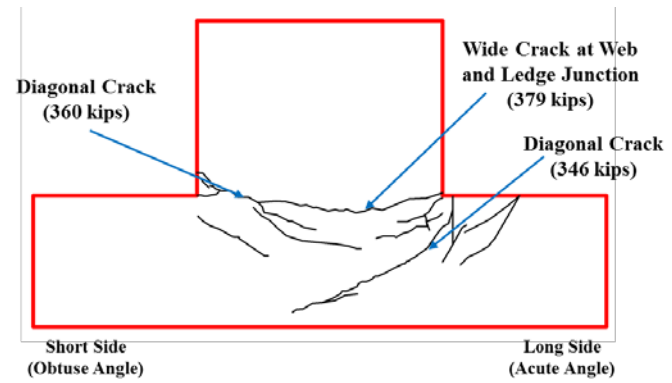


(d) Crack Pattern at West Side

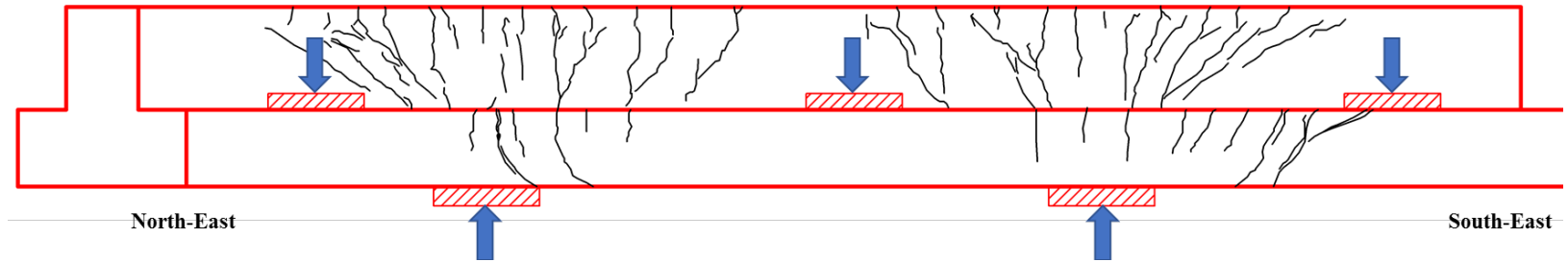
Figure 4.38. Cracking Pattern at Failure Stage for Specimen ITBC-30-T-2M



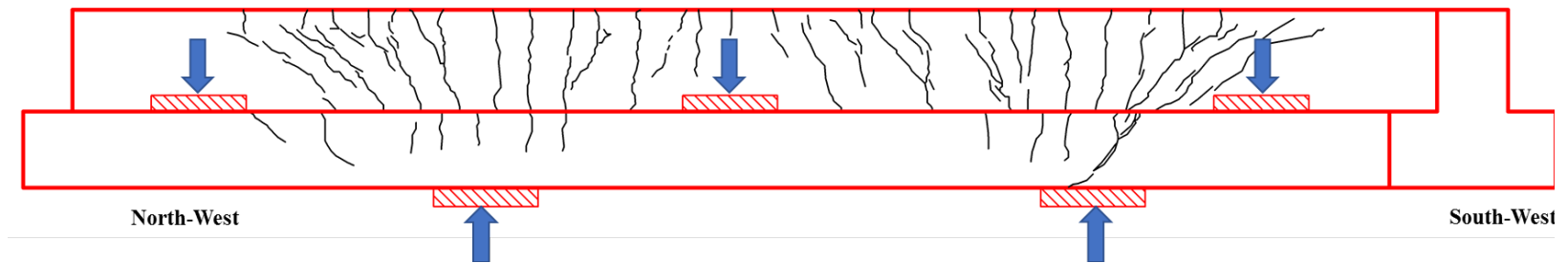
(a) North Face



(b) South Face

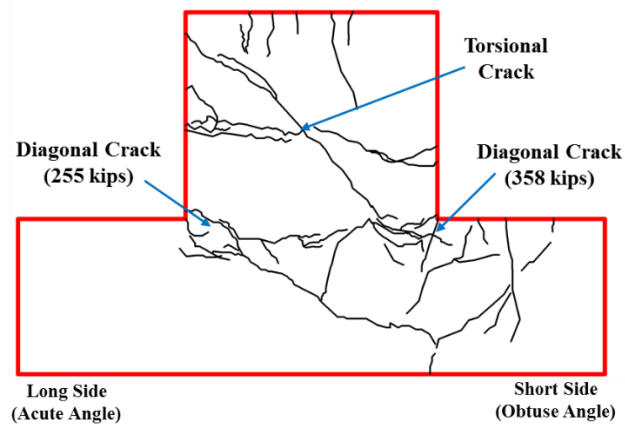


(c) Crack Pattern at East Side

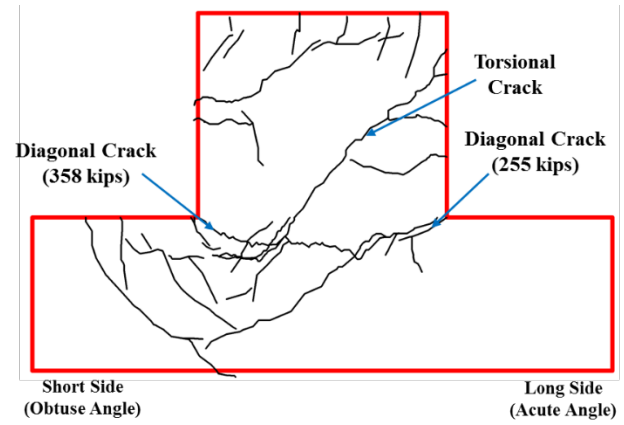


(d) Crack Pattern at West Side

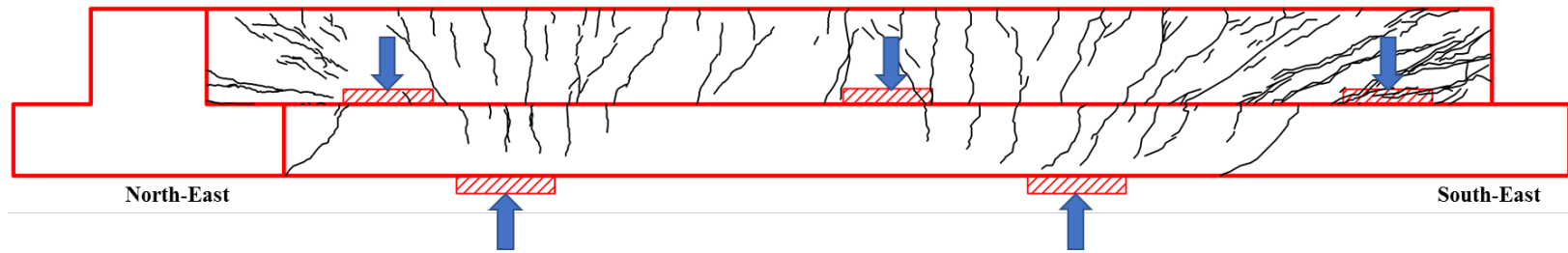
Figure 4.39. Cracking Pattern at Failure Stage for Specimen ITBC-30-S-2M



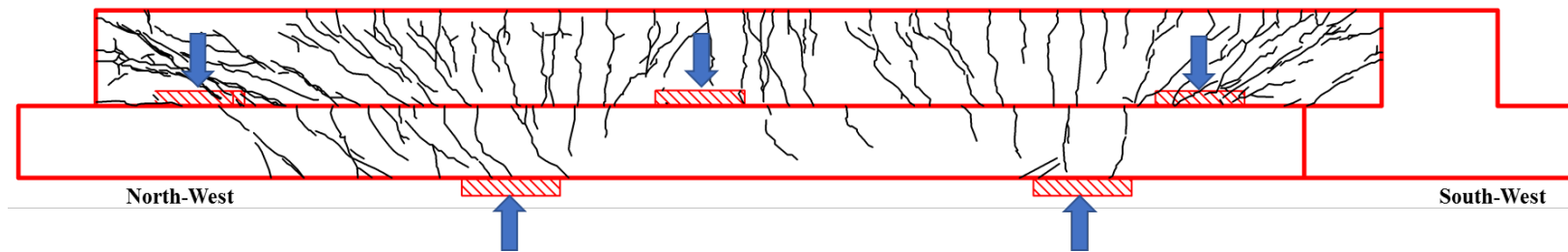
(a) North Face



(b) South Face

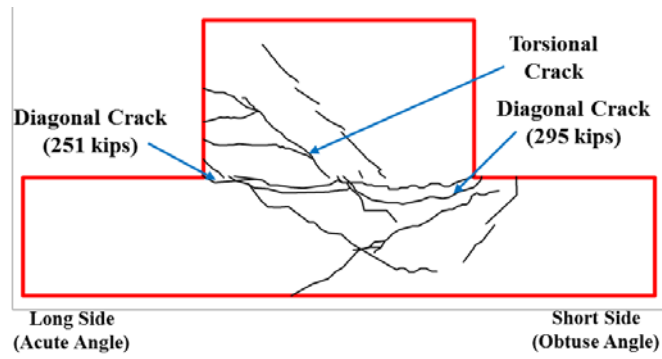


(c) Crack Pattern at East Side

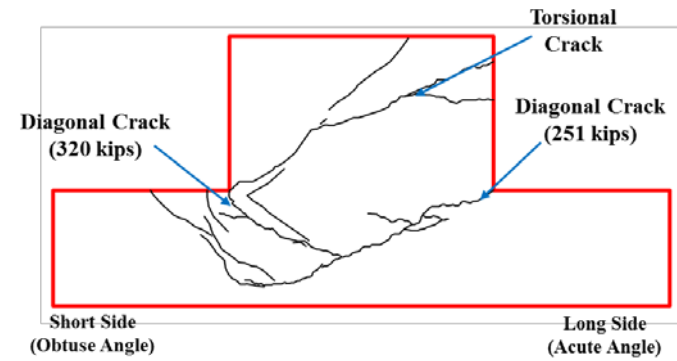


(d) Crack Pattern at West Side

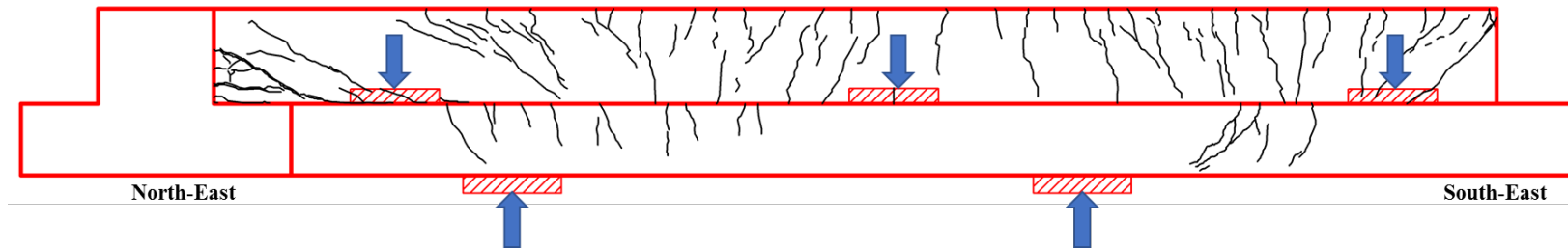
Figure 4.40. Cracking Pattern at Failure Stage for Specimen ITBC-45-T-2M



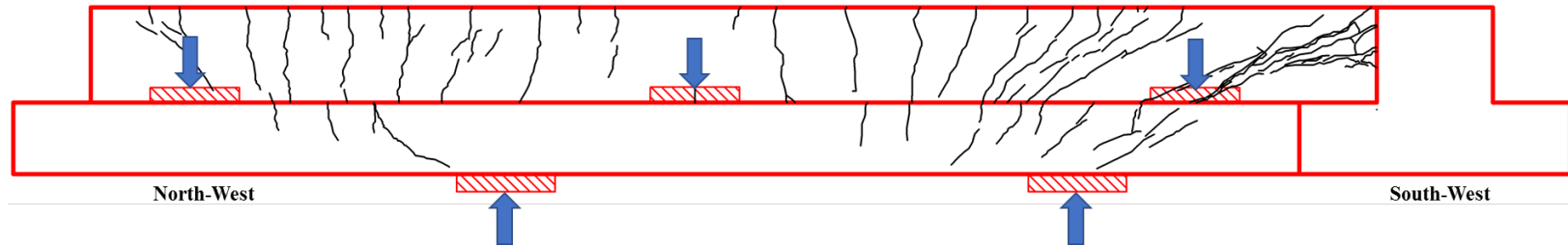
(a) North Face



(b) South Face



(c) Crack Pattern at East Side



(d) Crack Pattern at West Side

Figure 4.41. Cracking Pattern at Failure Stage for Specimen ITBC-45-S-2M

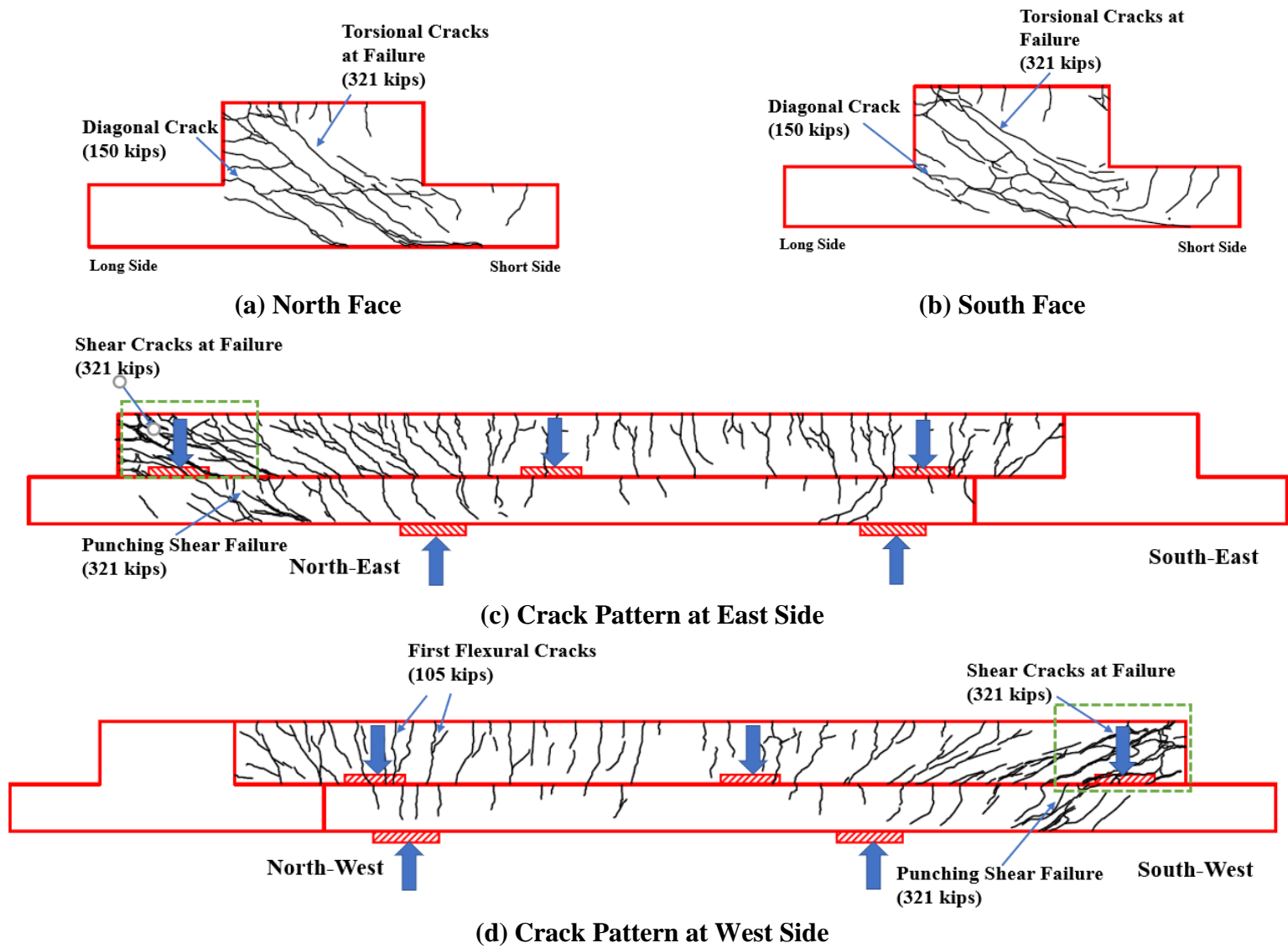


Figure 4.42. Cracking Pattern at Failure Stage for Specimen ITBC-60-T-2M

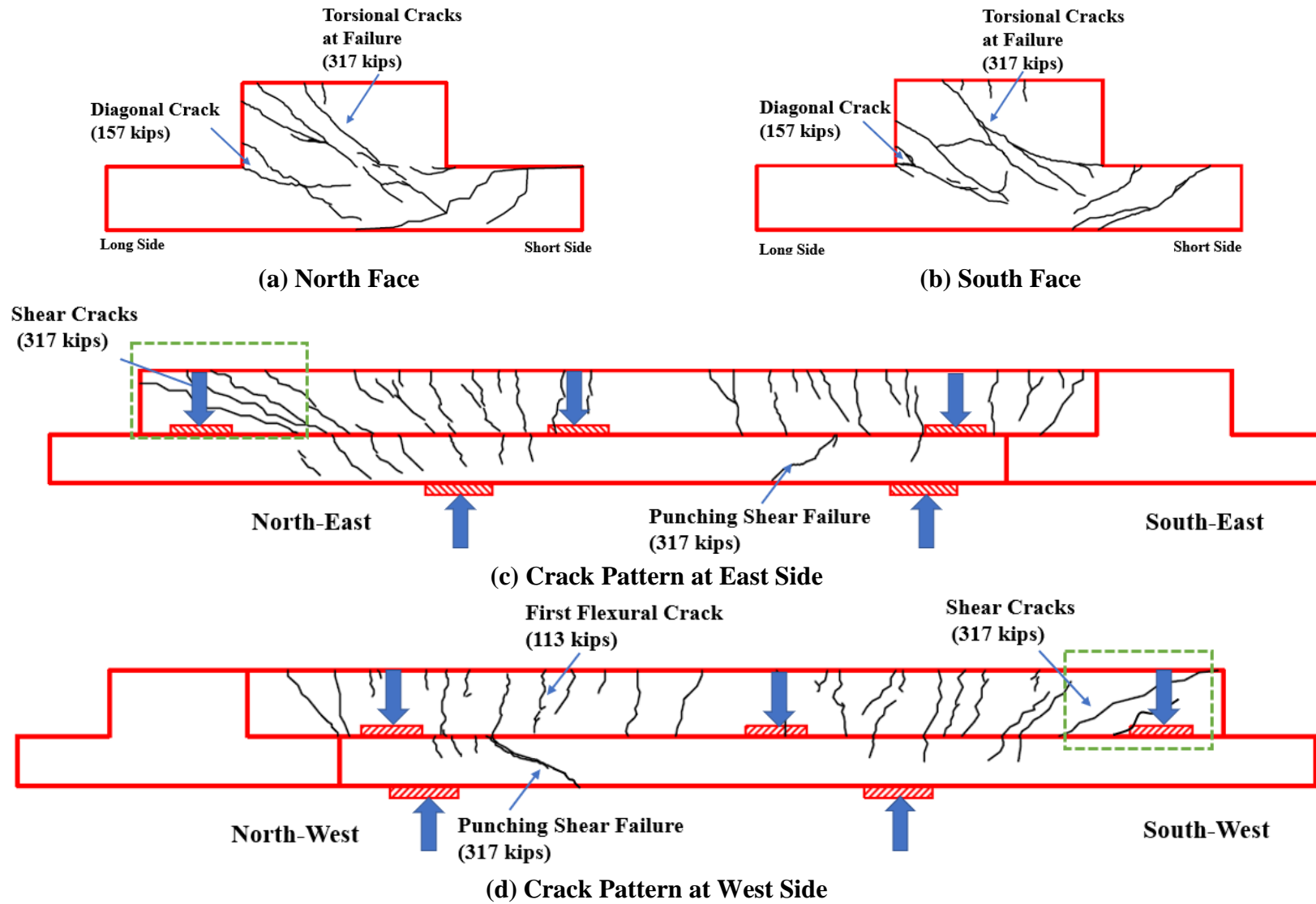
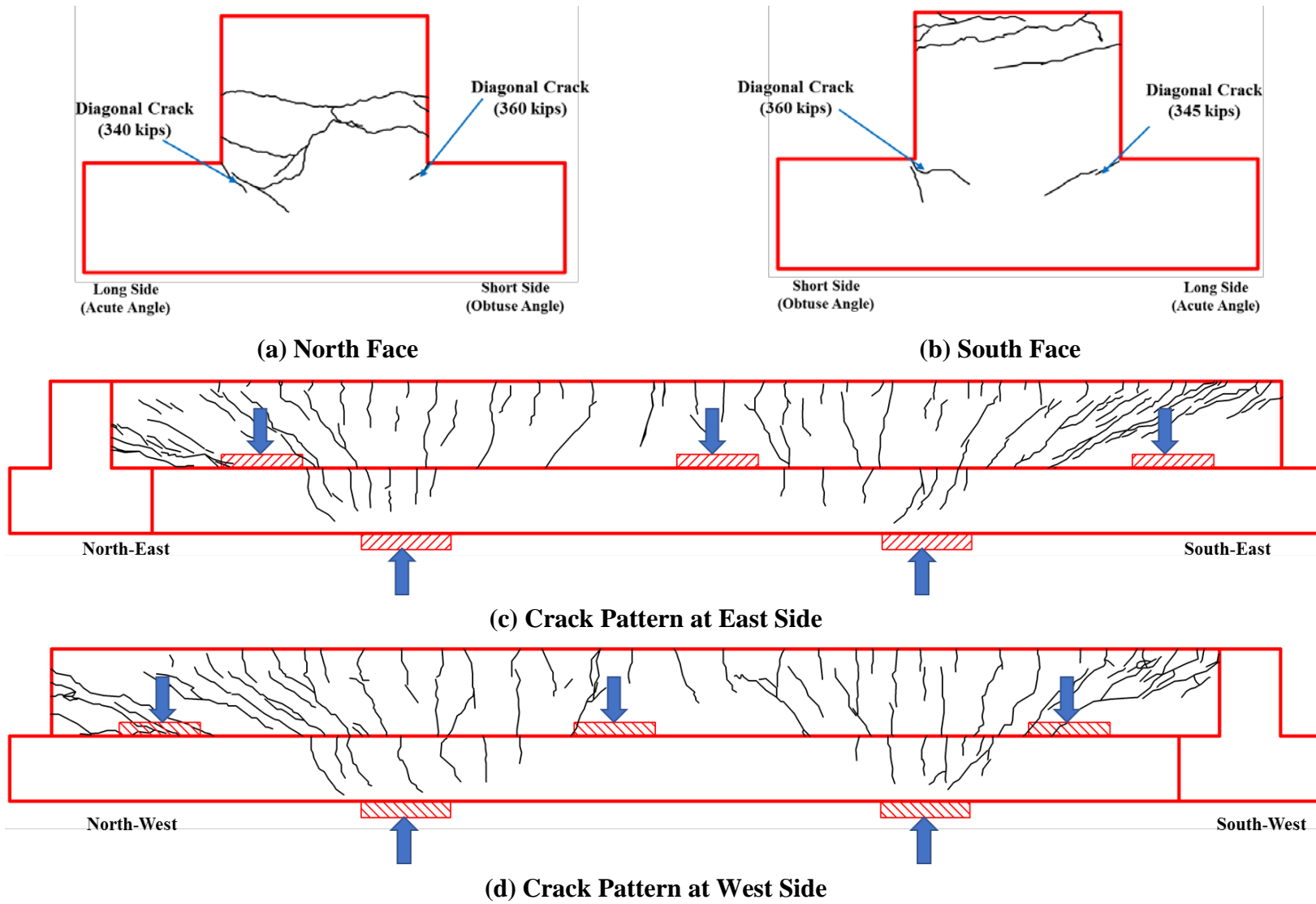


Figure 4.43. Cracking Pattern at Failure Stage for Specimen ITBC-60-S-2M



**Figure 4.44. Cracking Pattern at Failure Stage for Specimen ITBC-30-T-M**

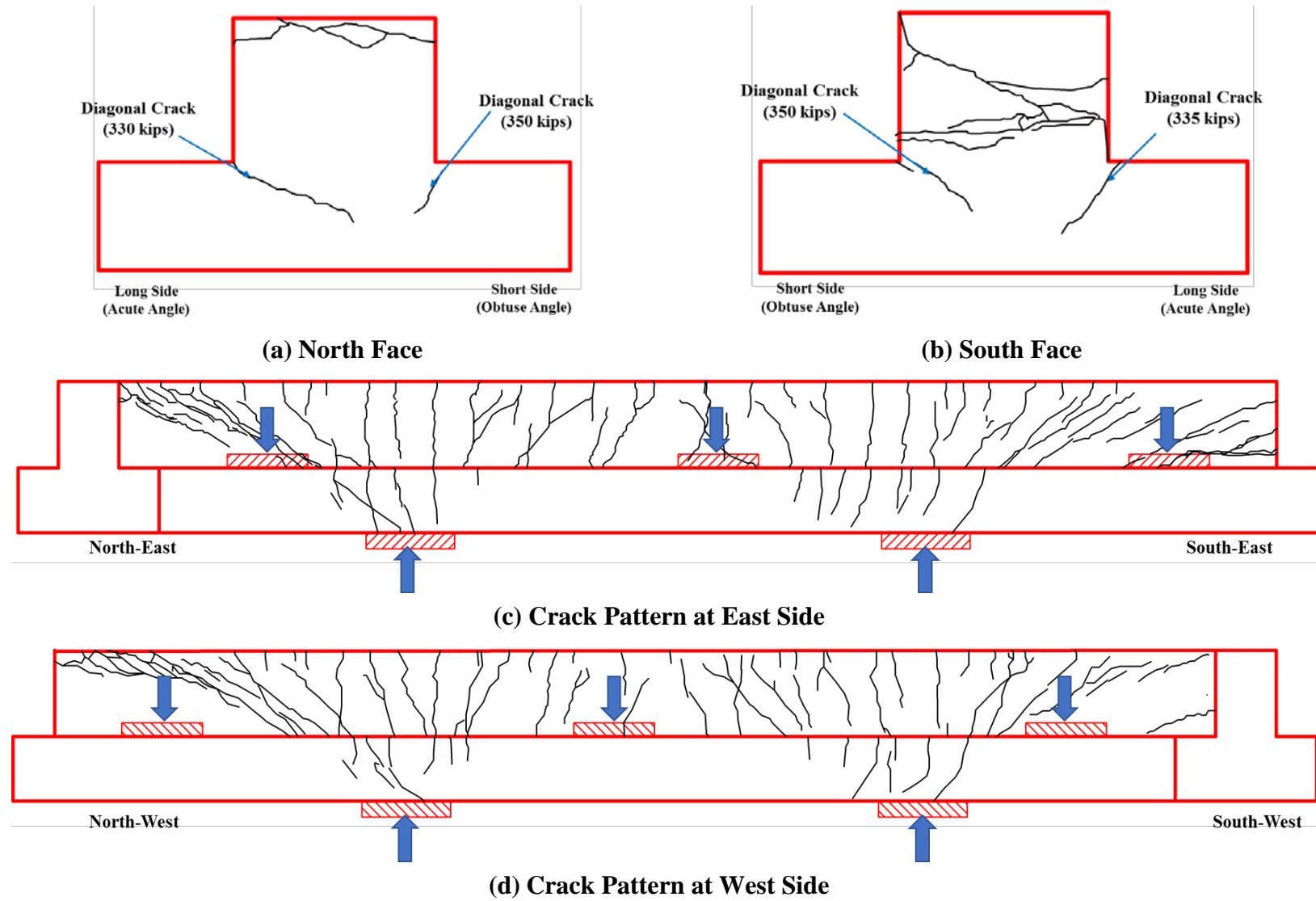


Figure 4.45. Cracking Pattern at Failure Stage for Specimen ITBC-30-S-M

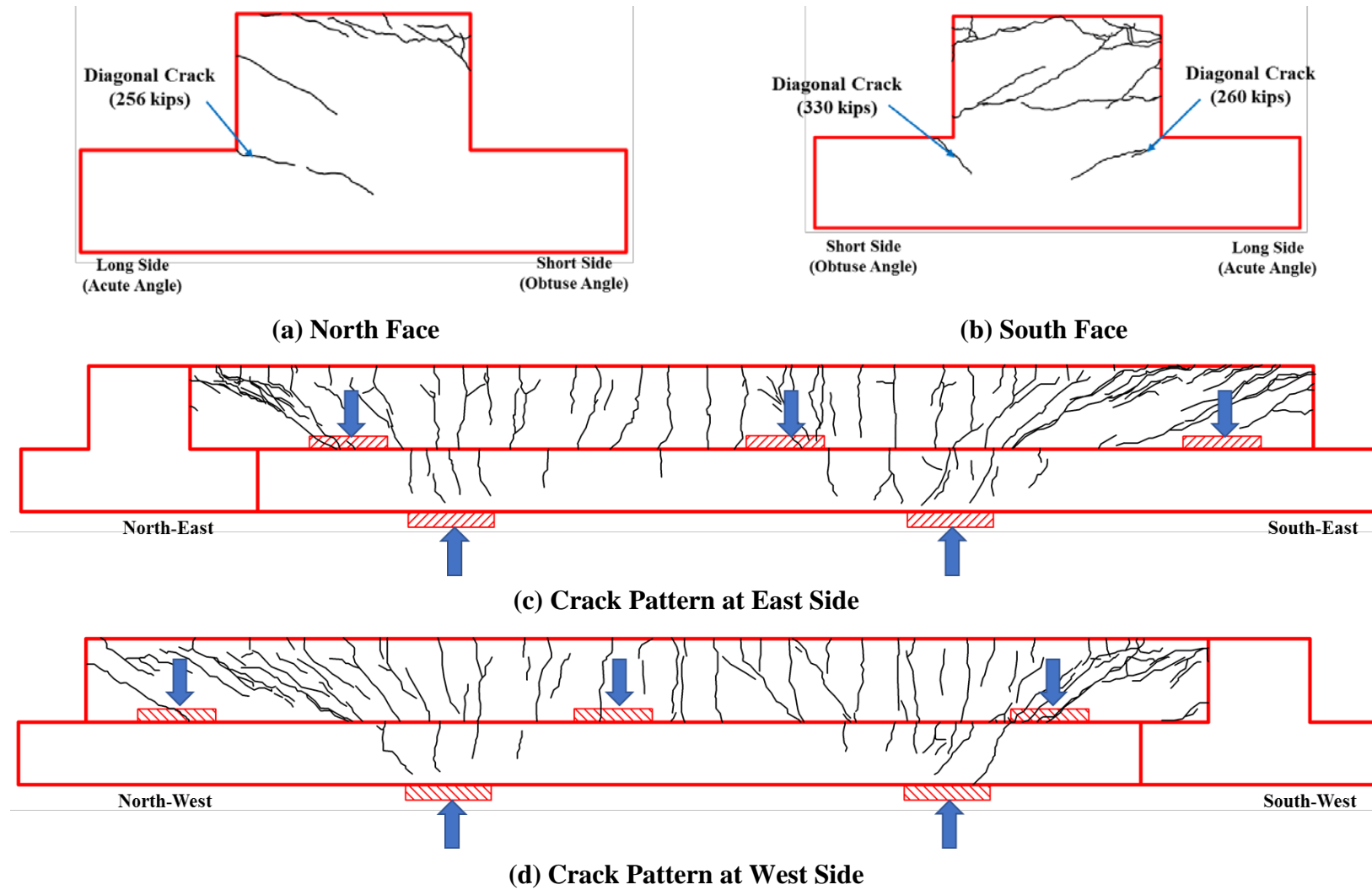
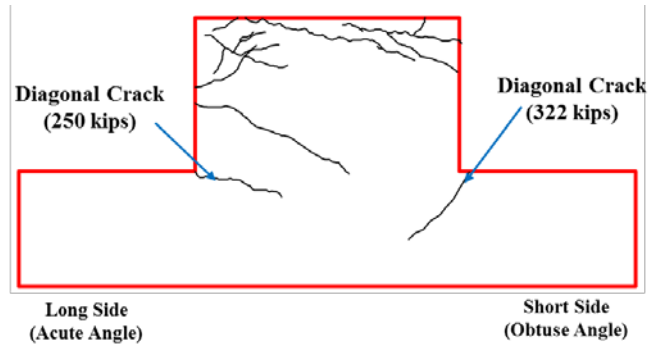
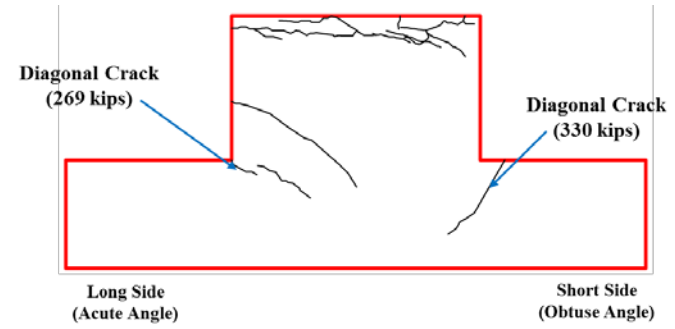


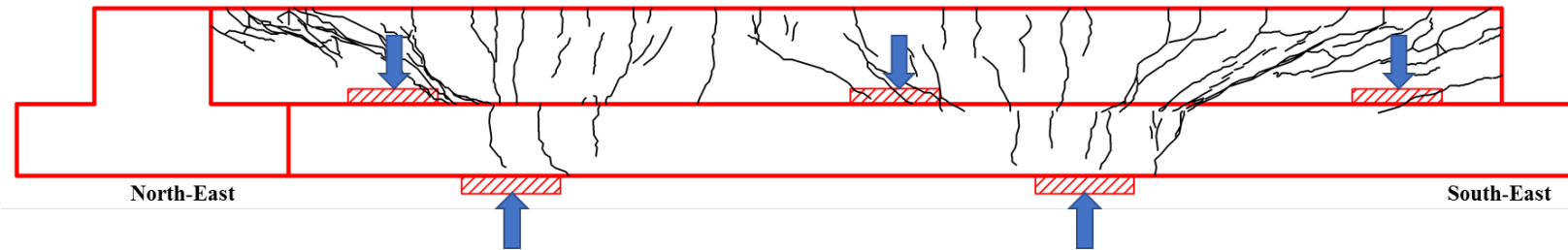
Figure 4.46. Cracking Pattern at Failure Stage for Specimen ITBC-45-T-M



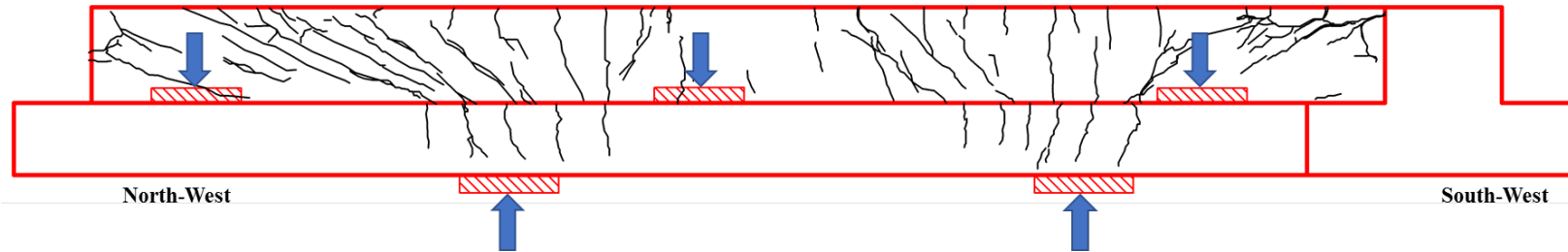
(a) North Face



(b) South Face



(c) Crack Pattern at East Side



(d) Crack Pattern at West Side

Figure 4.47. Cracking Pattern at Failure Stage for Specimen ITBC-45-S-M

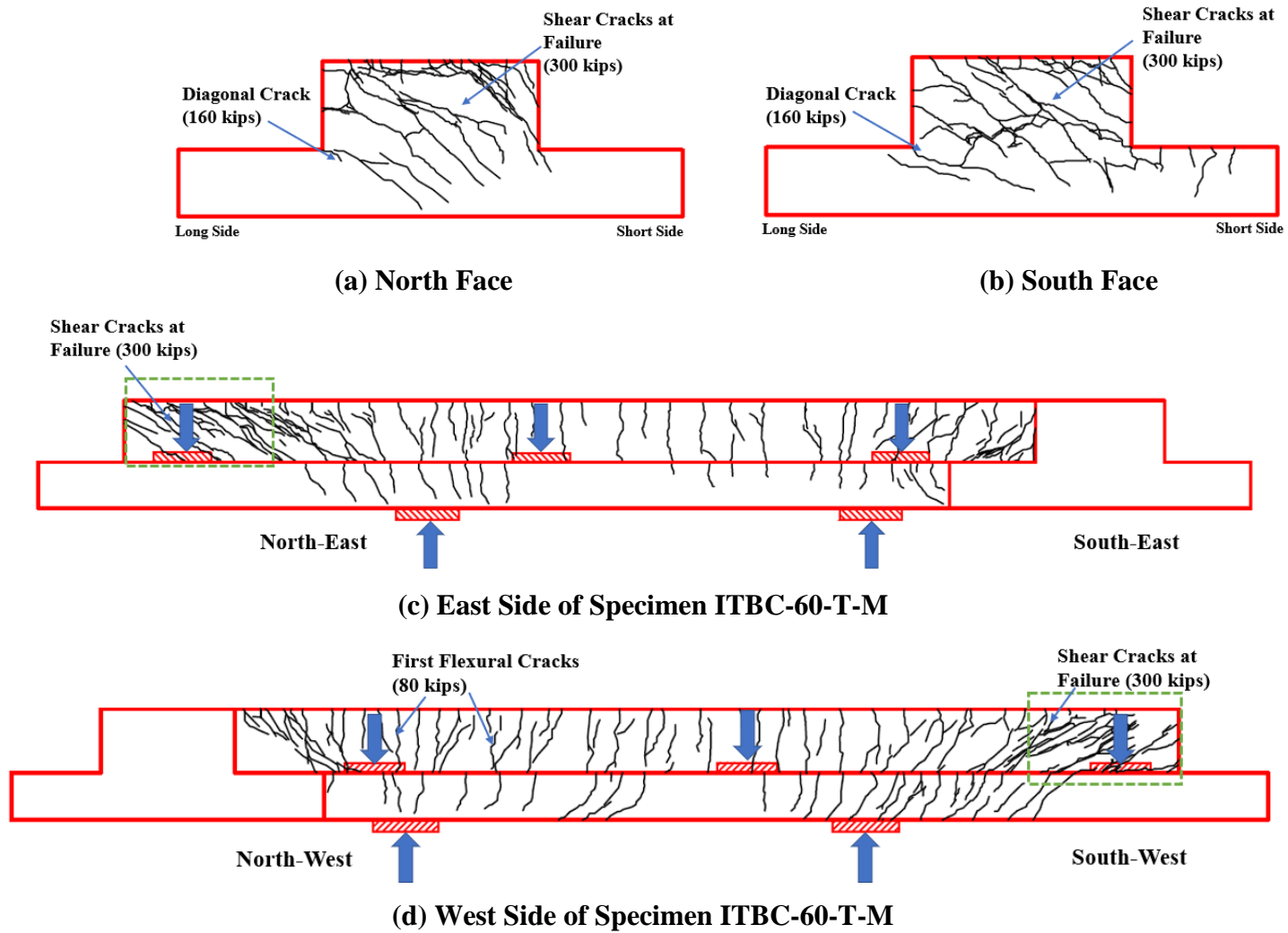


Figure 4.48. Cracking Pattern at Failure Stage for Specimen ITBC-60-T-M

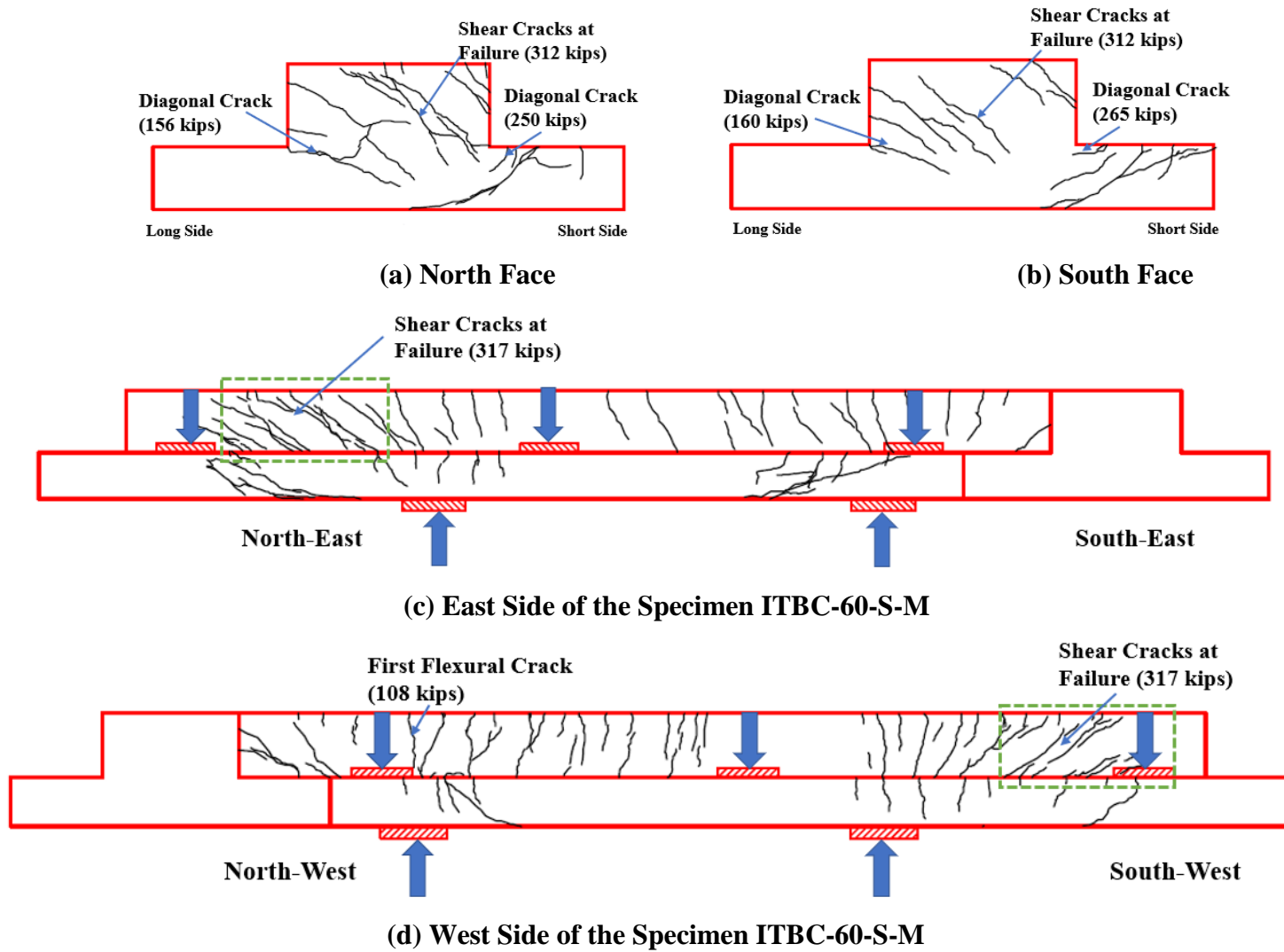


Figure 4.49. Cracking Pattern at Failure Stage for Specimen ITBC-60-S-M

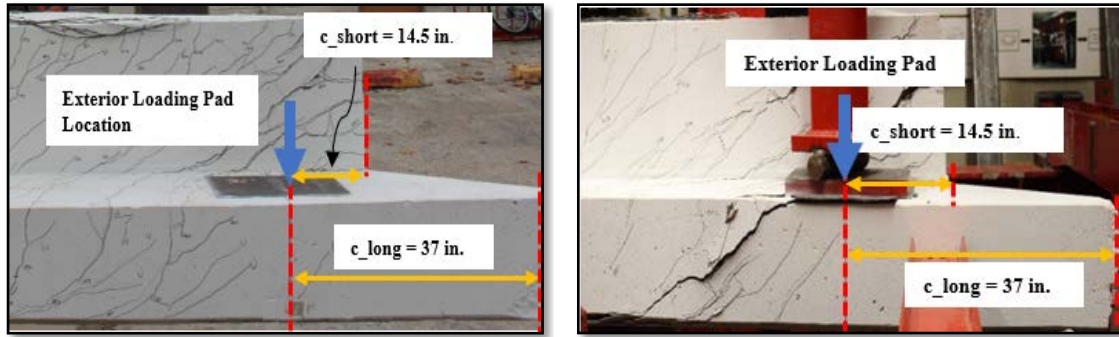
#### 4.5.4 Failure Modes of ITBC Specimens

For inverted-T bent caps designed with  $0^\circ$  and  $30^\circ$  transverse reinforcement, the failure was observed due to shear failure caused as a result of yielding of the shear reinforcements. This was further followed by the separation of the ledge from the web at both end face overhang parts of the specimen due to the failure of the transverse rebars located at the end region of the specimen. Since, the specimen was characterized  $0^\circ$  skew of transverse reinforcement, the torsional effect was not observed in this case.

Further, for two  $60^\circ$  specimens under Phase 1 designed with traditional transverse reinforcements (ITBC-60-T-2M) and proposed transverse skewed reinforcement (ITBC-60-S-2M), the common behavior at failure was observed. Both of the specimens failed at about the same peak support reaction (321 kips and 317 kips) under the torsional effect induced due to the high angle of skew apparently developing a large number of torsional cracks at the end regions (north and south) of the specimens. These cracks were not seen in the  $0^\circ$  skewed ITBC specimen. The yielding of transverse reinforcement at the peak load also contributed to the failure of the specimen.

In addition, the punching shear failure at the ledges was encountered in both of the specimens in Phase 1. In the case of ITBC-60-T-2M, the punching shear failure was observed in the ledges at both of the long sides of the specimen, designated as northeast and southwest side in Figure 4.41 (c) and (d). This type of failure could be attributed to the arrangement of transverse ledge reinforcement at the longer sides of the specimen. Figure 4.50 (a) and 4.50 (b) represent the punching shear failure of ledges observed for the specimen ITBC-60-T-2M at the northeast and southwest regions, respectively. Figure 4.51 shows the corresponding transverse reinforcement (partial) arrangement for the sections under consideration subjected to punching shear failure.

The reinforcement arrangement for the northeast end region as well as the southwest end region of the specimen is symmetrical as represented in Figure 4.51 since these are the identical long sides of the specimen at north and south end, respectively. In this region, ledge stirrups intersecting the face of the truncated pyramid can assist in supporting the concentrated load if anchorage of the stirrups is developed above and below the face of the truncated pyramid. However, no such contribution of stirrups is included in the punching shear equation provided by the AASHTO LRFD (2014) or TxDOT Bridge Design Manual (2015) due to complex checks on design and detailing of stirrups.



(a) North-east Ledge Region

(b) South-west Ledge Region

**Figure 4.50. Punching Shear Failure of Ledges in ITBC-60-T-2M**

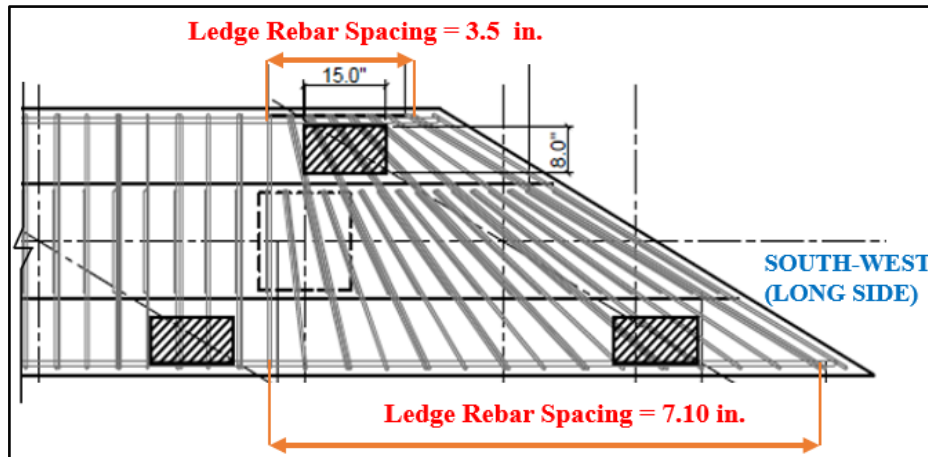


**Figure 4.51. Plan View of Partial Reinforcement Arrangement for ITBC-60-T-2M**

Thus, it is not possible to verify the contribution of provided ledge stirrups for the given sections subjected to punching shear failure. On the other hand, it is evident from the reinforcement arrangement depicted in Figure 4.51 that the spacing of the transverse ledge rebars in the region of punching shear failure is 7.10 inches which is twice the ledge rebar spacing of 3.5 inches provided at the short side of the specimen. With respect to the dense arrangement of ledge rebars on the short side, the punching shear failure could have possibly dominated at the ledges near both of the long sides of the specimen instead of short sides. In addition, TxDOT Bridge Design Manual guidelines recommend that the distance from the centerline of the exterior loading pad to the end of the inverted-T bent cap should be at least 24 inches to satisfy the adequate punching shear capacity requirement. For the ITBC-60-T-2M specimen, as shown in Figure 4.43 (a) and 4.43 (b), the distance between the centerline of the exterior loading pad and the longer edge ( $c_{long}$ ) is 37 inches which satisfies the requirement provided by TxDOT Bridge Design Manual. However, the distance between the centerline of the exterior loading pad and the shorter

edge ( $c_{short}$ ) of the specimen is 14.5 inches, which is less than the recommended distance for satisfying the punching shear capacity. This factor could also have contributed to the punching shear failure of ledges in the given specimen.

The phenomenon of punching shear failure was also observed in the case of the ITBC-60-S-2M specimen designed with proposed skewed transverse reinforcement. In the case of this specimen, the punching shear was observed at the ledges near the short sides of the specimen at the southeast and northwest end region, as represented in Figure 4.42 (c) and (d), respectively. Figure 4.52 (a) and (b) show the punching shear failure occurring at the southeast and northwest end of the ITBC-60-S-2M specimen, respectively.

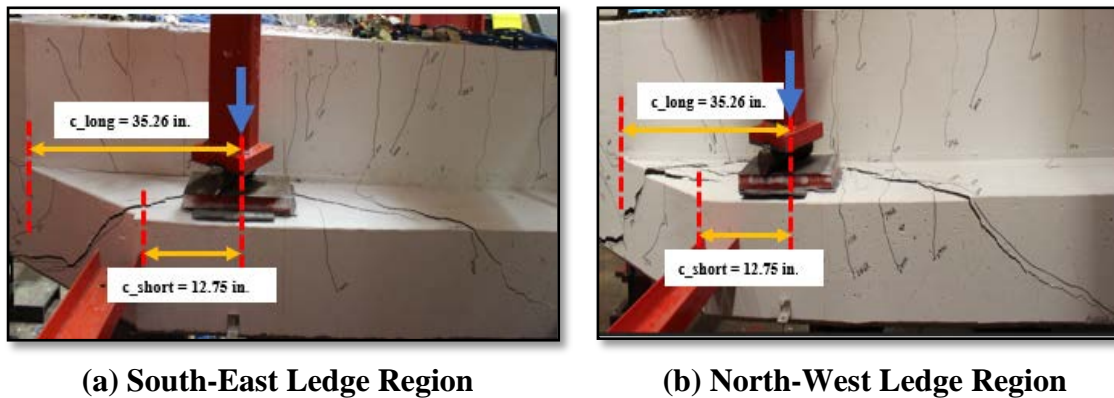


**Figure 4.52. Punching Shear Failure of Ledges in ITBC-60-S-2M**

Figures 4.47 and 4.48 show the torsional crack profile of 45 and 60-degree skew ITBC specimens with traditional and skew reinforcing. The number of torsional cracks that appeared is more severe in the case of the 45 and 60-degree traditional ITBC. Such torsional cracks were not observed in the case of any of the 30° ITBC specimens. This shows that the torsional effect becomes severe with a higher skew angle.

To summarize, all the inverted-T bent cap specimens characterized with skewed transverse reinforcement (traditional and proposed) were observed to be under the substantial effect of shear as well as torsion, and it was validated by the appearance of a large number of shear and torsional cracks at the failure stage. The punching shear failure of ledges was observed in both of the skewed ITBC specimens of Phase 1 whereas it did not arise in any of the specimens in Phase 2. The specimen designed with a 0° skewed angle in Phase 1 (ITBC-0-T-2M) did not seem to have any effect of torsion; however, the effect of shear was validated by the shear cracks observed at the failure stage.



(a)



(b)

**Figure 4.53. Torsional cracking profile at peak load :  
(a) ITBC-45-T-2M and (b) ITBC-45-S-2M**



(a)



(b)

**Figure 4.54. Torsional cracking profile at peak load:  
(a) ITBC-60-T-2M and (b) ITBC-60-S-2M**

## 4.6 CONCLUSIONS

The test matrix of this project consists of 13 ITBC specimens. Primary experimental results of strength and serviceability of the 13 specimens are summarized and discussed in this chapter. The difference of first yielding and peak capacities between the ITBCs with traditional and the corresponding skew transverse reinforcing is not significant, whereas the cracking performance of skew reinforcing is better than the traditional one. The number of shear cracks observed at peak reaction force in ITBCs with traditional reinforcing was more than that of ITBCs with skew reinforcing. The number of cracks observed in all the specimens with skew reinforcing is very close. Based on the test results, it is recommended that the skew ITBCs with skew reinforcing can be a better alternative to the traditional

reinforcing because the traditional detailing of transverse reinforcements in skew ITBCs brings complexity into the design and construction process. Therefore, any kind of improper detailing can cause poor placement of concrete and cracks within the concrete structure which would reduce the load carrying capacity and increase future maintenance costs. Faster and easier construction can be obtained if the skew transverse reinforcing steel is utilized and it can provide an alternative approach which will significantly reduce the design complexities and construction period.

## CHAPTER 5: FINITE ELEMENT (FE) ANALYSIS

### 5.1 OVERVIEW

In this chapter, the 3D finite element (FE) analysis model of all the test specimens using ABAQUS are calibrated against the test results of each ITBC specimen tested in this project. Also, a comprehensive parametric study has been presented in order to understand the overall structural behavior of skew reinforcement in inverted-T bridge bent caps.

### 5.2 FINITE ELEMENT ANALYSIS OF TEST SPECIMENS

#### 5.2.1 Finite Element Modeling

The finite element model of the ITBC test specimens was developed using 3D finite element (FE) software ABAQUS (2014), as shown in Figure 5.1. The two square rigid supports representing columns under the bridge bent cap are fixed at the bottom faces. There is a total of six loading pads tied on top of the ledges. The superstructure loads from bridge girders are transferred to the bridge bent cap through these loading pads.

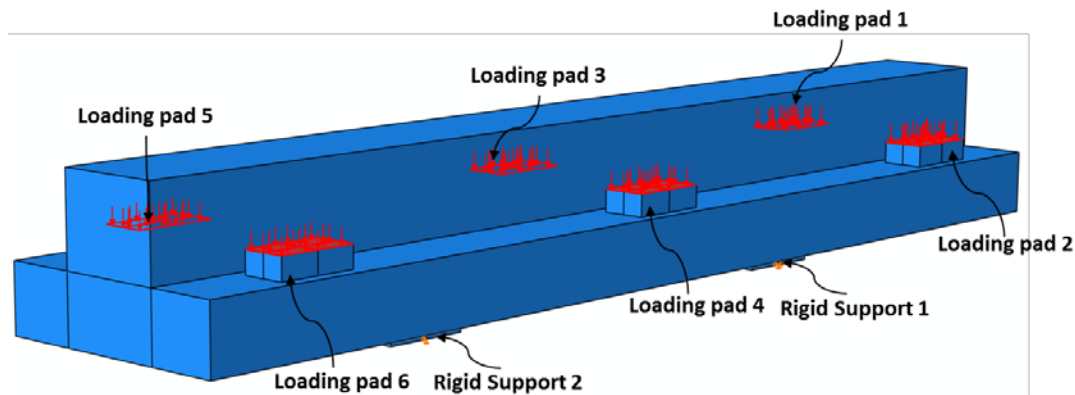


Figure 5.1. 3D FE Model of ITBC-0-T-2M

The concrete of the inverted-T bridge bent caps is modeled using an eight-node, reduced integration, hourglass control solid element (C3D8R). A 2-node linear three-dimensional (3-D) truss element (T3D2) is used to model the reinforcement because it is only subjected to axial force. The FE mesh of a 30° skew ITBC is shown in Figure 5.2. In the analysis, the same amount of loading was applied to each of the loading pads using the ABAQUS multiple points control method (MPC), which not only ensures the same loading condition for each pad, but also allows the displacement control during the loading process to gain the full performance curve of the inverted-T bridge bent cap specimen. The following constraint equation is established for the system:

$$\Delta_1 + \Delta_2 + \Delta_3 + \Delta_4 + \Delta_5 + \Delta_6 - 6\Delta_{cp} = 0 \quad (5.1)$$

where

$\Delta_i$  is the deflection of the  $i$  th loading pad in z-direction.

$\Delta_{cp}$  is the deflection of the control point in z-direction.

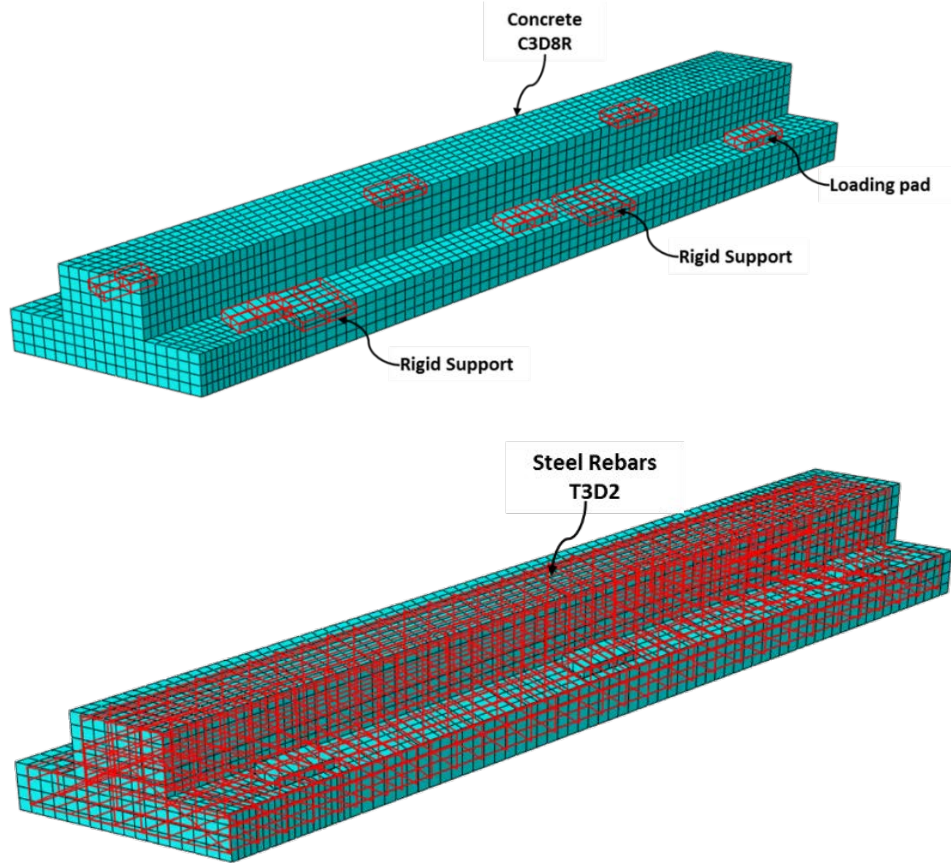


**Figure 5.2. 3D Finite Element Mesh of ITBC in ABAQUS:  
C3D8R Solid element for concrete and T3D2 truss element for reinforcements**

Two types of detailing of the transverse reinforcing bars, modeled in ABAQUS are shown in Figure 5.3(a)–5.3(m) for all 13 test specimens. The first detailing is current TxDOT skew inverted-T bridge caps using the traditional way of fanning out the rebars to match the skew angle. The second detailing, in which all transverse reinforcing bars are arranged in a complete skewed direction, is proposed to be used because it is much simpler in design and construction. The spacing and detailing of each rebars in ABAQUS are the same as during the design and construction stage of the test specimens.

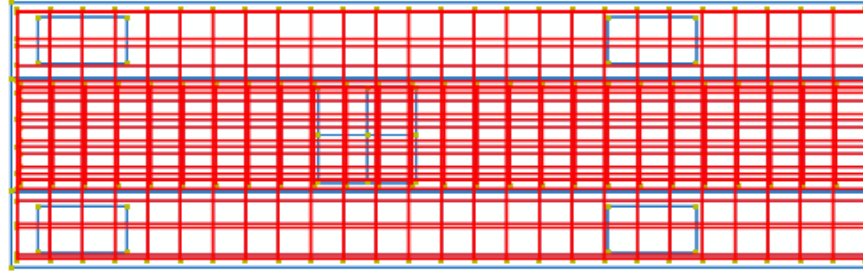
### 5.2.2 Material Models

The Concrete Damaged Plasticity (CDP) model is used as the constitutive model of concrete in the FEM model (Lee and Fenves, 1998). The CDP model requires the definition of uniaxial behavior in compression and tension. The stress-strain curves of concrete

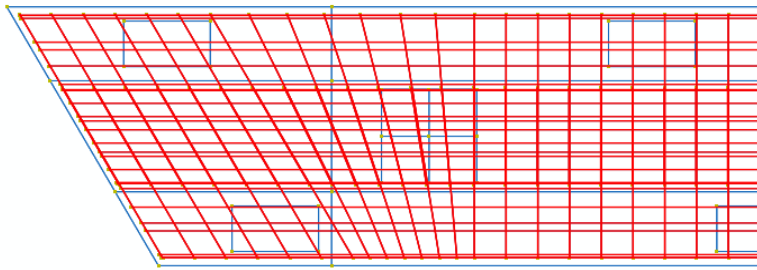
considered in the constitutive model are adopted from the book “Unified Theory of Concrete Structures” by Thomas T.C. Hsu and Y. L. Mo.

The uniaxial compression stress-strain behavior of concrete can be defined using the parabolic stress-strain model, as shown in Figure 5.4. Equation 1 is used to develop the compression stress-strain curve.

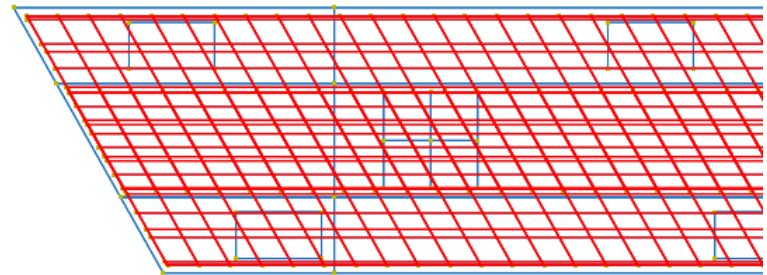
$$\sigma_c = f'_c \left[ \frac{2\varepsilon_c}{\varepsilon_0} - \left( \frac{\varepsilon_c}{\varepsilon_0} \right)^2 \right] \quad (\text{psi}) \quad \text{Eq. 5.2}$$



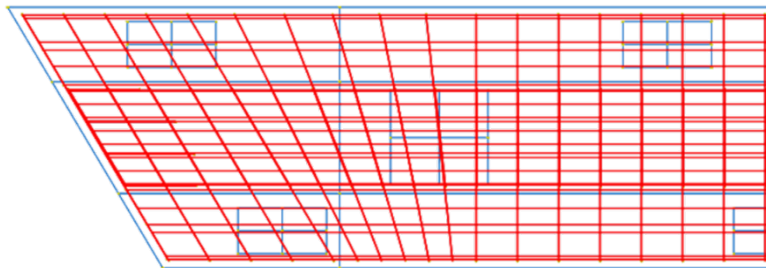
(a) ITBC-0-T-2M



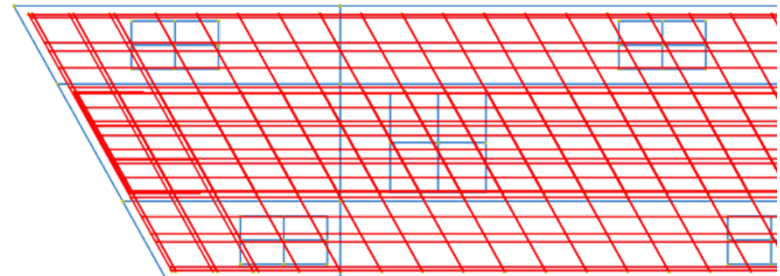
(b) ITBC-30-T-2M



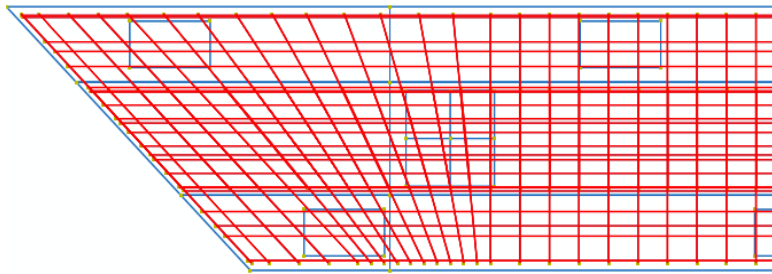
(d) ITBC-30-S-2M



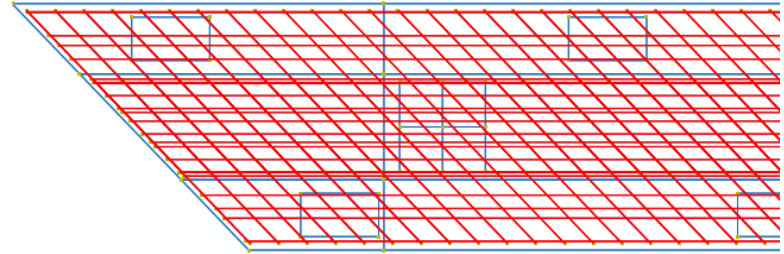
(c) ITBC-30-T-M



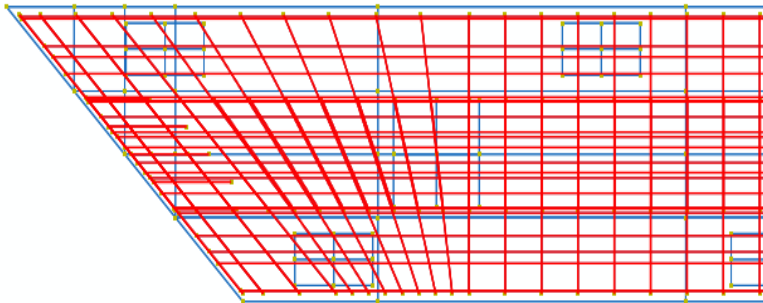
(e) ITBC-30-S-M



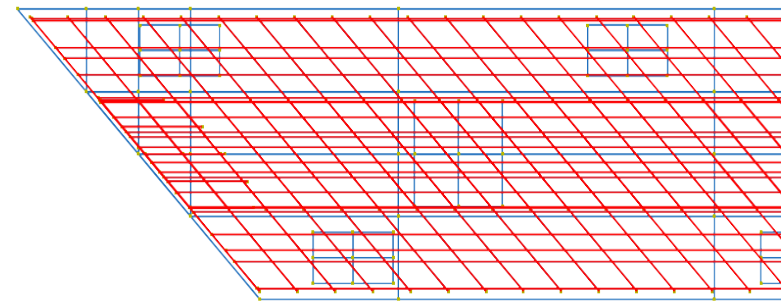
**(f) ITBC-45-T-2M**



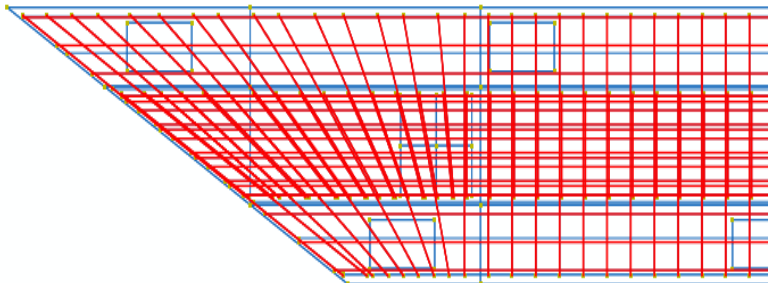
**(h) ITBC-45-S-2M**



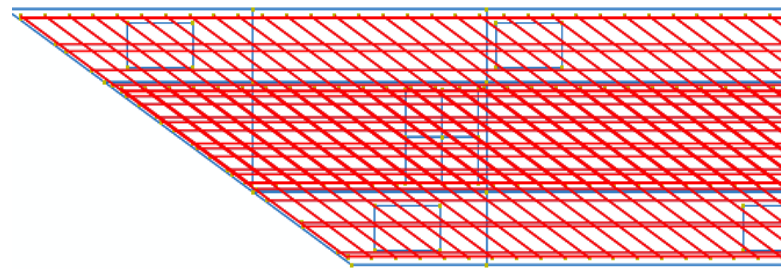
**(g) ITBC-45-T-M**



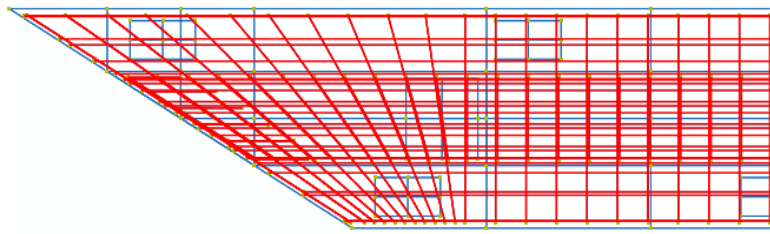
**(i) ITBC-45-S-M**



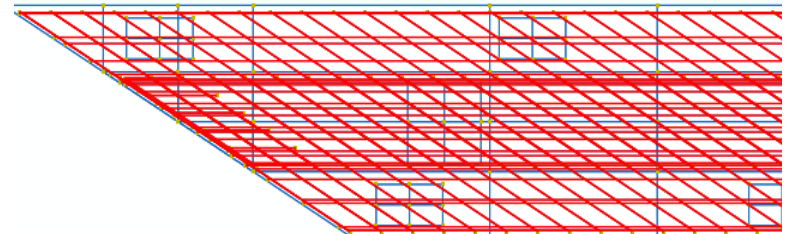
**(j) ITBC-60-T-2M**



**(l) ITBC-60-S-2M**



(k) ITBC-60-T-M



(m) ITBC-60-S-M

**Figure 5.3. Plan View of Partial Reinforcing in ABAQUS**

In ABAQUS, the model of concrete (Lubliner et al., 1989) requires the definitions of initial elastic modulus  $E_c$  and Poisson ratio  $\nu$ . The initial elastic modulus  $E_c$  can be calculated using the AASHTO empirical equation (AASHTO 2014):

$$E_c = 57000 \sqrt{f'_c} \text{ (psi)} \quad \text{Eq. 5.3}$$

The Poisson ratio of concrete under uniaxial compressive stress ranges from about 0.15 to 0.22, with a representative value of 0.19 or 0.2 (AASHTO). In this report, the Poisson ratio of concrete is assumed to be  $\nu = 0.2$ .

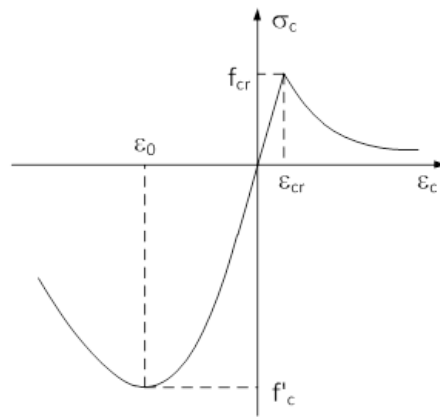


**Figure 5.4. Stress-Strain Curves of Concrete in Tension and Compression**

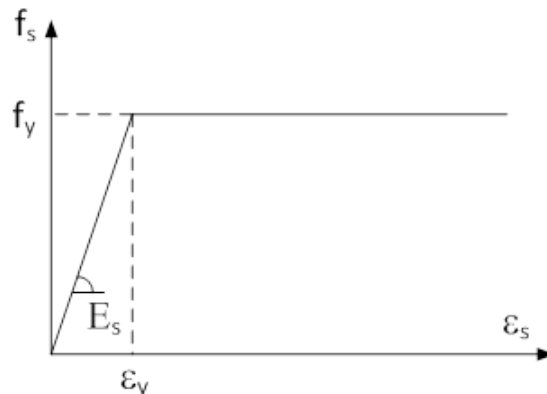


**Figure 5.5. Stress-Strain Curve of Mild Steel**

The uniaxial tension stress-strain behavior of smeared (average) concrete was proposed by Belarbi and Hsu (1994), as shown in Figure 5.4. Equations 5.4 and 5.5 are used to develop the tensile stress-strain curve.

Ascending branch:

$$\sigma_c = E_c \varepsilon_c \quad \varepsilon_c \leq \varepsilon_{cr} \quad (5.4)$$

Descending branch:

$$\sigma_c = f_{cr} \left( \frac{\varepsilon_c}{\varepsilon_{cr}} \right)^{0.4} \quad \varepsilon_c > \varepsilon_{cr} \quad (5.5)$$

where  $E_c$  = the elastic modulus of concrete;  $\varepsilon_{cr}$  = the cracking strain of concrete taken as 0.00008 and  $f_{cr}$  = the cracking stress of concrete taken as  $0.00008E_c$ .

The stress-strain curve of the reinforcing bar is assumed to be elastic and perfectly plastic as shown in Figure 5.5. In the ABAQUS program, the bond-slip effect between concrete and steel is not considered. In order to properly model the steel, the cross-section area, position and orientation of each steel bar within the concrete element needs will be specified.

Elastic branch:

$$f_s = E_s \varepsilon_s \quad \varepsilon_s \leq \varepsilon_y \quad (5.6)$$

Plastic branch:

$$f_s = f_y \varepsilon_s > \varepsilon_y \quad (5.7)$$

where  $E_s$  = the elastic modulus of steel taken as 29000 ksi and  $\varepsilon_y$  = the yielding strain of steel.

The details of material parameters of the concrete damaged plasticity model for Specimens 1 to 13 are listed in Table 5.1.

**Table 5.1. Material Parameters for the Concrete Damaged Plasticity Model**

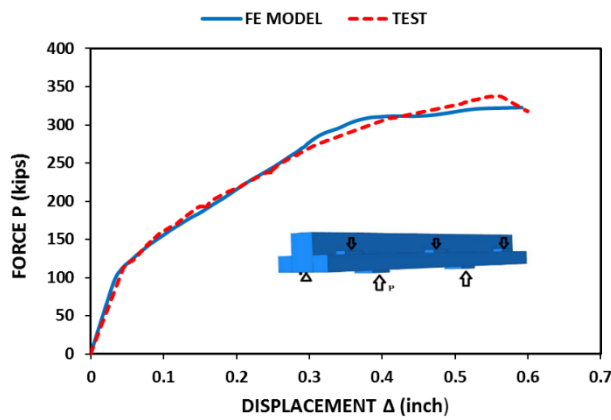
<b>Specimen designation</b>	<b>Young's modulus (ksi)</b>	<b>Poisson's ratio</b>	<b>Compressive strength (ksi)</b>	<b>Tensile strength (ksi)</b>	<b>Density (lb/ft<sup>3</sup>)</b>	<b>Dilation<sup>a</sup> angle (°)</b>	<b>Flow potential eccentricity<sup>a</sup></b>	<b>K<sup>a,b</sup></b>	<b>Viscosity coefficient (relaxation time)<sup>a</sup></b>
ITBC-0-T-2M	4936	0.2	7.3	0.3896	150	31	0.1	0.6667	1.0e-5
ITBC-30-T-2M	4936	0.2	7.5	0.3949	150	31	0.1	0.6667	1.0e-5
ITBC-30-T-M	5066	0.2	7.9	0.4053	150	31	0.1	0.6667	1.0e-5
ITBC-30-S-2M	4870	0.2	7.3	0.3896	150	31	0.1	0.6667	1.0e-5
ITBC-30-S-M	4837	0.2	7.2	0.3869	150	31	0.1	0.6667	1.0e-5
ITBC-45-T-2M	4969	0.2	7.6	0.3975	150	31	0.1	0.6667	1.0e-5
ITBC-45-T-M	5193	0.2	8.3	0.4154	150	31	0.1	0.6667	1.0e-5
ITBC-45-S-2M	5034	0.2	7.8	0.4027	150	31	0.1	0.6667	1.0e-5
ITBC-45-S-M	5162	0.2	8.2	0.4129	150	31	0.1	0.6667	1.0e-5
ITBC-60-T-2M	5317	0.2	8.7	0.4253	150	31	0.1	0.6667	1.0e-5
ITBC-60-T-M	4700	0.2	6.8	0.3760	150	31	0.1	0.6667	1.0e-5
ITBC-60-S-2M	5377	0.2	8.9	0.4302	150	31	0.1	0.6667	1.0e-5
ITBC-60-S-M	5130	0.2	8.1	0.4104	150	31	0.1	0.6667	1.0e-5

<sup>a</sup> Systemes (2014)

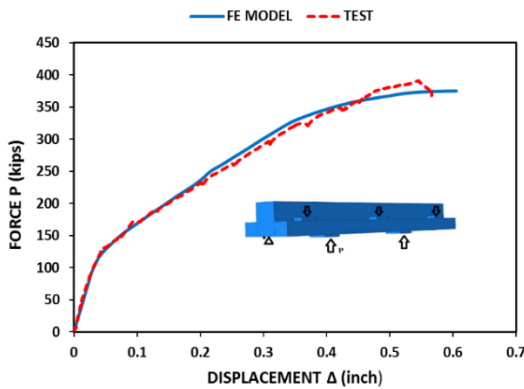
<sup>b</sup> Ratio K of the second stress invariant on the tensile meridian to that on the compressive meridian for the yield function

### 5.2.3 Finite Element Simulated Results

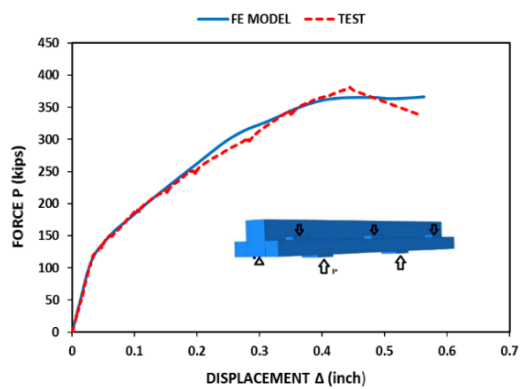
The comparison of the force-displacement curves between the test results and the finite element analysis outcomes for all the test specimens is shown in Figure 5.6. The y-axis is the reaction force ( $P$ ) from the north support in kips and the x-axis is the vertical displacement ( $\Delta$ ) of the cap's north free end in inches. It can be seen from the force-displacement curves of the specimens that both the analytical and test curves match well with each other at all the loading stages. Even though in most of the cases the simulated peak load is somewhat lower than that of the experimental result, the FE model can simulate the structural behavior of the test specimens well.



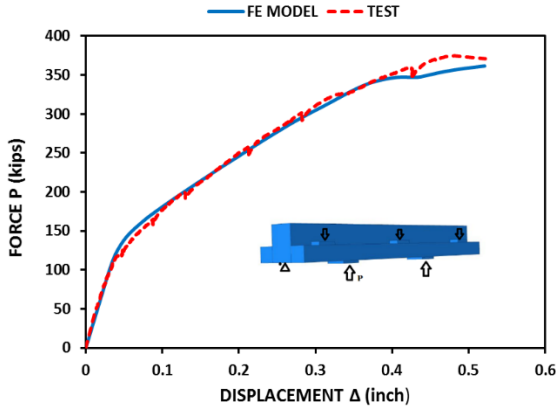
(a) ITBC - 0 -T-2M



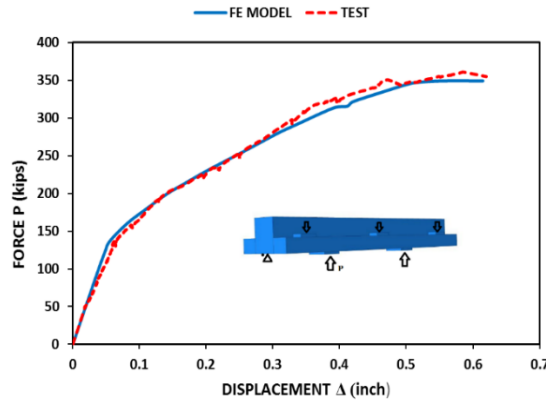
(b) ITBC - 30 -T-2M



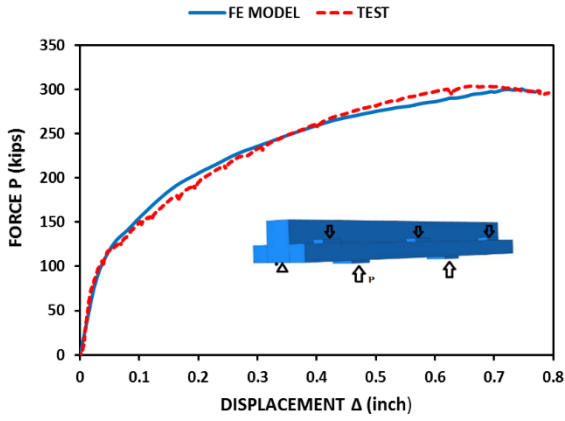
(c) ITBC - 30 -S-2M



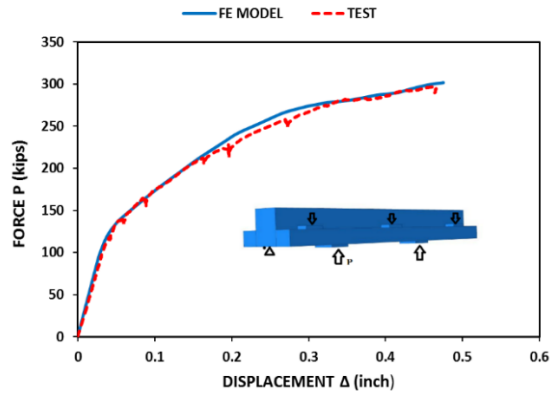
(d) ITBC - 45 -T-2M



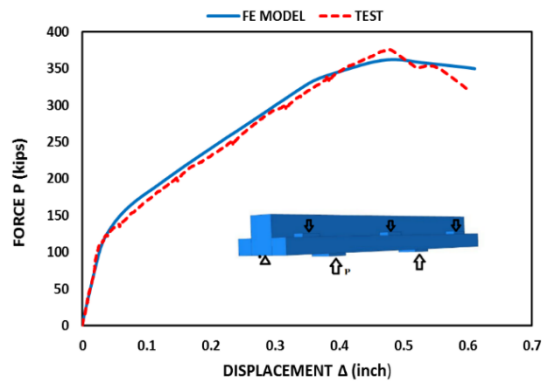
(e) ITBC - 45 -S-2M



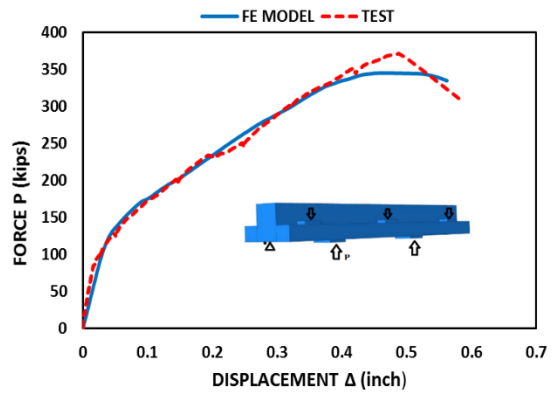
(f) ITBC - 60 -T-2M



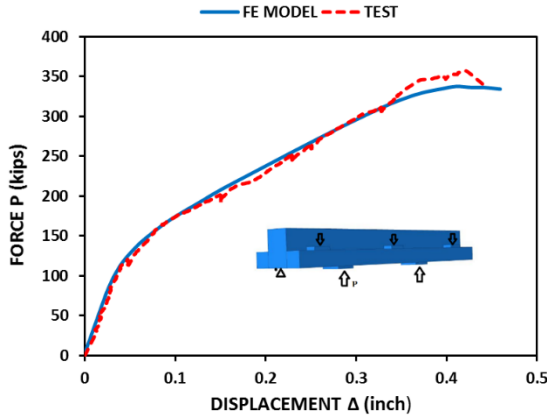
(g) ITBC - 60 -S-2M



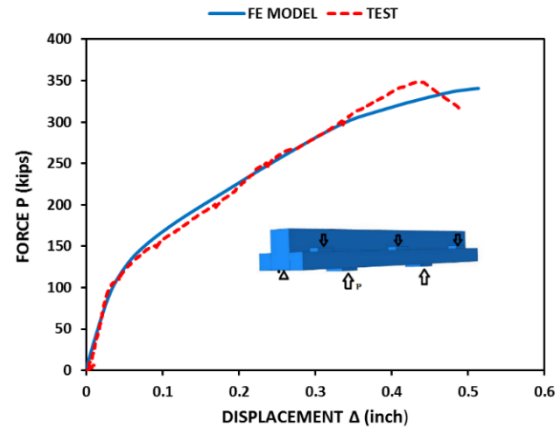
(h) ITBC - 30 -T-M



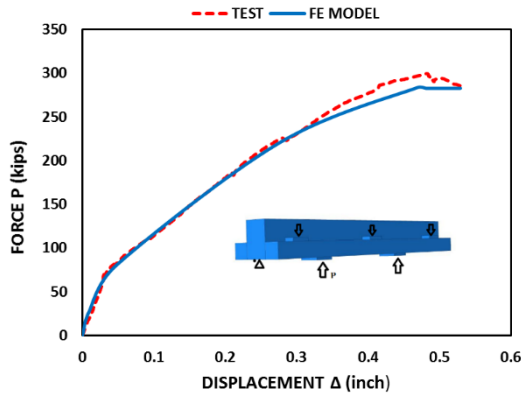
(i) ITBC - 30 -S-M



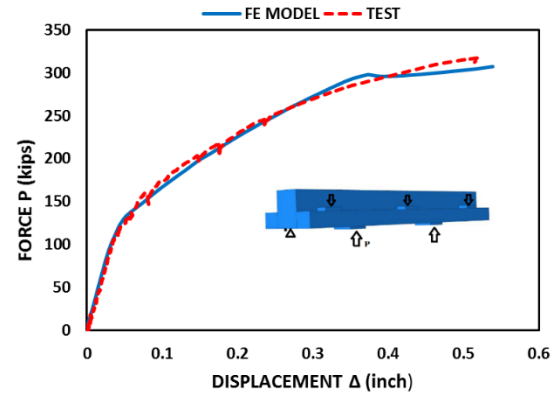
(j) ITBC - 45 -T-M



(k) ITBC - 45 -S-M



(l) ITBC - 60 -T-M



(m) ITBC - 60 -S-M

**Figure 5.6. Comparison of Force – Displacement Curves**  
**(red: TEST; blue: FE MODEL)**

### 5.3 PARAMETRIC STUDY

The parametric analysis is intended to identify and examine the effects of certain critical parameters. The simulation of inverted-T test specimens is performed in order to understand the overall structural behavior of skew reinforcement in inverted-T bridge bent caps taking into account unexplored parameters in the test matrix.

The analysis was performed with two loading cases. The first one is the service load which includes dead load and live load with the load combination factor equal to one. To determine the vertical dead load and the live load acting on the specimen, the dead load and live load acting on the full-scale bent cap will be estimated, and they will be scaled down with the scaling law to obtain the equivalent loads acting on the scaled specimen. The second loading case is the yielding load. In this case, the load will be applied (increased) until the crushing of the concrete of the test specimen (i.e., when the maximum

compressive strain of the concrete reaches 0.004). Moreover, the occurrence of the first yielding at transverse reinforcement for both traditional and skew cases will be monitored. For the parametric study, the analysis during the course is divided into several groups. In each group, the finite element models of the bridge caps were kept identical, except that one parameter (i.e., skew angle) was selected to change in order to examine the effect of this parameter on the behavior of the structure.

### 5.3.1 Comparison of Deformations for Various Skew Angles

Figure 5.7 shows the deformation patterns at the end of the bridge cap at the service load, corresponding to different values of the skew angle. As can be seen from the figure, there are unsymmetrical deformations in all skew cases except the 0° skew case. Even though the same amount of load is applied to each of the loading pads, the unsymmetrical deformations in all skew cases are caused by torsional moments generated by the unsymmetrical locations of bearing pads on the ledges of the bridge cap (see Figure 5.3 for the locations of the bearing pads). It can also be seen that the torsional deformations increase when the skew angle increases.

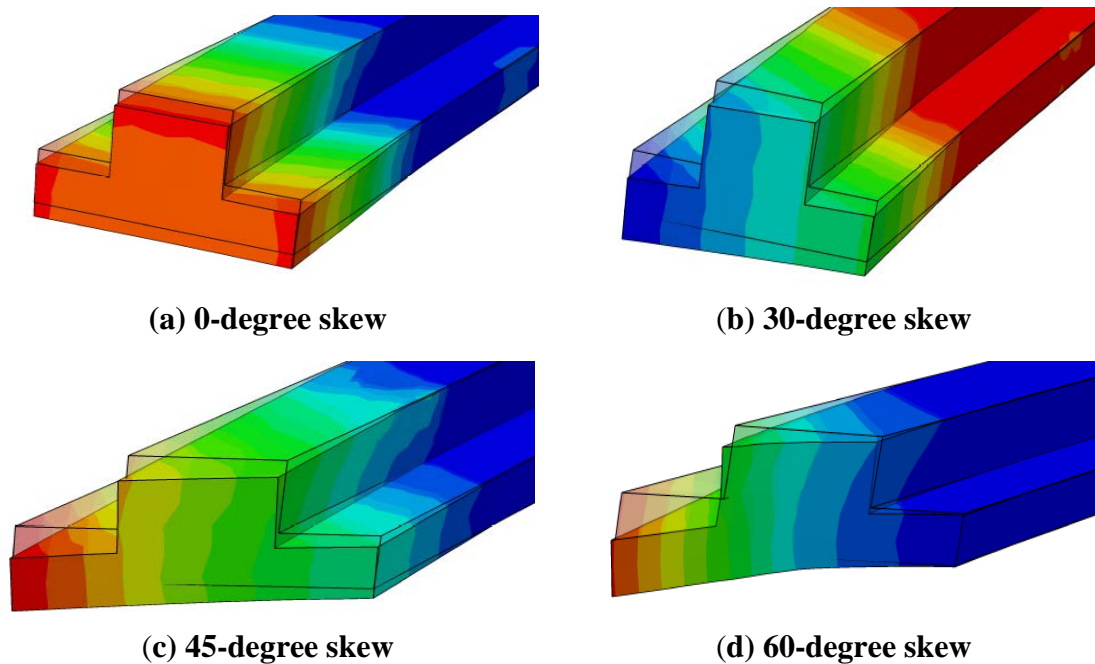
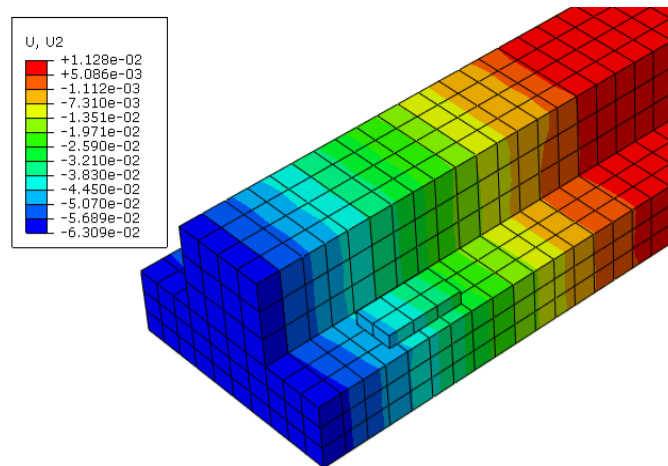


**Figure 5.7. Deformations of skew ITBCs for Various Skew Angles**

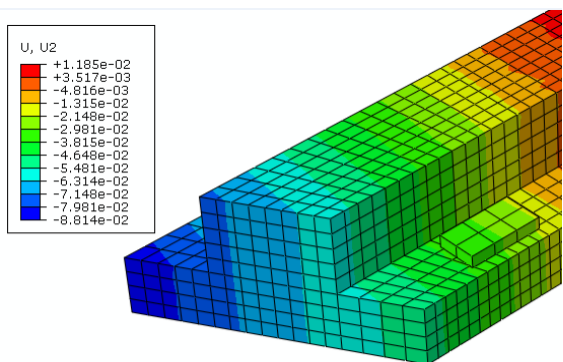
### 5.3.2 Comparison of Displacements at Service Load

Figure 5.8 shows the magnitude of the deformations at the end of the bridge cap at the service load, corresponding to skew angles 0, 30, 45 and 60 degrees for each of the traditional and skew reinforcements. As can be seen from the figure, for the 0-degree skew case there is the smallest deformation (i.e., 0.063 inches) whereas the largest deformation

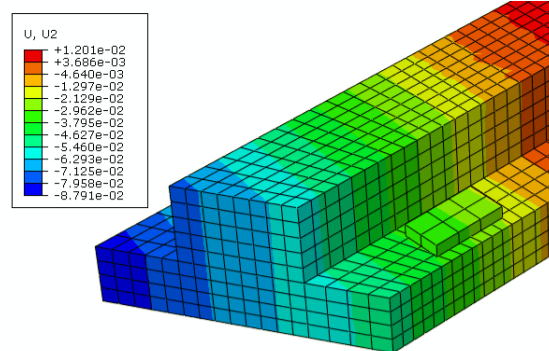
is found in the 60-degree skew case (i.e., 0.223 inches). The larger deformation in the 60-degree case can be attributed to torsion generated by the unsymmetrical locations of the bearing pads on the ledges of the bridge cap. In each figure, the deformations at the end of the bridge cap for the traditional and skew reinforcements are shown for comparison. It can be seen from Figures 5.8(b)–(m) that the deformation contour and maximum deformation in both cases are very similar. In other words, the bent caps using normal and skewed transverse reinforcement have similar structural behavior. However, for Phase 2 specimens with M amount of transverse reinforcements and side bars at the end face [Figure 2.2 (a)], the deformations at the end are smaller than the corresponding Phase 1 specimens with 2M transverse reinforcements. For example, the maximum displacement for ITBC-60-T-2M is 0.223 inches, whereas for ITBC-60-T-M is 0.181 inches. The same trend can also be observed in other cases. The maximum displacement is the deep blue color contour, and the negative sign indicates the displacement is downward. This smaller displacement is due to the use of end face rebars (U1, U2, and G bars) in all Phase 2 specimens.



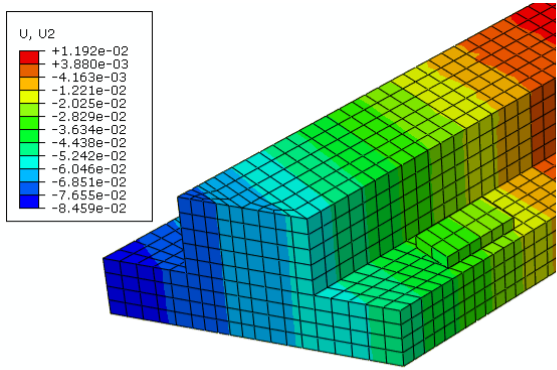
(a) ITBC-0-T-2M



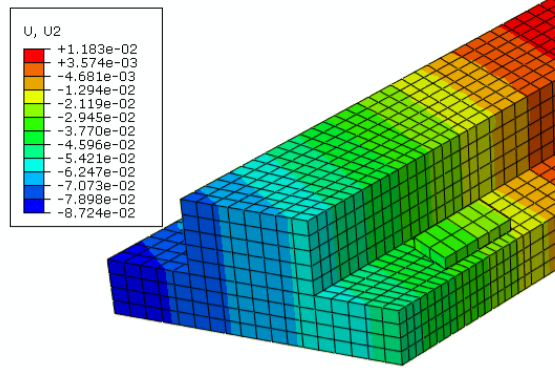
(b) ITBC-30-T-2M



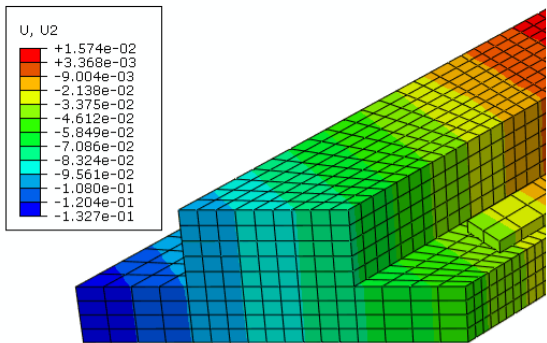
(c) ITBC-30-S-2M



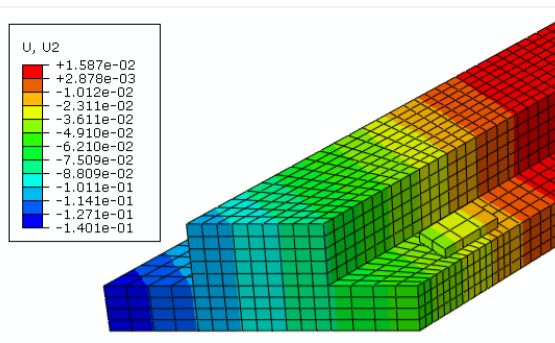
(d) ITBC-30-T-M



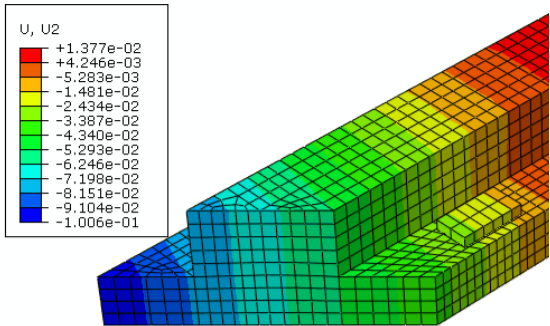
(e) ITBC-30-S-M



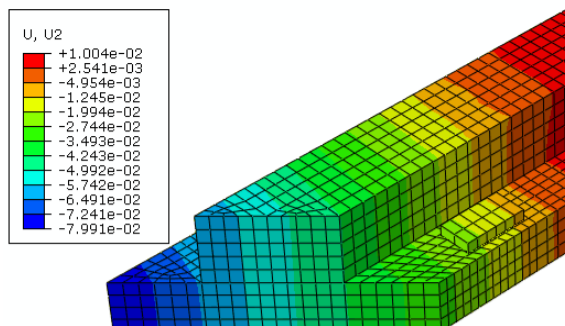
(f) ITBC-45-T-2M



(g) ITBC-45-S-2M



(h) ITBC-45-T-M



(i) ITBC-45-S-M

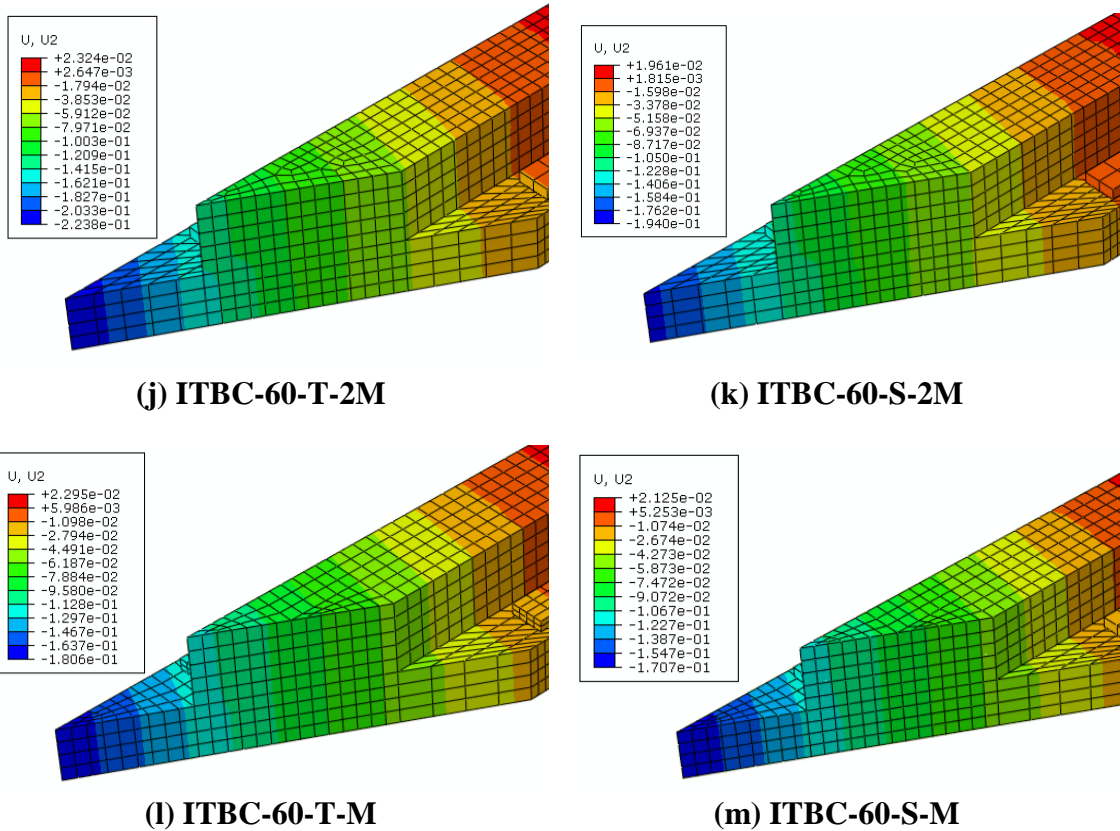
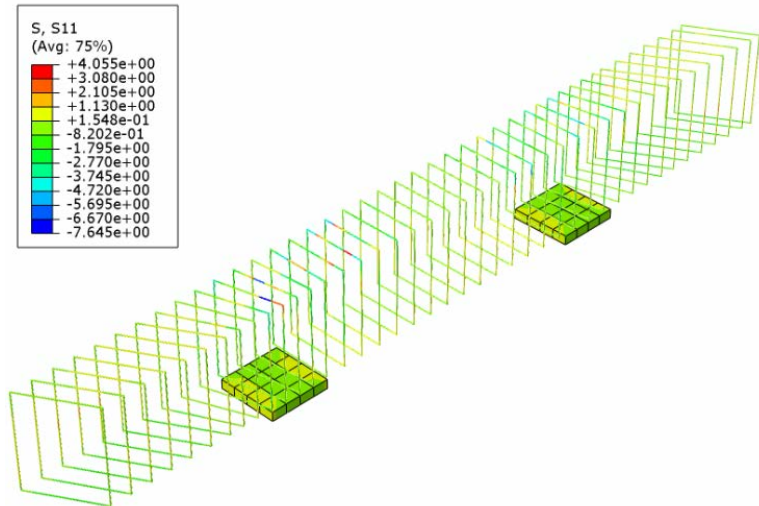


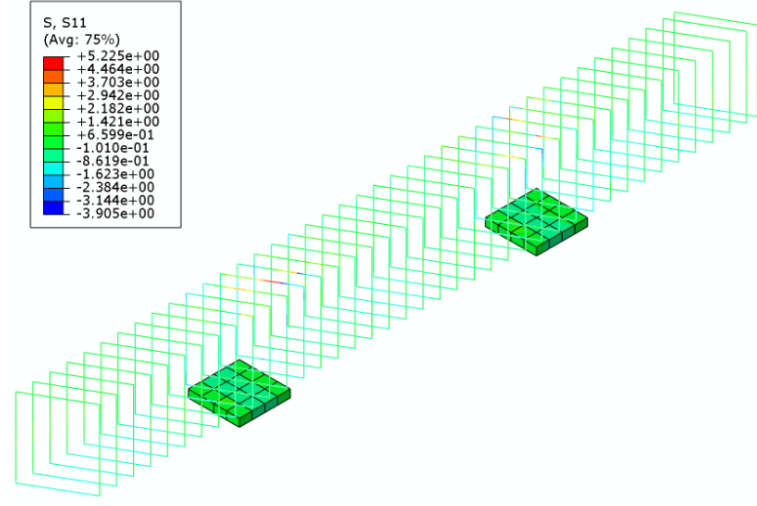
Figure 5.8. Displacement at Service Load for Various Skew Angle

### 5.3.3 Stresses in Transverse Rebars at Service Load

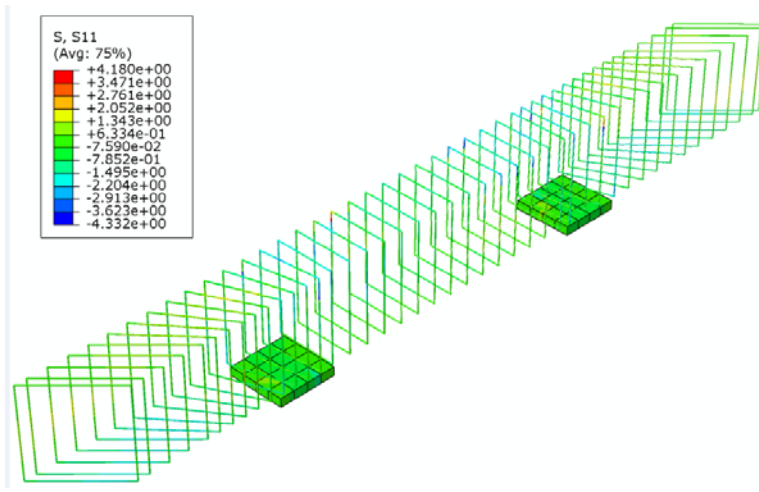
Figure 5.9 illustrates the contour plot of stresses in the transverse reinforcement of the skew bent caps of Phase 1 test specimens corresponding to skew angles of  $0^\circ$ ,  $30^\circ$ ,  $45^\circ$  and  $60^\circ$ , respectively. In each figure, the stresses in transverse rebars for the traditional and skew transverse reinforcement are shown for comparison. It can be observed that the stress contour and maximum stresses in transverse rebars for both cases are very similar. In other words, the bent caps using traditional and skew transverse reinforcement have similar structural behavior. The small difference in stresses between the traditional and skew transverse reinforcement can be attributed to the non-uniform spacing of traditional transverse reinforcements, unlike the skew transverse reinforcement where the spacing between all transverse reinforcements are uniform. A similar kind of trend in stresses was also observed for Phase 2 specimens.



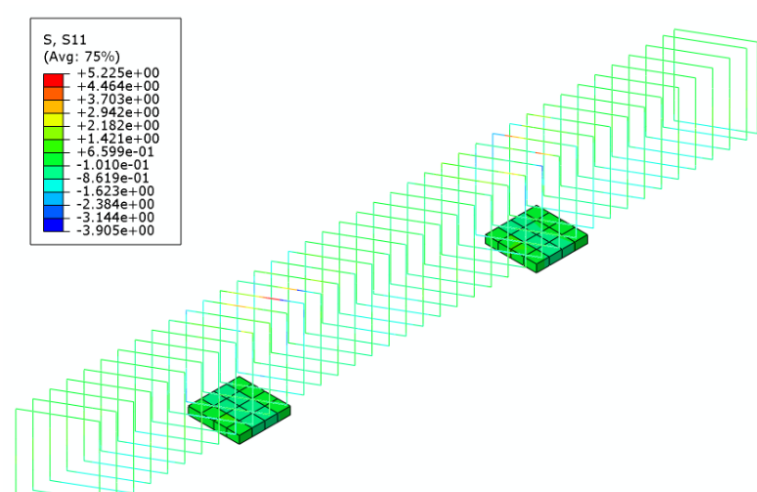
(a) ITBC-30-T-2M



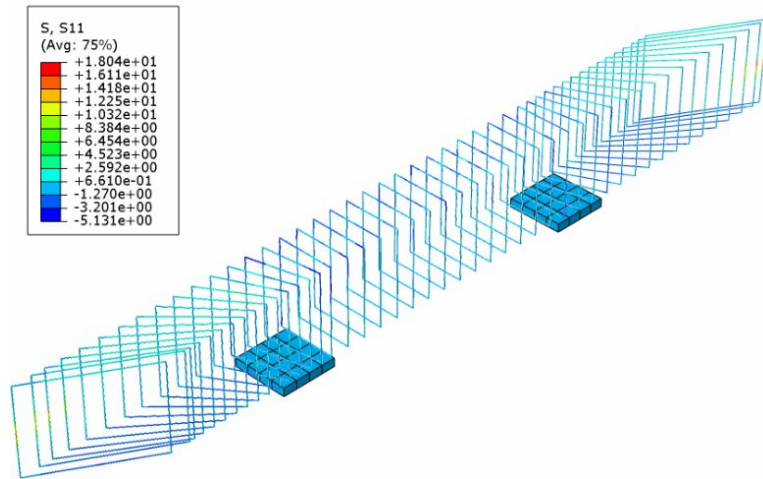
(b) ITBC-30-S-2M



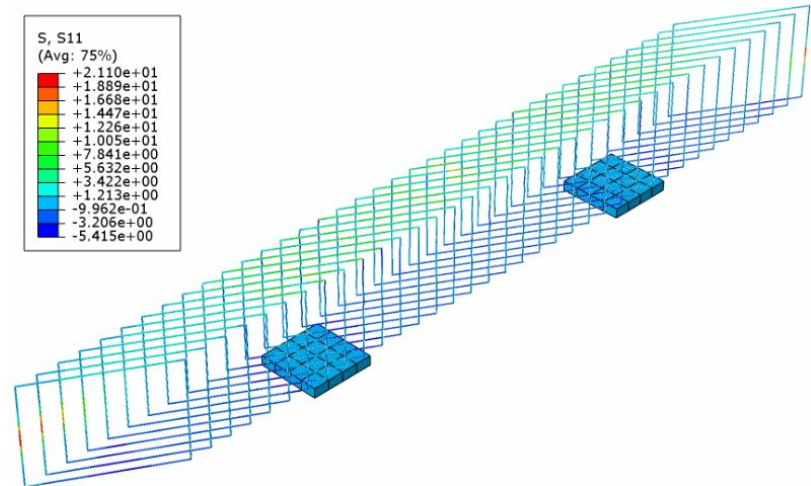
(c) ITBC-45-T-2M



(d) ITBC-45-S-2M



(e) ITBC-60-T-2M

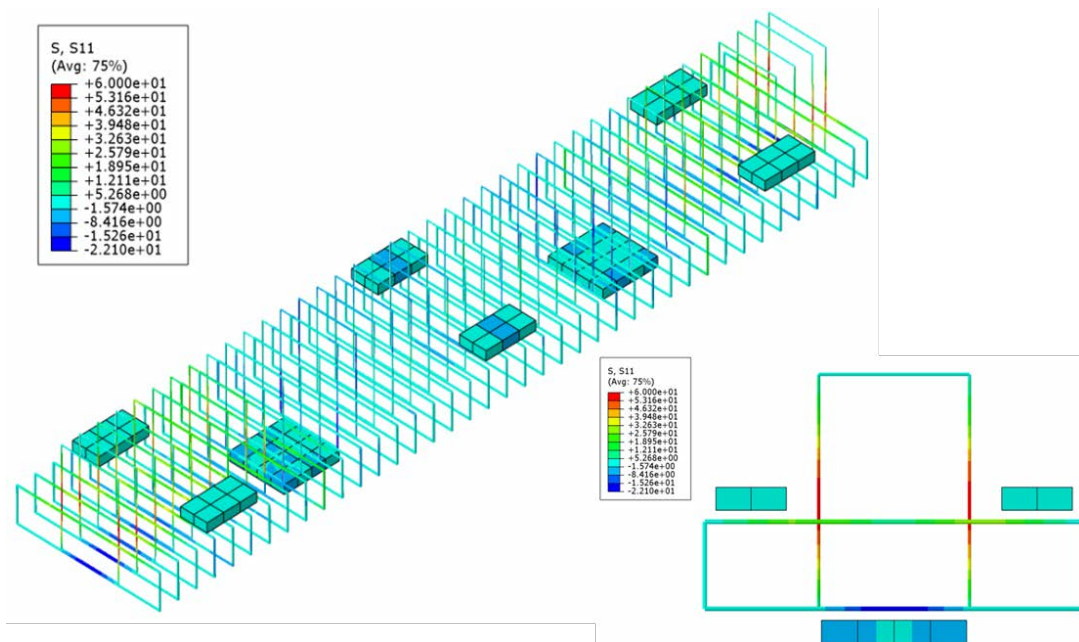


(f) ITBC-60-S-2M

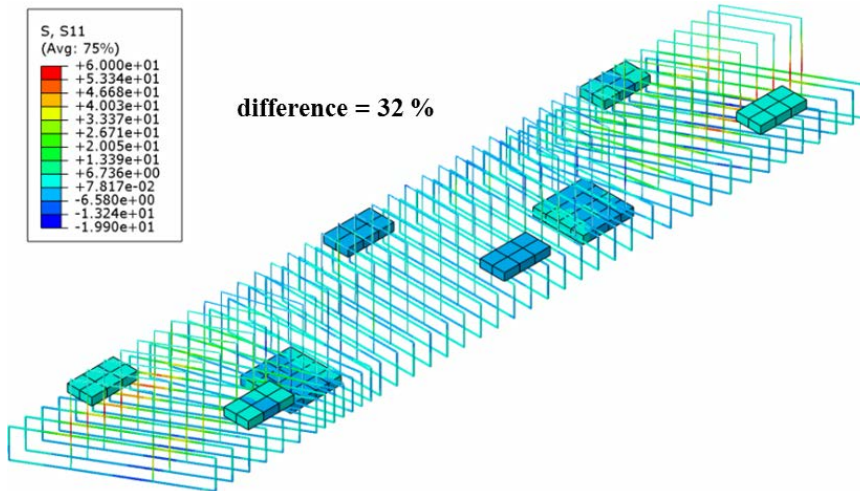
Figure 5.9. Transverse Rebar Stresses at Service Load for Various Skew Angle

### 5.3.4 Stresses in Transverse Rebars at Yielding

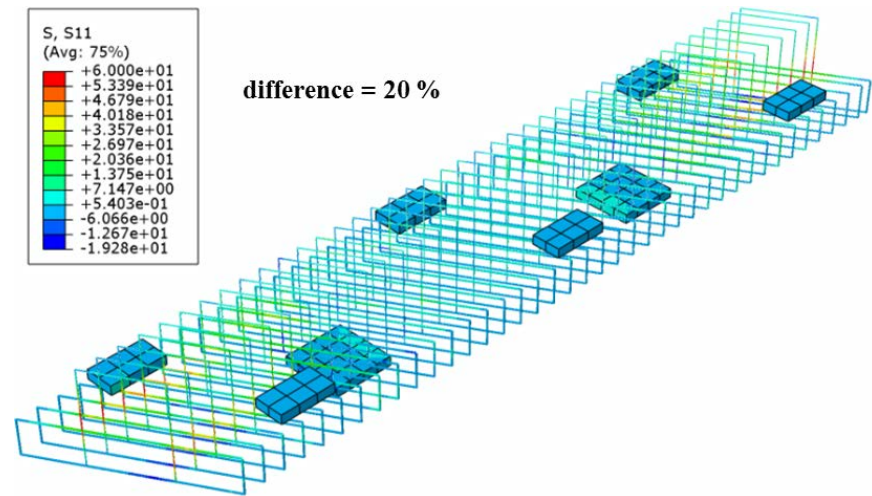
Figure 5.10 shows the contour plot of the stresses in the transverse rebars of the Phase 1 skew ITBCs at yielding load. In each figure, the stresses in transverse rebars for the traditional and skew transverse reinforcing are shown for comparison. When the skew angle is small, for example in the case of 0 and 30 degrees, yielding stresses happen almost simultaneously at both legs of the transverse reinforcing bars, as shown (red color) in Figures 5.10(a) and 5.10(b). In the case of a larger skew angle, for example in the case of 45 and 60 degrees, yielding stresses happen earlier at one leg while another leg has not yet yielded, as shown in Figures 5.10(c) and 5.10(d). This is due to the fact that the shear stress caused by shear and the shear stress caused by torsion are additive at one leg and subtractive at another leg. These results show that for the skew inverted-T bridge cap, the torsional effect is critical and needs to be considered. Moreover, it can be seen that the stress contour in transverse rebars for both traditional and skew reinforcement cases are very similar. In other words, the bent caps using traditional and skew transverse reinforcement have similar structural behavior.



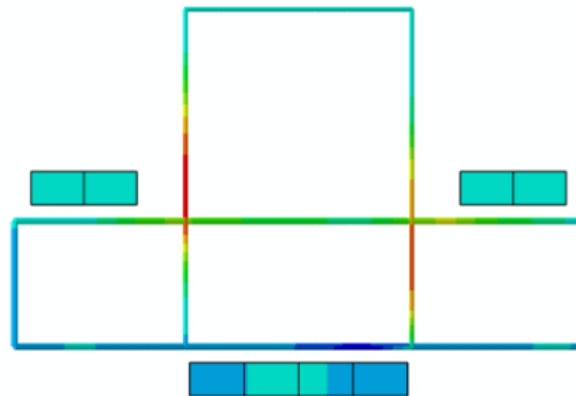
(a) ITBC-0-T-2M



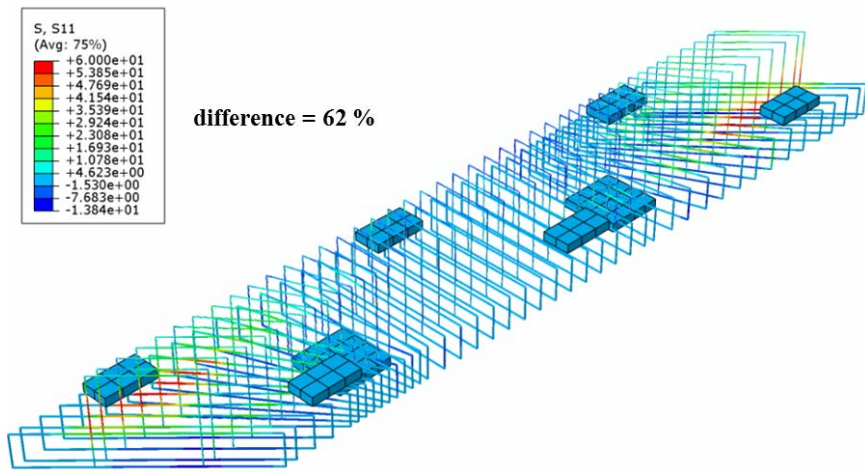
**(i) ITBC-30-T-2M**



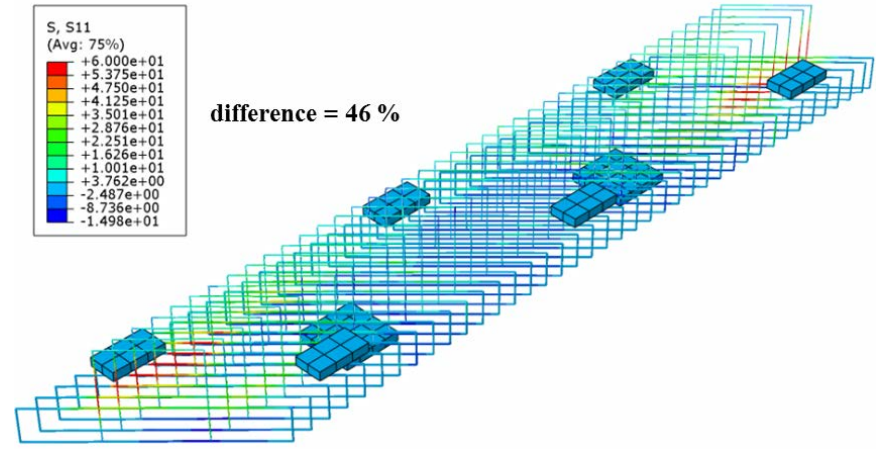
**(ii) ITBC-30-S-2M**



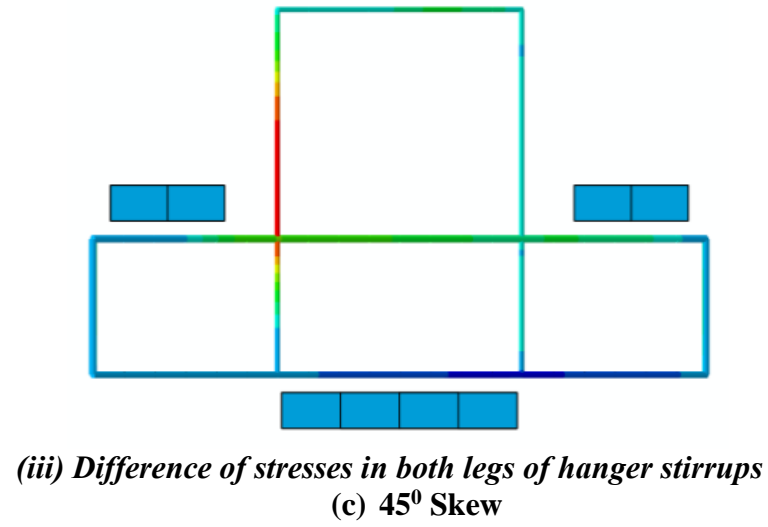
**(iii) Difference of stresses in both legs of hanger stirrups  
(b) 30° Skew**

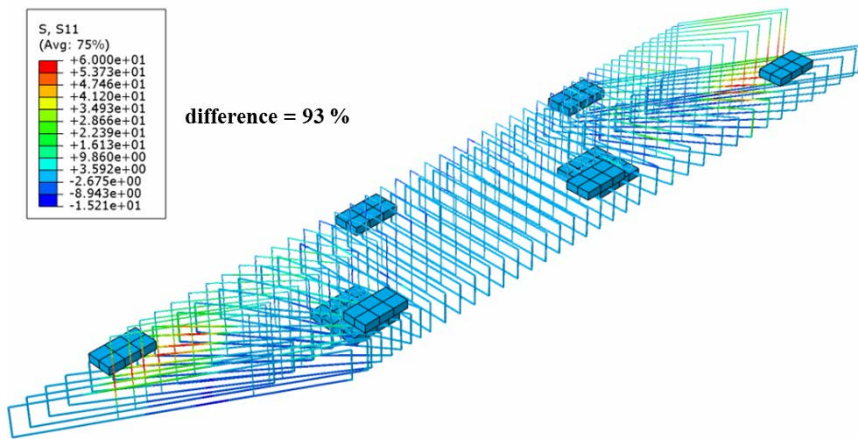


(i) *ITBC-45-T-2M*

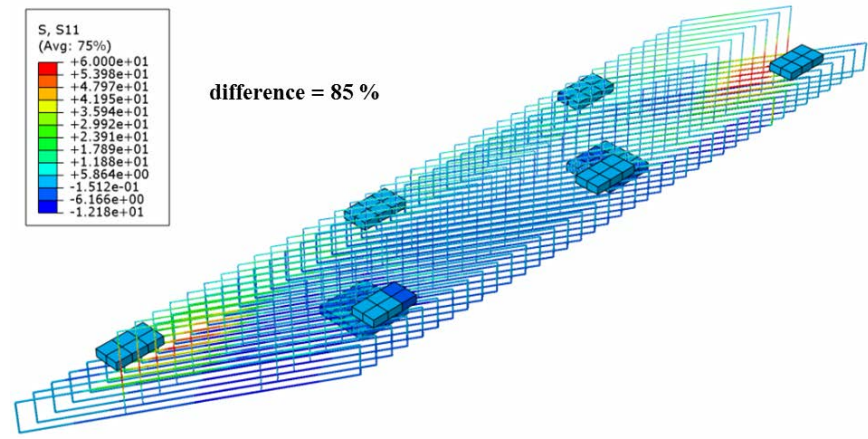


(ii) *ITBC-45-S-2M*

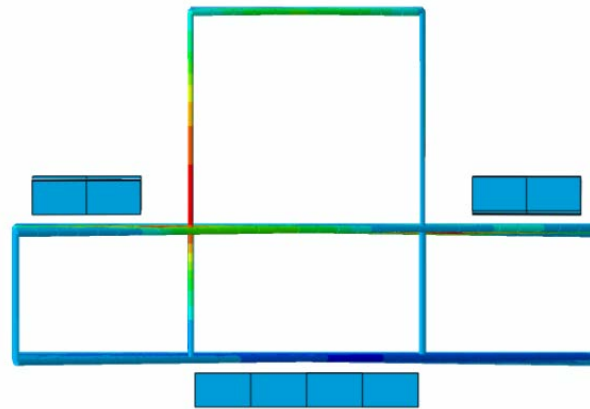




(i) *ITBC-60-T-2M*



(ii) *ITBC-60-S-2M*



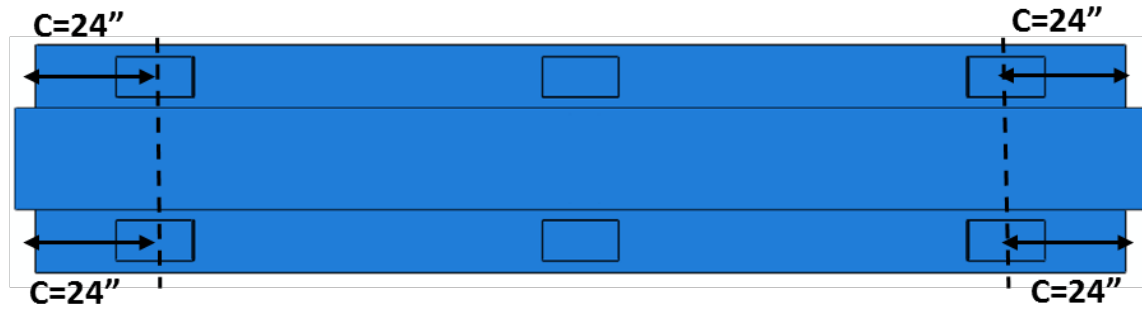
(iii)  
(d)  $60^\circ$  Skew

**Figure 5.10. Stresses in Hanger Rebars at Yielding:**  
(a)  $0^\circ$  Skew , (b)  $30^\circ$  Skew , (c)  $45^\circ$  Skew , (d)  $60^\circ$  Skew

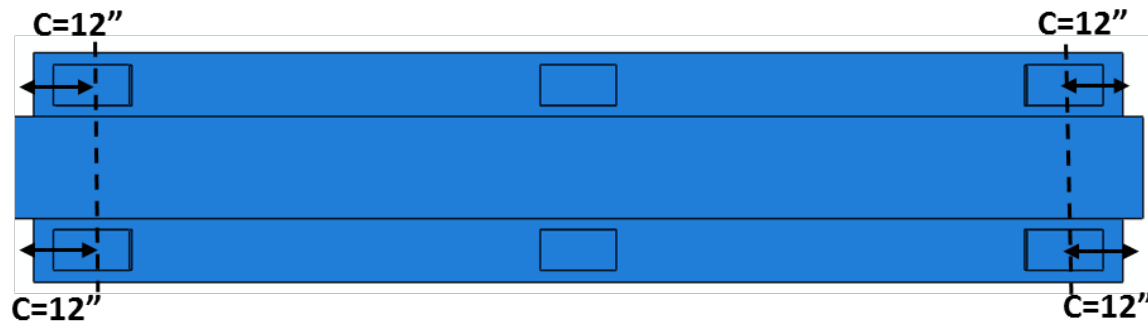
### 5.3.5 Effect of Loading Pad's Location on Transverse Rebars

The locations of the exterior loading pads on skew inverted-T bent caps highly affect their structural behavior as they can influence the hanger stresses in transverse rebar. This phenomenon was also witnessed from the experimental results of the test specimens of different skew angles. During the test at the UH Structural Lab, the external loading pads were placed at a 24-inch distance from the end faces. The distance between the end face and the central line of the exterior loading pad is designated as  $C$ . In most of the inverted-T bent caps in a real bridge system, the loading pads (bearing pads) are located very close to the end face. To investigate the effect of the locations of the loading pads, four different skew ITBCs are considered in this analytical study by placing them at a distance of  $C=24''$  and  $C=12''$ . The analysis was performed for four different skew angles,  $0^0$ ,  $30^0$ ,  $45^0$ , and  $60^0$  under the application of the same amount of load which is the service load. Figure 5.11 shows the locations of loading pads for two different configurations.

From the 3D finite element analysis, as shown in Figure 5.12, it is observed that the stress in the transverse rebars for the  $C=12''$  case is significantly higher than the case of  $C=24''$  under the same amount of loading. With the increase in the skew angle, this pattern of higher stresses in transverse rebars became more severe. Therefore, in most of the old ITBCs diagonal cracks are observed at the end faces, where the exterior bearing pads or loading pads are not placed at the appropriate distance from the end face. So, while designing the ITBCs, the locations of exterior bearing pads should be determined very judiciously. This distance will even play a crucial role in the case of skewed ITBCs as the locations of loading pads in both the ledges are unsymmetrical, thereby creating an unequal distance from the end faces.



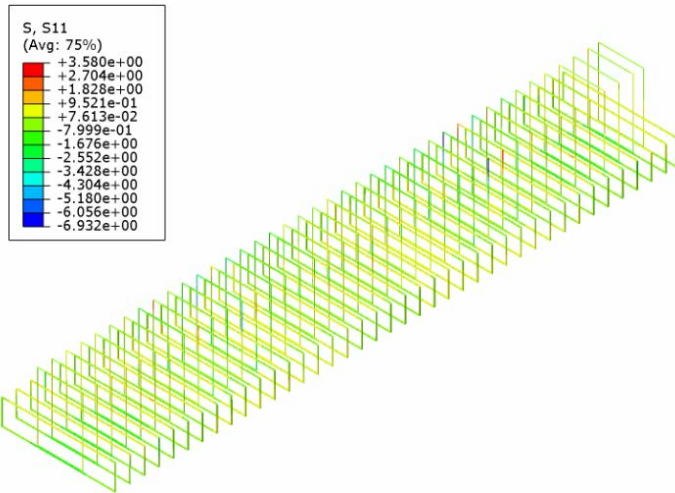
(a) Exterior loading pads at  $C=24''$  from the end face



(b) Exterior loading pad at  $C=12''$  from the end face

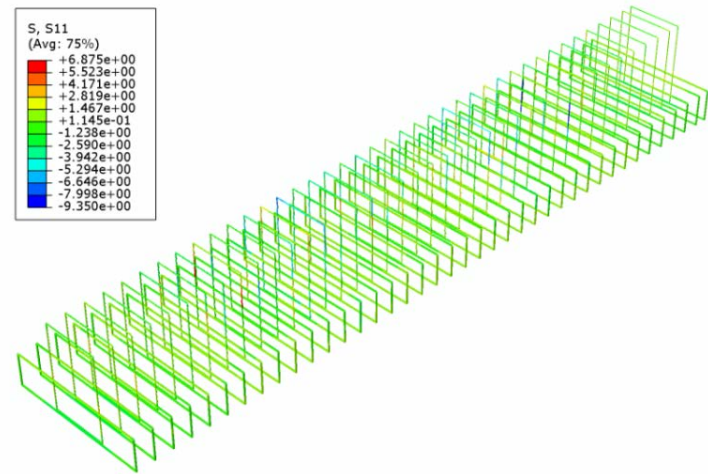
Figure 5.11. Different Configurations of Loading Pads

C = 24 inches

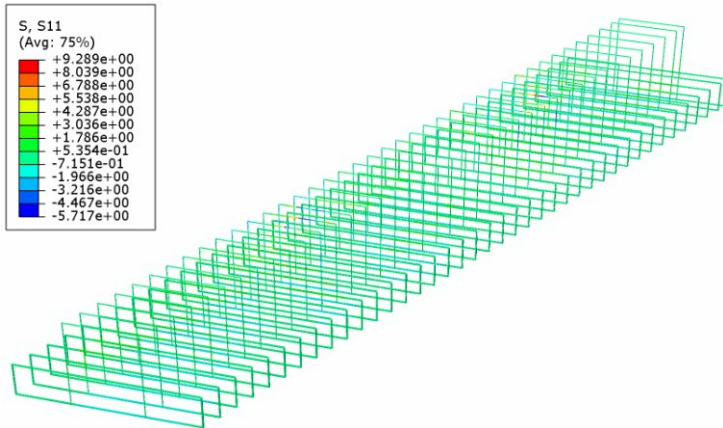


(a) ITBC-0-T-2M

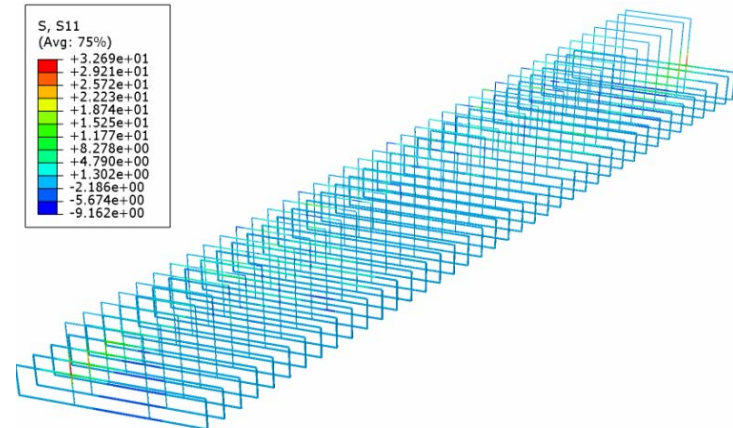
C = 12 inches



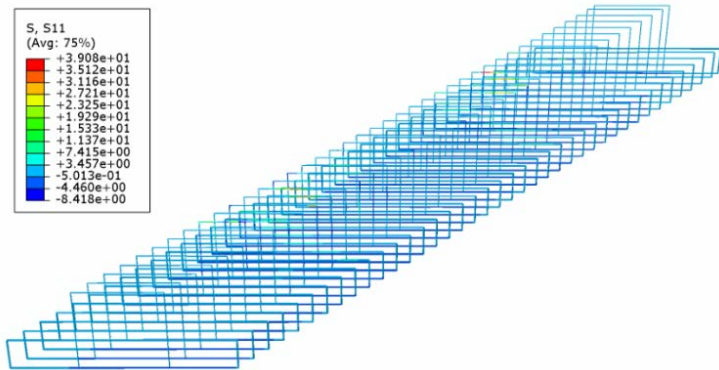
(b) ITBC-0-T-2M



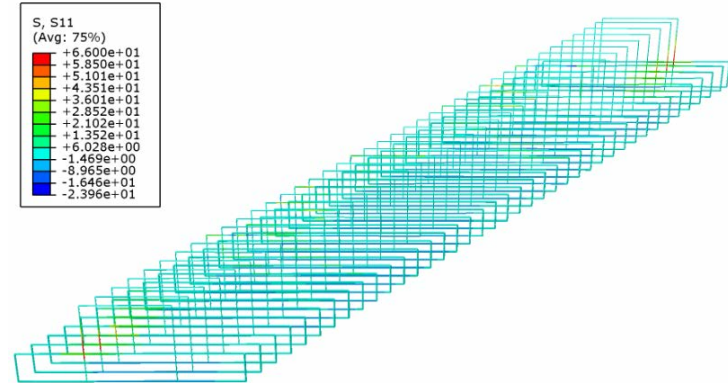
(c) ITBC-30-S-2M



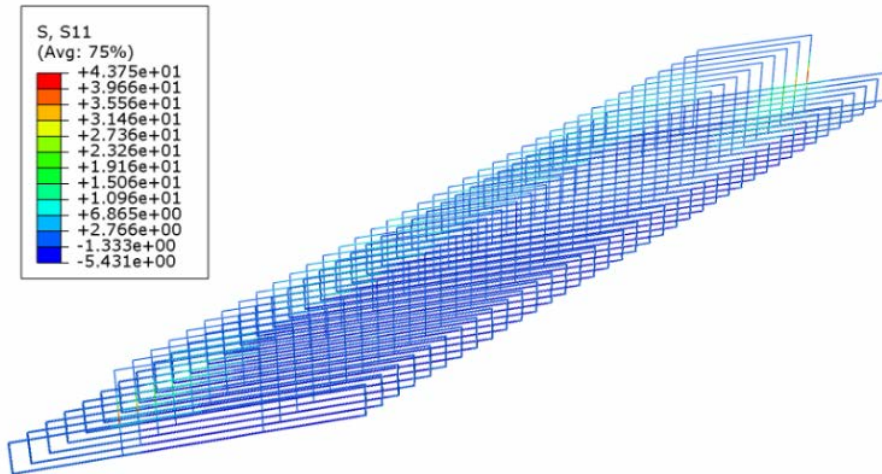
(d) ITBC-30-S-2M



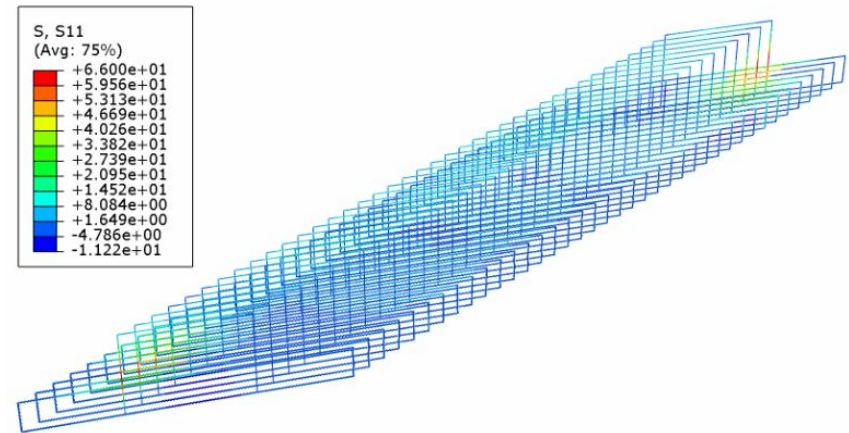
(e) ITBC-45-S-2M



(f) ITBC-45-S-2M



(g) ITBC-60-S-2M



(h) ITBC-60-S-2M

Figure 5.12. Stresses in Transverse Rebars for Various C

### 5.3.6 Effect of End Face Rebars

In contrast to the Phase 1 specimens, the end face bars U1, U2, and G were added to the Phase 2 specimens as shown in Figure 5.13. Figure 5.14 shows the contour plot of the stresses in the transverse rebars of the Phase 2 skew ITBCs for various skew angles varying from  $0^{\circ}$  to  $60^{\circ}$ . In the figure, the stresses in transverse rebars for the traditional and skew transverse reinforcements are shown for comparison. When the skew angle is small, for example in the case of  $30^{\circ}$ , the maximum tensile stresses in the transverse rebars are very similar for the specimens with and without end face bars, as shown in Figures 5.13(a) and (b), respectively. In the case of a larger skew angle, for example in the case of  $45^{\circ}$  and  $60^{\circ}$ , the maximum stresses in transverse rebars are significantly different for the specimens with and without end face rebars, as shown in Figures 5.14(c), (d), (e), and (f). These results show that for the skew ITBC with a larger skew angle the torsional effect is critical and needs to be considered.

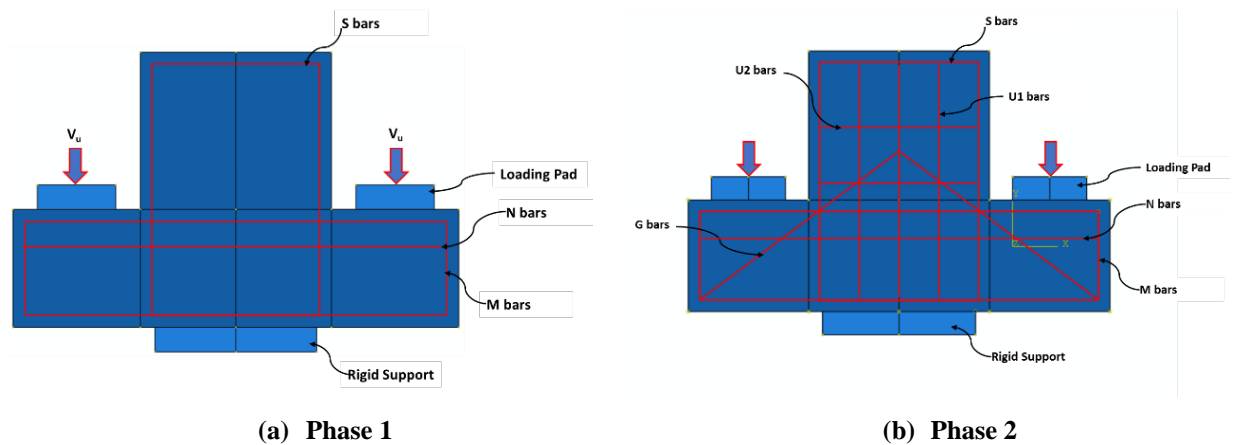
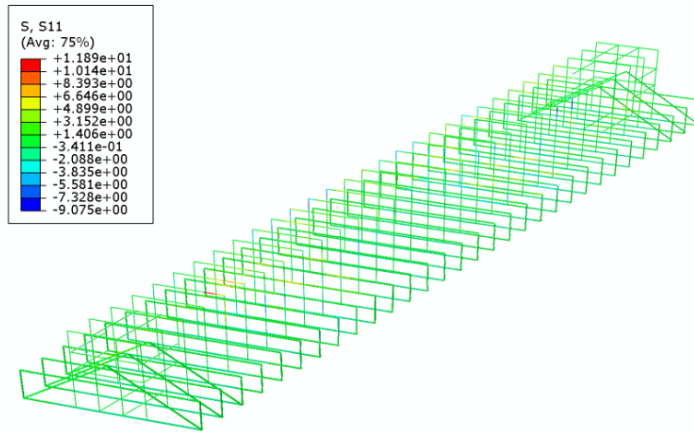


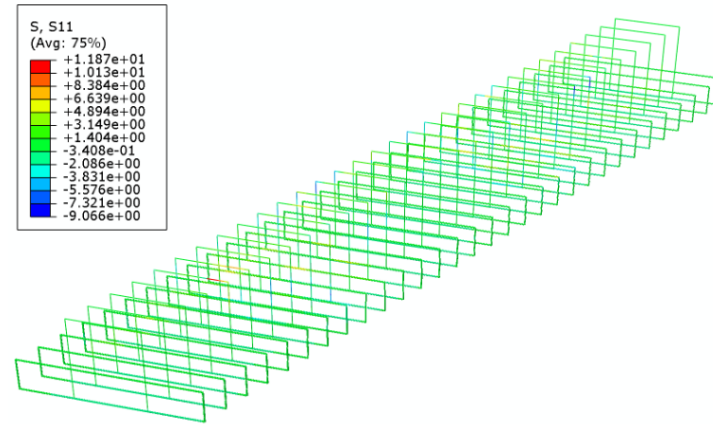
Figure 5.13. End Face Details

With End Face Bars

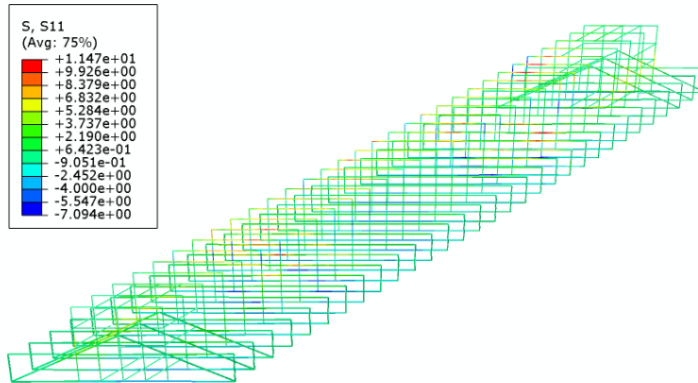


(a) ITBC-30-S-M

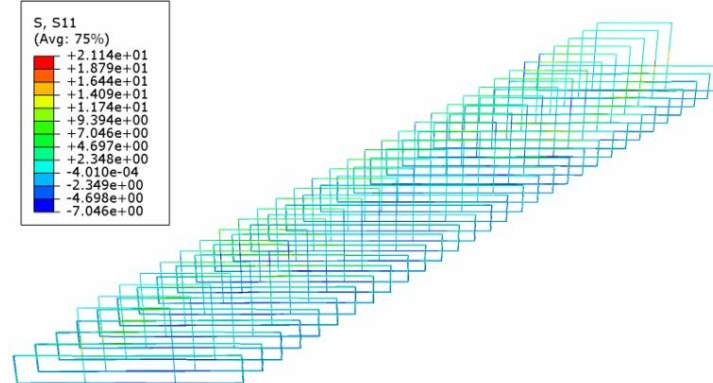
Without End Face Bars



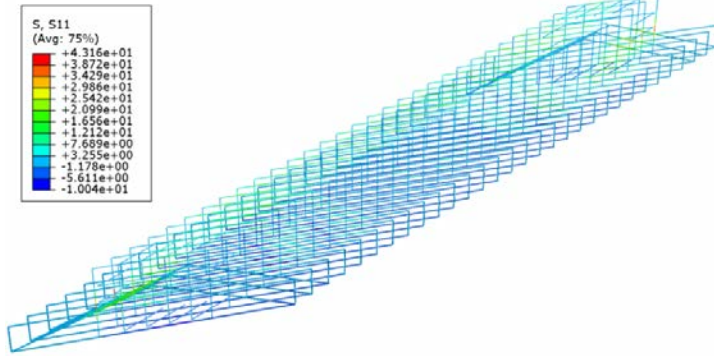
(b) ITBC-30-S-M



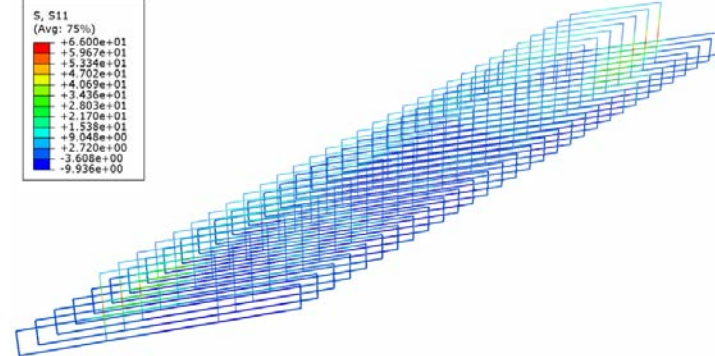
(c) ITBC-45-S-M



(d) ITBC-45-S-M



(e) ITBC-60-S-M

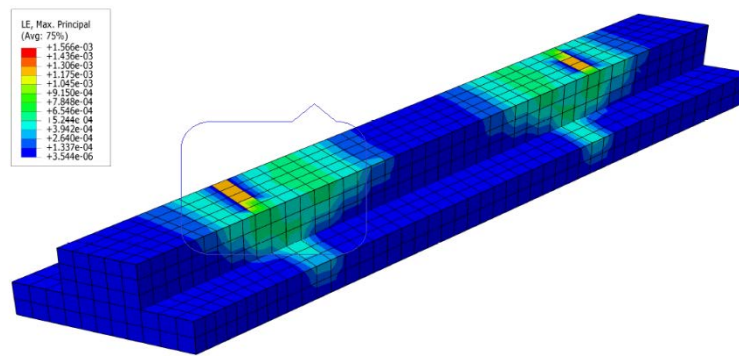


(f) ITBC-60-S-M

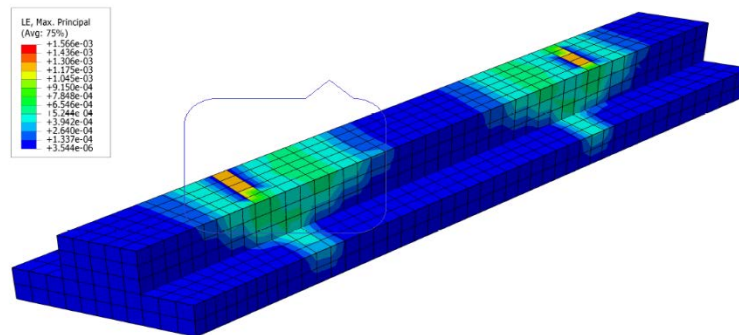
Figure 5.14. Stresses in Transverse Rebars for Various Skew Angles

### 5.3.7 Comparison of Principal Tensile Strain (Cracking Zone)

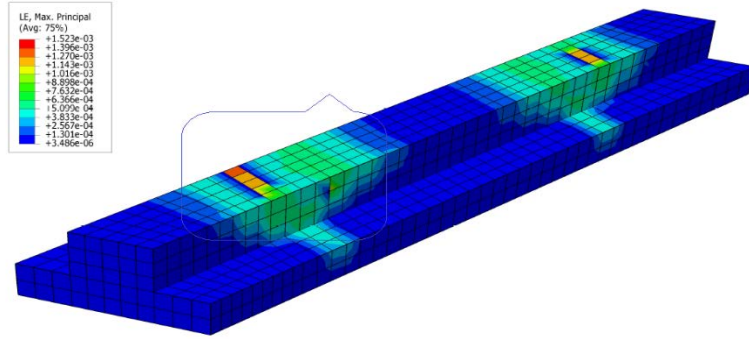
Figure 5.15 shows FE analysis results which address the comparison of the cracking problem between the two types. In the figure, the contour of the principal tensile strain in concrete is illustrated. To show the cracking zone, a lower limit of the principal strain (i.e., 0.00008) was defined so that the regions at which principal strain is less than cracking strain have a different color than the cracked regions. The other regions with different colors and surrounded by the rectangle, therefore, represent cracking zones. As can be seen from the figure, the bridge cap using skew reinforcing bars has an almost similar cracking area as the one using the traditional reinforcing bar under the service load. However, the maximum principal tensile strain is less in the case of the ITBC with skew reinforcing than the traditional one as shown in the following figures.



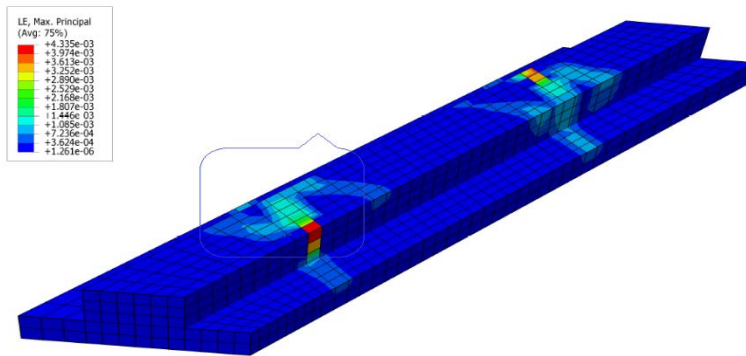
(a) ITBC-0-T-2M



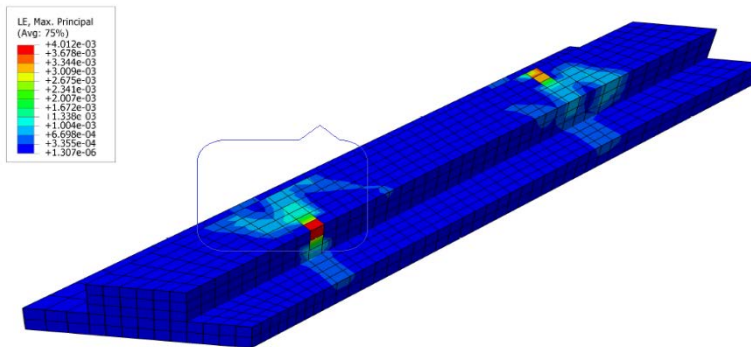
(b) ITBC-30-T-2M



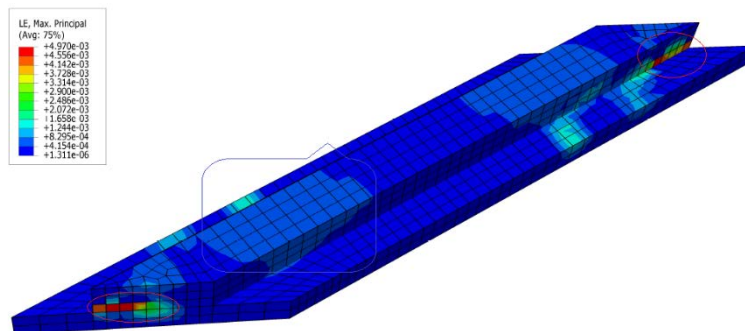
(c) ITBC-30-S-2M



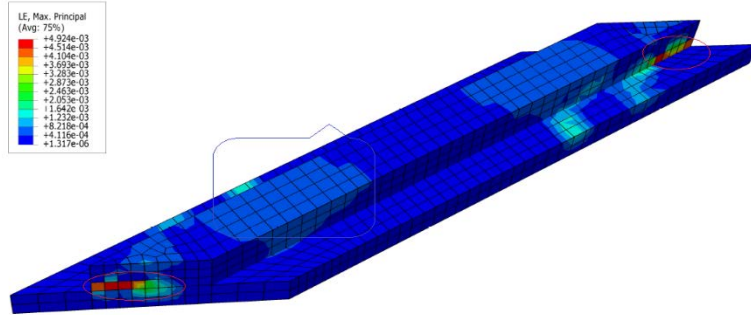
(d) ITBC-45-T-2M



(e) ITBC-45-S-2M



(f) ITBC-45-T-2M



(g) ITBC-45-T-2M

**Figure 5.15. Comparison of Principal Tensile Strain at Service Load**

## 5.4 CONCLUSIONS

The advanced numerical simulations of 13 specimens using 3D FE software ABAQUS are summarized in this task report. Moreover, a comprehensive parametric has been carried out to clearly understand the structural performance and response of the skew transverse reinforcing in inverted-T bridge caps. By comparing and studying the finite element models, the main conclusions are listed as follows: (1) The arrangement of transverse reinforcements does not show critical influence on the skew ITBC's structural performance and failure mechanism. (2) The locations of exterior loading pads are found to have a profound influence on the skew bent cap's structural behavior. Closer locations of loading pads to the end face of the ITBC increases the transverse rebar stresses significantly. This pattern is even worse in the case of higher skew angles. (3) The torsional deformations increase when the skew angle increases. Even though the same amount of load is applied to each of the loading pads, the unsymmetrical deformations in all skew cases are caused by torsional moments generated by the unsymmetrical locations of bearing pads on the ledges of the bridge cap.

## **CHAPTER 6: DESIGN RECOMMENDATIONS**

### **6.1 OVERVIEW**

In this chapter, the general design guidelines and typical drawings for the design and construction of the skew reinforcing in inverted-T bridge caps are provided. The general design recommendations presented in this section reflect the conclusions drawn as a result of the extensive experimental and FE program on inverted-T bridge caps with skew and traditional transverse reinforcing. For the design example, a seven-span bridge is chosen which is planned to be constructed on Donigan Road over IH10 near Brookshire in Waller County of Texas. In this bridge there are skew inverted-T bridge caps with two different skew angles such as  $43^{\circ}$  and  $33^{\circ}$ . The design example is provided for the  $43^{\circ}$  - bent cap. The preliminary data for the design and drawings are obtained from the Project team.

### **6.2 GENERAL DESIGN RECOMMENDATIONS**

All thirteen test specimens (including both the traditional and skew transverse reinforcing) were designed based on the current design provisions provided in the AASHTO LRFD and TxDOT BDM LRFD codes. The basic focus of this research is on the shear behavior of traditional and skewed transverse stirrups in inverted-T bridge caps with varying skew angles of  $0^{\circ}$ ,  $30^{\circ}$ ,  $45^{\circ}$  and  $60^{\circ}$ . Therefore, during the design stage of the test specimens, it was ensured that the flexure failure and the three local failure modes [i.e. (1) failure of hanger stirrups, (2) ledge failure due to punching shear and (3) ledge failure due to loss of shear friction] must be prevented before the yielding of the hanger stirrups in shear. In other words, the shear capacities of all the specimens were designed to be the lowest of all other capacities of inverted-T bridge caps.

In all the inverted-T test specimens, both the traditional and skew transverse reinforcements for shear and hanger resistance were designed by using the equations specified in AASHTO LRFD and TxDOT BDM LRFD provisions. The spacing of shear and hanger stirrups obtained as an outcome from the equations mentioned above was maintained for all the thirteen test specimens with various skew angles of  $0^{\circ}$ ,  $30^{\circ}$ ,  $45^{\circ}$  and  $60^{\circ}$ . As shown in the tests, the shear capacities of all the inverted-T bridge cap test specimens with skew angles of  $0^{\circ}$ ,  $30^{\circ}$ ,  $45^{\circ}$  and  $60^{\circ}$  and with traditional and skew transverse reinforcements are greater than those calculated in the design stage using the equations specified in AASHTO LRFD and TxDOT BDM LRFD provisions. The transverse shear reinforcements were yielded, and wide diagonal shear cracks were observed in the web before the failure of the specimens. The failure mode of the specimens was primarily attributed to the shear failure caused by the yielding of shear reinforcements at both the overhang ends of the specimen and followed by the initiation of crushing of the compression strut in the web. The strains in the longitudinal and ledge rebars are less than the yielding strain. Therefore, the present design equations provided in the AASHTO

LRFD and TxDOT BDM LRFD provisions (to determine the shear and hanger capacities of transverse stirrups) are reliable and can also be utilized to design the ITBC with skew transverse reinforcements having skew angles of  $0^{\circ}$ ,  $30^{\circ}$ ,  $45^{\circ}$  and  $60^{\circ}$ .

Following are the proposed essential recommendations for the design and construction of skew inverted-T bridge caps with transverse reinforcing:

- All S Bars (shear and hanger stirrups), M Bars (Primary ledge bars) and N Bars (secondary ledge bars) will be skewed to match the skew angle of the inverted-T bridge cap, as shown in Figure 6.1. The spacing of skew transverse reinforcements will be measured from center to center of the hanger and ledge stirrups along the central line of the skew bent cap (not the perpendicular distance between hanger or ledge stirrups).
- Avoid using shorter ledges. The distance between the central line of the exterior girder and the end face of the inverted-T bent cap should be maintained at least 24 inches to provide adequate punching shear capacity. This also delays the appearance of the diagonal crack at the re-entrant corner between the cantilever ledge and the web at the end faces of the ITBCs. Shorter ledges could increase the risk of ledge failures. TxDOT Projects 0-1854 and 0-6416 also emphasize this aspect.
- Vertical rebars should be provided across both end faces of the skewed web. The spacing of these rebars should be equivalent to the spacing of shear and hanger stirrups (at least 6") and will be provided along the end face. In addition to restricting the formation of cracks, vertical rebars at end faces help to reduce the stress concentration of the hanger and shear stirrups by redistributing at the cantilever end face. This aspect is illustrated in the section 6 with 3D FE simulated results.
- At the skewed end faces of cantilever spans, adding diagonal bars (G bars) do not help to prevent the formation of diagonal crack at the re-entrant corner between the cantilever ledge and the web. The most effective variables to control crack width is the distance from end face to the most exterior loading pad. As the skew angle increased from the 0 degree to 60 degree the diagonal crack at the junction of ledge and web occurred at lower load.
- A minimum area of transverse reinforcement is required to restrain the growth of diagonal (inclined) cracking, to increase the ductility and to prevent the sudden shear failure of the bent cap. In this study six skewed inverted-T bent caps are studied with minimum amount of transverse reinforcement using the equations 5.8.2.5 provided in AASHTO LRFD 2014. All the test results show that there was no sudden shear failures. Transverse rebars are considerably yielded before the failure of the specimens. Therefore, the equations in AASHTO LRFD 2014 can be used to design the minimum transverse reinforcing in skewed inverted-T bent caps.

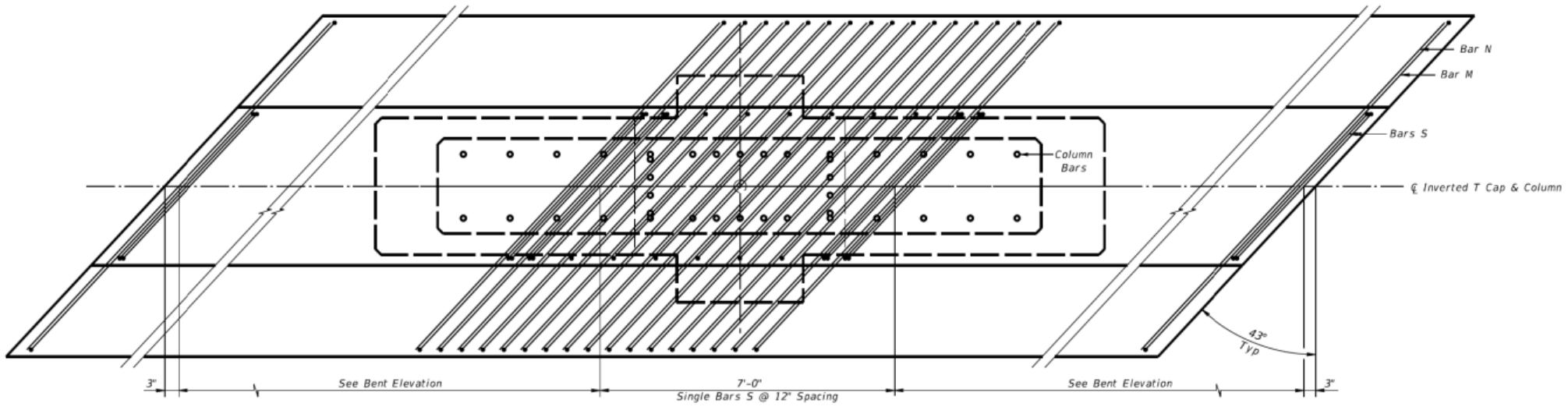


**Figure 6.1. Typical Stirrup Details ~ Plan View**

## **6.3 PROPOSED CHANGES TO TXDOT PRACTICE**

The following recommendations for designing inverted-T bridge caps resulted from the experimental and analytical work performed in this project.

### **6.3.1 Current TxDOT Practice**

For a skewed inverted-T bridge cap, the TxDOT Bridge Design Manual states only that hanger and ledge reinforcements should be placed perpendicular to the centerline of the skew bent. The detailing of the skewed ends of the bent should be done with a section of skewed stirrups and ledge reinforcements. Based on the availability of the space, typically, the transition of straight bars to the skewed bars is carried out over the column support where the transverse reinforcement spacing is less critical based on the availability of the space. The designer of ITBC flares the bars out to match the skew angle while trying to maintain a minimum and maximum spacing based on the outcome of the design calculations. Such detailing of transverse reinforcements creates unequal spacing in both sides of the web producing congestion of reinforcements in one side.

### **6.3.2 Proposed Change**

Instead of fanning out the hanger and ledge stirrups to match the skew angle of the bridge, skewed transverse reinforcing should be utilized all the way from one end of the skew bent cap to the other end maintaining the required spacing along the central line of the bent cap. This will create a uniform spacing and length of ledge and hanger stirrups throughout the bent cap unlike the traditional method of design and construction practice which create multiple spacing and length of ledge and hanger stirrups in the fanning out zone. Moreover, it will provide an alternative approach which will significantly reduce the design complexities and construction period.

## **6.4 DESIGN EXAMPLES**

### **6.4.1 Defining the Bent Cap**

For the design example, a seven-span bridge is selected which is planned to be constructed on Donigan Road over IH10 near Brookshire in Waller County of Texas. The preliminary data for the design example and drawings such as bent cap dimensions, service and factor load at each bearing location, design moments, etc., are obtained from the Project team. There is a total of six bent caps with two different skew angles ( $43^{\circ}$  and  $33^{\circ}$ ) in this bridge.

### **6.4.2 Illustrative Example**

A detailed design example of one of the  $43^{\circ}$  bent caps of this real bridge system is provided in this section. The design is carried out using the general guidelines provided in previous sections and the equations provided in AASTHO, TxDOT BDM and TxDOT

inverted-T design example. A typical design example for  $43^\circ$  skew angle is presented in Appendix 3. Figures 6.2 and 6.3 show the cross-sectional view of the designed bent cap at inner and end face locations, respectively. Figures 6.4 and 6.5 show the partial elevation and plan view of the designed bent cap over a column support. The skewed bent caps with skew angles up to  $60^\circ$  can be designed in similar procedures.

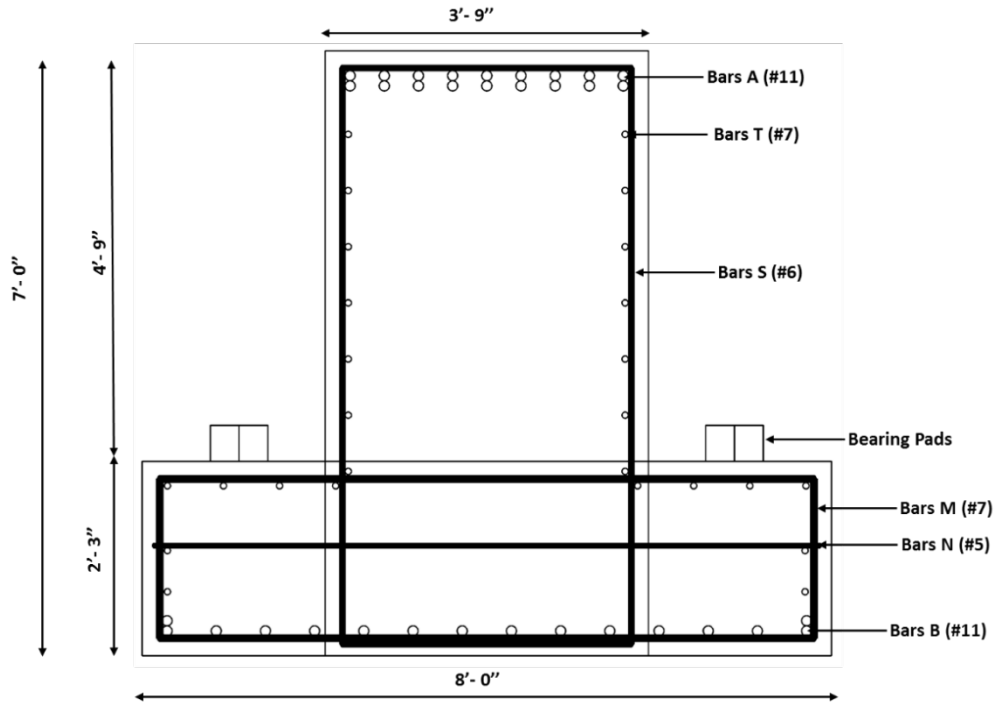


**Figure 6.2. Typical Bent Cap Cross Section**

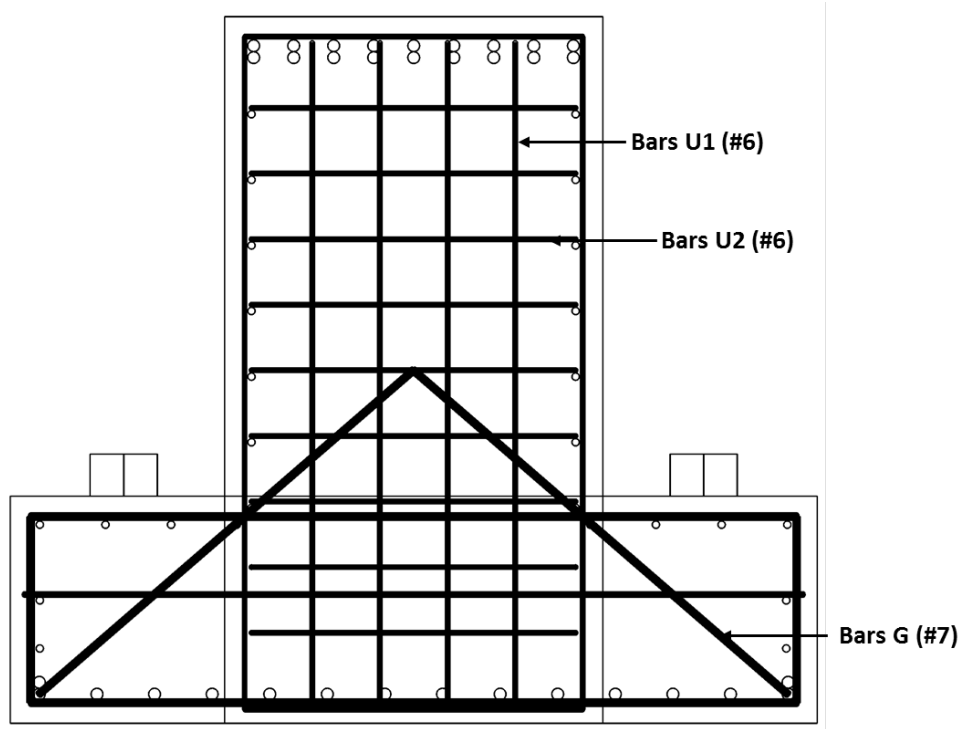


**Figure 6.3. Typical Bent Cap Cross Section at End Face**



**Figure 6.4. Partial Elevation View Over a Column**

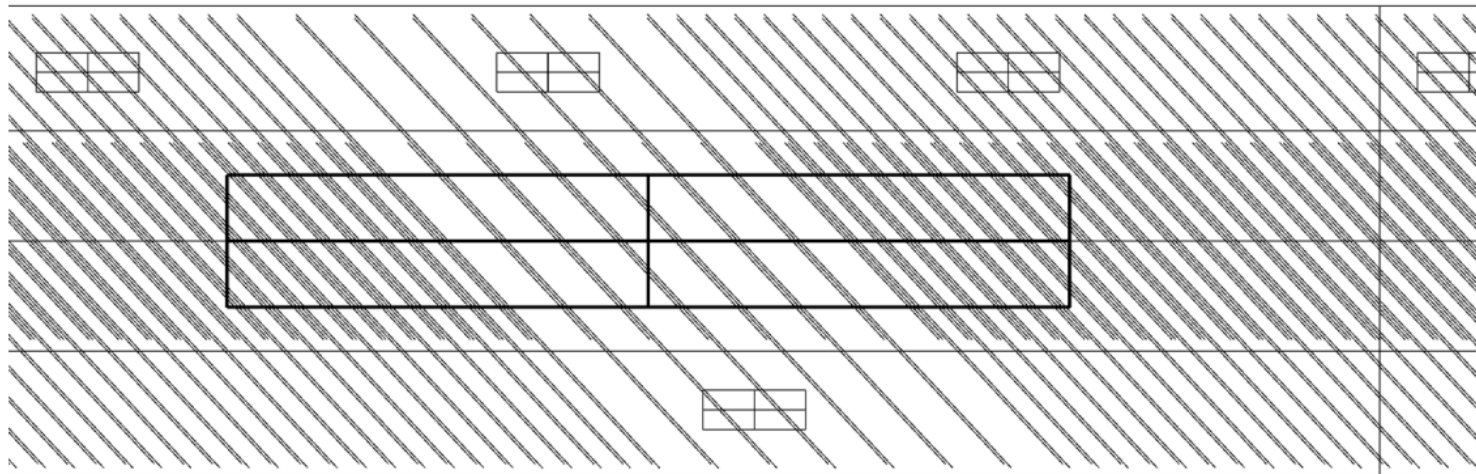


**Figure 6.5 Partial Plan view Reinforcement Detailing (Shows S, M & N Bars)**

## 6.5 3D FEA RESULTS OF THE FULL SCALE BENT CAP

The 3D finite element model of the designed inverted-T bridge cap is developed using the FE software, ABAQUS (2014). The concrete of the inverted-T bridge caps was modeled using an eight-node, reduced integration, hourglass control solid element (C3D8R). A 2-node linear three-dimensional (3-D) truss element (T3D2) was used to model the reinforcement because it is only subjected to axial force. The 3D FE model of the bent depicting a cross-section view and end face detailing is shown in Figure 6.6. The FE mesh of the partial bent cap is provided in Figure 6.7. The four rectangular rigid supports representing columns under the bridge bent cap are fixed at the bottom faces. There is a total of 24 bearing pads tied on top of the ledges. The superstructure loads from bridge girders are transferred to the bridge bent cap through these bearing pads.

The analysis is performed for service load which includes dead load and live load with the load combination factor equal to one. The analysis is performed for the same bent cap in two stages. First, the bent cap with the vertical rebars at the end faces and second, with the vertical rebars at the end faces. Figure 6.8 shows the tensile stress contour (S11) in ksi under the application of service loading. It is evident from the figure that the maximum tensile stress in the rebars is 9.086 ksi (red) and this occurred in the transverse rebars at the end face (marked in the circle). Figure 6.9 depicts the stress contour of the bent cap without side bars at end faces. It shows that the maximum tensile stress in the rebars is 13.59 ksi (red). By providing the vertical rebars at both the ends, the tensile stresses are lower by 33% and are well distributed among the rebars at the end.

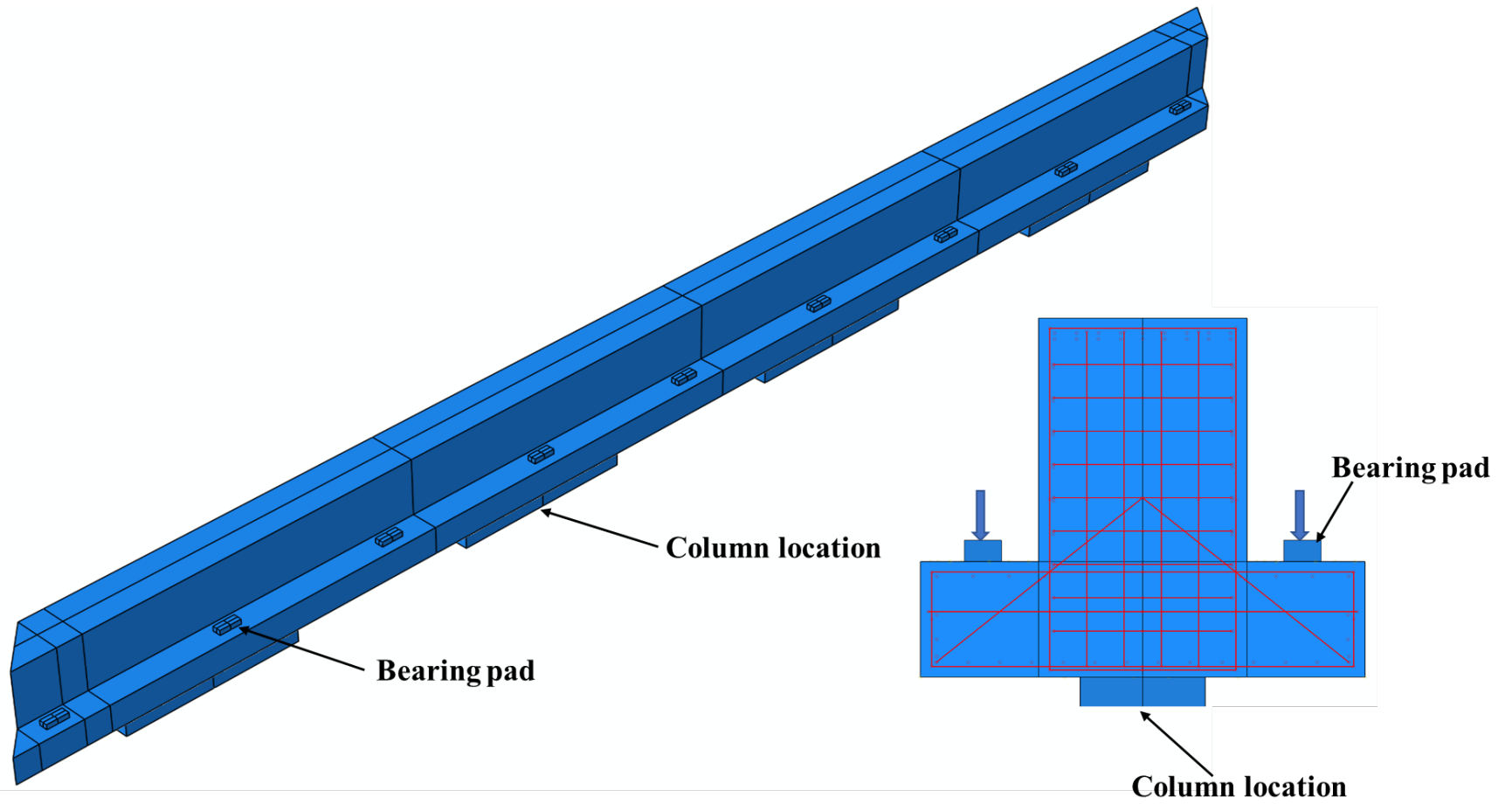


**Figure 6.6. 3D Finite Element Model of the Designed Bent Cap with Skew Angle  $43^{\circ}$**

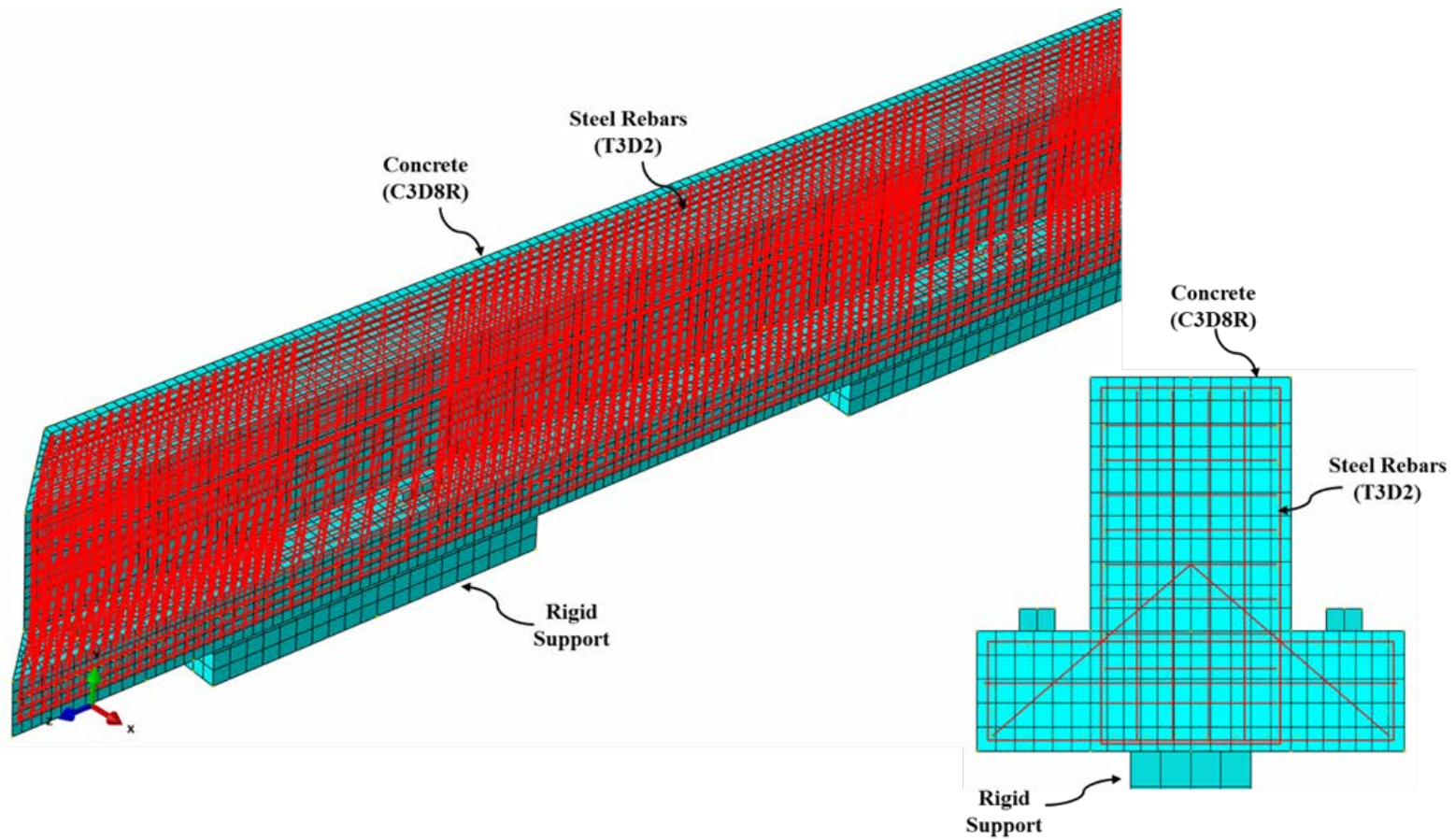


**Figure 6.7. Partial 3D Finite Element Mesh of the Designed Bent Cap**

Tensile stress contour

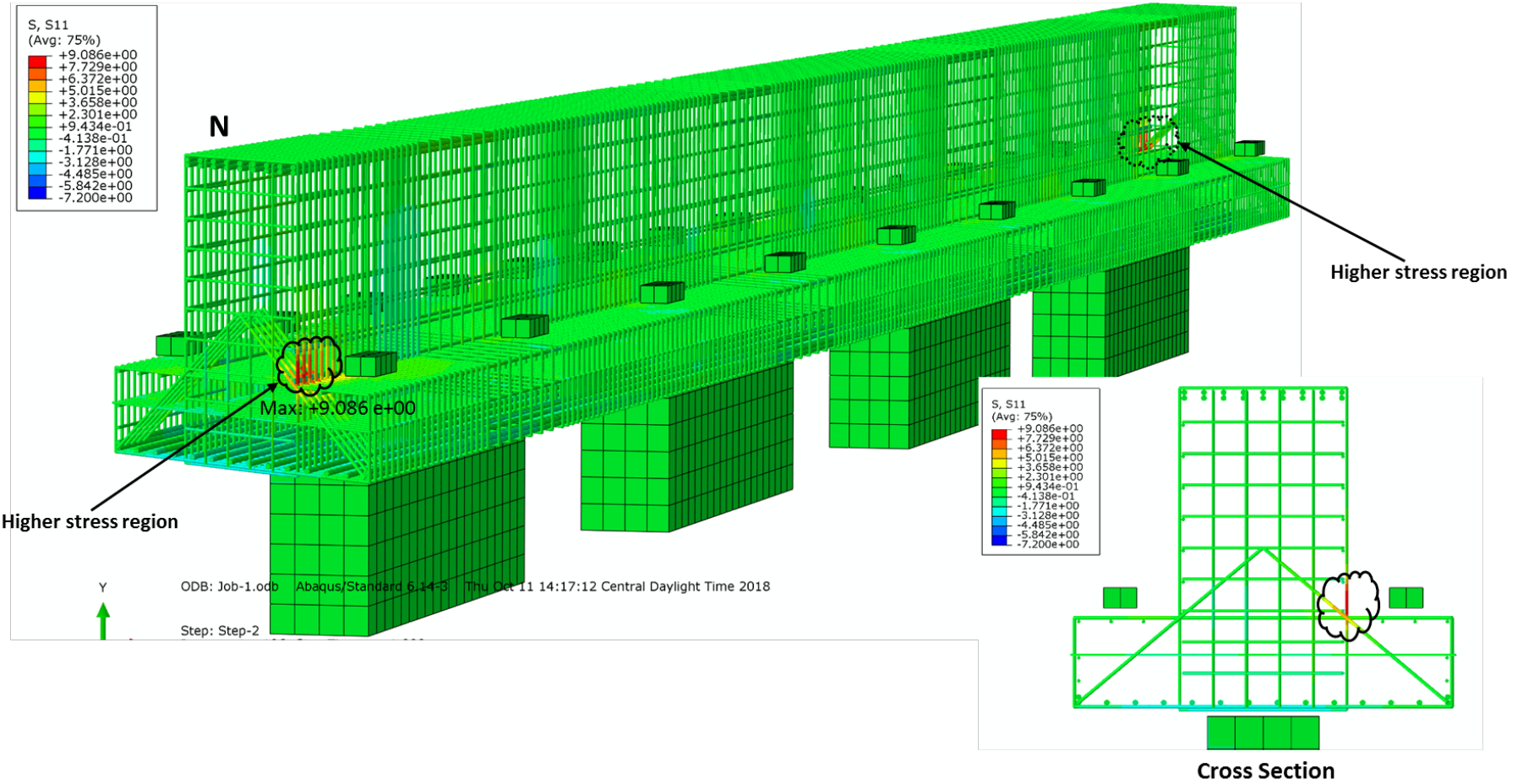
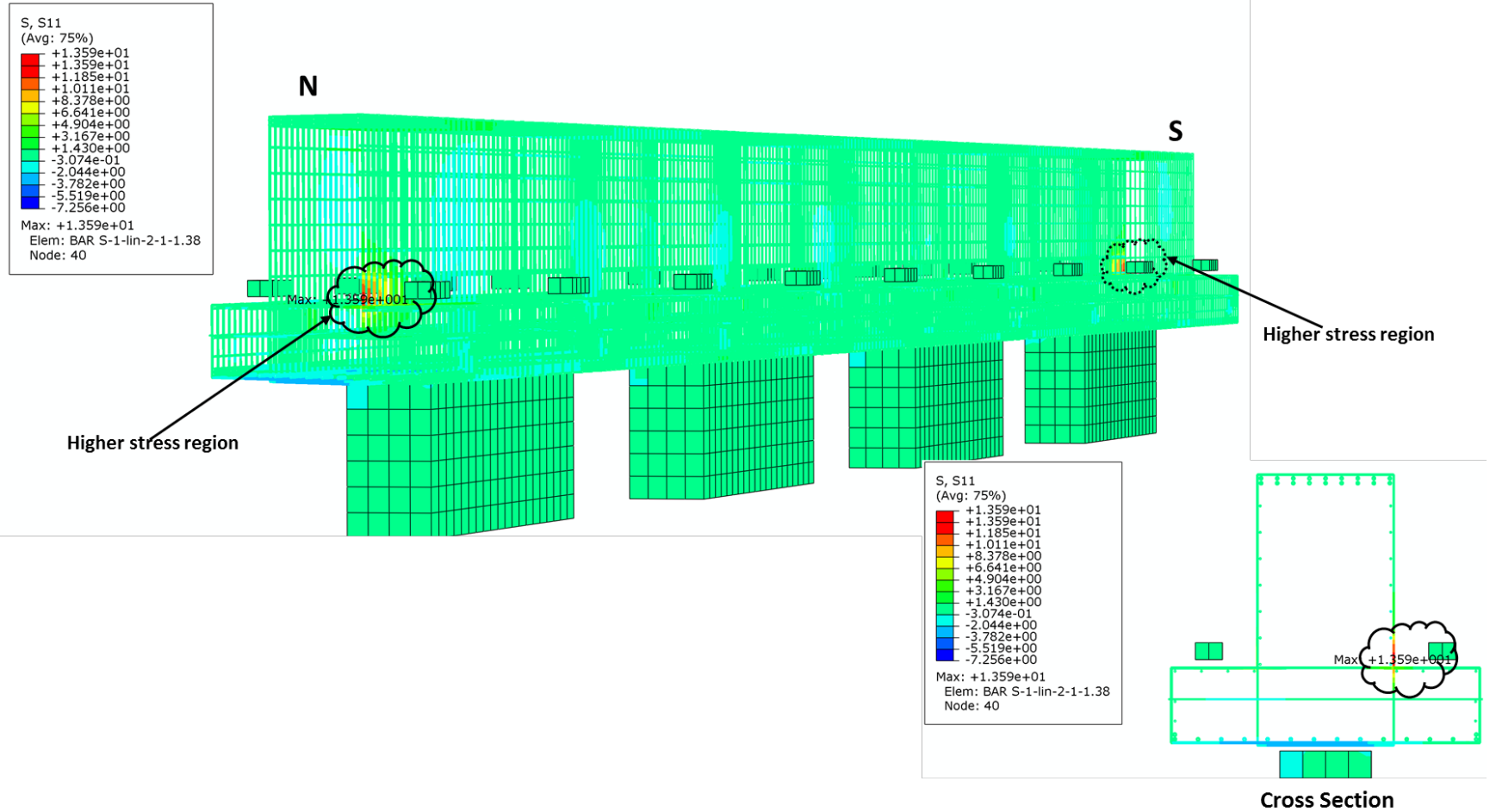


Figure 6.8. Tensile stress Contour at Service Load (With End Face Rebars)

[S11 = Tensile stresses in ksi in Rebars – Red (Top) : Maximum stress, Blue (Bottom): Minimum stress]

**Tensile stress contour**



**Figure 6.9. Tensile stress Contour at Service Load (Without End Face Rebars)**

[S11 = Tensile stresses in ksi in Rebars – Red (Top) : Maximum stress, Blue (Bottom): Minimum stress]

## **6.6 CONCLUSIONS**

During construction, the spacing of skew transverse reinforcements will be measured from center to center of the hanger and ledge stirrups along the central line of the skew bent cap. Shorter ledges should be avoided. The distance between the central line of the exterior girder and the end face of the inverted-T bent cap should be at least 24 inches to provide adequate punching shear capacity and to delay the appearance of a diagonal crack at the re-entrant corner between the cantilever ledge and the web at the end faces of the exterior portions of the ITBCs. Vertical rebars should be provided across both end faces of the skewed web. In addition to restricting the formation of cracks, vertical rebars at both end faces help to reduce the stress concentration of the hanger and shear stirrups at the cantilever end face and resist cracking.

## **CHAPTER 7: SUMMARY AND CONCLUSIONS**

### **7.1 SUMMARY OF THE RESEARCH WORK**

The summary of the test and analytical results on inverted-T bent cap specimens under the scope of this project work can be expressed as per following:

- To investigate the structural performance of skew inverted-T bent caps with traditional transverse reinforcement and proposed skewed transverse reinforcement, a total of thirteen half-scaled specimens are designed using AASHTO LRFD (2014), TxDOT BDM (2015) guidelines, constructed and tested under static compression loading to study the behavior of inverted-T bent caps under shear and torsion.
- The experimental program for ITBC specimens was divided into two phases. Phase-1 included seven ITBC specimens ITBC-0-T-2M, ITBC-30-T-2M, ITBC-30-S-2M, ITBC-45-T-2M and ITBC-45-S-2M, ITBC-60-T-2M and ITBC-60-S-2M, with . Phase-2 of the program included ITBC-30-T-M and ITBC-30-S-M, ITBC-45-T-M, ITBC-45-S-M, ITBC-60-T-M, and ITBC-60-S-M.
- The three critical parameters considered in the research program include the skew angle ( $0^{\circ}$ ,  $30^{\circ}$ ,  $45^{\circ}$  and  $60^{\circ}$ ), the detailing of transverse reinforcement (traditional and skewed) and the amount of transverse reinforcements ((2\* Minimum (AASHTO), Minimum (AASHTO)).
- To study and compare the performance of all ITBC specimens in terms of strength and serviceability, all the data gathered from the experimental tests and FEA was scrutinized and demonstrated under different sections.
- The performance of the test specimens was analyzed and compared using the load-displacement curves, normalized shear capacities, strain-load data, crack patterns, number of cracks, crack width as well as failure modes of the specimens.

### **7.2 CONCLUSIONS**

After performing the structural tests and FEA on the inverted-T bent caps considered under the research project and comparing their performance, the conclusions can be presented as per following: By comparing and studying the finite element models, the main conclusions are listed as follows:

1. The arrangement of transverse reinforcements does not show critical influence on the skew ITBC's structural performance and failure mechanism. The peak load carrying capacity is slightly affected because of the various uneven spacing of the shear and hanger reinforcements. For skew ITBC the dimensions and spacings of skewed transverse reinforcements are similar, thus reducing the labor cost of making complex transverse reinforcements in the end zone of the bridge cap. Considering the

construction convenience and time-efficiency, the skewed arrangement plan is better than the traditional arrangement for practical applications.

2. The influence of shear and torsion is highly dominant in the bent caps with higher skew angle. The inverted-T bent cap with a zero-degree skew angle is significantly affected by shear however it does not have any effect of torsion. The effect of torsion on the behavior of the ITBC specimens is more effectively seen with an increase in the skew angle where a sixty-degree being the highest skew angle for overall ITBC specimens.
3. The larger the skew angle is, the weaker the specimen will be. This is due to the fact that a larger skew angle creates higher asymmetry in the bearing pad's locations, thereby introducing a much larger torsion. Therefore, skew ITBC with a skew angle of more than 45° is prone to torsional failure.
4. The torsional deformations increase when the skew angle increases. Even though the same amount of load is applied to each of the loading pads, the unsymmetrical deformations in all skew cases are caused by torsional moments generated by the unsymmetrical locations of bearing pads on the ledges of the bridge cap.
5. The locations of exterior loading pads are found to have a profound influence on the skew bent cap's structural behavior. Closer locations of loading pads to the end face of the ITBC increases the transverse rebar stresses significantly. This pattern is even worse in the case of higher skew angles. Therefore, while in the design stage of the skew inverted-T bent caps, the locations of exterior bearing pads should be scrutinized very carefully.
6. The long sides of the skew ITBCs are always under the influence of prevailing additive shear responsible for early stage yielding of transverse reinforcement in the given region developing a greater number of cracks as compared to short sides.
7. The ultimate shear capacity of the ITBC specimens decreases with respect to the increase in the skew angle. The normalized shear capacity of all sixty-degree specimens was observed to be 20% lesser as compared to other skew specimen. On the other hand, the arrangement of transverse reinforcement did not induce any notable difference in the shear capacities of the 30, 45 and 60-degree skew specimens.
8. As compared to the traditional transverse reinforcement, the proposed arrangement of skew transverse reinforcement can be more effective and function better in terms sustaining the applied loads up to the yielding stage.
9. The cracking performance of ITBC specimens is enhanced with a provision of proposed skew transverse reinforcement spaced evenly generating comparatively less number of flexural shear, shear and torsional cracks as well as lower crack width as compared to the ITBC specimens designed with traditional transverse reinforcement.

10. The punching shear failure of ledges observed in the specimen with traditional arrangement of transverse reinforcement in Phase-1 can be avoided by increasing the edge distance 'c' as well as by reducing the spacing between ledge reinforcement at the long sides. In addition, for the specimen with proposed skew transverse reinforcement, the punching shear in ledges can be prevented by adjusting the distance between the exterior loading pad and the provided support at short sides.
11. Even though the cracking zone is similar for both types of reinforcing arrangements, the lower principal tensile strain is observed in the case of skew reinforcing than that of the traditional one under the application of the same load. The maximum principal tensile strain is a direct indicator of crack width. From the test results, it was observed that the crack width measured in ITBC with skew reinforcing was smaller than that of a traditional one. This is due to the even spacing of skew reinforcing.
12. All S Bars (shear and hanger stirrups), M Bars (Primary ledge bars) and N Bars (secondary ledge bars) will be skewed to match the skew angle of the inverted-T bridge cap, as shown in Figure 6.1. The spacing of skew transverse reinforcements will be measured from center to center of the hanger and ledge stirrups along the central line of the skew bent cap (not the perpendicular distance between hanger or ledge stirrups).
13. Avoid using shorter ledges. The distance between the central line of the exterior girder and the end face of the inverted-T bent cap should be maintained at least 24 inches to provide adequate punching shear capacity. This also delays the appearance of the diagonal crack at the re-entrant corner between the cantilever ledge and the web at the end faces of the ITBCs. Shorter ledges could increase the risk of ledge failures. TxDOT Projects 0-1854 and 0-6416 also emphasize this aspect.
14. Vertical rebars should be provided across both end faces of the skewed web. The spacing of these rebars should be equivalent to the spacing of shear and hanger stirrups (at least 6") and will be provided along the skew face. In addition to restricting the formation of cracks, vertical rebars at end faces help to reduce the stress concentration of the hanger and shear stirrups by redistributing at the cantilever end face. This aspect is illustrated in the section 6 with 3D FE simulated results.
15. At the skewed end faces of cantilever spans, adding diagonal bars (G bars) do not help to prevent the formation of diagonal crack at the re-entrant corner between the cantilever ledge and the web. The most effective variables to control crack width is the distance from end face to the most exterior loading pad. As the skew angle increased from the 0 degree to 60 degree the diagonal crack at the junction of ledge and web occurred at lower load.
16. A minimum area of transverse reinforcement is required to restrain the growth of diagonal (inclined) cracking, to increase the ductility and to prevent the sudden shear

failure of the bent cap. In this study six skewed inverted-T bent caps are studied with minimum amount of transverse reinforcement using the equations 5.8.2.5 provided in AASHTO LRFD 2014. All the test results show that there was no sudden shear failures. Transverse rebars are considerably yielded before the failure of the specimens. Therefore, the equations in AASHRO LRFD 2014 can be used to design the minimum transverse reinforcing in skewed inverted-T bent caps.

Thus, to summarize, based on the test and analytical results, it is recommended that the skew ITBCs with skew reinforcing can be a better alternative to the traditional reinforcing because the traditional detailing of transverse reinforcements in skew ITBC brings complexity in the design and construction process. Faster and easier construction can be obtained if the skew transverse reinforcing steel is utilized, and it can provide an alternative approach which will significantly reduce the design complexities and the construction period.

## REFERENCES

- AASHTO. (2014). Load Resistance Factor Design (LRFD) Bridge Design Specifications. American Association of State Highway and Transportation Officials (AASHTO), Washington, DC.
- ACI 318. (2014). Building Code Requirements for Structural Concrete (ACI 318-14) and Commentary. Farmington Hills
- Bridge Design Practice. (2015). State of California Department of Transportation. Fourth Edition.
- Gomez, F. (2012). Design criteria for strength and serviceability of inverted-T straddle bent caps (Doctoral dissertation).
- Kuo, W. W., Hsu, T. T., & Hwang, S. J. (2014). Shear strength of reinforced concrete beams. *ACI Structural Journal*, 111(4), 809.
- Larson, N., Gomez, E. F., Garber, D., Bayrak, O., & Ghannoum, W. (2013). *Strength and serviceability design of reinforced concrete inverted-T beams* (No. FHWA/TX-13/0-6416-1).
- Mirza, S. A., & Furlong, R. W. (1983, July). Serviceability Behavior and Failure Mechanisms of Concrete Inverted T-Beam Bridge Bent Caps. In *Journal Proceedings* (Vol. 80, No. 4, pp. 294-304).
- TxDOT Project 0-6905. (2018). Performance of Skew Reinforcing in Inverted-T Bridge Caps. Technical Memorandum-Task 4.
- TxDOT Project 0-6905. (2018). Performance of Skew Reinforcing in Inverted-T Bridge Caps. Technical Memorandum-Task 5.
- TxDOT. (2015). Bridge Design Manual (L.R.F.D). Texas Department of Transportation (TxDOT), Austin, TX.
- TxDOT. (2010). Inverted Tee Bent Cap Design Example. ([ftp://pub.txdot-info/library/pubs/bus/bridge/inverted\\_t.pdf](ftp://pub.txdot-info/library/pubs/bus/bridge/inverted_t.pdf)).
- Zhu, R. H., Dhonde, H., & Hsu, T. T. C. (2003). Crack Control for Ledges in Inverted 'T' Bent Caps (No. Research Report 0-1854-5). University of Houston, Department of Civil & Environmental Engineering.

**APPENDIX 1: STRAIN GAUGE LOCATIONS OF TEST SPECIMENS**

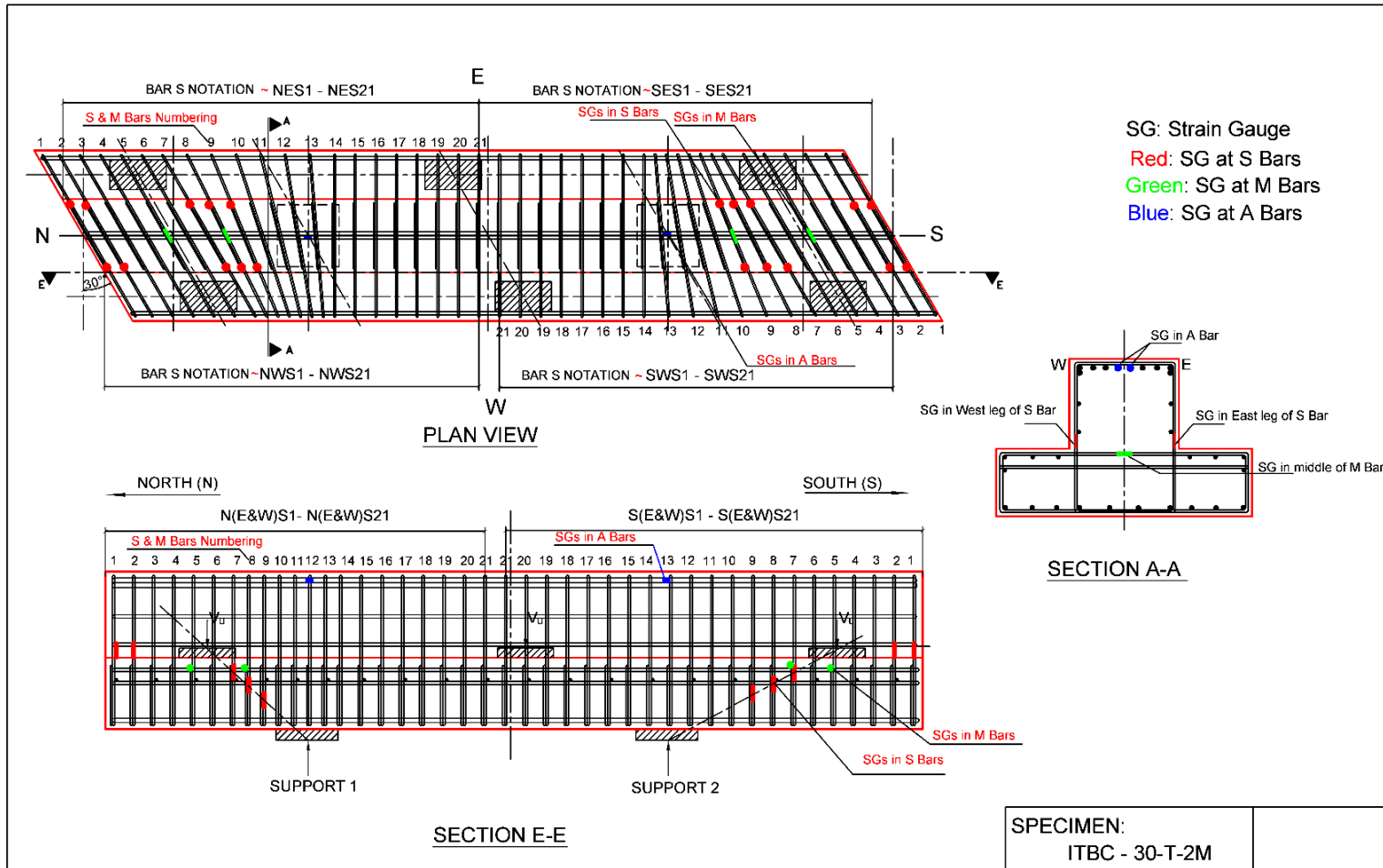


Figure A1.1. Strain gauge locations for Specimen ITBC-30-T-2M

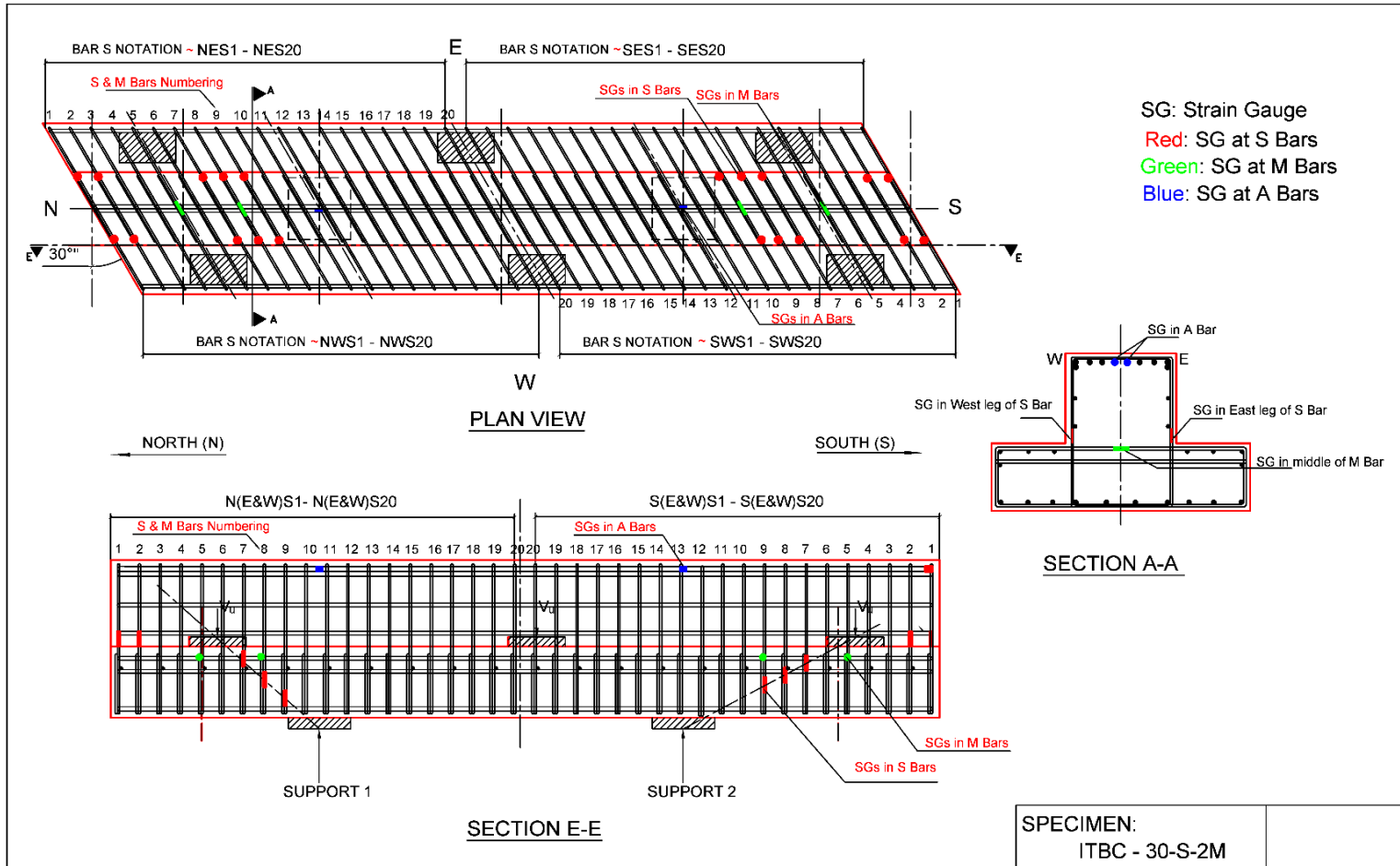


Figure A1.2. Strain gauge locations for Specimen ITBC-30-S-2M

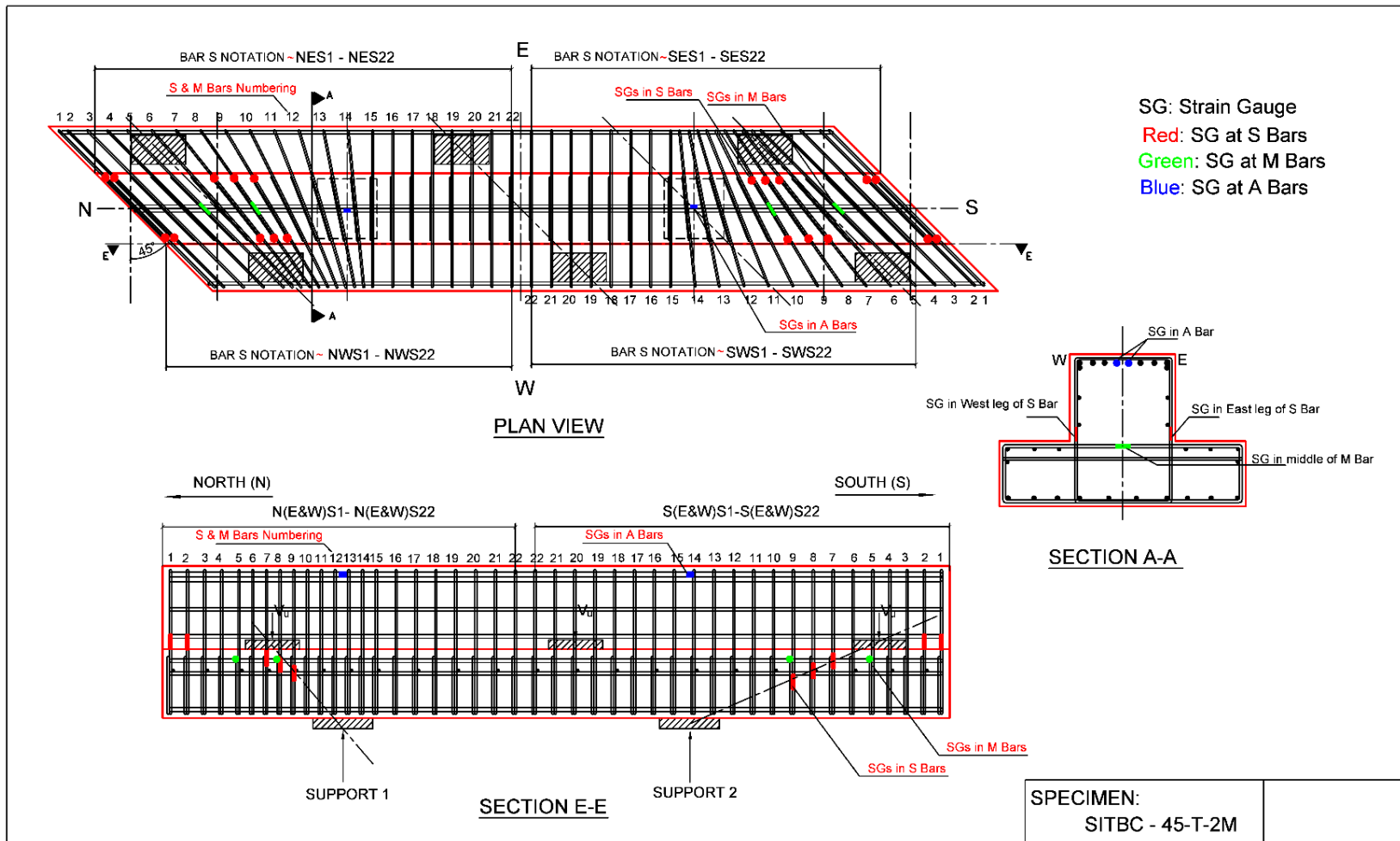


Figure A1.3. Strain gauge locations for Specimen ITBC-45-T-2M

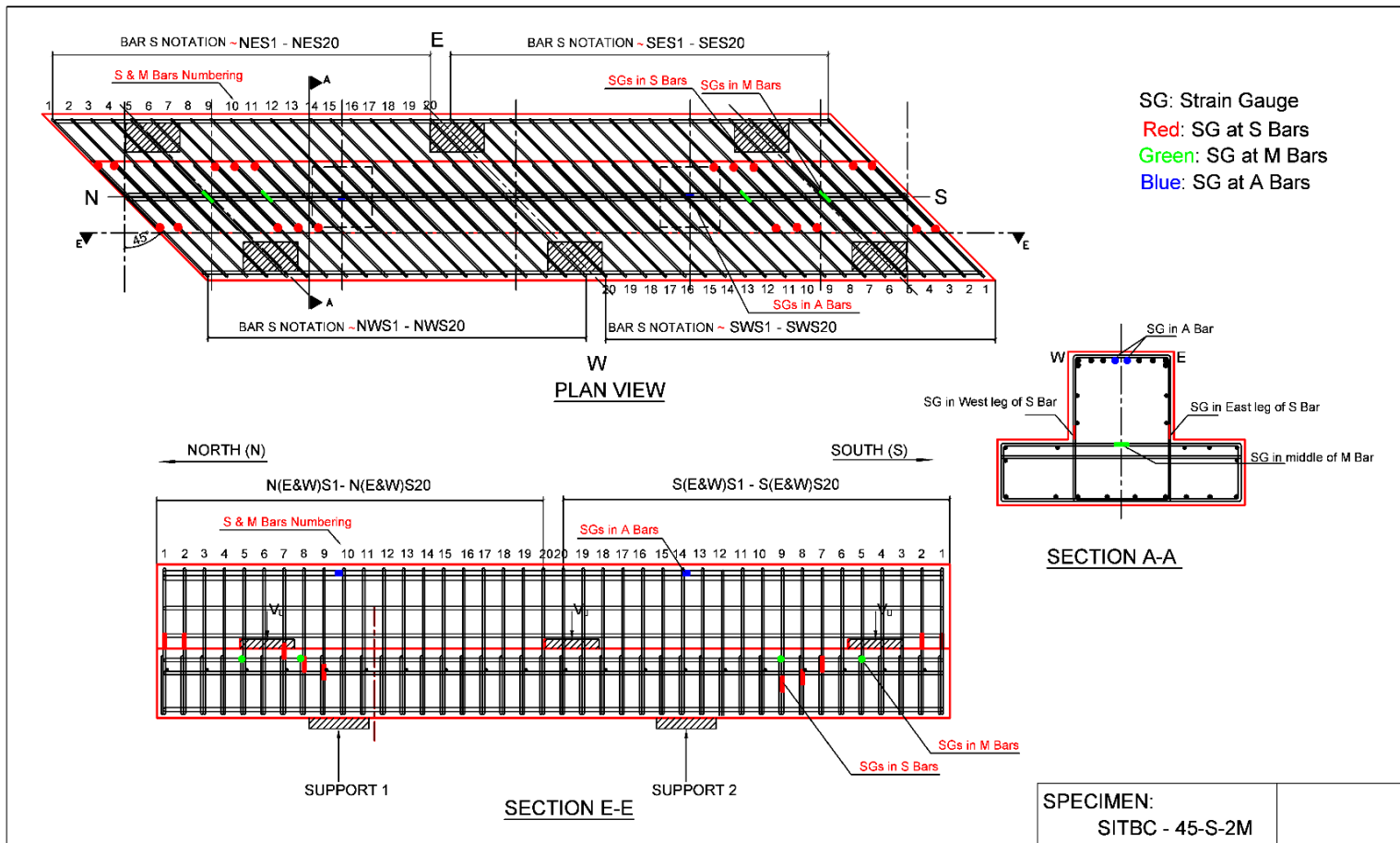
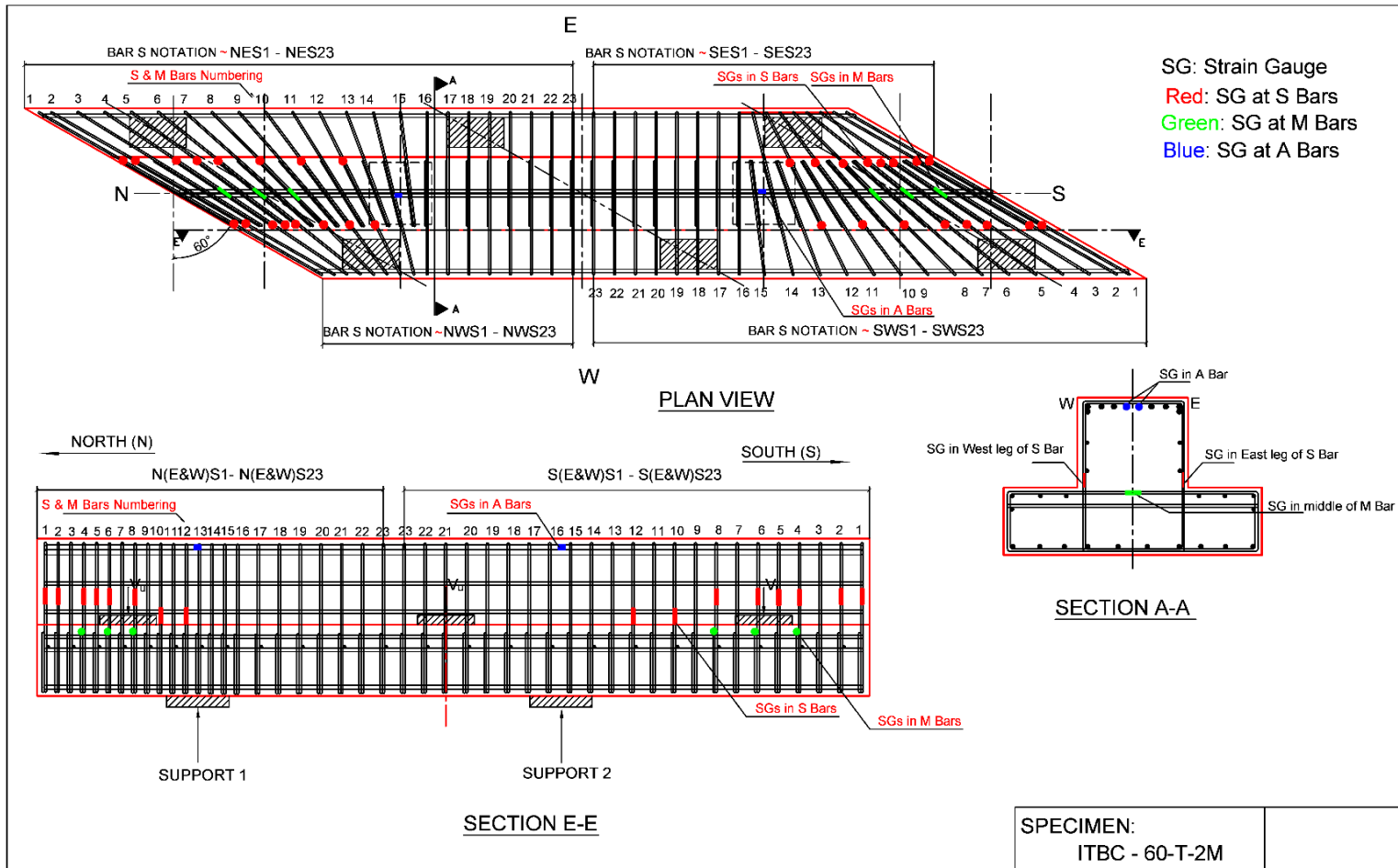


Figure A1.4. Strain gauge locations for Specimen ITBC-45-S-2M



**Figure A1.5. Strain gauge locations for Specimen ITBC-60-T-2M**

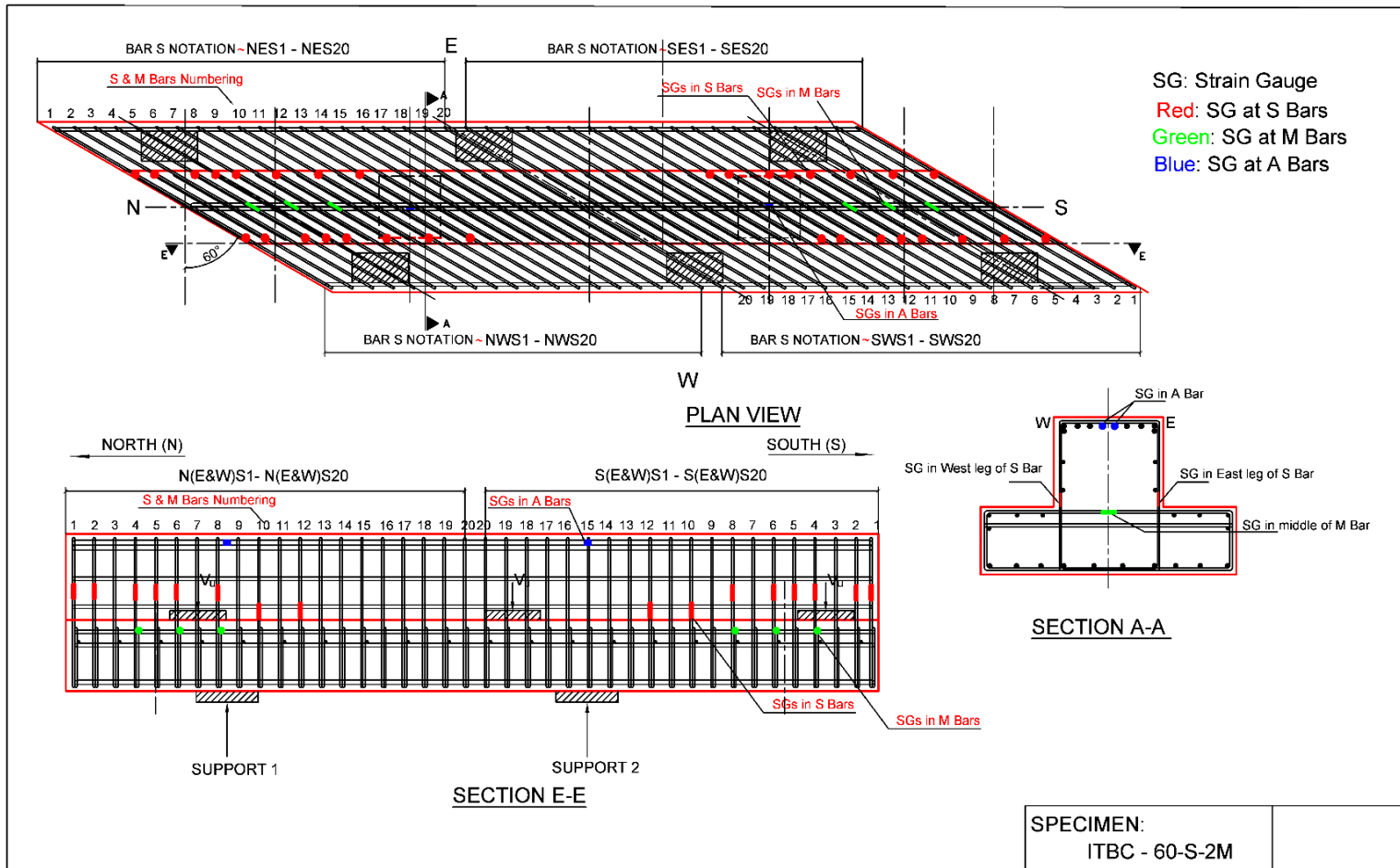


Figure A1.6. Strain gauge locations for Specimen ITBC-60-S-2M

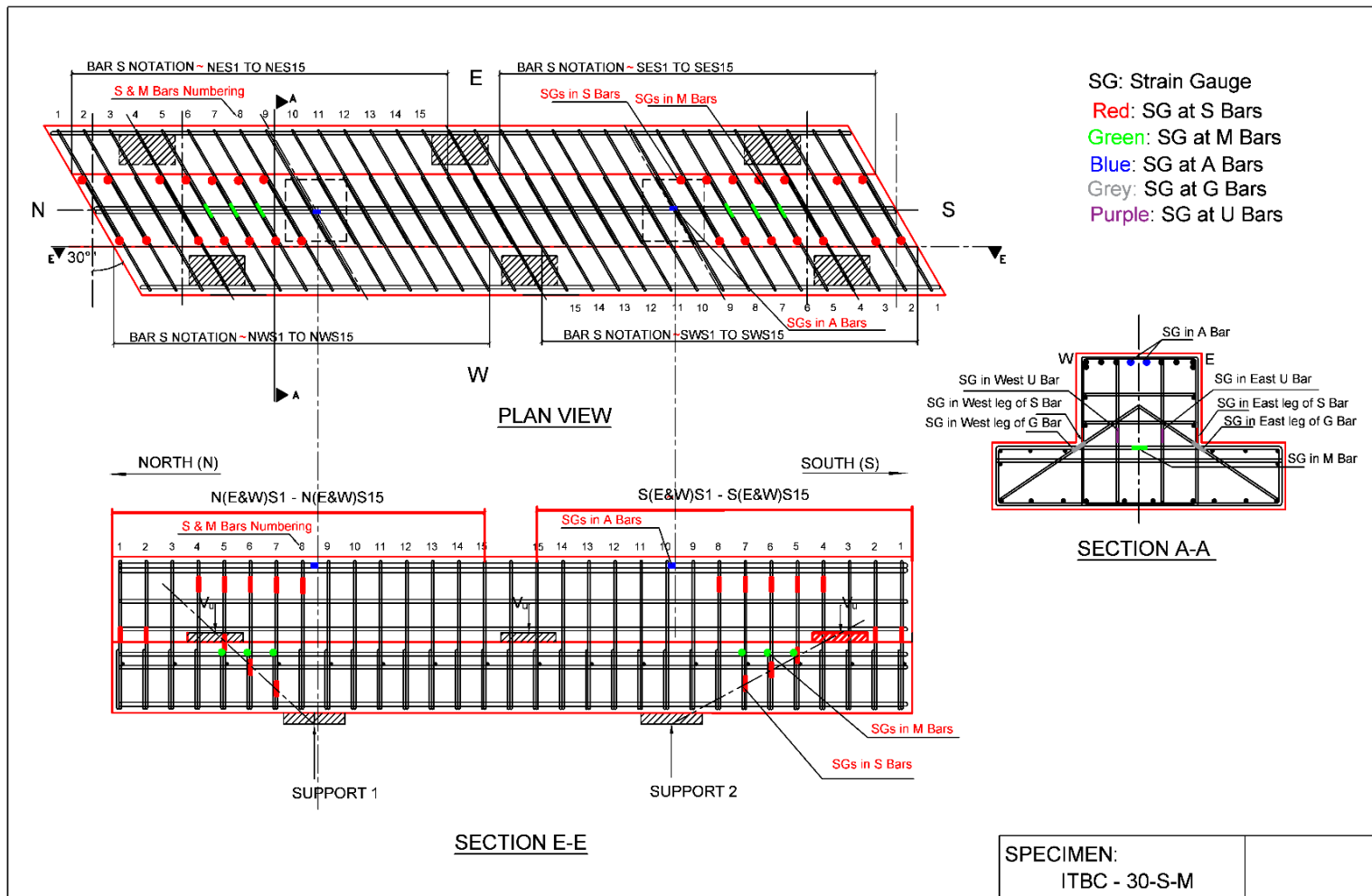


Figure A1.7. Strain gauge locations for specimen ITBC-30-T-M

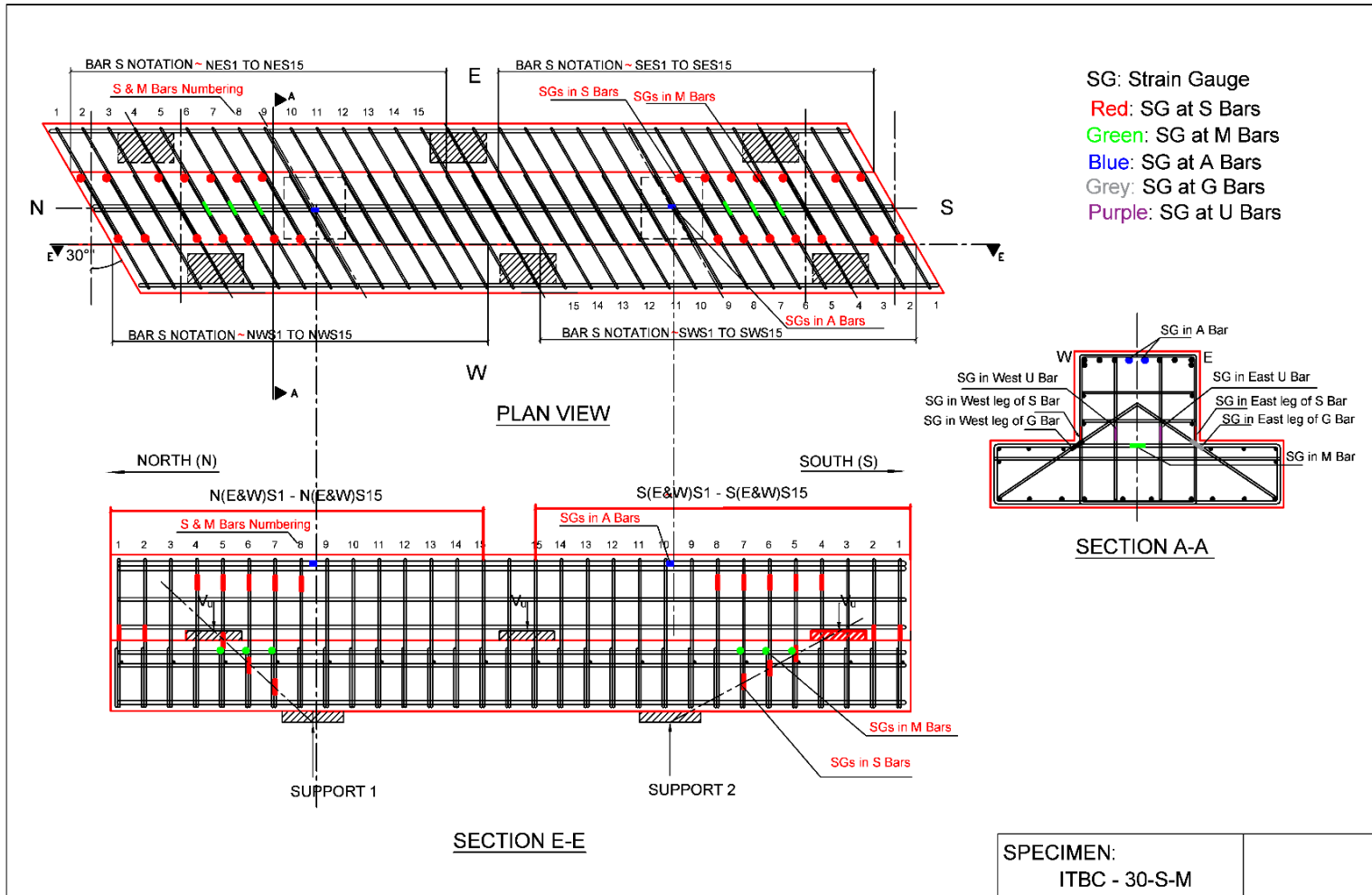
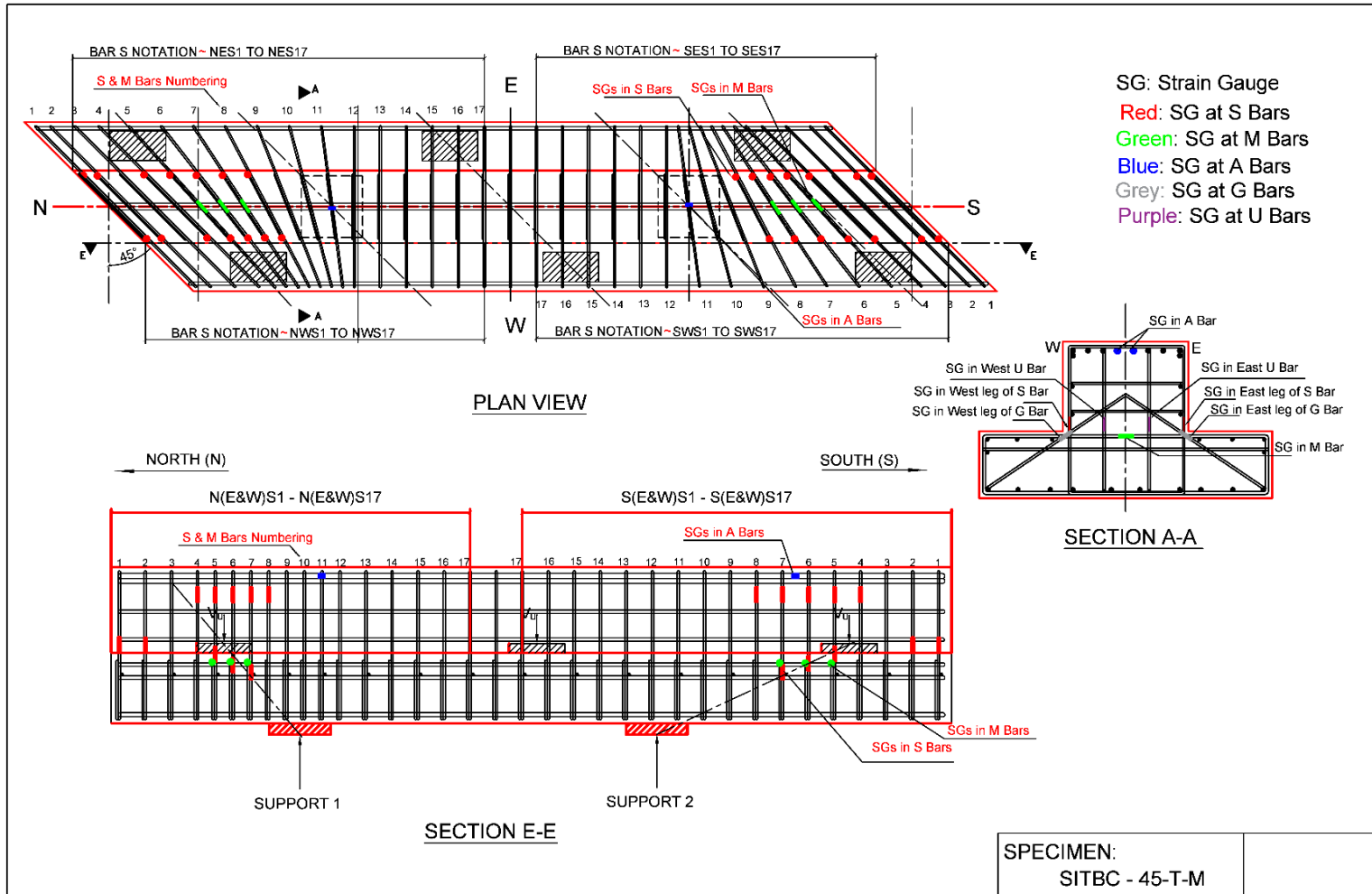


Figure A1.8. Strain gauge locations for specimen ITBC-30-S-M



**Figure A1.9. Strain gauge locations for specimen ITBC-45-T-M**

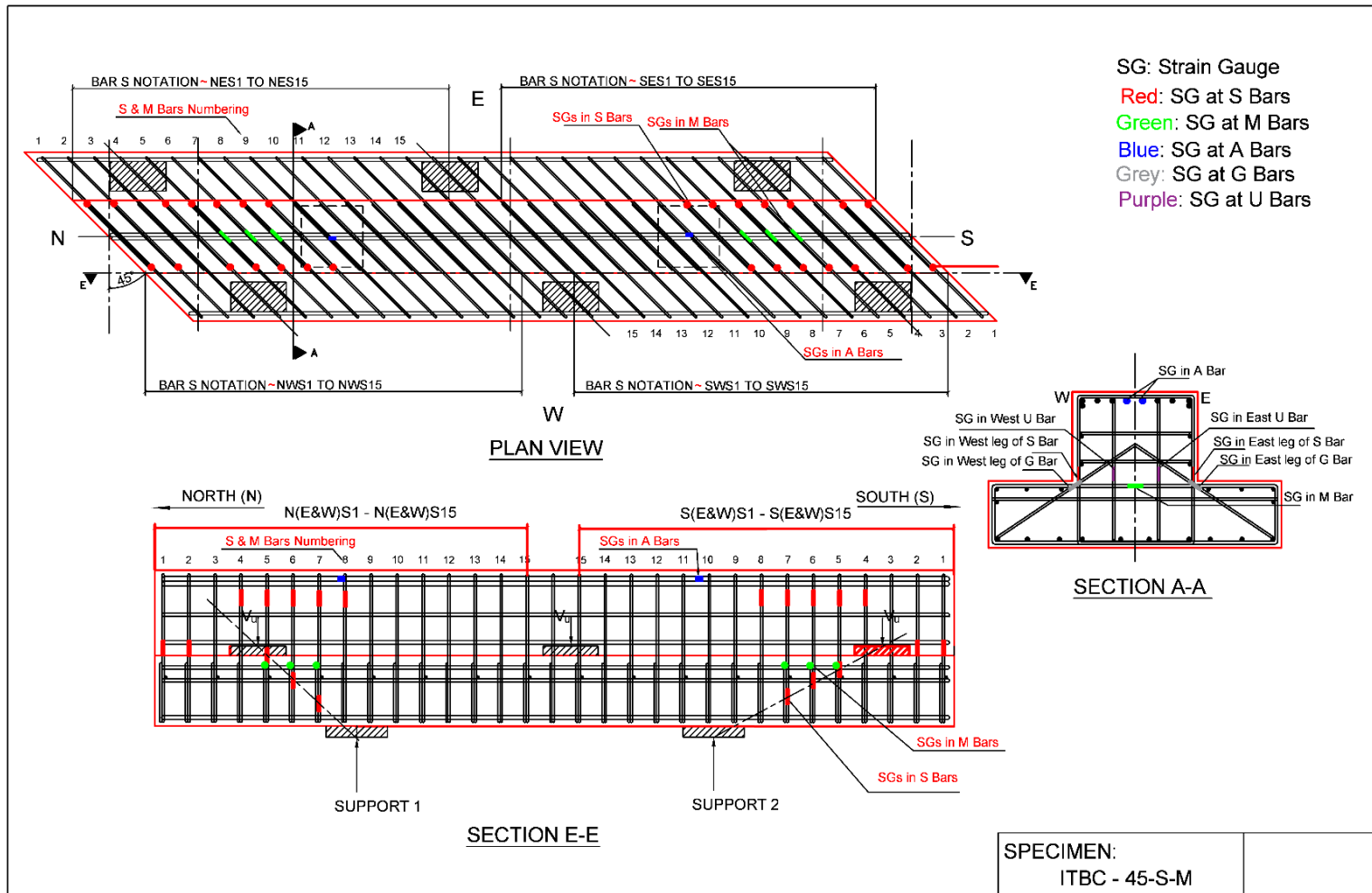
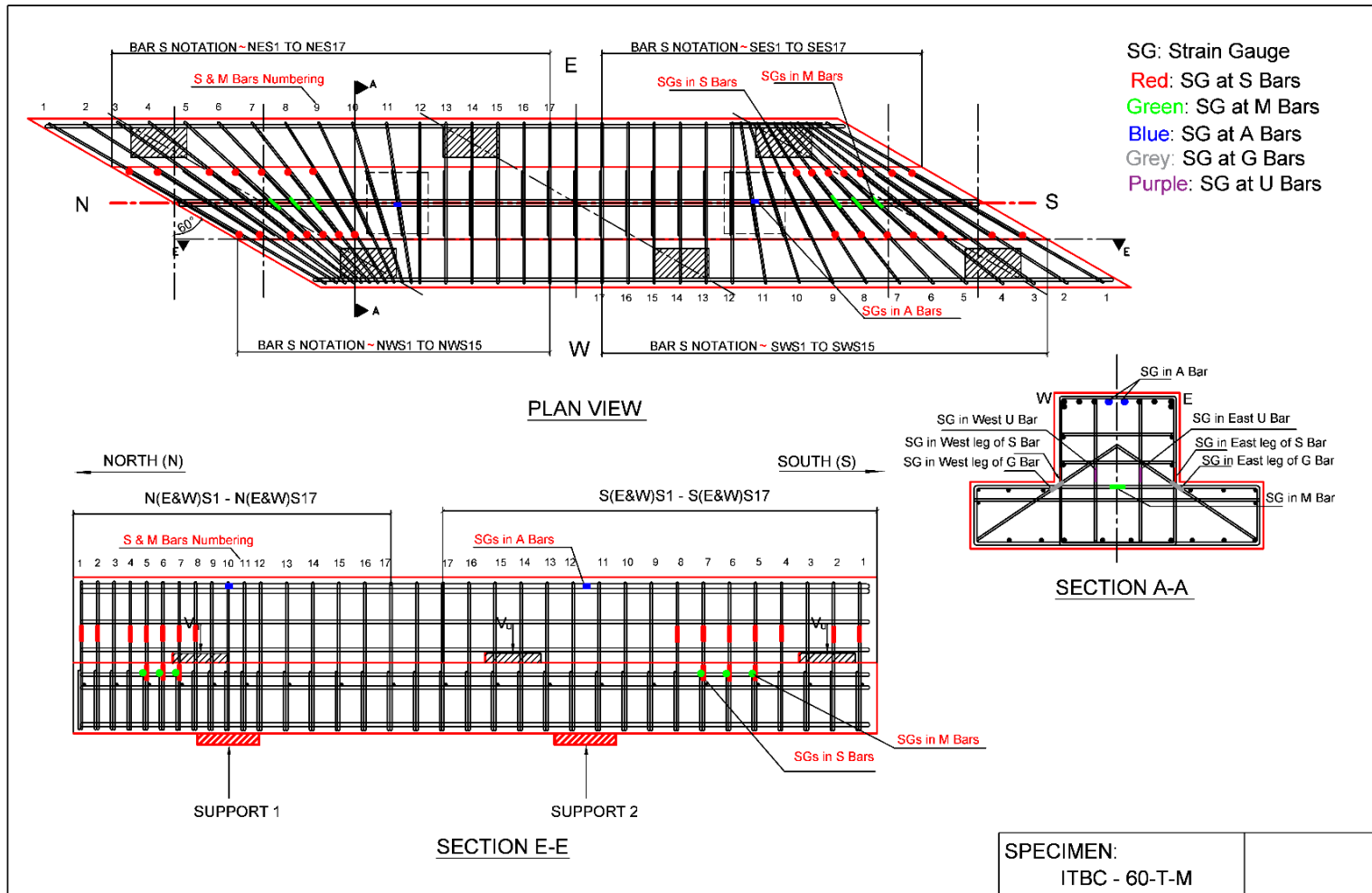


Figure A1.10. Strain gauge locations for specimen ITBC-45-S-M



**Figure A1.11. Strain gauge locations for specimen ITBC-60-T-M**

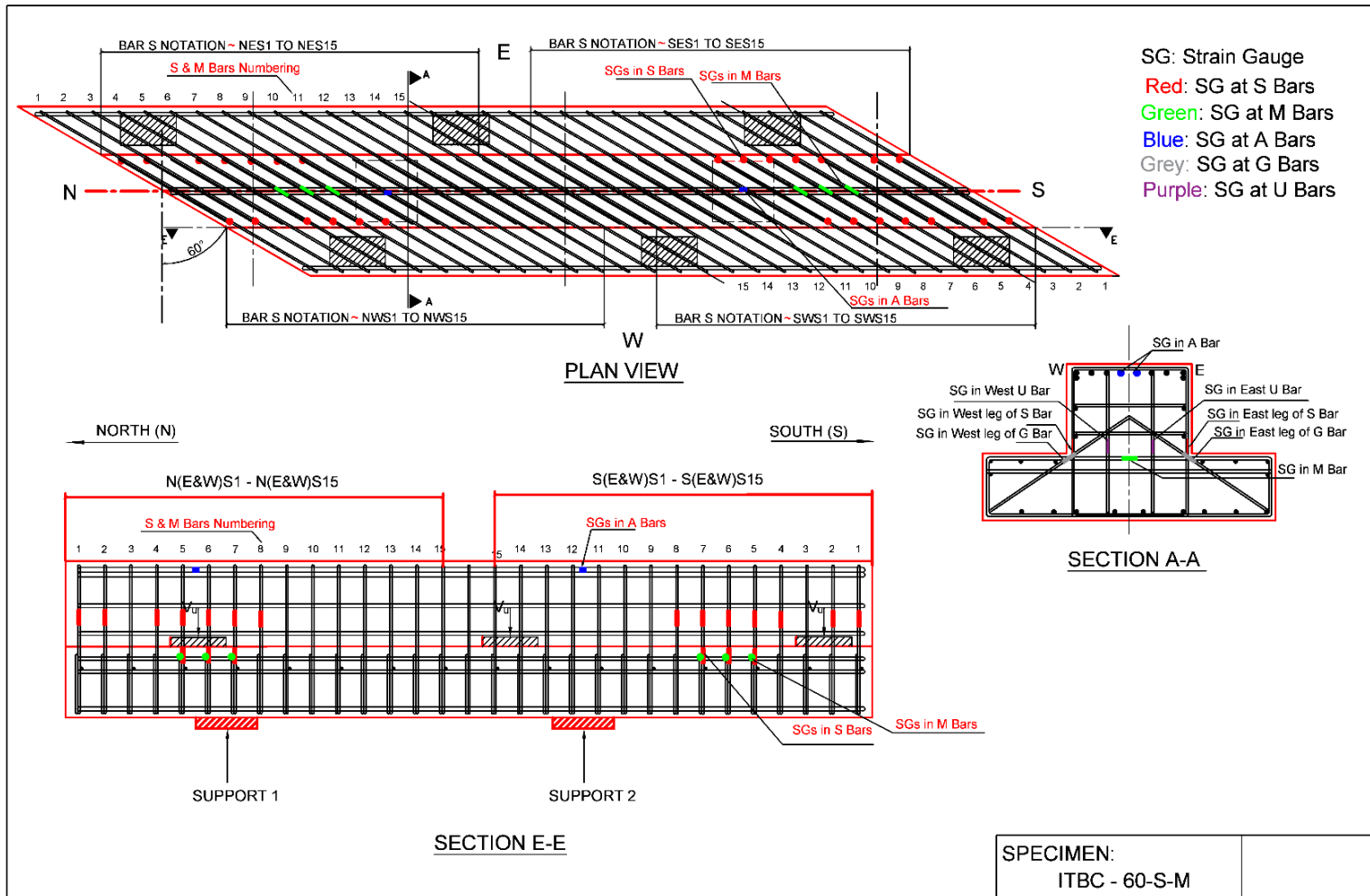


Figure A1.12. Strain gauge locations for specimen ITBC-60-S-M

## APPENDIX 2 : STRAIN IN THE REBARS OF TEST SPECIMENS

**Table A2.1. Specimen ITBC-0-T-2M**

Strain gauge Location	Yielding force (kips)	Strain values ( $\epsilon \times 10^{-6}$ )	
		At 1 <sup>st</sup> yielding	At peak force
NES1	245	1850	13349
NWS1	238	2303	7204
NES2	248	1656	7774
NWS2	244	1810	13136
NES7	334	729	10165
NWS7	326	647	23350
NES8	320	450	7438
NWS8	337	387	13634
NES9	NY	38	744
NWS9	NY	48	327
NL	NY	1215	1461
NM9	NY	99	120
NM5	NY	55	790
SES1	240	192	15746
SWS1	248	123	18109
SES2	271	88	11120
SWS2	329	238	23657
SES7	324	587	6609
SWS7	337	597	19096
SES8	333	227	48958
SWS8	337	366	12707
SES9	331	104	16232
SWS9	320	167	18053
SL	NY	1109	1602
SM5	NY	28	1303
SM8	NY	37	328

**Table A2.2. Specimen ITBC-30-T-2M**

Strain gauge Location	Yielding force (kips)	Strain values ( $\epsilon \times 10^{-6}$ )	
		At 1 <sup>st</sup> yielding	At peak force
NES1	321	2315	15920
NWS1	376	862	15023
NES7	362	1183	2606
NWS7	380	750	25146
NES8	358	1799	10208
NWS8	377	618	2808
NES9	346	2225	3520
NWS9	375	1964	2690
NL	NY	1405	1721
NM5	NY	54	480
NM9	NY	50	364
SES1	360	27	15593
SWS1	325	716	9539
SES7	356	830	13366
SWS7	360	533	3483
SES8	351	436	3834
SWS8	358	170	8023
SES9	363	262	11732
SWS9	384	874	2898
SL	NY	1284	1631
SM5	NY	13	320
SM8	NY	12	480

**Table A2.3. Specimen ITBC-30-S-2M**

Strain gauge	Yielding load (kips)	Strain values ( $\epsilon \times 10^{-6}$ )	
		At 1 <sup>st</sup> yielding	At peak load
NES1	332	2308	14235
NWS1	341	573	3755
NES7	NY	372	1200
NWS7	NY	519	1463
NES8	NY	48	1500
NWS8	347	1468	2204
NES9	NY	58	137
NWS9	NY	1082	1338
NL	NY	1500	1859
NM5	NY	29	48
NM9	NY	55	64
SES1	341	460	13728
SWS1	337	2294	7730
SES7	NY	447	1066
SWS7	NY	89	1028
SES8	354	1039	11647
SWS8	NY	26	1328
SES9	375	183	2360
SWS9	NY	21	174
SL	NY	1599	1987
SM5	NY	16	109
SM8	NY	55	64

**Table A2.4. Specimen ITBC-45-T-2M**

Strain gauge	Yielding load (kips)	Strain values ( $\epsilon \times 10^{-6}$ )	
		At 1 <sup>st</sup> yielding	At peak load
NES1	332	2308	14235
NWS1	341	573	3755
NES7	NY	372	1200
NWS7	NY	519	1463
NES8	NY	48	1500
NWS8	347	1468	2204
NES9	NY	58	137
NWS9	NY	1082	1338
NL	NY	1500	1859
NM5	NY	29	48
NM9	NY	55	64
SES1	341	460	13728
SWS1	337	2294	7730
SES7	NY	447	1066
SWS7	NY	89	1028
SES8	354	1039	11647
SWS8	NY	26	1328
SES9	375	183	2360
SWS9	NY	21	174
SL	NY	1599	1987
SM5	NY	16	109
SM8	NY	55	64

**Table A2.5. Specimen ITBC-45-S-2M**

Strain gauge	Strain values ( $\epsilon \times 10^{-6}$ )		Yielding force (kips)
	At 1 <sup>st</sup> yielding	At peak force	
NES1	2300	16141	293
NWS1	11	13348	348
NES7	922	8746	324
NWS7	355	14205	302
NES8	858	2383	320
NWS8	41	2245	361
NES9	439	1763	NY
NWS9	3	705	NY
NL	1212	1682	NY
NM5	26	792	NY
NM9	31	1794	NY
SES1	49	6230	315
SWS1	2303	21930	295
SES7	*	*	*
SWS7	2214	9636	301
SES8	31	2245	360
SWS8	1132	2263	348
SES9	17	1305	NY
SWS9	745	1715	NY
NL	488	1230	NY
SM5	55	1586	NY
SM8	18	33	NY

**Table A2.6. Specimen ITBC-60-T-2M**

Strain gauge	Yielding force (kips)	Strain values ( $\epsilon \times 10^{-6}$ )	
		At 1 <sup>st</sup> yielding	At peak force
NES1	171	2313	24738
NWS1	NY	7	1195
NES2	180	1489	14258
NWS2	NY	7	1499
NES4	195	13	13643
NWS4	291	3	7040
NES5	234	7	6266
NWS5	295	6	3556
NES6	*	*	*
NWS6	NY	11	1980
NES8	294	4	3034
NWS8	303	50	2463
NES10	290	21	5298
NWS10	NY	58	920
NES12	NY	23	1032
NWS12	NY	195	798
NL	NY	687	1636
NEM4	260	872	9239
NEM6	254	946	12975
NEM8	285/273	158	8346
SES1	NY	11	526
SWS1	179	2313	11762
SES2	NY	9	1115
SWS2	190	493	13149
SES4	NY	1	1693
SWS4	220	1	45069
SES5	290	3	3755
SWS5	241	4	13257
SES6	NY	33	318
SWS6	274	11	7821
SES8	NY	25	582
SWS8	297	21	3985

Strain gauge	Yielding force (kips)	Strain values ( $\epsilon \times 10^{-6}$ )	
		At 1 <sup>st</sup> yielding	At peak force
SES10	NY	264	581
SWS10	NY	-51	1160
SES12	NY	14	742
SWS12	NY	16	1137
SL	NY	981	1759
SWM4	284	438	13245
SWM5	314	141	2223
SWM8	NY	94	1601

**Table A2.7. Specimen ITBC-60-T-2M**

Strain gauge	Yielding force (kips)	Strain values ( $\epsilon \times 10^{-6}$ )	
		At 1 <sup>st</sup> yielding	At peak force
NES1	216	1109	10937
NWS1	NY	3	1313
NES2	214	1232	7698
NWS2	NY	7	1499
NES4	260	84	10984
NWS4	NY	14	1114
NES5	262	49	7794
NWS5	295	6	3556
NES6	271	0	2905
NWS6	NY	7	274
NES8	280	2	2678
NWS8	NY	173	530
NES10	271	10	3922
NWS10	NY	234	444
NES12	NY	-35	345
NWS12	NY	40	69
NL	NY	498	790
NEM4	NY	986	1886
NEM5	254	-88	6
NEM8	NY	586	1520
SES1	NY	1	1252
SWS1	210	2312	25516
SES2	NY	9	1115
SWS2	245	1248	12820
SES4	NY	0	700
SWS4	264	269	10984
SES5	NY	66	1290

Strain gauge	Yielding force (kips)	Strain values ( $\epsilon \times 10^{-6}$ )	
		At 1 <sup>st</sup> yielding	At peak force
SWS5	245	14	15023
SES6	NY	27	434
SWS6	267	9	13788
SES8	NY	136	227
SWS8	283	14	2875
SES10	NY	8	441
SWS10	NY	46	1750
SES12	NY	41	1009
SWS12	NY	42	1332
SL	NY	498	1600
SWM4	238	514	10786
SWM6	*	*	*
SWM8	NY	509	1833

**Table A2.8. Specimen ITBC-30-T-M**

Strain gauge	Yielding force (kips)	Strain values ( $\epsilon \times 10^{-6}$ )	
		At 1 <sup>st</sup> yielding	At peak force
NES1	NY	228	1529
NWS1	NY	17	620
NES2	NY	197	1481
NWS2	NY	42	502
NES4	NY	18	1204
NWS4	NY	170	1740
NES5	367	71	6329
NWS5	339	220	8891
NES6	292	2311	12661
NWS6	328	1267	5727
NES7	298	1799	5011
NWS7	336	115	3306
NES8	NY	1394	1601
NWS8	NY	558	941
NEU1	NY	34	1675
NWU1	NY	4	755
NEG1	*	*	*
NWG1	*	*	*
NM4	*	*	*
NM7	NY	57	111
NL	NY	717	1027
SES1	*	*	*
SWS1	NY	145	1391
SES2	NY	24	474
SWS2	NY	167	1217
SES4	*	*	*
SWS4	NY	6	1737
SES5	344	835	7609
SWS5	NY	113	1403
SES6	335	1387	6165
SWS6	336	543	10228
SES7	329	1902	3685
SWS7	338	1268	2764
SES8	NY	785	1181
SWS8	337	1505	2489
SEU1	NY	-24	178

Strain gauge	Yielding force (kips)	Strain values ( $\epsilon \times 10^{-6}$ )	
		At 1 <sup>st</sup> yielding	At peak force
SWU1	NY	0	606
SEG1	NY	52	650
SWG1	NY	183	1030
SL	NY	1394	2025
SM4	*	*	*
SM8	NY	43	98

**Table A2.9. Specimen ITBC-30-S-M**

Strain gauge	Yielding force (kips)	Strain values ( $\epsilon \times 10^{-6}$ )	
		At 1 <sup>st</sup> yielding	At peak force
NES1	NY	35	928
NWS1	NY	12	127
NES2	NY	29	482
NWS2	NY	42	488
NES4	NY	18	1918
NWS4	346	1158	4321
NES5	360	19	24445
NWS5	362	869	4610
NES6	295	2304	22248
NWS6	348	1333	2830
NES7	299	1010	9260
NWS7	NY	688	1079
NES8	NY	359	815
NWS8	NY	313	426
NEU1	NY	4	439
NWU1	NY	4	38
NEG1	NY	165	1100
NWG1	NY	69	1214
NM5	NY	24	31
NM7	NY	604	1785
NL	NY	1447	2242
SES1	*	*	*
SWS1	370	103	8223
SES2	NY	30	426
SWS2	NY	150	1548
SES4	344	922	3066
SWS4	367	16	4276
SES5	326	539	16140
SWS5	346	20	13058
SES6	354	524	3824
SWS6	336	240	14680
SES7	NY	1323	2093
SWS7	316	1118	4032

Strain gauge	Yielding force (kips)	Strain values ( $\epsilon \times 10^{-6}$ )	
		At 1 <sup>st</sup> yielding	At peak force
SES8	NY	57	156
SWS8	NY	1322	2030
SEU1	NY	22	774
SWU1	*	*	*
SEG1	NY	42	1203
SWG1	NY	47	1735
SM4	NY	10	1111
SM6	NY	14	22
SL	NY	1319	2280

**Table A2.10. Specimen ITBC-45-T-M**

Strain gauge	Yielding force (kips)	Strain values ( $\epsilon \times 10^{-6}$ )	
		At 1 <sup>st</sup> yielding	At peak force
NES1	NY	99	995
NWS1	NY	5	20
NES2	NY	137	1431
NWS2	NY	10	20
NES4	NY	-17	1061
NWS4	269	1751	13801
NES5	237	50	3828
NWS5	276	1694	15574
NES6	277	1345	18187
NWS6	445	1025	2361
NES7	253	2300	9604
NWS7	NY	1093	1343
NES8	NY	1346	1993
NWS8	NY	1031	1173
NEU1	NY	99	1011
NWU1	NY	4	73
NL	NY	1776	2102
SWS1	NY	20	915
SES2	NY	10	543
SWS2	NY	19	1574
SES4	342	38	7146
SES5	NY	445	2620
SWS5	NY	18	2492
SES6	302	1616	2255
SWS6	NY	25	7491
SES7	NY	1316	1730
SWS7	308	1283	7045
SES8	NY	558	1722
SWS8	NY	1368	1859
SEU1	NY	-33	11
SWU1	NY	18	1253
SL	NY	1371	2259

**Table A2.11. Specimen ITBC-45-S-M**

Strain gauge	Yielding force (kips)	Strain values ( $\epsilon \times 10^{-6}$ )	
		At 1 <sup>st</sup> yielding	At peak force
NES1	NY	588	1518
NWS1	*	*	*
NES2	NY	686	2159
NWS2	NY	11	54
NES4	373	-7	2604
NWS4	306	600	2430
NES5	356	26	26200
NWS5	287	1636	3677
NES6	*	*	*
NWS6	347	1096	10847
NES7	292	1234	2779
NWS7	360	1015	4290
NES8	NY	1326	1726
NWS8	NY	45	63
NEU1	NY	271	2076
NWU1	NY	8	103
SES1	NY	9	238
SES2	NY	27	409
SES4	310	69	2285
SES5	268	2310	3966
SES6	350	946	5140
SWS6	NY	62	1143
SES7	NY	17	261
SWS7	280	1959	6592
SWS8	NY	792	1832
SEU1	NY	26	189
SWU1	NY	9	64

**Table A2.12. Specimen ITBC-60-T-M**

Strain gauge	Yielding force (kips)	Strain values ( $\epsilon \times 10^{-6}$ )	
		At 1 <sup>st</sup> yielding	At peak force
NES1	229	2021	3915
NWS1	300	-32	2214
NES2	221	2312	7015
NWS2	NY	-30	432
NES4	298	236	2942
NWS4	NY	298	2069
NES5	265	347	2349
NWS5	297	595	4431
NES6	293	11	3113
NWS6	NY	120	1284
NES7	NY	1433	1603
NWS7	NY	435	1447
NES8	280	1148	2874
NWS8	NY	59	288
NEU1	NY	1038	1654
NWU1	NY	567	1344
NL	NY	967	1423
SES1	300	-86	2312
SWS1	226	1674	2602
SES2	NY	-84	1582
SWS2	293	931	3692
SES4	NY	-45	2091
SWS4	NY	-31	285
SES5	294	-7	4289
SWS5	293	-22	3692
SES6	NY	74	1187
SWS6	290	680	3297
SES7	NY	139	1499
SWS7	NY	301	1380
SES8	NY	142	475
SWS8	NY	561	2039
SEU1	NY	-30	3676
SWU1	292	550	4167
SL	NY	992	1650

**Table A2.13. Specimen ITBC-60-S-M**

Strain gauge	Yielding force (kips)	Strain values ( $\epsilon \times 10^{-6}$ )	
		At 1 <sup>st</sup> yielding	At peak force
NES1	248	1251	8453
NES2	241	2302	11769
NES4	260	838	18752
NWS4	296	244	3248
NES5	292	799	4992
NWS5	NY	27	406
NES6	293	282	4425
NWS6	NY	96	480
NES7	247	53	2825
NWS7	NY	116	478
NES8	251	1209	6038
NWS8	NY	236	501
NEU1	276	1249	17744
NWU1	292	481	2497
SES1	296	4	5253
SWS1	260	1885	15537
SES2	281	20	6044
SWS2	247	1039	14355
SES4	NY	376	901
SWS4	267	276	2431
SES5	NY	1135	1855
SWS5	253	2	11321
SES6	255	473	2252
SWS6	284	4	3694
SES7	NY	422	646
SWS7	277	63	2253
SES8	NY	35	127
SWS8	NY	773	1836
SEU1	NY	70	1424
SWU1	NY	220	2007

\* Not Applicable (Damaged)

## **APPENDIX 3: ILLUSTRATIVE DESIGN EXAMPLE**

# Design Example

## Material Properties

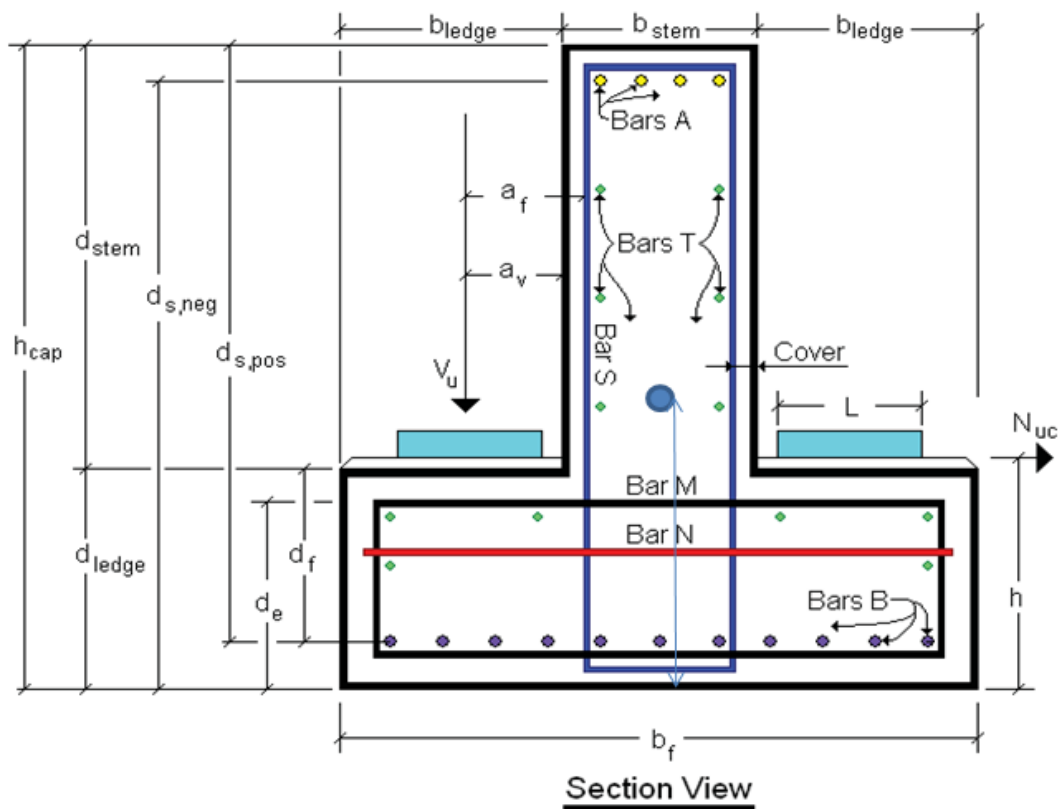
$f_c := 5.0 \text{ ksi}$  "Compressive strength of concrete"

$W_{ce} := 0.145 \text{ kcf}$  "Unit weight of concrete"

$E_c := 33000 \cdot W_{ce}^{1.5} \cdot \sqrt{f_c} = 4074.281 \text{ ksi}$  "Elastic modulus of concrete"

$f_y := 60 \text{ ksi}$  "Yield strength of steel rebars"

$E_s := 29000 \text{ ksi}$  "Elastic modulus of Steel rebars"



## Summary of Rebar Details

Longitudinal Rebars (Bar A, #11) :

$$d_{bar\_A} := 1.41 \text{ in}; \quad A_{bar\_A} := \frac{\pi}{4} \cdot (d_{bar\_A})^2 = 1.561 \text{ in}^2$$

$$BarANo := 18 \quad ; \quad As := BarANo \cdot A_{bar\_A} = 28.106 \text{ in}^2$$

Longitudinal Rebars (Bar B, #11) :

$$d_{bar\_B} := 1.41 \text{ in}; \quad A_{bar\_B} := \frac{\pi}{4} \cdot (d_{bar\_B})^2 = 1.561 \text{ in}^2$$

$$BarBNo := 14 \quad ; \quad As' := BarBNo \cdot A_{bar\_B} = 21.86 \text{ in}^2$$

Transverse Rebars (Bar S, #6) :

$$d_{bar\_S} := 0.75 \text{ in} \quad ; \quad A_{bar\_S} := \frac{\pi}{4} \cdot (d_{bar\_S})^2 = 0.442 \text{ in}^2 \quad ; \quad n_{leg\_S} := 4$$

$$A_V := n_{leg\_S} \cdot A_{bar\_S} = 1.767 \text{ in}^2 \quad ; \quad S_{bar\_S} := 6 \text{ in}$$

$$A_{hr} := \frac{A_V}{2} = 0.884 \text{ in}^2$$

Ledge Rebars (Bar M, #7) :

$$d_{bar\_M} := 0.875 \text{ in}; \quad A_{bar\_M} := \frac{\pi}{4} \cdot (d_{bar\_M})^2 = 0.601 \text{ in}^2 \quad ; \quad S_{bar\_M} := 6 \text{ in}$$

Skin Reinforcements (Bar T, #7) :

$$d_{bar\_T} := 0.875 \text{ in}; \quad A_{bar\_T} := \frac{\pi}{4} \cdot (d_{bar\_T})^2 = 0.601 \text{ in}^2$$

Secondary Ledge Rebars (Bar N, #5) :

$$d_{bar\_N} := 0.625 \text{ in}; \quad A_{bar\_N} := \frac{\pi}{4} \cdot (d_{bar\_N})^2 = 0.307 \text{ in}^2$$

## Inverted-T Bent Cap Dimensions & Cross Sectional Properties

$$Skew := 43$$

$$BearingNo. := 24 \quad \text{"Total number of bearing pad locations in the bent cap"}$$

$$L := 8 \text{ in} \quad \text{"Length of bearing pad"}$$

$$W := 21 \text{ in} \quad \text{"Width of bearing pad"}$$

$$a_v := 12 \text{ in} \quad \text{"Distance from the face of stem to center of bearing"}$$

$$S := 68.93 \text{ in} \quad \text{"Spacing of girders"}$$

$$C := 27.024 \text{ in} \quad \text{"Distance from the center of exterior girder to the edge of the bent cap"}$$

$$Cover := 2.0 \text{ in}$$

$$d_{ledge} := 27 \text{ in} \quad \text{"Depth of the ledge"}$$

$$b_{ledge} := 25.5 \text{ in} \quad \text{"Width of the ledge"}$$

$$d_{stem} := 57 \text{ in} \quad \text{"Depth of the stem"}$$

$$b_{stem} := 45 \text{ in} \quad \text{"Width of the stem"}$$

$$b_w := b_{stem} = 45 \text{ in}$$

$$h_{cap} := d_{stem} + d_{ledge} = 84 \text{ in} \quad \text{"Depth of the cap"}$$

$$d_e := d_{ledge} - Cover = 25 \text{ in}$$

$$d_f := d_{ledge} - Cover - \frac{d_{bar_M}}{2} - \frac{d_{bar_B}}{2} = 23.858 \text{ in}$$

$$a_f := a_v + Cover = 14 \text{ in}$$

$$b_f := 2 \cdot b_{ledge} + b_{stem} = 96 \text{ in}$$

$$LeverArm := a_v + 0.5 \cdot b_{stem} = 34.5 \text{ in}$$

$$h := 28.5 \text{ in}$$

$$A_g := (d_{ledge}) \cdot (b_f) + (d_{stem}) \cdot (b_{stem}) = 5157 \text{ in}^2$$

$$Ybar := \frac{(d_{ledge}) \cdot (b_f) \cdot \frac{1}{2} \cdot (d_{ledge}) + (d_{stem}) \cdot (b_{stem}) \cdot \left(d_{ledge} + \frac{1}{2} \cdot d_{stem}\right)}{A_g} = 34.39 \text{ in}$$

"Distance from the bottom of the cap to the center of gravity of the cap"

$$I_{ledge} := \frac{b_f \cdot d_{ledge}^3}{12} + b_f \cdot d_{ledge} \cdot \left(Ybar - \frac{1}{2} \cdot d_{ledge}\right)^2 = 1288597.993 \text{ in}^4$$

"Moment of Intertia of the ledge"

$$I_{stem} := \frac{b_{stem} \cdot d_{stem}^3}{12} + b_{stem} \cdot d_{stem} \cdot \left(Ybar - \left(d_{ledge} + \frac{1}{2} \cdot d_{stem}\right)\right)^2 = 1837514.417 \text{ in}^4$$

"Moment of Intertia of the stem"

$$I_g := I_{ledge} + I_{stem} = 3126112.41 \text{ in}^4$$

"Gross Moment of Intertia "

## Summary of Cap Loads & Moments

### Cap Loads

$M_{posDl} := 0.10 \text{ ft}\cdot\text{kip}$	"Positive moment due to dead load"
$M_{posServ} := 1210 \text{ ft}\cdot\text{kip}$	"Positive moment due to service load"
$M_{negUlt} := 1831 \text{ ft}\cdot\text{kip}$	"Positive moment due to ultimate load"
$M_{negDl} := 2122.40 \text{ ft}\cdot\text{kip}$	"Negative moment due to dead load"
$M_{negServ} := 3150 \text{ ft}\cdot\text{kip}$	"Negative moment due to service load"
$M_{negUlt} := 4470 \text{ ft}\cdot\text{kip}$	"Negative moment due to ultimate load"

### Ledge Loads

$V_{S\_Int} := 222.48 \text{ kip}$	"Service load at interior bearing pads"
$V_{U\_Int} := 334.84 \text{ kip}$	"Factor load at interior bearing pads"
$V_{S\_Ext} := 240.19 \text{ kip}$	"Service load at exterior bearing pads"
$V_{U\_Ext} := 365.82 \text{ kip}$	"Factor load at exterior bearing pads"

### Maximum Torsion, Shear and Moment

*Maximum Torsion* :  $Tu := 522 \text{ ft}\cdot\text{kip}$

*Maximum Shear* :  $Vu := 808.00 \text{ kip}$

## 1. Check for Punching Shear

$$\phi_s := 0.9$$

(1) AASHTO LRFD(2014) (AASHTO LRFD 5.13.2.5.4)

(i) Interior Girder

$$V_{nps\_int1} := 0.125 \cdot \sqrt{fc} (W + 2 \cdot L + 2 \cdot d_e) \cdot d_e = 607.931 \quad kip$$

$$\phi_s \cdot V_{nps\_int1} = 547.138 \quad kip$$

(ii) Exterior Girder

$$V_{nps\_ext1} := 0.125 \cdot \sqrt{fc} (0.5 \cdot W + L + d_e + C) \cdot d_e = 492.801 \quad kip$$

$$\phi_s \cdot V_{nps\_ext1} = 443.521 \quad kip$$

(2) TxDOT BDM LRFD(2015)

(i) Interior Girder

$$V_{nps\_int2} := 0.125 \cdot \sqrt{fc} (W + 2 \cdot L + 2 \cdot d_f) \cdot d_f = 564.911 \quad kip$$

$$\phi_s \cdot V_{nps\_int2} = 508.42 \quad kip$$

(ii) Exterior Girder

$$V_{nps\_ext2} := 0.125 \cdot \sqrt{fc} (W + 2 \cdot L + 2 \cdot d_f) \cdot d_f = 564.911 \quad kip$$

$$V_{nps\_ext2.1} := 0.125 \cdot \sqrt{fc} (0.5 \cdot W + L + d_f + C) \cdot d_f = 462.662 \quad kip$$

$$\phi_s \cdot V_{nps\_ext2.1} = 416.396 \quad kip$$

$$\therefore V_{nps\_int} := \min(\phi_s \cdot V_{nps\_int1}, \phi_s \cdot V_{nps\_int2}) = 508.42 \quad kip$$

$$V_{nps\_ext} := \min(\phi_s \cdot V_{nps\_ext1}, \phi_s \cdot V_{nps\_ext2.1}) = 416.396 \quad kip$$

$$V_{U\_Int} < V_{nps\_int} \quad \text{Punching Shear Check = "OK"}$$

$$V_{U\_Ext} < V_{nps\_ext} \quad \text{Punching Shear Check = "OK"}$$

## 2. Check for Shear Friction (AASHTO LRFD 5.13.2.5.2)

Checks are for concrete only

### (i) Interior Girder

$$c1 := 0 \quad \mu := 1.4 \quad Pc := 0 \quad \phi_{sf} := 0.9$$

$$b_{s\_int} := \min(W + 4 \cdot a_v, S) = 68.93 \text{ in}$$

$$A_{cv\_Int} := d_e \cdot b_{s\_int} = 1723.25 \text{ in}^2$$

$$V_{nsf\_Int} := \min(0.2 \cdot fc \cdot A_{cv\_Int}, 0.8 \cdot A_{cv\_Int}) = 1378.6 \text{ kip}$$

$$\phi_{sf} \cdot V_{nsf\_Int} = 1240.74 \text{ kip}$$

### (ii) Exterior Girder

$$c1 := 0 \quad \mu := 1.4 \quad Pc := 0 \quad \phi_{sf} := 0.9$$

$$b_{s\_Ext} := \min(W + 4 \cdot a_v, S, 2 \cdot C) = 54.048 \text{ in}$$

$$A_{cv\_Ext} := d_e \cdot b_{s\_Ext} = 1351.2 \text{ in}^2$$

$$V_{nsf\_Ext} := \min(0.2 \cdot fc \cdot A_{cv\_Ext}, 0.8 \cdot A_{cv\_Ext}) = 1080.96 \text{ kip}$$

$$\phi_{sf} \cdot V_{nsf\_Ext} = 972.864 \text{ kip}$$

$$V_{U\_Int} < \phi_{sf} \cdot V_{nsf\_int} \quad \text{Shear Friction Check = "OK"}$$

$$V_{U\_Ext} < \phi_{sf} \cdot V_{nsf\_ext} \quad \text{Shear Friction Check = "OK"}$$

### 3. Check for Bearing of the Ledge (AASHTO LRFD 5.7.5)

$$\phi_b := 0.7$$

$$A_1 := W \cdot L = 168 \text{ in}^2$$

#### (i) Interior Girder

$$B := \min \left( (b_{ledge} - a_v) - 0.5 \cdot L, (a_v + 0.5 \cdot b_{stem}) - 0.5 \cdot L, 2 \cdot d_{ledge}, 0.5 \cdot S - 0.5 \cdot W \right) = 9.5 \text{ in}$$

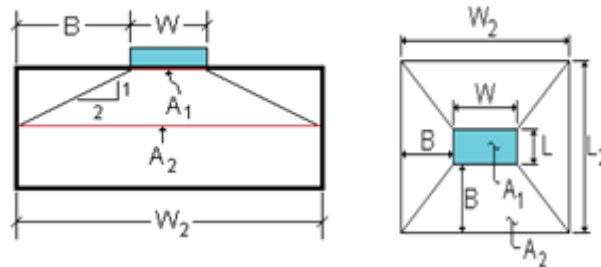
$$L_2 := L + 2 \cdot B = 27 \text{ in}$$

$$W_2 := W + 2 \cdot B = 40 \text{ in}$$

$$A_2 := L_2 \cdot W_2 = 1080 \text{ in}^2$$

modification factor :

$$m := \min \left( \sqrt{\frac{A_2}{A_1}}, 2 \right) = 2$$



Elevation

Plan

$$V_{nb\_Int} := 0.85 \cdot f_c \cdot A_1 \cdot m = 1428 \text{ kip}$$

$$\phi_b \cdot V_{nb\_Int} = 999.6 \text{ kip}$$

#### (ii) Exterior Girder

$$B := \min \left( (b_{ledge} - a_v) - 0.5 \cdot L, (a_v + 0.5 \cdot b_{stem}) - 0.5 \cdot L, 2 \cdot d_{ledge}, 0.5 \cdot S - 0.5 \cdot W, C - 0.5 \cdot W \right) = 9.5$$

$$L_2 := L + 2 \cdot B = 27 \text{ in}$$

$$W_2 := W + 2 \cdot B = 40 \text{ in}$$

$$A_2 := L_2 \cdot W_2 = 1080 \text{ in}^2$$

modification factor :

$$m := \min \left( \sqrt{\frac{A_2}{A_1}}, 2 \right) = 2$$

$$V_{nb\_Ext} := 0.85 \cdot f_c \cdot A_1 \cdot m = 1428 \text{ kip}$$

$$\phi_b \cdot V_{nb\_Ext} = 999.6 \text{ kip}$$

$$V_{U\_Int} < \phi_b \cdot V_{nb\_Int}$$

Bearing Check = "OK"

$$V_{U\_Ext} < \phi_b \cdot V_{nb\_Ext}$$

Bearing Check = "OK"

## 4. Flexural Reinforcement For Negative and Positive Bending

### 1. Flexural Reinforcement For Negative Bending

#### Cracking Moment :

$$I_g := I_{ledge} + I_{stem} = 3126112.41 \text{ in}^4 \quad \text{"Gross Moment of Intertia"}$$

$$h_{cap} := d_{stem} + d_{ledge} = 84 \text{ in} \quad \text{"Height of the cap"}$$

$$f_r := 0.24 \cdot \sqrt{f_c} = 0.537 \text{ ksi} \quad \text{"Modulus of Rupture"}$$

$$y_t := h_{cap} - Ybar = 49.61 \text{ in} \quad \text{"Distance from center of gravity to extreme tension fiber"}$$

$$S := \frac{I_g}{y_t} = 63013.822 \text{ in}^3 \quad \text{"Section Modulus"}$$

$$M_{cr} := S \cdot \frac{f_r}{12} = 2818.064 \text{ ft}\cdot\text{kip} \quad \text{"Cracking Moment"}$$

$$M_u := M_{negUlt} = 4470 \text{ ft}\cdot\text{kip}$$

$$M_f := \min(1.2 \cdot M_{cr}, 1.33 M_u) = 3381.677 \text{ ft}\cdot\text{kip}$$

#### Moment Capacity Design

Try 18 #11 bars at top

$$d_{bar\_A} := 1.41 \text{ in}$$

$$A_{bar\_A} := \frac{\pi}{4} \cdot (d_{bar\_A})^2 = 1.561 \text{ in}^2$$

$$A_{s\_A} := 18 \cdot A_{bar\_A} = 28.106 \text{ in}^2$$

$$d_{s\_neg} := h_{cap} - Cover - \frac{d_{bar\_S}}{2} - d_{bar\_A} = 80.215 \text{ in}$$

$$\beta_f := \begin{cases} \text{if } f_c \leq 4.0 \\ \quad \left| \begin{array}{l} 0.85 \\ \text{else} \\ 0.85 - 0.05 \left( \frac{f_c \cdot 1000 - 4000}{1000} \right) \end{array} \right| \end{cases}$$

$$\beta_1 := \beta_f = 0.8$$

$$c_f := \frac{A_{s_A} \cdot f_y}{0.85 \cdot f_c \cdot \beta_1 \cdot b_f} = 5.167$$

$$ac := c_f \cdot \beta_1 = 4.133$$

$$M_{n\_neg} := A_{s_A} \cdot f_y \cdot \left( \frac{d_{s\_neg} - \frac{ac}{2}}{12} \right) = 10982.231 \text{ ft}\cdot\text{kip}$$

$$\varepsilon_s := 0.003 \cdot \left( \frac{d_{s\_neg} - c_f}{c_f} \right) = 0.044$$

$$\varepsilon_s > 0.005 \quad \text{Flexure Behavior} = \text{"Tension Controlled"}$$

$$\phi_M := 0.9$$

$$M_r := \phi_M \cdot M_{n\_neg} = 9884.008 \text{ ft}\cdot\text{kip}$$

### Checking Serviceability

$$n := \frac{E_s}{E_c} = 7.118 \quad \text{"Modular ratio"}$$

$$\rho_A := \frac{A_{s_A}}{b_f \cdot d_{s\_neg}} = 0.004 \quad \text{"Tension reinforcement ratio"}$$

$$k := \sqrt{(2 \cdot \rho_A \cdot n) + (\rho_A \cdot n)^2} - (\rho_A \cdot n) = 0.203$$

$$d_{s\_neg} \cdot k = 16.319 \text{ in} \quad d \cdot k < d_{ledge}$$

$$j := 1 - \frac{k}{3} = 0.932$$

$$M_s := 3150 \text{ ft}\cdot\text{kip}$$

$$f_{ss} := \frac{M_s \cdot 12}{A_{s_A} \cdot j \cdot d_{s\_neg}} = 17.986 \text{ ksi}$$

$$f_a := 0.6 \cdot f_y = 36 \text{ ksi}$$

$$\therefore f_{ss} < f_a \quad \text{Serviceability Check} = \text{"OK"}$$

## Checking Dead Load Stress:

TxDOT limits the dead load stresses to 22 ksi. This is due to the observed cracking under dead load.

$$\therefore f_{dl} := 22 \text{ ksi}$$

$$M_{dl} := 2122.40 \text{ ft}\cdot\text{kip}$$

Allowable Dead Load Moment

$$M_{a\_dl} := A_{s\_A} \cdot d_{s\_neg} \cdot j \cdot \frac{f_{dl}}{12} = 3853.014 \text{ ft}\cdot\text{kip}$$

$$\therefore M_{dl} < M_{a\_dl} \quad \text{Check} = \text{"OK"}$$

## 2. Flexural Reinforcement For Positive Bending

### Cracking Moment

$$y_{t1} := Ybar = 34.39 \text{ in} \quad \text{"Distance from center of gravity to extreme compression fiber"}$$

$$S_1 := \frac{I_g}{y_{t1}} = 90901.647 \text{ in}^3 \quad \text{"Section Modulus"}$$

$$M_{cr1} := S_1 \cdot \frac{f_r}{12} = 4065.245 \text{ ft}\cdot\text{kip} \quad \text{"Cracking Moment"}$$

$$M_{u1} := 1831.00 \text{ ft}\cdot\text{kip}$$

$$M_{f1} := \min(1.2 \cdot M_{cr}, 1.33 M_{u1}) = 2435.23 \text{ ft}\cdot\text{kip}$$

### Moment Capacity Design

**Try 14 #11 bars at top**

$$d_{bar\_A} := 1.41 \text{ in}$$

$$A_{bar\_B} := \frac{\pi}{4} \cdot (d_{bar\_A})^2 = 1.561 \text{ in}^2$$

$$A_{s\_B} := 14 \cdot A_{bar\_A} = 21.86 \text{ in}^2$$

$$d_{s\_pos} := h_{cap} - Cover - \frac{d_{bar\_M}}{2} - \frac{d_{bar\_B}}{2} = 80.858 \text{ in}$$

$$\beta_f := \begin{cases} \text{if } fc \leq 4.0 \\ \quad \parallel 0.85 \\ \text{else} \\ \quad \parallel 0.85 - 0.05 \left( \frac{fc \cdot 1000 - 4000}{1000} \right) \end{cases}$$

$$\beta_1 := \beta_f = 0.8$$

$$c_f := \frac{A_{s_B} \cdot f_y}{0.85 \cdot fc \cdot \beta_1 \cdot b_{stem}} = 8.573$$

$$ac := c_f \cdot \beta_1 = 6.858$$

$$M_{n_{pos}} := A_{s_B} \cdot f_y \cdot \left( \frac{d_{s_{pos}} - \frac{ac}{2}}{12} \right) = 8463.044 \quad \text{ft} \cdot \text{kip}$$

$$\varepsilon_s := 0.003 \cdot \frac{(d_{s_{pos}} - c_f)}{c_f} = 0.025$$

$$\varepsilon_s > 0.005 \quad \text{Flexure Behavior = "Tension Controlled"}$$

$$\phi_M := 0.9$$

$$M_r := \phi_M \cdot M_{n_{pos}} = 7616.74 \quad \text{ft} \cdot \text{kip} \quad \text{good}$$

### Checking Serviciability

$$n := \frac{E_s}{E_c} = 7.118 \quad \text{"Modular ratio"}$$

$$\rho_B := \frac{A_{s_B}}{b_{stem} \cdot d_{s_{pos}}} = 0.006 \quad \text{"Tension reinforcement ratio"}$$

$$k_1 := \sqrt{(2 \cdot \rho_B \cdot n) + (\rho_B \cdot n)^2} - (\rho_B \cdot n) = 0.253$$

$$d_{s_{pos}} \cdot k_1 = 20.44 \quad \text{in} \quad d \cdot k < d_{stem}$$

$$j_1 := 1 - \frac{k_1}{3} = 0.916$$

$$M_{s1} := 1210 \text{ ft}\cdot\text{kip}$$

$$f_{ss1} := \frac{M_{s1} \cdot 12}{A_{s\_B} \cdot j1 \cdot d_{s\_pos}} = 8.971 \text{ ksi}$$

$$f_a := 0.6 \cdot f_y = 36 \text{ ksi}$$

$$f_{ss1} < f_a \quad \text{Check} = \text{"OK"}$$

### Checking Dead Load Stress

TxDOT limits the dead load stresses to 22 ksi. This is due to the observed cracking under dead load.

$$\therefore f_{dl} := 22 \text{ ksi}$$

$$M_{dl1} := 0.1 \text{ ft}\cdot\text{kip}$$

### Allowable Dead Load Moment

$$M_{a\_dl1} := A_{s\_B} \cdot d_{s\_pos} \cdot j1 \cdot \frac{f_{dl}}{12} = 2967.478 \text{ ft}\cdot\text{kip}$$

$$\therefore M_{dl} < M_{a\_dl} \quad \text{Check} = \text{"OK"}$$

### Flexural Reinforcement Summary:

Provide 18 #11 bars A on the Top and 14#11 bars B on the Bottom

## 5. Ledge Reinforcement (Bars M & N)

The ledge reinforcements will be designed for Shear friction, flexure and axial tension. Let's provide

$$S_{bar\_M} := 6.00 \text{ in}$$

$$S_{bar\_N} := 6.00 \text{ in}$$

### Calculation of Distribution Width

#### 1. Distribution width for Shear friction : (AASHTO LRFD 5.13.2.2.2)

##### (i) Interior Girder :

$$b_{s\_int} := \min(W + 4 \cdot a_v, S) = 69 \text{ in}$$

##### (ii) Exterior Girder :

$$b_{s\_ext} := \min(W + 4 \cdot a_v, S, 2 \cdot C) = 54.048 \text{ in}$$

#### 2. Distribution width for bending and axial tension : (AASHTO LRFD 5.13.2.2.3)

##### (i) Interior Girder :

$$b_{m\_Int} := \min(W + 5 \cdot a_f, S) = 91 \text{ in}$$

##### (ii) Exterior Girder :

$$b_{m\_Ext} := \min(W + 5 \cdot a_f, S, 2 \cdot C) = 54.048 \text{ in}$$

### Reinforcing Required for Shear Friction

$$c1 := 0 \quad \mu := 1.4 \quad Pc := 0 \quad \phi_{sf} := 0.9$$

#### Minimum Reinforcing for Shear Friction (AASHTO LRFD 5.5.4.2.1)

$$A_{cv\_int} := d_e \cdot b_{s\_int} = 1725 \text{ in}^2$$

$$A_{vf\_min} := 0.05 \cdot \frac{A_{cv\_int}}{f_y} = 1.438 \text{ in}^2$$

$$a_{vf\_min} := \frac{A_{vf\_min}}{b_{s\_int}} \cdot 12 = 0.25 \text{ ft}$$

## Shear Friction Reinforcing :

### (i) Interior Girder :

$$A_{cv\_int} := d_e \cdot b_{s\_int} = 1725 \quad \text{in}^2$$

$$A_{vf\_int} := \left( \frac{1}{\mu} \cdot \left( \frac{V_{U\_Int}}{\phi_s \cdot fy} - c1 \cdot \frac{A_{cv\_int}}{fy} \right) - \frac{Pc}{fy} \right) = 4.429 \quad \text{in}^2$$

$$a_{vf\_int} := \frac{A_{vf\_int}}{b_{s\_int}} \cdot 12 = 0.77 \quad \frac{\text{in}^2}{\text{ft}}$$

### (ii) Exterior Girder :

$$A_{cv\_ext} := d_e \cdot b_{s\_ext} = 1351.2 \quad \text{in}^2$$

$$A_{vf\_ext} := \left( \frac{1}{\mu} \cdot \left( \frac{V_{U\_Ext}}{\phi_s \cdot fy} - c1 \cdot \frac{A_{cv\_ext}}{fy} \right) - \frac{Pc}{fy} \right) = 4.839 \quad \text{in}^2$$

$$a_{vf\_ext} := \frac{A_{vf\_ext}}{b_{s\_ext}} \cdot 12 = 1.074 \quad \frac{\text{in}^2}{\text{ft}}$$

## Reinforcing Required for Flexure

### (i) Interior Girder :

$$V_{U\_Int} := 334.84 \quad \text{kip}$$

$$N_{uc\_Int} := 0.2 \cdot V_{U\_Int} = 66.968 \quad \text{kip}$$

$$M_{u\_Int} := V_{U\_Int} \cdot a_v + N_{uc\_Int} \cdot (h - d_e) = 4252.468 \quad \text{in} \cdot \text{kip}$$

$$\beta_1 := 0.85$$

Guess Values	$A_{f\_Int} := 1.0$
	$c_{l\_Int} := \frac{A_{f\_Int} \cdot fy}{0.85 \cdot fc \cdot \beta 1 \cdot b_{m\_Int}}$
	$a_{l\_Int} := c_{l\_Int} \cdot \beta 1$
Constraints	$0.9 \cdot A_{f\_Int} \cdot fy \cdot \left( d_e - \frac{a_{l\_Int}}{2} \right) \geq M_{u\_Int}$
Solver	$A_{f\_Int} := \text{find}(A_{f\_Int}) = 3.16 \quad in^2$

$$a_{f\_int} := \frac{A_{f\_Int}}{b_{m\_Int}} \cdot 12 = 0.417 \quad \frac{in^2}{ft}$$

## (ii) Exterior Girder :

$$V_{U\_Ext} := 365.82 \quad kip$$

$$N_{uc\_Ext} := 0.2 \cdot V_{U\_Ext} = 73.164 \quad kip$$

$$M_{u\_Ext} := V_{U\_Ext} \cdot a_v + N_{uc\_Ext} \cdot (h - d_e) = 4645.914 \quad in \cdot kip$$

$$\beta 1 := 0.85$$

Guess Values	$A_{f\_Ext} := 1.0$
	$c_{l\_Ext} := \frac{A_{f\_Ext} \cdot fy}{0.85 \cdot fc \cdot \beta 1 \cdot b_{m\_Ext}}$
	$a_{l\_Ext} := c_{l\_Ext} \cdot \beta 1$
Constraints	$0.9 \cdot A_{f\_Ext} \cdot fy \cdot \left( d_e - \frac{a_{l\_Ext}}{2} \right) \geq M_{u\_Ext}$
Solver	$A_{f\_Ext} := \text{find}(A_{f\_Ext}) = 3.459 \quad in^2$

$$a_{f\_Ext} := \frac{A_{f\_Ext}}{b_{m\_Ext}} \cdot 12 = 0.768 \frac{in^2}{ft}$$

## Reinforcing Required for Axial Tension

### (i) Interior Girder :

$$N_{uc\_Int} := 0.2 \cdot V_{U\_Int} = 66.968 \text{ kip}$$

$$A_{n\_Int} := \frac{N_{uc\_Int}}{0.9 \cdot f_y} = 1.24 \text{ in}^2$$

$$a_{n\_Int} := \frac{A_{n\_Int}}{b_{m\_Int}} \cdot 12 = 0.164 \frac{in^2}{ft}$$

### (ii) Exterior Girder :

$$N_{uc\_Ext} := 0.2 \cdot V_{U\_Ext} = 73.164 \text{ kip}$$

$$A_{n\_Ext} := \frac{N_{uc\_Ext}}{0.9 \cdot f_y} = 1.355 \text{ in}^2$$

$$a_{n\_Ext} := \frac{A_{n\_Ext}}{b_{m\_Ext}} \cdot 12 = 0.301 \frac{in^2}{ft}$$

## Minimum Reinforcing Required

$$a_{s\_min} := 0.04 \cdot \frac{f_c}{f_y} \cdot d_e \cdot 12 = 1 \frac{in^2}{ft}$$

## Check Reinforcing Required

$$\text{Primary ledge reinforcing : } a_s := \frac{A_{bar\_M}}{S_{bar\_M}} \cdot 12 = 1.203 \frac{in^2}{ft}$$

$$\text{Secondary ledge reinforcing : } a_h := \frac{A_{bar\_N}}{S_{bar\_N}} \cdot 12 = 0.614 \frac{in^2}{ft}$$

## Ledge Reinforcement Summary:

Provide #7 bars M and #5 bars N @ 6" c/c spacing.

## 6. Hanger Reinforcement (Bars S)

### Input Data

$$d_{bar\_S} := 0.75 \text{ in}$$

$$S_{bar\_S} := 6 \text{ in}$$

$$A_{bar\_S} := \frac{\pi}{4} \cdot (d_{bar\_S})^2 = 0.442 \text{ in}^2$$

$$A_{hr} := \frac{A_V}{2} = 0.884 \text{ in}^2$$

$$A_V := 4 \cdot A_{bar\_S} = 1.767 \text{ in}^2$$

$$V_{s\_Int} := 222.48 \text{ kip}$$

$$V_{s\_Ext} := 240.19 \text{ kip}$$

$$V_{u\_Int} := 334.84 \text{ kip}$$

$$V_{u\_Ext} := 365.82 \text{ kip}$$

$$T_u := 522.35 \text{ ft}\cdot\text{kip}$$

$$V_u := 808.00 \text{ kip}$$

$$M_u := -1634.00 \text{ ft}\cdot\text{kip}$$

$$M_n := M_{n\_neg} = 10982.231 \text{ ft}\cdot\text{kip}$$

### Minimum Transverse Reinforcement (AASHTO LRFD 5.8.2.5-1)

$$b_V := b_w = 45 \text{ in}$$

$$A_{V\_min} := 0.0316 \cdot \sqrt{f_c} \cdot \left( \frac{S_{bar\_S} \cdot b_V}{f_y} \right) = 0.318 \text{ in}^2$$

**Check Service Limit State** (AASHTO LRFD 5.13.2.5.5)

$$A_{hr} := \frac{A_V}{2} = 0.884 \text{ in}^2$$

$$\phi_h := 0.9$$

**(i) Interior Girder:**

$$V_{all\_Int} := \min \left( \left( \left( \frac{A_{hr} \cdot \binom{2}{3} \cdot fy}{S_{bar\_S}} \right) \cdot (W + 3 \cdot a_v) \right), \left( \left( \frac{A_{hr} \cdot \binom{2}{3} \cdot fy}{S_{bar\_S}} \right) \cdot S \right) \right) = 335.758 \text{ kip}$$

**(ii) Exterior Girder:**

$$V_{all\_Ext} := \min \left( \left( \left( \frac{A_{hr} \cdot \binom{2}{3} \cdot fy}{S_{bar\_S}} \right) \cdot \left( \frac{W + 3 \cdot a_v}{2} + C \right) \right), \left( \left( \frac{A_{hr} \cdot \binom{2}{3} \cdot fy}{S_{bar\_S}} \right) \cdot \left( \frac{S}{2} + C \right) \right) \right) = 327.063 \text{ kip}$$

**Check Strength Limit State** (AASHTO LRFD 5.13.2.5.5)

**(i) Interior Girder:**

$$V_{nh\_Int} := \min \left( \left( \frac{A_{hr} \cdot fy}{S_{bar\_S}} \right) \cdot S, \left( 0.063 \cdot \sqrt{fc} \cdot b_f \cdot d_f + \frac{A_{hr} \cdot fy}{S_{bar\_S}} \cdot (W + 2 \cdot d_f) \right) \right) = 929.79 \text{ kip}$$

$$\phi_h \cdot V_{nh\_Int} = 836.811 \text{ kip}$$

$$V_{U\_Int} < \phi_h \cdot V_{nh\_int}$$

**Ultimate Check = OK**

*fishy*

**(ii) Exterior Girder:**

$$V_{nh\_Ext} := \min \left( \left( \left( \frac{A_{hr} \cdot fy}{S_{bar\_S}} \right) \cdot \left( \frac{S}{2} + C \right) \right), V_{nh\_Int}, \left( \left( 0.063 \cdot \sqrt{fc} \cdot b_f \cdot d_f \right) + \frac{A_{hr} \cdot fy}{S_{bar\_S}} \cdot \left( \frac{W + 2 \cdot d_f}{2} + C \right) \right) \right) = 864.993 \text{ kip}$$

$$\phi_h \cdot V_{nh\_Ext} = 778.494 \text{ kip}$$

$$V_{U\_Ext} < \phi_h \cdot V_{nh\_ext}$$

**Ultimate Check = OK**

## Combined Shear and Torsion Check

$$A_{ps} := 0 \quad f_{ps} := 0 \quad d_p := 0 \quad \beta := 2.38 \quad \theta := 33.70 \text{ deg}$$

$$d_s := d_{s\_neg} = 80.215 \text{ in}$$

$$d_s := \frac{A_{ps} \cdot f_{ps} \cdot d_p + A_{s\_A} \cdot f_y \cdot d_s}{A_{ps} \cdot f_{ps} + A_{s\_A} \cdot f_y} = 80.215 \text{ in}$$

$$d_v := \max \left( \frac{M_{n\_neg} \cdot 12}{A_{ps} \cdot f_{ps} + A_{s\_A} \cdot f_y}, 0.9 \cdot d_{s\_neg}, 0.72 \cdot h \right) = 78.148 \text{ in}$$

$$A_t := 0.44 \text{ in}^2 \quad \text{"}A_t\text{" is the area of outer stirrups}$$

$$A_{oh} := (d_{stem}) \cdot (b_{stem} - 2 \cdot Cover) + (d_{ledge} - 2 \cdot Cover) \cdot (b_f - 2 \cdot Cover) = 4453 \text{ in}^2$$

" $A_{oh}$ " is the area inside the central line of the exterior stirrups

$$A_o := 0.85 \cdot A_{oh} = 3785.05 \text{ in}^2$$

$$p_h := (b_{stem} - 2 \cdot Cover) + 2 \cdot (b_{ledge}) + (b_f - 2 \cdot Cover) + 2 \cdot (h_{cap} - 2 \cdot Cover) = 344 \text{ in}$$

" $p_h$ " is the perimeter of the centerline of Bar S

## Equivalent Shear Force

(AASHTO LRFD 5.8.2.1-6)

$$V_{u\_Eq.} := \sqrt{(V_u)^2 + \left( \frac{0.9 \cdot p_h \cdot T_u}{2 \cdot A_o} \right)^2} = 808.282 \text{ kip}$$

## Shear Steel Required

$$\phi_v := 0.9 \quad V_p := 0$$

$$b_v := b_{stem} = 45 \text{ in}$$

$$V_{n\_max} := 0.25 \cdot f_c \cdot b_v \cdot d_v + V_p = 4395.846 \text{ kip} \quad \text{(AASHTO LRFD 5.8.3.3-2)}$$

$$\phi_v \cdot V_{n\_max} = 3956.261 \text{ kip}$$

$$\therefore V_u \leq \phi_v \cdot V_{n\_max} \quad \text{Maximum Shear Check = OK}$$

$$V_c := 0.0316 \cdot \beta \cdot \sqrt{f_c} \cdot b_v \cdot d_v = 591.4 \quad \text{kip} \quad \text{"Shear resisted by concrete"}$$

$$\beta := 2.38 \quad \theta := 33.70$$

$$V_s := \frac{A_V \cdot f_y \cdot d_v \cdot \left( \cot\left(\theta \cdot \frac{\pi}{180}\right) + \cot\left(90 \cdot \frac{\pi}{180}\right) \right) \cdot \sin\left(90 \cdot \frac{\pi}{180}\right)}{6.0} = 2070.716 \quad \text{kip}$$

"Shear resisted by steel"

$$a_{v\_req} := \frac{V_u - V_c - V_p}{\phi_v \cdot f_y \cdot d_v \cdot \left( \cot\left(\theta \cdot \frac{\pi}{180}\right) + \cot\left(90 \cdot \frac{\pi}{180}\right) \right) \cdot \sin\left(90 \cdot \frac{\pi}{180}\right)} \cdot 12 = 0.523 \quad \begin{matrix} \text{in}^2 \\ \text{ft} \end{matrix}$$

"Required shear steel"

### Torsional Steel Required

$$\phi_T := 0.9$$

$$T_u < \phi_T \cdot T_n \quad \text{(AASHTO LRFD 1.3.2.1-1)}$$

$$T_n := \frac{2 \cdot A_o \cdot A_t \cdot f_y \cdot \cot\left(\theta \cdot \frac{\pi}{180}\right)}{S_{bar\_S} \cdot 12} = 4161.992 \quad \text{in} \cdot \text{kip} \quad \text{(AASHTO LRFD 5.8.3.6.2-1)}$$

$$a_{t\_req} := \frac{T_u \cdot 12^2}{\phi_T \cdot 2 \cdot A_o \cdot f_y \cdot \cot\left(\theta \cdot \frac{\pi}{180}\right)} = 0.123 \quad \begin{matrix} \text{in}^2 \\ \text{ft} \end{matrix}$$

### Total Required Transverse Steel

$$a_{req} := a_{v\_req} + 2 \cdot a_{t\_req} = 0.768 \quad \begin{matrix} \text{in}^2 \\ \text{ft} \end{matrix}$$

$$a_{prov} := \frac{A_V}{S_{bar\_S}} \cdot 12 = 3.534 \quad \begin{matrix} \text{in}^2 \\ \text{ft} \end{matrix}$$

$$\therefore a_{prov} > a_{req} \quad \text{Transverse rebars Check = OK}$$

## Check for Spacing of Transverse Reinforcement (AASHTO LRFD 5.8.2.7)

$$v_u := \frac{V_u - \phi_v \cdot V_p}{\phi_v \cdot b_v \cdot d_v} = 0.255 \text{ ksi}$$

$$0.125 \cdot f_c = 0.625 \text{ ksi}$$

$$S_{max} := \begin{cases} \text{if } v_u < 0.125 \cdot f_c & = 24 \text{ in} \\ \left\| \min(0.8 \cdot d_v, 24) \right\| & \\ \text{else} & \\ \left\| \min(0.4 \cdot d_v, 12) \right\| & \end{cases}$$

But TxDOT limits the maximum transverse reinforcement spacing to 12", therefore

$$S_{max} := 12 \text{ in}$$

$$\therefore S_{bar\_S} < S_{max}$$

Maximum Spacing Check =OK

### Hanger Reinforcement Summary :

Provide double #6 transverse stirrups @ 6" c/c spacing.  
Spacing of the stirrups should be measured from center to center along the length of the bent cap.

Also provide #6 bars at the each end face along the skew direction @ 6" c/c spacing.

## 7. Skin Reinforcements (Bars T)

Try 7~#7 brs in Stem and 3~#7 in Ledge on each side

$$A_{bar\_T} := 0.60 \text{ in}^2$$

$$NoTBarsStem := 7$$

$$NoTBarsLedge := 3$$

"a" must be within 2/3 of de

$$\frac{2}{3} \cdot d_e = 16.667 \text{ in}$$

### Required Area of Skin Reinforcement

$$A_{sk\_Req} := 0.012 \cdot (d_{s\_neg} - 30) = 0.603 \text{ in}^2$$

$$A_{sk\_max} := \max \left( \left( \frac{A_{bar\_A} \cdot BarANo}{4} \right), \left( \frac{A_{bar\_B} \cdot BarBNo}{4} \right) \right) \cdot 12 = 2.102 \text{ in}^2$$
$$\left( \frac{d_{s\_neg}}{2} \right), \left( \frac{d_{s\_pos}}{2} \right) \text{ ft}$$

$$A_{skReq} := \min(A_{sk\_Req}, A_{sk\_max}) = 0.603 \text{ in}^2$$

### Required Spacing of Skin Reinforcement

$$S_{req} := \min \left( \frac{A_{bar\_T} \cdot 12}{A_{skReq}}, \frac{d_{s\_neg}}{6}, \frac{d_{s\_pos}}{6}, 12 \right) = 11.949 \text{ in}$$

### Check Actual Spacing of Skin Reinforcement

#### (i) Check T bars Spacing in Stem

$$h_{top} := d_{stem} - \left( Cover + \frac{d_{bar\_S}}{2} + \frac{d_{bar\_A}}{2} \right) + \left( Cover + \frac{d_{bar\_M}}{2} + \frac{d_{bar\_T}}{2} \right) = 56.795 \text{ in}$$

$$s_{skStem} := \frac{h_{top}}{NoTBarsStem + 1} = 7.099 \text{ in}$$

$$S_{req} > s_{skStem}$$

**(ii) Check T bars Spacing in Stem**

$$h_{bot} := d_{ledge} - \left( Cover + \frac{d_{bar\_M}}{2} + \frac{d_{bar\_T}}{2} \right) - \left( Cover + \frac{d_{bar\_S}}{2} + \frac{d_{bar\_B}}{2} \right) = 21.045 \text{ in}$$

$$s_{skLedge} := \frac{h_{bot} - 6}{NoTBarsLedge - 1} = 7.523 \text{ in}$$

$$S_{req} > s_{skLedge}$$

**Skin Reinforcement Summary :**

Provide double 7 #7 rebars in stem and 3#7 bars in the ledge on each side. .